University of Louisville

ThinkIR: The University of Louisville's Institutional Repository

Electronic Theses and Dissertations

5-2015

Critical insights into the pathogenesis of clinical isolates of pandemic influenza A(H1N1) 2009 virus in mouse and ferret models.

Jeremy V. Camp 1980-
University of Louisville

Follow this and additional works at: https://ir.library.louisville.edu/etd

Part of the Immunology and Infectious Disease Commons, and the Microbiology Commons

CRITICAL INSIGHTS INTO THE PATHOGENESIS OF

CLINICAL ISOLATES OF PANDEMIC INFLUENZA A(H1N1)2009 VIRUS

IN MOUSE AND FERRET MODELS

By

Jeremy V. Camp
B.S. Auburn University, 2003
M.S. Georgia Southern University, 2006

A Dissertation
Submitted to the Faculty of the
School of Medicine of the University of Louisville
in Partial Fulfillment of the Requirements
for the Degree of

Doctor of Philosophy
in Microbiology and Immunology

Department of Microbiology and Immunology
University of Louisville
Louisville, KY

May 2015

CRITICAL INSIGHTS INTO THE PATHOGENESIS OF

CLINICAL ISOLATES OF PANDEMIC INFLUENZA A(H1N1)2009 VIRUS

IN MOUSE AND FERRET MODELS

By

Jeremy V. Camp
B.S. Auburn University, 2003
M.S. Georgia Southern University, 2006

A Dissertation Approved on

March 26, 2015

by the following Dissertation Committee:

_____

Colleen B. Jonsson, Ph.D.

_____

Mostafa Fraig, M.D.

_____

Matthew B. Lawrenz, Ph.D.

_____

Thomas C. Mitchell, Ph.D.

_____

Silvia M. Uriarte, Ph.D.

ABSTRACT

CRITICAL INSIGHTS INTO THE PATHOGENESIS OF CLINICAL ISOLATES OF

PANDEMIC INFLUENZA A(H1N1)2009 VIRUS IN MOUSE AND FERRET

MODELS

Jeremy V. Camp
March 26, 2014

Influenza A virus (IAV) is a minus-sense, segmented, single-stranded RNA virus that

infects the respiratory tract of humans and can cause severe illness. Novel IAV variants

perpetually emerge on every continent, and the emergence of variants with increased

transmissibility and/or pathogenesis in the human population is a serious concern for

global public health. Infection with IAV typically causes an acute, self-limiting upper

respiratory tract disease. However, severe IAV disease is characterized by infection of

the lower respiratory tract which can lead to pneumonia and may result in the

development of acute respiratory distress syndrome (ARDS). Viral and host

contributions to the development of ARDS are poorly understood, however IAV

pathogenesis has been linked mutations in the receptor binding protein and the viral

polymerase. Ferrets and mice are two important laboratory animal models for studying

IAV pathogenesis. In 2009, a novel H1N1 subtype IAV (H1N1pdm) emerged in the

human population and displayed variable pathology in humans. Using a mouse model,

we show the variability of clinical isolates of H1N1pdm is driven by viral mutations,

iv

and that the timing of the inflammatory response is correlated with disease severity. To investigate spatiotemporal aspects of potential host and viral contributions to influenza pathogenesis, we developed a live imaging platform for ferrets infected with a human clinical isolate of H1N1pdm. We detected an early recruitment of neutrophils into ferret lungs following infection, which accumulated at foci of H1N1pdm infection within specific anatomical regions of the lung by 24 hours post-infection. The neutrophil response was biphasic, characterized by the recruitment of two populations with differing gene expression profiles, and baseline neutrophil levels were increased throughout the entire lung, including areas with no apparent viral infection. Changes in the viral microenvironment resulted in the regeneration of lung epithelium during recovery phase of infection, and this was imaged with PET-CT using a radiolabeled glucose analog. In summary, these data illustrate critical features of the immune response to IAV, and emphasize important considerations about the timing and accuracy of innate immune responses in studying viral pathogenesis.

TABLE OF CONTENTS

LIST OF TABLES

LIST OF FIGURES

CHAPTER I

INTRODUCTION

1. Establishing a role for neutrophils in influenza A viral pneumonia

Influenza A virus (IAV) infection is the cause of a respiratory disease that poses a significant global public health concern (1-5). Influenza disease is commonly relatively mild and self-limiting, although highly pathogenic forms exist (6-13). The major complication from IAV infection is the formation of severe influenza pneumonia (SIP) which may develop into an acute respiratory distress syndrome (ARDS) (7-9, 11-15). The reason(s) why infection with IAV may lead to severe viral pneumonia and ARDS is poorly understood, but is thought to involve both host and viral factors. The respective and combined contributions of the host immune response and viral factors to the timing and severity of SIP are poorly understood. Neutrophils are immune cells that are well-known to be present during many types of lung diseases associated with ARDS, and may contribute to acute lung injury (16-25). Neutrophils are present in the respiratory tract during infection with mild seasonal IAV, moderate and severe IAV infection, and highly pathogenic avian influenza viruses (HPAI) (7, 8, 14, 26-30). During SIP and HPAI infection, an increase in the number of neutrophils in the lower respiratory tract (LRT) is correlated with disease severity (7, 8, 14, 28-30). However, neutrophils are poorly studied with respect to viral infection, respiratory viral disease, and specifically IAV infection.   Herein, the contribution of neutrophils to IAV disease pathogenesis is reviewed.

IAV poses a concern for global public health due to emergence of strains with increased human transmission and/or increased pathology (2, 5, 31-34). In 2009, an H1N1 subtype IAV (H1N1pdm) emerged that was observed to have increased transmission and caused moderate to severe pathology relative to seasonal human IAV (1, 6, 28, 35-46). Clinical isolates of H1N1pdm have relatively little genetic variability yet caused variable clinical outcomes from moderate to severe pathology, including ARDS (1, 30, 38, 44, 45). Therefore they are well suited to understand host and viral contributions to IAV pathogenesis. Laboratory animal models, such as mice and ferrets, provide a way to study and test hypotheses about the pathogenesis of IAV, specifically about the contributions of viral and host determinants to severe disease (47-50). There are common occurrences in the formation of severe IAV (including SIP and ARDS) in humans, ferrets, and mice; these include increased cytokine secretions in the lung, diffuse alveolar damage (bronchointerstitial pneumonia in veterinary pathology), and neutrophilic infiltration (9, 14, 47, 50-56).

The lung has a global inflammatory response to infection, and this response includes the infiltration of neutrophils and macrophages in response to chemotactic signaling which originates in the lung (16, 18, 25, 57-64). However, the immune system requires additional information to control specific causes of infection. In other words, although similar cellular and systemic signaling systems are activated in response to infection of the lungs, in general the type I interferons (IFN) and interferon-stimulated genes (ISGs) are necessary to signal a benevolent immune response during a viral infection (65-68). During experimental IAV infection in mice, a breakdown of transmission of "viral" information causes malevolent immune responses, and a dysregulated immune response is lethal (e.g., via suppression of type I IFN, or productive infection of major IFN-producing cells, the alveolar macrophages) (69-75). Ultimately, all forms of respiratory infection require resolution of the infection and

2

inflammation. Interferons are essential components of initiating sterilizing immunity via the adaptive immune system (*i.e.*, resolution of infection), at which point the resolution of inflammation can effectively proceed (67, 68, 76). In regards to resolution of both infection and inflammation, neutrophils may be a keystone cell type in determining pathologic outcomes in the viral microenvironnment. Although the mechanisms are poorly understood, through their direct antiviral actions and indirect actions on the lung microenvironment (*e.g.*, efferocytosis of apoptotic neutrophils by macrophages), neutrophils have the ability to influence outcomes towards successful resolution as well as towards the formation of ARDS (16, 18, 25, 26, 57, 77-84). In general, the interactions of neutrophils with IAV, the antiviral microenvironement, and resident lung cells deserve further study.

Here, the role of neutrophils in IAV disease is reviewed. First, the various presentations of disease caused by IAV infection are introduced followed by a description of the viral replication cycle. This is essential for understanding viral determinants of disease severity in humans, as well as the justification for the use of animal models in studying IAV pathogenesis. Finally, the host acute (exudative) response to IAV is reviewed, focusing on the role of neutrophils in disease and data from both human, mouse, and ferret studies. The role of neutrophils in the generation of adaptive immunity and resolution have been established in a mouse model of IAV, however, this aspect of the relationship between neutrophils and IAV infection is beyond the scope of this review (26, 83, 85-87). The intention here is to present what is known about the interaction between neutrophils and early events within the airways following IAV infection. In doing so, this review will also discuss the relationships between neutrophils and other respiratory virus infections to establish a role for neutrophils in respiratory viral disease.

2. Influenza A virus pathology

Although clinical pathology suggests that a spectrum of disease results from IAV infection, there are at least three disease "phenotypes" caused by infection with IAV, listed by increasing case fatality rate: a mild URT tract infection, a SIP which can lead to ARDS, and a LRT infection which can lead to hypercytokinemia (Figure 1.1). As discussed below, the virological basis for disease phenotype is related to IAVs adaptation to humans, for which some mechanisms have been well defined; thanks in part to the use of experimental animal models (2, 32, 33, 49, 88-91). An "ideal" viral infection (*i.e.*, one that is successful for the virus and non-lethal for the host) may be considered a balance between virus replication and an immune response necessary to promote viral shedding, typical of mild seasonal ("epidemic") IAV. In general emergent IAV, directly or indirectly from avian enzootic cycles, have increased pathology in humans, the most fatal form of which is a syndrome of complete immune dysregulation (10, 11, 14, 92-95). IAV is genetically highly variable, and mechanisms for increased disease severity are multifactorial, involving host and viral factors, and thus are poorly understood.

2.1 Uncomplicated influenza.

The majority of yearly, seasonal IAV infections in the world cause a relatively mild, self-limiting URT disease (96). Influenza disease is characterized by an abrupt onset fever, myalgia and malaise, with symptoms similar to other URT infections, such as sneezing, coryza, and rhinorrhea (7, 97). Symptoms can last anywhere from 1-5 days, and are clinically indistinguishable from other "flu"-like illnesses, including bacterial and viral infections that cause the common cold (e.g., *Streptococcus pneumoniae, Haemophilus influenzae*, human rhinovirus infection, human respiratory syncytial virus infection, and

coronavirus infection) (97-100). Experimental infection of humans with IAV suggests that the virus is mainly restricted to the URT, although sampling the LRT is difficult (7, 8, 99, 101). While fever typically begins two days post-infection, virus is shed from the URT in nasal secretions as quickly as 24 hours post-infection, allowing efficient transmission prior to symptom onset, and continues until 4-5 days post-infection (98, 99, 101). Rhinorrhea is coincident with neutrophilic rhinitis and shedding of necrotic nasal epithelium (7, 102, 103). Surprisingly, the LRT seems to be involved in uncomplicated IAV infection, although this observation is frequently overlooked or unaddressed in studies (8, 104). In humans, local and systemic concentrations of IL6, CXCL8/IL8, and MCP1/CCL2 correlate with increased disease severity (*i.e.,* symptoms and increased virus shedding) (99-101, 105).

2.2 Pandemic influenza and SIP.

Histopathology. The 2009 H1N1pdm virus spread quickly throughout the globe, much like previous pandemic viruses such as the 1918 H1N1 "Spanish flu". H1N1pdm infections also presented with typical flu-like symptoms (*e.g.*, fever, cough), however there was an increased number of cases presenting with dyspnea, respiratory distress, and pneumonia (1, 6, 28, 35-37, 39-45, 106, 107). Additionally, retrospective assessments show a proportionately greater number of adolescents and adults with severe disease compared to typical seasonal influenza, and patients with comorbidities such as obesity and asthma were at higher risk of severe infection (30, 108-110). In general, the virus causes infection of URT, as well as bronchitis and bronchiolitis, and a high proportion of cases presented with severe disease in the form of viral pneumonia (6, 30, 108). Histopathologic changes in autopsies revealed extensive cytonecrosis, desquamation, and inflammatory infiltration of the bronchus and trachea, mild to severe necrotizing bronchiolitis (6, 28, 30, 111). The primary pathologic finding of SIP

was sporadic to diffuse alveolar damage with hyaline membrane formation, edema, and occasionally hemorrhage (6, 28, 30, 111). As is typical of influenza infections, some patients experienced bacterial co-infection although this was not in a majority of patients, including those dying from ARDS (6, 28, 30, 45, 105, 111-115). This may distinguish the 2009 H1N1pdm virus from the 1918 H1N1 "Spanish" IAV, for which bacterial super-infection was determined to cause a majority of the deaths (116, 117), although this may more accurately reflect improved hygiene and standard of care. As discussed below, studies of the reconstructed 1918 H1N1 IAV using animal models suggest that this virus was highly pathogenic irrespective of secondary bacterial pneumonia (53, 118-120).

Immune response. Across many cohorts of clinical patients, serum concentration of IL-6, CCL2, and CXCL8 were significantly elevated in severe cases of H1N1pdm pneumonia when compared to patients with other confirmed illnesses including seasonal IAV, mild forms of H1N1pdm, bacterial pneumonia, or other viral respiratory infection (*Human respiratory syncytial virus* [hRSV], human rhinovirus [HRV], human adenovirus [hAdv]) (105, 112-114, 121). These cytokines and chemokines remained elevated over time (up to 6 days following hospital admission) in cases of severe H1N1pdm pneumonia, where as they decreased as patients recovered from seasonal and mild H1N1pdm infection (105, 112). In severe cases of H1N1pdm infection, decreased type I IFN and ISG production was occasionally noticed compared to adult patients with seasonal IAV infection (105). The H1N1pdm viruses have received much scrutiny and a large dataset of the genetics and pathogenic phenotypes of virus isolates exists in human and animal models. The H1N1 subtype IAV are highly important viruses due to their pandemic potential, as supported by the historical record (8, 53, 122). Some H1N1pdm viruses can infect the lower respiratory tract in humans and in the ferret animal model, which makes them excellent laboratory

viruses to investigate the involvement of the LRT in pathogenesis, specifically in the development of severe disease (6, 123-127). Their overall genetic similarity makes for excellent comparison studies between natural clinical isolates, and reverse genetics systems exist to study molecular pathogenicity (1, 107, 125, 128-138). This review will focus on the H1N1pdm viruses for these reasons.

2.3 HPAI and cytokine storm.

H5N1 HPAI. Avian IAV has sporadically entered the human population in the last 20 years, emerging first in China in 1997 (11, 93, 139, 140). It is likely that this (H5N1 avian IAV) and other emergent strains result from contact with infected domestic poultry who are infected with HPAI (93). The disease caused by H5N1 IAV is characterized by diffuse alveolar damage, alveolar necrosis, and alveolar hemorrhage (human disease, including pathology, is reviewed in (94)). There is evidence of viremia and systemic spread; IAV antigen has been detected in the trachea, bronchi and alveolar pneumocytes (10, 29), as well as infrequently in the brain and gastric epithelium (9, 29, 94). The innate cellular immune response in the lungs was characterized by an increase in inter-alveolar macrophages/histiocytes (9, 10, 12, 14, 92, 141) and only moderate infiltration of lymphocytes and neutrophils (10, 29). Systemically, patient serum had high concentrations of CXCL10, CCL2, IL6, IL8, and IL10 compared to matched control patients with either seasonal H3/H1 IAV, and these concentrations were correlated with viral load in throat (9, 10, 14). In lethal cases, the result of infection and immune dysregulation led to multiple organ failure, (e.g., kidney tubular inflammation, necrotic lesions in brain, impaired liver function) and abnormal clotting. Reactive histiocytes undergoing hemophagocytosis were

frequently found in bone marrow and lungs of patients, which is indicative of diseases involving hypercytokinemia.(9, 11, 14, 92, 94, 142).

Continuing emergence of avian IAV. Other events involving avian IAV transmission to humans are known, and are often associated with veterinary or other animal workers; for example a 2004 case of H7N7 infection in a veterinarian in Europe showed severe fatal pneumonia and DAD (143). It was reported that 1 L of serosanguineous fluid was drained from his chest upon autopsy. In 2013, another avian IAV emerged in Southeast Asia; this time an H7N9 virus (12, 13, 141, 144). The histopathology was similar to H5N1; severe pneumonia, diffuse alveolar damage, and epithelial necrosis were common features of infection with both viruses (12, 13). Patients infected with either virus had high levels of CXCL10, CCL2, IL-6, and CXCL8 in the plasma and displayed peripheral blood leukopenia and neutrophilia (10, 14, 92, 141, 142, 144). There were slightly more bacterial co-infections in cases of H7N9 compared to H5N1 avian IAV (12, 13, 92). In a direct comparison, serum from patients with infected with H5N1 avian IAV had higher concentrations of IFNa and IFNg in the blood and lower levels of IL8, whereas the opposite was true for patients with H7N9 (145). Similarly, CXCL9 and CXCL10 were higher in patients with H5N1 avian IAV, whereas CCL4 concentrations were higher in patients with H7N9 avian IAV (145). Infection with either virus resulted in higher blood C-reactive protein (CRP) (141).

3. Influenza A virus components and replicative cycle

IAV was first isolated in 1933 as a "filterable agent" that was capable of infecting ferrets and satisfied Koch's postulates in ferrets (146-148). It caused a respiratory tract disease in ferrets that was very similar to influenza disease in humans (147-149). Currently, many aspects of

IAV replication cycle are understood through the use of cell culture techniques. Modern

molecular genetic techniques have developed a reverse genetics system, which allows direct

manipulation of the viral genome to study biochemical properties of viral proteins (128, 150).

Today, efforts by the WHO and agencies in collaborating countries have standardized

techniques for the isolation and description of clinical IAV to provide constant, world-wide

IAV monitoring with the goal of preventing or predicting future pandemics .

3.1 Virion structure and components.

IAV are enveloped, minus sense, RNA viruses in the family Orthomyxoviridae (151). Each

virion carries one copy of the genome, which is composed of eight segments of viral RNA

(151, 152) (Figure 1.2). In the virion, each genomic segment is bound with a polymeric

helical viral nucleoprotein and a single molecule of the trimeric viral RNA-dependent RNA

polymerase (RDRP) (153-156). This ribonucleoprotein (RNP) complex is encased in a shell

of matrix (M1) protein, which is enveloped by a phospholipid bilayer membrane derived

from host plasma membrane (157, 158). The IAV viral envelope contains three

transmembrane proteins: the HA, the NA, and the M2 ion channel protein (158-162). The

pleiomorphic virions are approximately 100 nanometers in diameter, and filamentous virus

particles are produced which are typically greater than 1 micrometer in length (163-165).

The complexities of virion assembly are not fully understood, particularly with respect to the

formation of these filamentous particles and the production of virions lacking a complete

genome (158, 163, 165-167).

3.2 Receptor binding, fusion, and entry.

Influenza viruses bind to glycosylated host proteins via the viral HA, which has a specificity for glycans with terminal SA residues (159, 168, 169) (Figure 1.3, step 1). Currently, it is thought that this receptor binding maintains the virus in close proximity of the plasma membrane until the virus can be taken up by clathrin-mediated endocytosis, although other forms of uptake are possible (170, 171). Clathrin-mediated endocytosis results in a gradually acidified endosome, which allows a two-step conformational change in the HA protein (172, 173). The HA is classified as a class II membrane fusion protein, and the conformational change results (1) in the insertion of an alpha helical domain near the cleavage site into the host's endosomal membrane followed by (2) a "pinching" movement at approximately pH 5.5 which fuses the host endosomal membrane with the viral envelope (159, 172, 174-176) (Figure 1.3, step 2). For this high energy fusion reaction, the HA must undergo a maturation step prior to endocytosis in which a host protease cleaves a residue on the pre-fusion conformation of the HA protein to prepare the protein for membrane fusion (177-181). During endocytosis, the M2 ion channel allows for the acidification of the interior of the virion simultaneously during the acidification of the endosome by host processes (182, 183). This prepares the matrix (M1) protein to release the viral RNPs into the cytoplasm once the membrane fusion event has occurred (157, 184, 185).

3.3 Viral replication and gene expression.

Nuclear localization signals designate transport of the RNP and other viral proteins to the host cell's nucleus where replication and transcription can occur (184, 186-189) (Figure 1.3, step 3). Once in the nucleus, the viral RDRP initiates these processes by creating complementary plus-sense copies of the gene segments (cRNA), which can be then replicated

back into vRNA (190, 191). The RDRP has a "cap-snatching" function, which removes a 5'-terminal methylated structures from host mRNA and attaches it to viral cRNA to make viral mRNA (192, 193). IAV lack methyltransferases, so this is an essential step for mRNA translation initiation on ribosomes (192, 193). This is also necessary to evade intracellular immune systems which detect $2'$-O and $5'$-penultimate unmethylated RNA structures in the cytoplasm (194, 195). Viral mRNA is exported and translated on ribosomes in the cytoplasm, while transmembrane glycoproteins are co-translated on the endoplasmic reticulum (Figure 1.3, step 4).

3.4 Non-structural gene products.

There are several non-structural gene products encoded by IAV. All seem to have the primary function of modulating the host's immune response (151, 196-198) (Figure 1.3, step 5). As discussed below, NS1A protein reduces anti-viral type I IFN responses in infected cells through a variety of hypothesized mechanisms (reviewed in (199-201)). The IAV PB1-F2 is thought to modulate host cell apoptosis by targeting the mitochondrial activator MAVS and interfering with mitochondrial membrane potential (196, 197, 202, 203). Recently, several other gene products have been discovered (e.g., PB1-N40, PA-X) by identifying start codons in alternate reading frames (204). The approach to understanding these has been to use reverse genetics systems to create viruses with mutations in the polypeptide's ORF or insert a stop codon to disrupt translation of the putative polypeptide in a way that does not affect the full-length protein and test the effects compared to the wild type virus *in vitro* or *in vivo* (205-207). With this approach, it is difficult to control the effects on other gene products; therefore the relative importance of these lesser-known non-structural proteins pathogenesis is currently unknown.

3.5 Virion assembly and budding.

As IAV proteins are being made, the RNP complex escapes the nucleus via the interaction of NS2 (nuclear export protein, NEP) with nuclear pore proteins (208). Transmembrane proteins, such as the HA, NA, and M2, are translated on rough ER and transported through the Golgi body to the plasma membrane (151). Currently, it is thought that the cytoplasmic domains of glycoproteins, the M1, and the M2 proteins coordinate the assembly of all eight RNPs at cytosolic locations near plasma membrane rafts of viral membrane proteins (166, 209, 210) (Figure 1.3, step 6). New virions deform the membrane outwards, eventually budding off from the host membrane (158, 166) (Figure 1.3, step 7). Release from the host cell is performed by the NA protein, which is a viral receptor destroying enzyme. Destroying SA receptors on the infected host cell may be beneficial by preventing re-infection of that cell. There is strong evidence in both natural and experimental systems for coevolution of the HA and NA proteins to enable an efficient balance between receptor binding and receptor destruction (211-215).

4. Influenza A virus ecology and epidemiology

4.1 Sources of IAV variation and subtypes.

There are two important rules governing the transmission cycle of IAV in nature: (1) the error-prone viral RDRP creates mutations which allow viral progeny to quickly adapt to new selective pressures (*e.g.*, "drift" over time within a host taxon), (2) optimized virus "solutions" to replication become genetically fixed across host taxa due to host-adapting selective pressures such as receptor binding (2, 32, 216). It is thought that host herd

immunity is the driving factor behind drift, and this makes influenza unique amongst RNA

viruses ((217),reviewed in (218)). However, variation of the glycoproteins does not exist in a

spectrum and certain "solutions" have been fixed in the IAV gene pool (219, 220). "Fixed"

subtypes of IAV have been classified according to antigenic characteristics of the envelope

glycoproteins, HA or NA (*i.e.,* antibody cross-reactivity) (2, 32, 221). This system is well-

supported genetically, and viruses are identified using an "H" number and "N" number to

specify the antigenic subtype of each. There are 16 subtypes of HA and 9 subtypes of NA

which have been described from influenza viruses found in mammals and birds (219, 220,

222, 223). Recently two additional influenza-like viruses have been described from bats

which have H17N10 and H18N11 glycoprotein subtypes (224-227). Biologically, the two

membrane glycoproteins, HA and NA, have important roles in the viral life cycle, and are

important features for the generation of host adaptive immunity via neutralizing antibodies.

4.2 IAV zoonoses.

Host restriction is intrinsically linked to the initial receptor binding step; thus HA subtypes

remain antigenically stable within reservoir species with some drift (reviewed in (216)).

Subtypes of HA can be classified by their ability to bind specific SA terminal linkages ((223),

reviewed in (159)). For example, avian IAV have undergone selection to bind preferentially

to SA forming a terminal linkage to the carbon-3 of a penultimate galactose (i.e., alpha 2,3-

linked SA), which is the most common type of linkage in the avian gastro-intestinal tract (95,

169, 228, 229). In mammalian hosts, the isomeric linkage of SA to the carbon-6 of galactose

is more common, resulting in alpha 2,6-linked SA which are found throughout the

mammalian respiratory tract (95, 169, 228-230). The first step in determining whether

transmission between taxa can occur is if receptor binding can occur in the new taxon. Once

in a new host species, gradual mutations in the HA and other viral proteins (*i.e.,* drift) may allow for increased efficiency of replication and transmission and establish these viruses within a new enzootic cycle (216, 231). For example, equine H7N7 and H3N8 IAV circulates in horses, canine H3N8 IAV circulates in dogs and originated from the horse strain, and swine H1N1, H1N2, H3N2, and the "variant H3N2" IAV circulates in domestic pigs (2, 38, 232-234). Throughout the last century there is evidence that novel H1N1, H2N2, and H3N2 subtypes of IAV have entered an endemic human cycle of transmission from an epizootic event and are now responsible for "seasonal" influenza (122). As the viruses drift and adapt with their host, the subtype proteins retain their original antigenicity; thus, for example, the canine, equine, human, and swine "H3" are genetically distinct, yet they are more similar to one another than any are to an "H1" (reviewed in (2, 216)).

4.3 Avian IAV.

Birds are natural reservoirs for all HA and NA subtypes of IAV (with the recent exceptions noted above), and as such all known influenza A viruses are avian influenza viruses (235-238). Avian viruses may infect domestic poultry, *i.e.,* chickens or turkeys (order Galliformes), and can be divided into highly pathogenic avian influenza viruses (HPAI) or low pathogenicity avian influenza viruses (LPAI) according to their pathogenicity in domestic birds (236-238). HPAI causes significant mortality in humans but transmits poorly between humans, and thus the 2003 H5N1 and 2013 H7N9 IAV outbreaks in China were contained (10, 11, 145, 239, 240). The reason(s) for the poor transmissibility of avian IAV between mammals is not known, although recently two laboratories have attempted to experimentally answer this question using ferrets (89, 91).

4.4 Epizootic transmission of IAV.

The hypothesis explaining the emergence novel IAV in the human population is that swine act as intermediate hosts between human population and the avian reservoirs (2, 31-34). Pigs have the ability to become infected with an avian virus and may foster adaption of avian viruses to mammalian SA linkages (241, 242). Additionally, coinfection allows for the reassortment of gene segments into novel viruses with altered virulence (241-244). Combined with the population size of modern pig farming (60 million in the U.S. alone) and the conditions in which the pigs are kept (i.e., overcrowding), this creates conditions for the emergence of novel IAV variants. An excellent recent example is the March 2009 emergence of a triple reassortant H1N1 IAV in a single pig farm in Mexico (H1N1pdm), which spread globally within three months and eliciting a WHO worldwide pandemic alert by June 2009 (1, 132). There is evidence that this H1 is the ancestor of the 1918 H1N1 virus that has remained in swine reservoirs, and in the years following the 2009 H1N1pdm, a reassortment event with H3N2 viruses have been associated with swine at agricultural fairs in the U.S. (1, 234, 245)

4.5 Human IAV.

Influenza viruses are present year-round in the human population, and the seasonality may be related to cold weather influencing human behavior (*e.g.,* spending winters indoors and increasing transmission rates) and favoring the persistence of the virus on fomites (246). Since the beginning of the 20th century, three main subtype combinations are readily transmitted within the human population: H1N1, H2N2, and H3N2 (122). For most of the last century, a novel antigenic form has displaced the previously circulating forms, *e.g.,* the

15

"Asian flu" H2N2 IAV from 1957 no longer circulates in the human population (122). The

1957 H2N2 IAV was instead replaced by a reassortment event with circulating H3N2 viruses,

which were subsequently related to the cause of the 1968 H3N2 "Hong Kong" IAV pandemic

(122). However the latest 2009 H1N1 failed to displace the seasonal human H3N2, and has

even led to the formation of variant H3N2 IAV, which is a reassortant of the two as a direct

result of mixing in the pig "vessel" (1, 132, 234, 247). Since 2005 other subtypes,

particularly highly pathogenic subtypes, have been transmitted to humans from avian species,

although so far they have resulted in dead ends for the virus (13, 141, 144). In summary,

viral reassortment (antigenic shift) and random mutations under selection the reservoir host

(antigenic drift) account for genetic complexity and adaptability of IAV (238). In the last

100 years, several emergent IAV have been recorded with varying levels of pathogenicity

and transmissibility in humans.

5. Studying pathogenesis of IAV.

5.1 Mouse model of IAV.

Mouse IAV disease. Mouse IAV disease is characterized by increased infection of the

respiratory epithelium (55, 248, 249) (Figure 1.4). This is often dose-dependent, and viral

replication is typically in both the URT and the LRT (reviewed in (248, 249)).

Histopathologic findings after mouse intranasal IAV infection include pneumonia, alveolar

edema, and mixed inflammatory infiltrates (248, 249). Infection of the LRT is not always

fatal in mice, although the severity of disease in mice is difficult to assess. Signs of severe

disease in mice include: hypothermia (as opposed to fever in humans), lethargy, hunched

posture, ruffed fur, dehydration, and weight loss, the latter of which is typically used as a

humane endpoint (248, 249). Mouse respiratory epithelial cells display mainly alpha 2,3-linked SAs, and viruses with increased binding affinity to this receptor are known to replicate to a higher titer in mice which may result in a lethal disease (50, 230, 247). Human isolates (*e.g.*, seasonal IAV) do not replicate well in mouse lungs and cause minimal disease, however 1918 H1N1 IAV ("Spanish" flu) and avian IAV both infect mouse lungs to high titer and systemic spread of viral infection is frequently noted (50, 55, 118, 250-254). This may be due to receptor binding affinity of the HA, as well as the presence of a multi-basic HA cleavage site in avian IAV (253-255). As discussed below, the innate immune system of mice has many similarities to humans.

Benefits and limitations of mice in IAV research. Mice are the most frequently used experimental animal model in modern biological laboratories, and in IAV research. (49, 50, 248, 249, 256, 257)(Figure 1.4) Genetically, laboratory mice are well-defined, homogeneous, and capable of experimental manipulation (*i.e.*, transgenic mice). Housing and husbandry costs are relatively low which allows for a comfortable level of statistical replication in experiments. Reagents and tools are commercially readily available for mice, which are important for studying the immune system. However mice are not natural hosts of IAV infection, and their lung anatomy, including the frequency and distribution of IAV receptors within the respiratory tract, is different compared to humans (49, 50, 248, 249, 256, 257). Mice are capable of becoming infected with certain IAV and may develop lower respiratory disease that has similarities to human influenza disease in a general sense (i.e., a viral inflammatory immune response and the development of specific adaptive immunity) (49, 50, 248, 249, 256, 257). The pathogenicity of a given IAV isolate (e.g., human or avian) is variable between mouse strains, and does not always match human disease susceptibility (250, 258). The most well-studied host factor that contributes to increased pathology in mice

is the lack of a functional Mx1 gene (an ISG) in certain laboratory mouse strains (259-262).

To overcome these limitations to studying IAV pathogenesis, strains of IAV may evolved to

increased pathogenicity upon experimental passage through mice (49, 50, 248, 249, 256,

257).

5.2 Ferret model of IAV.

Ferret IAV disease. Ferrets are considered the best laboratory animal model for human IAV

pathogenesis and transmission (47, 49, 50, 249, 256, 257, 263-266). They have a similar

anatomy and physiology of the respiratory tract as compared to humans, including SA

receptor frequency and distribution (267, 268) (Figure 1.4). They can be infected with

human isolates of IAV without adaptation, and they are, themselves, natural hosts of IAV

with human-like SA linkages (267, 268). Ferrets display signs of disease following infection

that are very similar to humans, including fever, malaise, rhinorrhea, sneezing, dyspnea, and

inappetence (47, 49, 50, 249, 256, 257, 263-266). Pathology from experimental IAV

infection of ferrets may match human IAV pathology depending on IAV strain, specifically

URT disease (71, 102, 103, 269) and bronchointerstitial pneumonia (related to human diffuse

alveolar damage), although the latter is not as common as expected, possibly due to the

practice of inoculating with an intranasal bolus (48, 270-272). Similar to human cases,

infection with avian IAV causes infection of the LRT, and pathology shows severe

pneumonia, inflammatory infiltrates of the lung, blood neutrophilia and leukopenia (56, 266).

However ferrets display distinct neurological symptoms after infection with avian H5N1

IAV, a feature that was not common during human outbreaks (56, 273, 274). Importantly,

viral traits that are associated with increased pathogenicity in humans are thought to be

similar in ferrets: for example, viral receptor affinity that affects infection of the LRT verses

URT, increased polymerase activity, and to viral mechanisms of immune modulation (e.g., type I IFN suppression by viral NS1A) (56, 69, 89, 91, 275, 276). The ferret model is an enormous benefit for evaluating novel IAV for pandemic potential, measuring aspects of both transmission and pathogenicity, as well as testing vaccines and therapeutics for human use.

Benefits and limitations of ferrets in IAV research. Although ferrets are an excellent model for studying transmission and pathogenicity of IAV, and despite their use in IAV research for 80 years, the ferret model is poorly characterized compared to the mouse (47, 48, 148, 249, 264). The complete genome and transcriptome of the domestic ferret have been completed and published only very recently (277, 278). Laboratory ferrets are outbred and are therefore genetically diverse. In addition, there are very few ferret-specific tools and reagents commercially available, and these are poorly validated (279, 280). As a result, aspects of the ferret immune system remain unknown with respect to specific similarities/differences to the human immune (compared to the mouse, about which much more is known). Ferrets require special handling, housing and care, they are expensive and they are considerably larger than mice (47, 48, 264). This has the effect of reducing experimental sample size and, ultimately, reducing the statistical power achieved with many ferret studies. Perhaps for these reasons there is still variation in the experimental methods employed in IAV studies using ferrets (*e.g.*, inoculation volume, sex, and age are not standardized), and clinical endpoints continue to become better defined (263, 265, 266, 272). Finally, many commercial vendors do not house ferrets in barrier facilities and it is possible, and very likely, that many research ferrets are not naïve to influenza infection.

6. Viral determinants of increased pathogenicity.

6.1 HA tropism and cleavage.

Sialic acid receptor binding. As discussed above, variation in viral HA leads to changes in amino acid constellations that affect receptor binding preference. This leads to increased efficiency of infection within a given host taxon. Just as different species have different frequencies of SA linkages, epithelial cell types within a given host various have different frequencies of certain SA linkages. The central dogma of the increased pathogenicity of avian IAV in humans has been that a preference of avian IAV for alpha 2,3-linked SAs enables the virus to replicate in the lower respiratory tract (52, 88, 231, 281, 282). IAV that cause severe pneumonia, such as H1N1pdm and 1918 H1N1 have an increased ability to bind to alpha 2,3-linked SAs, whereas mild seasonal IAV and H1N1pdm viruses with low pathogenicity have binding affinities to alpha 2,6-linked SA (88, 116, 282-284) (Figure 1.1). Further support of the link between receptor specificity and disease in a natural system came in 2013, where emergent avian H7N9 IAV had dual receptor specificity and caused viral pneumonia and ARDS, and not hypercytokinemia (145). The fact that H5 does not bind alpha 2,6-linked SA may be tied to the unique pathogenicity of avian H5N1 IAV, a disease marked by hypercytokinemia (88, 94, 145, 282) (Figure 1.1).

HA determines site of infection. The human URT and most of the LRT contain alpha 2,6-linked SAs, whereas the alveolar epithelium, submucosal epithelium, and alveolar macrophages contain mostly alpha 2,3-linked SAs (228, 229, 282). It is not known how avian H5N1 IAV is able to bypass the anatomical and chemical defenses of the URT to begin infection of the LRT, however ferret aerosol inoculation suggests IAV can be deposited in

the LRT (285). On the contrary, it has been shown that if H1N1pdm viruses are manipulated to have altered tropism to alpha 2,6- or alpha 2,3-linked SAs, this has no major effect in pathogenicity in ferrets (116). Therefore, properties of these viruses other than HA binding affinity (*e.g.,* binding avidity of HA or contributions of other gene segments) cannot be ignored. In summary, replication in the URT may progress to pneumonia and ARDS if viral HA allows LRT replication; but replication in the LRT, alone and without URT involvement, is linked to a disease characterized by hypercytokinemia. Likewise, it is clear that HA receptor affinity is important for transmission of avian IAV to mammals and between mammals, and is therefore an important not only as a virulence but also for pandemic potential.

HA maturation and cleavage. Other features of the HA that are related to increased pathogenicity are related to viral entry and membrane fusion. The immature HA requires cleavage by host proteases so that fusion can occur during the reduced pH of the endosome (177, 179, 181).   A feature of the HA of HPAI, compared to LPAI, is the presence of a polybasic cleavage site (177-180, 286). The polybasic cleavage site allows for cleavage by the ubiquitous protease furin, which makes it possible for the virus to replication in many mammalian tissues (178, 181). Additionally, it was recently observed that some H1N1pdm isolates carried a mutation that altered their specific pH of fusion (287). HA typically fuses within the late endosome at pH 5.5, and specific amino acid mutations that stabilize the pre-fusion complex may reduce the pH of fusion (172, 174, 287-290). This may change the endosomal compartment where IAV undergoes fusion, although the ultimate effects of this are unknown.

6.2 Replication in mammalian cells.

The rate of viral replication in the host cell is dependent upon the RDRP. Host adaptation has shaped a key residue in the polymerase subunit, PB2, which allows increased RDRP activity in either mammalian or avian cells (275, 291-296). Avian IAV adapted to human cells (E627K) have a distinct increase in RDRP activity at 33°C, the temperature of the human respiratory tract, whereas a glutamate at the site has a maximum RDRP activity at 42°C (296, 297). Similar to the viral properties bestowed by HA, this alteration is important for pathogenicity as well as the transmission and pandemic potential of avian IAV in mammals.

6.3 NS1A and IFN.

Many viruses have evolved strategies to counteract an efficient host response to infection, which almost unanimously includes the ability to interrupt the type I IFN system (66-68). IAV accomplishes this through NS1A, a non-structural protein that is involved in direct and indirect disruption of the type I IFN response system (198, 298). Using reverse genetics techniques, IAV lacking NS1A functionality or lacking NS1A altogether can be made and can infect cells (299). However, these viruses are very sensitive to cellular type I IFN stimulation, and cells infected with these viruses produce much more type I IFN than cells infected with wild-type IAV (299-301). Through studies with these viruses, it has been shown that NS1A masks cytoplasmic viral nucleic acids by interacting with dsRNA molecules (299-301). This effectively hides (sequesters) dsRNA from cytoplasmic PRRs such as 2'5'oligoadenylate synthase (OAS)-RNaseL, protein kinase R (PKR), and the RLR

family of helicases (such as RIG-I and MDA5). The binding of cytoplasmic viral dsRNA by RIG-I or MDA5 begins downstream transcriptional activation of type I IFN (299-301). In addition, NS1A may also bind these host cell factors, either directly or via co-binding to dsRNA, to inhibit the translation of host cell mRNA to counteract establishment of an anti-viral state (198, 302). The interactions of NS1A are an illustration of IAV as a master at effecting an acceptable and necessary level of inflammation and cellular activation (291, 303-305), and the pathogenicity of some isolates may result from an inability of IAV to manage the balance between cell activation and immune suppression (199, 306). For example, delay of type I IFN signaling via NS1 mediated increased virulence in ferrets (69). In this scenario, inflammation (*e.g.*, NFkB-mediated effectors) would result in leukocytic infiltration without the appropriate information (*i.e.*, type I IFN) to generate a "correct" anti-viral response (65, 69, 70, 300, 301, 307). Powerful effector cells like neutrophils may respond inappropriately, and begin a cascade of immune dysregulation (70, 71, 301).

7. Immune response to IAV infection

7.1 Site of infection.

IAV infects and replicates in epithelial cells of the respiratory mucosa (151). The human respiratory system is divided functionally and anatomically into URT and LRT at the larynx, by convention. The function of the respiratory system is to facilitate gas exchange between the host blood and the atmosphere. The LRT is the primary site of gas exchange, and it is highly sensitive to (and highly protected from) inflammation. The URT serves as a mechanical and chemical barrier, protecting the sensitive LRT from infection and debris.

The upper respiratory tract. The URT is made up of the nasal cavity, the sinuses, and the

pharynx (often the laryngopharynx and larynx are included in the URT). The nasal cavity

and nasopharynx are lined with a pseudostratified columnar epithelium which contains both

ciliated and non-ciliated cells. Anatomical barriers in the URT include the vibrissae and

nasal turbinates (conchae) which block large particles and vortex air to remove smaller

particulate matter. During this process the air is warmed and humidified, and receptors

transmit chemical information to the brain via the olfactory nerves. Particulates which

become trapped in the mucous of the URT are moved up and out of the URT via beating of

the ciliated epithelial cells, rhinorrhea and sneezing. The nasal turbinates are heavily

vascularized, and during inflammation may be the site of extreme leukocytic infiltration.

Neutrophils, mast cells, and eosinophils contribute to both allergic and infectious

inflammation which leads to rhinitis and associated symptoms (especially rhinorrhea).

The lower respiratory tract. The LRT begins below the larynx, and includes the trachea and

main bronchus. These structures are supported by cartilage, and the mucosal barrier consists

of a thick layer of a psuedostratified, ciliated, columnar epithelium with non-ciliated

columnar and basal cells (Figure 1.5). Fibroblasts and antigen presenting cells are found in

the lamina propria, which is supported by a submucosa that is thick with connective tissue.

Specialized non-ciliated cells, goblet and/or clara cells, are vacuolated secretory cells within

the epithelial layer which contribute primary chemical defenses to the respiratory mucosae in

the form of mucous containing defensins and other innate immune effector proteins (Figure

1.5). Similarly, invaginations of the bronchial epithelium which extend into the submucosae

contain patches of additional specialized secretory epithelial cells, the seromucinous (or

submucosal) glands (Figure 1.5). They also contribute to the mucosal lining which protects

the epithelium and is the vehicle of the mucociliary elevator. These features of the URT and

the upper portion of the LRT appear to exist solely to protect the sensitive alveolar spaces below.

Beginning with the branching of the trachea into the main bronchi, the LRT (the lung, proper) is divided into lobes fed by branches of the bronchi which split into smaller bronchioles and even smaller alveoli. This arrangement creates an enormous surface area in a minimal volume. The alveoli are arranged in acini and are composed of two types "alveolar" epithelial cells: the thin type I pneumocytes at the air/water interface and the cuboidal type II pneumocytes that secrete surfactant lipids and proteins ("I" and "II" in Figure 1.5). Associated with the bronchioles are pulmonary blood vessels which branch into smaller capillaries that cover the alveolar clusters as the lung microvasculature. The individual capillaries are typically composed of a single cell of endothelium creating a tube that is thinner than a single red blood cell. The thin capillaries and thin type I pneumocytes facilitate the efficient transport of gases between the blood and air. The barriers to infection and debris in the alveoli consist of surfactant proteins and patrolling alveolar macrophages. Surfactant proteins help buffer the surface tension of the mucosal lipid layer to prevent the collapse of the alveoli. Surfactant protein-A and surfactant protein-D are lectins (specifically they are C-type lectins, collectins, that resemble C1q complement protein) that opsonize certain viruses for phagocytosis by alveolar macrophages, including IAV (reviewed in (308)).

Alveolar macrophages. Alveolar macrophages are resident phagocytic myeloid cells within the lungs, and are the most abundant immune cells in the lung, comprising over 90% of cells in lung lavage fluid (reviewed in (309, 310)). Alveolar macrophages perform anti-inflammatory functions during homeostasis, and their capacity as phagocytic cells constantly

clears debris from the sensitive alveoli . Despite extensive anatomical and chemical barriers, the alveoli inevitably receive both harmful and harmless antigens (311). Alveolar macrophages rely on immune "ignorance" to maintain homeostasis, and suppress dendritic cell and T cell activation via secretion of IL-10, TGFb, and/or NO *in vitro* (311, 312). Phenotypically alveolar macrophages are similar to dendritic cells, and they perform similar functions by constantly sampling the alveolar microenvironment for antigens and PAMPs (313). For the most part they are self-renewing cells, but they can be replaced by bone marrow-derived monocytes upon depletion (314, 315). They are in constant contact with the pneumocytes, and this provides essential feedback for both cells in the form of CD200/CD200R which maintains an anti-inflammatory state (316-318). As discussed below, they are the "keystone" cells in the lung, and they have important functions in modulating inflammation, cell death, and regeneration in the sensitive LRT (313, 319-323).

7.2 Cellular response to IAV infection.

The initial universal response to the detection of viral PAMPs is the secretion of type I IFN (reviewed in (66, 68)). The release of type I IFN triggers interferon receptor pathways which activate transcriptional regulators to initiate production of ISGs via JAK-STAT signaling (reviewed in (324)). This operates in an autocrine and paracrine manner in an effort to stop the infection process and prevent neighboring cells from becoming infected. The ISGs include pro-inflammatory cytokines and chemokines such as type I IFN, CXCL1 and CXCL10, as well as cytoplasmic anti-viral proteins such as Mx1, OAS, RNaseL, and PKR (reviewed in (325)). Similarly, these initiate well-studied inflammatory systems, such as activation of the transcriptional regulator NF-kappaB, to release other cytokines and chemokines, such as IL-6, CCL2, and CXCL8. The net effect on cells is an increased ability

to detect to viral PAMPs, a blockade on cytoplasmic translation, the initiation of apoptosis, the display of viral epitopes on major histocompatibility complexes, and pro-inflammatory signaling to alert neighboring cells and recruit inflammatory cells. IAV has mechanisms to buffer the activation of these cascades via NS1A-mediated suppression of type I IFN translation or anti-apoptosis via PB1-F2 (196-198, 300, 301).

7.3 Epithelial cell response to infection.

In the URT, IAV infects epithelial cells. Non-immune cells (non-myeloid) have cellular sensors of viruses that rely on detection of viral nucleic acids, and mammalian immune systems rely chiefly on the presence of dsRNA in the cytoplasm to recognize these viruses (326, 327). Double-stranded RNA is a common intermediate to the replicative cycles of both RNA and DNA viruses. RLRs are cytosolic helicases, such as RIG-I or MDA-5, which recognize dsRNA (327, 328). These activate pathways leading to transcription factors that initiate type I IFN secretion from the cell (Figure 1.6). Similarly, PKR is capable of recognizing and responding to viral dsRNA after activation via type I IFN signaling. TLRs (for detecting PAMPs in the extracellular and endosomal spaces) are typically not as abundant in epithelial cells as they are in myeloid cells (326, 327, 329).

In vitro infection of well-differentiated human primary respiratory epithelial cell culture systems and primary lung explants allows the study of the interaction between IAV and epithelial cells without confounding comorbidities in human patients (75, 330-334). In addition, this allows side-by-side comparison of various IAV isolates in the same human genetic background. Infection of these cultures with many IAV isolates causes the

production of type I IFN, IL-6, CCL2, and CXCL8, indicating that the epithelial cells contribute to the immune response, specifically by recruiting leukocytes to the site of infection (331, 334-338). There are differences between the response to infection with seasonal, H1N1pdm, and HPAI viruses; for example, seasonal IAV infection causes increase in the cytokines mentioned above, indicating that H1N1pdm viruses may be suppressing the immune response of these cells (viral titers were similar) (331, 334) and there is indication that this is strain-specific (331, 333, 335, 336). Interestingly, this was only true for apical secretion of cytokines and chemokines from these cells – we have shown that H1N1pdm viruses have increased basal secretion of cytokines and chemokines, such as IL6, CXCL8, CCL2, CCL4, and CCL5, from IAV-infected well-differentiated normal human bronchial epithelial cells grown in collagen-coated inserts (331). Moreover, infection of human epithelial cells with H5N1 viruses causes a comparatively higher level of IL6, CXCL8, CXCL10, TNFa, and CCL5 secretion in side-by-side studies (332, 334). Heat-inactivated virions (i.e., fusion-competent but non-replicating) were sufficient to activate human neutrophil chemoattractant gene signatures, such as CXCL1 and CXCL8 (333). Finally, necrotic epithelial cells are typical of severe influenza infection, and these cells provide a source of immune signals, as they release CXCL8 upon death (338).

7.4 Alveolar macrophages shape the viral microenvironment.

Alveolar macrophages play an important role in contributing to and limiting inflammation from epithelial cells and infiltrating macrophages during infection with IAV. In mice, depletion of alveolar macrophages prior to IAV infection results increased viral replication in the lungs, increased cytokine and chemokine production in the lungs, increased neutrophil infiltration, and increased lung pathology (322, 323, 339). Unlike epithelial cells, *in vitro*

experiments using human alveolar macrophages show that they release a wide variety of cytokine, chemokines, lipid mediators, and ROS into the environment upon sensing virus or via cytokine/chemokine receptors (75, 340-342). While pneumocytes are capable of immune signaling and release of cytokines following IAV infection, alveolar macrophages are the cells that shape the early lung microenvironment following IAV infection, and determine the pattern infiltration of leukocytes to the lung (61, 320-322, 337, 343-345).

Disrupting homeostasis. Upon introduction of IAV into the alveolar space, the alveolar space contains virus, pulmonary surfactant, and alveolar macrophages (Figure 1.5). Upon infection of either the epithelium or the alveolar macrophage, homeostatic cross-talk between alveolar macrophages and epithelial cells (e.g., CD200/CD200R) may become temporarily disrupted as type I IFN is released into the alveolus (316, 346). An important consequence of type I IFN in the alveoli is the triggered apoptosis of infected epithelial cells by activated macrophages via death receptors (65, 343, 344, 347, 348). Additionally, infection with IAV causes increased apoptosis and necrosis in epithelial cells and in monocytes without addition aid of death receptor ligation (202, 251, 334, 349-352). Desquamation of alveolar epithelium is characteristic of ARDS; on histological preparations from severe human cases the alveolar epithelium is replaced by an eosinophilic hyaline membrane (6-8).

Infection of alveolar macrophages and sensing IAV. *In vitro* studies using mouse (73, 353) and human alveolar macrophages (75, 341, 342) show that infection is abortive, suggesting that alveolar macrophages are not contributing to increased virus in the lung during infection. In mice, infection with a pathogenic IAV causes a necrotic depletion of alveolar

29

macrophages, which can be rescued by administering GM-CSF (313, 354). However, abortive infection is critical for sensing infection by activating virus-specific PRR and initiating adaptive immunity via MHC-I presentation on antigen presenting cells (355, 356). Detection of pathogens via TLR signaling relies heavily on myeloid cells, such as plasmacytoid DCs and alveolar macrophages (326, 357, 358), and detection of IAV relies heavily on RIG-I signaling (327). Both of which lead to induction of the type I IFN system and provides a crucial link with the innate and adaptive immune systems (67, 329, 348). Although there is an established trend that IAV with increased pathogenicity stimulate a decreased inflammatory response from alveolar macrophages *in vitro* (74, 340, 341, 359), to my knowledge no studies have investigated the effects on the normal anti-inflammatory functions of alveolar macrophages during IAV infection (*e.g.,* TGFb secretion).

7.5 Systemic inflammation.

As the local inflammatory environment grows, macrophages and endothelial cells amplify and transmit the inflammation systemically in the form of chemokines, pyrogenic cytokines, and growth-stimulating factors (360) (Figure 1.6). Chemokines recruit innate immune cells to the site of infection (reviewed in (361)). Following infection, cells such as natural killer cells (NK), inflammatory monocytes and macrophages, as well as neutrophils infiltrate the airways from peripheral blood circulation (70, 253, 360, 362, 363). As discussed below, these cells become activated while in the peripheral blood circulation, continue to activate during migration to the site of inflammation, and then perform effector functions to at the site of inflammation in response to the microenvironment. The activation of the innate immune response is immediate and acute, whereas the adaptive immune system requires time but is more specific. In the following, the role of specific early innate immune cells are discussed.

30

NK cells. In the context of viral infection, NK cells recognize "missing self" and the presentation of death receptors to destroy infected epithelial cells. Interestingly, mammalian NK cells are known to contain cell surface proteins, NKp46 and NKp44 in humans (NCR1 in mice and ferrets), which activates the cell upon recognition of IAV HA (364-367). IAV seems to have NK evasion strategies that include direct infection of NK cells as well as increasing the display of NK cell-inhibiting ligands on infected cells (368). Even so, NK cells seem to be dispensable for the response to influenza, and patients lacking NK cells recover fully from IAV infection (369, 370). In animal models, NK cells are essential for clearing viral infection, and they accomplish this by contributing to the generation of a robust adaptive immune response (*i.e.*, Th1), potentially through the release of massive amounts of IFNg (367, 371, 372).

Inflammatory Monocytes and Macrophages. Macrophages are terminally differentiated cells present in tissues (315). During inflammation their precursors (monocytes) are recruited from the peripheral blood circulation and the bone marrow to the site of infection to differentiate in response to *in situ* signals (reviewed in (309)). These signals may polarize these cells to differentiate towards various phenotypes, some of which have pro-inflammatory features and some have anti-inflammatory functions to various degrees (373). Infiltrating inflammatory monocytes and macrophages have a different phenotype than alveolar macrophages, and have different susceptibilities to infection by IAV (359, 374, 375). Depending on the *in vitro* preparation of macrophages and the viral strains used, their importance in IAV disease is still uncertain. However, in general it seems that infiltrating monocytes and macrophages have a clear pro-inflammatory response to IAV infection (72,

31

351, 376-378). In a CCR2$^{-/-}$ mouse model of IAV, even a minor delay in infiltrating

macrophages drastically increases the influx of neutrophils into the lung by exacerbating the

CXCL1/CXCL2 response (379). Macrophages are the main producers of CXCL9 and IFNb

(380) following mouse IAV infection. An interesting experiment used intraperitoneal

injection of IAV to show that infection of inflammatory macrophages by IAV stimulates an

immune response *in vivo* without contribution of epithelial cells (375).

Neutrophils. Neutrophils are another subset of phagocytic myeloid cells, and exist in steady-

state as mature, terminally differentiated cells. They are well known to be associated with

acute lung injury and inflammation in the lungs, and are typically among the first immune

cells to arrive during many types of infection and inflammation (16, 18, 381). They are well-

studied with respect to bacterial infection, although their role in viral infection is not clear.

Neutrophils are present during acute phases of IAV infection of both the URT and LRT, as

well as during infection with other respiratory viruses (343). A common feature of the

immune response to pathogenic influenza viruses in human and animal models is an

excessive infiltration of neutrophils into the LRT (70, 85, 86, 253, 323). However,

experimental depletion of neutrophils prior to infection with IAV leads to increased lung

pathology, increased inflammatory cytokines and chemokines in the lung, and increased virus

replication (84, 86). Neutrophil activation and their migration to the lungs are steps that are

critical to recovery from IAV infection (26, 78-80, 83, 84, 86, 323). Neutrophils are short-

lived during inflammation, and contribute significantly to the cellular debris that accumulates

in the lung during infection, although they are capable of phagocytosis of IAV-infected

epithelial cells (79). There is very little known about neutrophils in the context of viral

infection. In the next section, the possible roles for neutrophils in IAV disease will be discussed in detail.

8. Neutrophils in IAV infection

Neutrophils are increased in the lungs and blood after infection with pathogenic IAV in mice, humans, and ferrets (294, 363, 382). Neutrophils are necessary for recovery from severe, but not mild, IAV infection (86, 381). Studies in mice show that neutrophils have effects during both early and late stages of disease (85). Signals from both alveolar macrophages and macrophages initiate neutrophil chemotaxis and activation to the lungs. For example, TLR7 recognition of IAV dsRNA and Myd88-mediated release of TNFa and CCL3 by mononuclear cells is important for neutrophil recruitment to the site of infection (383, 384). Interestingly, TLR3^{-/-} mice have increased neutrophilia and fewer macrophages in the lungs, yet have increased survival after infection with IAV (385, 386). In cell co-culture, human neutrophils were seen to interact specifically with IAV-infected cells (387), although the nature of this interaction in the infected lung is unknown. Transgenic mice have been used to study the contribution of specific cytokines and chemokines to inflammation following IAV infection, particularly as this relates to "hypercytokinemia", and are summarized in Tables 1.1-1.4. The signals from the infected lung are propagated systemically by endothelial cells, which recruit and tether neutrophils. The complex interactions governing neutrophil extravasation, migration through the interstitium, and crossing the alveolar epithelium are well known in relation to many forms of ALI and the development of ARDS with the exception of conditions surrounding viral infection (16-18, 20, 388, 389). Due to the mechanical

stimulation of passing through the small diameter of the microvasculature of the lung, neutrophils in the lung are more activated than peripheral neutrophils (17).

8.1 Neutrophil migration.

Neutrophil chemotaxis in humans is thought to be mediated by many factors, such as the chemokine CXCL8, cytokines IL-1 and TNFa, and complement C5a (388, 390, 391). During both mild and severe IAV disease, patients show increased blood CRP and activation of C5a (392), as well as increased secretion of CXCL8, TNFa, and IL-1 in nasal washes which correlate with disease severity (99, 101, 105, 393-395). Studies using mice have offered insight into the relationships between inflammation and neutrophil chemoattraction during influenza infection. For example, chemical reduction of C5a during IAV infection reduced lung neutrophilia (396). Similarly, cytokines such as IL-1b and IL-6 are important for neutrophil activation and migration to the lungs during mouse IAV infection (Table 1.1) (397-399). Mice do not possess CXCL8, but CXCL1 and CXCL2 have equivalent functions. Neutrophils contribute CXCL2 to the IAV-infected mouse lung to further stimulate neutrophil recruitment (380). More recently it was shown that removing a CXCL1 repressor (*Setdb2*) does not increase recruitment of neutrophils to the lungs of mice infected with IAV PR8, rather it reduces the ability to respond to bacterial superinfection (400). In addition, it was shown that another ISG, CXCL10, operates on a unique subset of CXCR3+ neutrophils present during mouse IAV infection in an autocrine manner, increasing chemotaxis, oxidative burst and enhancing inflammation (380) (Tables 1.3 and 1.4). Finally, aryl hydrocarbon receptor is somehow linked to increases in NO and neutrophilia in the lungs of IAV-infected mice independently of known neutrophil chemoattractants or mechanisms of neutrophil extravasation (401-404).

8.2 Neutrophil extracellular PRRs and phagocytosis.

Neutrophils are phagocytic cells, and their methods for sensing extracellular pathogens relies on TLRs (390). Stimulation of neutrophils through TLRs has been recorded to promote cytokine secretion (CXCL8 and TNFa via NFkB and AP-1), ROS formation, phagocytosis, granule secretion, NET formation, and migration (388, 390, 391). Human neutrophils highly express nucleic acid-detecting TLRs, specifically endosomal TLR8 (405, 406), but do not express nor respond to activators of TLR3 or TLR7 (82, 405, 406). TLR4 is required for LPS-induced neutrophil migration to the lung (407); however, TLR4-stimulation does not lead to the production of type I IFN in neutrophils (82, 408). Surfactant protein D, a lung collectin, is an innate immune defense against a variety of viruses, which marks them for phagocytosis by neutrophils which cause the production of ROS (409-415). Human neutrophil defensins are short basic peptides released from neutrophil granules during inflammation (388, 415, 416). They have been shown to interact with IAV, reducing infectivity, and promote neutrophil phagocytosis and clearance of IAV (415-419). Defensins may also buffer the oxidative burst from neutrophils that follows from phagocytosis of viruses that have been opsonized by surfactant protein D (415-417). One study indicated that neutrophils do not interact with immunoglobulin-bound IAV (420), however another showed that protective anti-IAV antibody therapy only protected mice in the presence of neutrophils (78).

8.3 Neutrophil intracellular PRRs.

Neutrophils express sialic acid receptors and may become infected with IAV (26, 421, 422). Neutrophils infected with IAV have increased apoptosis, but infection does not result in the

production of virus (422). Infection of human neutrophils with IAV treated at 56°C to denature the viral replicase but not HA suggested that infection alone, but not replication, is sufficient to stimulate the release of CXCL8 and CCL4 in human neutrophils (423). Neutrophils infected with IAV have rapid up-regulation (<9 hpi) of type I IFN pathways, including cytoplasmic PRRs, IFNb, and ISGs (422), which is counter to the long-held dogma that neutrophils were incapable of gene expression. This is may be due to RLR sensing of viral dsRNA, as neutrophils transfected with poly(I:C) (a viral RNA mimic) have a similar response (82). Additionally, neutrophils express nod-like receptors (NLRs) but it is unclear how these interact with IAV infection (424, 425). In general, inflammasome and pro-IL1 activation following IAV infection is poorly understood (307, 397, 398, 426). However, studies of IAV infection using caspase-1, IL-1b, or IL-1R transgenic mice show modulation of neutrophil infiltration and pathology, and suggest that it is an IAV subtype-dependent effect (397, 426-430) (Tables 1.1 and 1.2). Furthermore, it has been demonstrated that the HA of some IAV isolates suppresses neutrophil activation, providing further evidence for IAV subtype-dependent effects on neutrophils (421, 422, 431).

8.4 Neutrophil activation and degranulation.

Activation of TLRs and RLRs trigger degranulation and the upregulation of CD11b (82), which pairs with CD18 to form the "Mac-1" integrin dimer that binds collagen (432). This facilitates migration through tissues, and release of gelatinase or collagenase (MMP-2 and MMP-9) from neutrophils assist in clearing connective tissue from the path. At the site of infection, neutrophils release microbial effectors (reviewed in (81, 388)). Neutrophils develop granules sequentially (azurophilic, specific, gelatinase, secretory) and secrete granules in the reverse order (388). Secretory and gelatinase granules are released shortly

after endothelial transmigration and contain membrane proteins essential for movement (extracellular matrix [ECM]-binding integrins) and pathogen recognition (immunoglobulin [FcR] and complement receptors) (388). Specific and azurophilic granules contain tissue-destroying enzymes and anti-microbial proteins. For example, neutrophil MPO may contribute to lung injury during IAV infection (77), however it may have direct antiviral effects on IAV (433). An investigation found no difference between IAV infection of a wild-type and neutrophil elastase knockout mouse, measuring lung function, chemokine secretion, and neutrophil recruitment (434) (Table 1.5). The contents of the granules can be secreted to destroy ECM (such as MMP-9) or directed towards phagosomes to destroy engulfed microbes. The production of hypochlorous acid (HOCl) is the main oxidant used in phagosomal killing, and its production is dependent on the generation of reactive oxygen by the neutrophils. Interestingly, infection by IAV was related to the inhibition of phagosomal killing of bacteria (431).

8.6 Oxidative burst.

Neutrophil degranulation primes neutrophils for ROS generation by mobilizing NADPH oxidase components to the plasma membrane (388) and exocytosis of MPO. IAV infection causes the generation of reactive oxygen species in neutrophils (435). Oxidative burst is thought to have direct microbial effects, however the direct effect on IAV has not been published (436). IAV infection benefits from the presence of ROS in the environment (437, 438), yet IAV also suppresses NADPH oxidase activity within infected phagocytes (439, 440). Many have investigated the effects of ROS and NO on lung inflammation during IAV infection and found that reduction of oxidative stress in the form of both ROS and NO alieves IAV-dependent lung injury (439, 441-446) (Table 1.5). For example, oxidized lipids in the

lung environment may trigger TLR4, activating immune cells and contributing to increased lung injury (447-449).

8.7 Neutrophil netosis.

Neutrophils undergo a form of programmed cell death called netosis, in which NETs are formed (450). NETs have the effect of killing many pathogens, including bacteria (389), fungi (451), and protozoans (452). NETs are becoming the focus of study in autoimmune disease atherosclerosis, since they damage endothelium (453-455). Recently, it was shown that hantavirus stimulates NET production during infection which leads to the generation of autoantibodies and may provide a mechanism for the hemorrhagic fever caused by Old World hantaviruses (456). NETs are typically found with histones, MPO, and neutrophil elastase, and the effect is to isolate the effects of these molecules directly onto the pathogen surface with a "sticky" NET of nucleic acid. NETs contribute to acute lung injury and alveolar capillary damage during IAV infection (381). Yet very little is known about the relationship between NETs and viral infection in viral disease pathogenesis (457).

8.8 Contribution to the viral microenvironment.

Resolving inflammation. At some point, neutrophil infiltration into the lung must stop, and increased neutrophils are present in lethal cases of ARDS. This may be regulated by secretion of IL-1RA and chemokine-destroying factors by recruited macrophages (373, 458). Additionally, it has been proposed that efferocytosis of apoptotic neutrophils is a key step in resolution of inflammation (459-461), and occurs in the lung during bacterial pneumonia (462). It is unclear if this happens during IAV infection. Finally neutrophils act as antigen

presenting cells during IAV infection of mice and enhance cytotoxic T cell responses (26, 83), contributing to resolution via the production of an adaptive immune response.

Prolonging inflammation. Factors that prolong the life span of neutrophils in the lungs increase the probability that they may contribute to immunopathology. IL-6 and G-CSF are immune mediators present in the lung during infection and are known to prolong survival of neutrophils in mouse lungs following IAV infection (463). Both neutrophils and macrophages are known to phagocytose apoptotic epithelial cells in mouse lungs during IAV infection (79). The cells may be recruited via chemokines or damage receptors. For example, necrotic IAV-infected epithelial cells are a source of CXCL8 (338), which attract neutrophils to dying cells. In addition, neutrophils can detect DAMPs such as S100A9 (464). It has been shown that extracellular S100A9 is abundant during IAV infection in mice (465). Antibody-mediated neutralization of S100A9 decreased lung inflammation in mice and improved disease outcome (465). Apart from potential tissue-destroying effects of neutrophil proteases, the presence of NETs may induce even more inflammation in the lungs (80, 381). Thus, there are limited data supporting directly malevolent actions of neutrophils (Table 1.5), yet factors that increase their presence and prolong their survival in the lung are correlated with increased disease severity.

9. Neutrophils in viral respiratory disease

There appears to be a correlation between IAV infection and neutrophils, but this may not be a causal relationship. In bacterial pneumonia, there is direct evidence of the importance of neutrophils in disease: bacterial PAMPs upregulate neutrophil activating and chemoattractant chemokines, bacteria have defined anti-neutrophil functions, and some bacteria, *e.g.,*

39

Mycobacterium tuberculosis, rely on neutrophils to establish their granulomatous niche (19, 466, 467). Similarly, in ARDS there are data that directly support the role of neutrophils as both beneficial and detrimental (16, 57, 58). To substantiate a link between neutrophils and IAV, evidence for the role of neutrophils in viral respiratory disease is briefly reviewed below. Although scarce, evidence presented here relies heavily on prospective clinical data as well as pathological reports from human cases of respiratory infection of confirmed viral and bacterial etiologies. Specific animal models are not considered here due to differences in the types of cells called neutrophils between species, as well as limitations in animal models to directly recapitulate human disease from these specific pathogens.

For both viral and bacterial etiologies, the most severe clinical complications result from infection of the LRT. Infection of the LRT by viruses such as human parainfluenza viruses, H1N1pdm, HPAI, New World hantavirus infections (causing hantavirus pulmonary syndrome), *Severe acute respiratory syndrome-related coronavirus* (SARS-Cov), and Middle East respiratory syndrome coronavirus (MERS-CoV) may develop into ARDS (22, 23, 51, 63, 143, 468-470). Clinically defined, ARDS has three phases; and most patents die within the first phase, the acute or "exudative" phase (reviewed in (25, 57, 58)). This phase is characterized by an increased immune response with high production of pro-inflammatory cytokines and chemokines, increased neutrophil infiltration and accumulation in the alveoli, and disruption of the alveolar epithelial-capillary barrier, which leads to increased vascular permeability and edema (57). The distinctive role for lung neutrophil infiltration in viral infection is summarized as follows: some, but not all, viruses that infect the LRT result in clinically-defined ARDS, and lung neutrophil infiltration is associated with viruses that do and do not lead to ARDS (16, 18, 22, 23, 51, 77, 143, 468-472). Therefore, perhaps there are

specific viral factors or virus-induced host factors that indicate a common mechanism for neutrophil infiltration into the respiratory tract (Table 1.6).

9.1 Viruses that cause neutrophilic infiltration.

Human rhinovirus. Infection with HRV is a well-studied virus for which there are several studies on the link between neutrophils and disease (87, 473-475) (Table 1.7). HRV are plus-sense single-stranded RNA viruses with an icosahedral nucleocapsid in the *Picornaviridae* family, genus *Enterovirus* (476). HRV virions enter nasal epithelial cells via endocytosis, yet, unlike influenza, infection does not cause major damage to the nasal epithelium (476-478). Neutrophilic rhinitis, increased vascular permeability, and mucus hypersecretion are the key pathological features of HRV infection (87, 473, 474, 477), and infected epithelium seems to be the source of large amounts of neutrophil chemotactic molecules, particularly CXCL8 and kinins (473, 475, 479, 480). Interestingly, *in vitro* studies have shown that TLR3 and MDA5, but not RIG-I, are important for detecting dsRNA, and HRV capsid is recognized by TLR2 on the epithelial surface (473, 481). Thus, viral recognition shares features with hRSV, but is somewhat different than with IAV (300, 327, 482). Even so, *in vitro* infection of nasal epithelial cells with HRV indicates similar secretion of inflammatory mediators is the result of these respiratory diseases: HRV causes upregulation of IL-1, IL-6, CXCL8, GM-CSF, CCL5, CCL11, and type I IFN (483). It has been established that there are virus-specific and cell-specific differences in sensing RNA viruses via primarily TLR- and/or RLR- pathways (and even in a preference for RIG-I versus MDA5), yet these pathways may have similar general endpoints, such as chemokine and cytokine signaling (326, 327, 329).

Paramyxoviruses. Numerous viruses in the family *Paramyxoviridae* infect the human respiratory tract and may cause significant pathology (Table 1.6). Paramyxoviruses are minus-sense single-stranded RNA viruses that include hRSV, which is the leading cause of childhood bronchiolitis and pneumonia during interpandemic years of IAV transmission (484). Infection with hRSV causes neutrophilic infiltration in the LRT, where thick luminal mucous plugs filled with neutrophils may cause bronchiolar obstruction (485, 486). Nasal washes and BAL from patients with hRSV contain neutrophil chemoattractant chemokines (21, 487-489) and there is evidence that neutrophils and other respiratory cells may recognize hRSV virions directly through TLR2/6 (482, 490). Other viruses within this family include *Measles virus*, *Human metapneumovirus* (MPV), and the highly pathogenic emerging viruses, *Hendra virus* and *Nipah virus*; all of which have reports of neutrophilic infiltration at sites of infection to various degrees (491-494). Interestingly, there are no reports of neutrophils associated with infection from any of the human parainfluenza viruses (PIV) (495). Human PIV infects ciliated epithelium of the respiratory tract and may cause bronchiolitis and alveolitis (470). However, infection does not cause a cytopathic effect, which is thought to be due to viral proteins which block PRR signaling and apoptosis (470, 496). Even so, cases of severe PIV infection have elevated chemokines in nasal washes (CCL3, CCL4, CCL5, CXCL8, CXCL9, and CXCL10), some of which are neutrophil chemoattractants indicating that neutrophils may be present at some point in the disease progression (470, 480, 495-497).

Coronaviruses. Members of the family *Coronaviridae* are plus-sense single-stranded RNA viruses and infect a wide variety of mammalian and avian species (498) (Table 1.7). Two genera of coronaviruses are important human pathogens: members of the genus *Alphacoronavirus* include *Human coronavirus NL63* (HCoV-NL63); and the genus

Betacoronavirus includes HCoV-HKU1 and the highly pathogenic SARS-CoV and MERS-CoV (498). Human coronaviruses, such as HCoV-HKU1, HCoV-NL63, HCoV-OC43, and HCoV-229E, have recently been identified and are thought to cause both URT and LRT infections (499, 500). Very little is known about specific pathology associated with HCoV infection. However, much more is known about infection with SARS-CoV and MERS-CoV. These emergent viruses infect pneumocytes in the LRT and may cause a severe disease that can lead to ARDS and even have pathophysiological symptoms of hypercytokinemia (22-24). Infection with either of these viruses is correlated with increased IL-6, CCL2, CXCL8, and CXCL10 in the blood and respiratory tract, and neutrophils are noted in respiratory tissues from lethal cases of infection with either of these viruses (23, 24, 501).

Other respiratory viral infections. Human adenovirus (hAdV, members of the family *Adenoviridae,* genus *Mastadenovirus*) infections have been documented to cause an initial neutrophilic alveolitis that may progress to a viral pneumonia (specifically serotype hAdv-7), which may be related to the release of CXCL8 and CXCL10 from infected epithelial cells (502) (Table 1.7). Human cytomegalovirus (family *Herpesviridae*) may cause a viral pneumonia that includes hyaline membrane formation and neutrophilic alveolar exudates (503). Autopsies from patients who died from hantavirus pulmonary syndrome, caused by infection with New World hantaviruses, were seen to have neutrophilic infiltration surrounding antigen positive lung lesions (504) (Table 1.7). These cases are particularly remarkable, since hantaviruses infect and cause inflammation of the endothelium, often with no apparent damage to the epithelium (504). However, hantavirus pulmonary syndrome (HPS) is a severe pulmonary infection characterized by interstitial pneumonitis, focal hyaline membrane formation, and left-shifted neutrophilic leukocytosis (504).

9.2 Comparisons of respiratory viral infections.

Cytopathic effect. A key question is whether virus-induced cytopathy drives neutrophilia or whether it is the result of host response to viral infection. Infections with H1N1pdm, HPAI, SARS-CoV, and MERS-CoV are thought to cause acute lung injury which results in ARDS; characterized by excessive damage to the alveolar epithelium and involving the infiltration of neutrophils (7, 8) (Tables 1.6 and 1.7). However, less pathogenic strains such as HRV infections do not cause significant damage to the respiratory mucosa, yet neutrophils are present (477, 478). Conversely, viruses that cause moderate, focal cytopathy in the lungs, for example seasonal IAV and hRSV, are known to cause neutrophilic infiltration (478-480). Therefore, neutrophils are not necessarily associated with direct cytopathic effect, nor are they exclusively associated with severe disease.

Host response to viral versus bacterial infection. Specific host responses to infection may act as a driving force behind neutrophil infiltration. As evidenced above, many viral infections associated with neutrophil infiltration have RNA genomes. Host cells detect RNA viruses primarily through RLR as well as TLR, whereas bacteria rely on a different group of PRRs to detect extracellular PAMPs (327, 328, 357, 505). Because of the importance in diagnostics, many studies have focused on biomarkers that identify bacterial versus viral infection (*e.g.*, (506, 507)). Although it is debated, these studies routinely point to CRP as a correlate of bacterial infection (506-511). However, cases of IAV and hRSV infection are known to activate complement and often show increased CRP (392, 396, 512, 513). In short a single reliable biomarker of bacterial versus viral infection has yet to be found. In a recent study, it was among a group of early conserved differentially expressed genes across species (mouse and macaque) and pathogens (IAV and bacterial), all of which were the direct result

of an upregulation of ISGs (505). For example, IFNb, IL-1a, IL-6, IL-23a, TIMP1, M-CSF, ISG15, CCL2, CCL5, CXCL10, and CD40 were all common to the early host immune response to lung infection (505). The control of signaling through TLR versus cytoplasmic is controlled by complex intracellular adaptor proteins (*e.g.*, allowing the characteristically bacteria-specific TLR4 to signal the upregulation of viral-specific type I interferons (514)), the implications of this require much more research (reviewed in (515)).

Specific immune response signatures to different viruses. The relative number of neutrophils during viral infection may reflect the different strategies used by viruses to manipulate the host defenses, and viral infections such as HRV, hRSV, and IAV may create unique or "signature" immune responses that are involved in neutrophil attraction relative to MPV, PIV, or HCoV (the latter group have fewer neutrophils during infection). In other words, where there are often redundancies in a typical "viral" immune response, investigating differences between these patterned immune responses *en masse* between viruses may be informative (*e.g.,* (516)). Unfortunately, there are very few studies that approach this topic. In general, clinical studies have shown that viruses causing increased concentrations of CXCL8, TNFa and IL-1 are associated with increased neutrophilia, confirmed in patients with HRV, IAV, and hRSV infection (480, 517), yet CXCL8 is only correlated with symptom scores for HRV and IAV (480). Interestingly, the lung microenvironment to hRSV has been shown to be different from IAV, specifically in the presence of IL-4 (508, 518). It is thought that this is driven by the presence of alternatively activated macrophages during RSV infection (519). It is not known if this directs differences in neutrophil chemoattraction, yet IL-4 is known to drive a Th2 ("bacterial" or antibody-biased) immune response (520).

CXCL10. Patients with ARDS resulting from infection with SARS-CoV (501), H1N1pdm (105), or H5N1 HPAI (10, 54, 330, 521) had a common marker of inflammation: high levels of CXCL10. A prospective study of patients with severe respiratory disease found BAL concentrations of CXCL10 (but not CXCL8) and eotaxin/CCL11 were significantly upregulated in confirmed cases of viral infection (HRV, IAV, hRSV, MPV, HCoV-NL63, PIV, hAdv, or polyomavirus) compared to non-viral respiratory disease (522). CXCL10 is an ISG that binds the CXCR3 receptor on NK cells and plasmacytoid DCs and induces chemotaxis, apoptosis, cell growth, and angiostasis (523-527). CXCL10 is released during many viral infections, not just respiratory viral infections. Although it is not a classical neutrophil chemottractant, it is also known to operate in an autocrine manner with a unique subset of CXCR3+ neutrophils during influenza infection (380).

9.3 Neutrophils in the viral microenvironment.

In general, immune activation pathways that involve the activation of NFkappaB lead to the secretion of neutrophil chemotactic chemokines (reviewed in (528)). This is heavily driven by PAMPs, and during a viral infection type I IFNs and ISGs are the unique elements in the virus-inflamed lung environment (reviewed in (66-68, 324, 325)). This single difference between viral and bacterial infections could have drastic effects on the actions of neutrophils once in the lung. Moreover, without this information (*e.g.,* pathogenic viruses that suppress type I IFN) neutrophils may respond to inflammation in an inefficient way, potentially with pathologic effects (65, 69-71, 298, 300, 301, 422, 529, 530). Neutrophils are known to respond to IAV and type I IFN by upregulation of ISGs (422). In systemic lupus erythematosus, neutrophils may be a large contributor of type I IFN (531, 532). During increased inflammation, left-shifted or immature neutrophils emerge from the bone marrow –

a classic sign for sepsis, but also known to be present during some severe viral respiratory diseases (*e.g.,* HPS) (504). It is known that immature neutrophils do not express IFNα/β receptor, nor many other cytokine receptors (530). It is unknown what affect this would have during increased inflammation during pathogenic influenza infection, although their role in other inflammatory conditions suggests it may affect their functions (529, 530, 533, 534).

Concluding remarks.

Are neutrophils associated with viral infection? Are they associated with respiratory viral infection? When, where, and how are they associated? In the context of viral infection, what is a productive response of neutrophils? Is a productive response determined by type I IFN? There is substantial data that suggest neutrophils are a part of a viral response to infection. Neutrophils are among the first responders to IAV infection in the lung, and they remain in great numbers throughout the development of ARDS. However, many questions remain before it is determined what part they play in mild and severe disease.

Human Influenza A virus Disease

| Uncomplicated Influenza | → | Pneumonia & Diffuse Alveolar Damage | ← → | Hypercytokinemia |

Mild Seasonal IAV *e.g.*, A(H3N2), A(H1N1)

Mo
Nφ

Nasopharyngeal-Tracheal Epithelium

| Cytokine Release | Adaptive Immunity |

Resolution

IFNa, IFNb, IL6, TNFa
CXCL8, CXCL10, CCL2, CCL5

Severe IAV *e.g.*, A(H1N1)pdm09

Endothelium

Bronchiolar & Alveolar Epithelium

| Apoptosis Necrosis | ↑ Leukocyte Infiltration |

| Edema | ROS |

IFNa, IFNb, IL6, TNFa
CXCL8, CXCL10, CCL2, CCL5

Highly Pathogenic Avian Influenza; *e.g.*, A(H5N1)

AMφ

Endothelium

Alveolar Epithelium Alveolar macrophages

| Hyper-Cytokine Release | Delayed/ Absent IFNα/β |

Hema-phagocytosis

Enhanced Virus Replication Immune dysregulation

Figure 1.1 Three disease states caused by human infection with influenza A virus.

Human infection with influenza A virus (IAV) produces three main types of disease.

Seasonal human IAV (left) causes upper respiratory tract disease that is characterized as

an acute, self-limiting flu-like illness. Seasonal IAV and some emergent IAV can cause a

severe influenza pneumonia (center), which involves infection and inflammation of the

lower respiratory tract.   Some highly pathogenic avian IAV (right) cause a lethal

infection characterized by a dysregulated immune response; this can also lead to severe

pneumonia. Beneath each heading are the viral strains that typically cause each disease,

following by a cartoon diagram showing primary site of viral replication. Arrows below

point to pathological outcomes, followed by typical immune responses measured in

humans (increased pathology is associated with increases in the underlined immune

proteins).
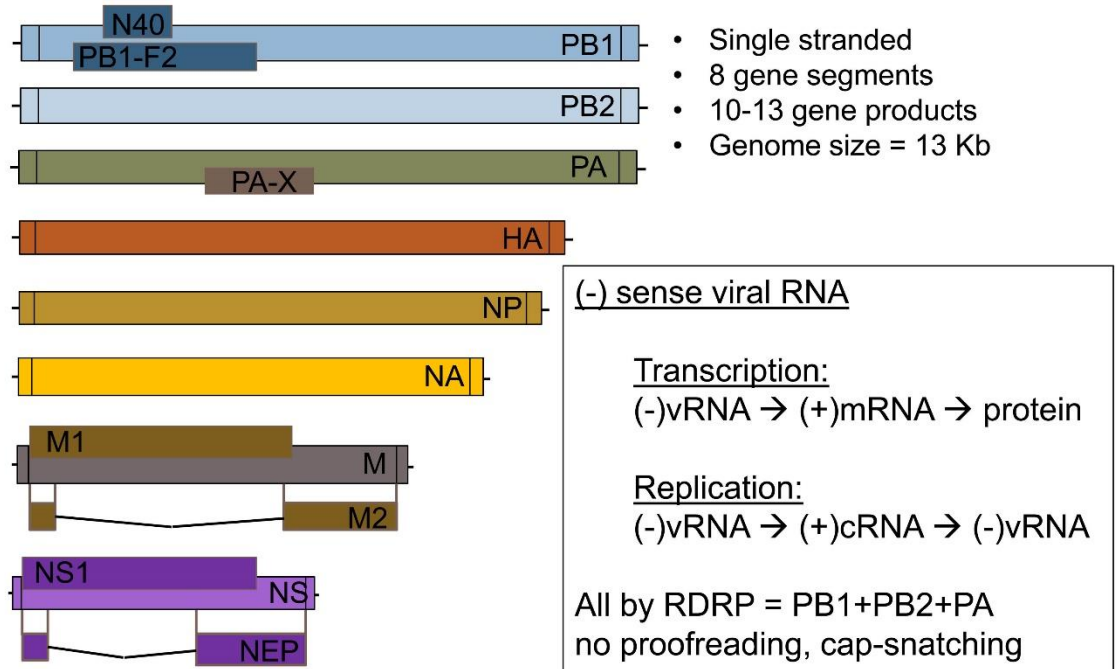
Figure 1.2 Influenza A virus genome.

Influenza A viruses have an 8-segmented, single-stranded, negative sense RNA genome that codes for 10-13 gene products. The cartoon shows the arrangement of those gene products along each gene segment. Gene segments are sized relative to each other, and the total genome is over 13 kb in length. The basic formulas for making protein and replicating the genome are shown in the box; most steps are performed by the viral RNA-dependent RNA polymerase (RDRP), which consists of three viral proteins.
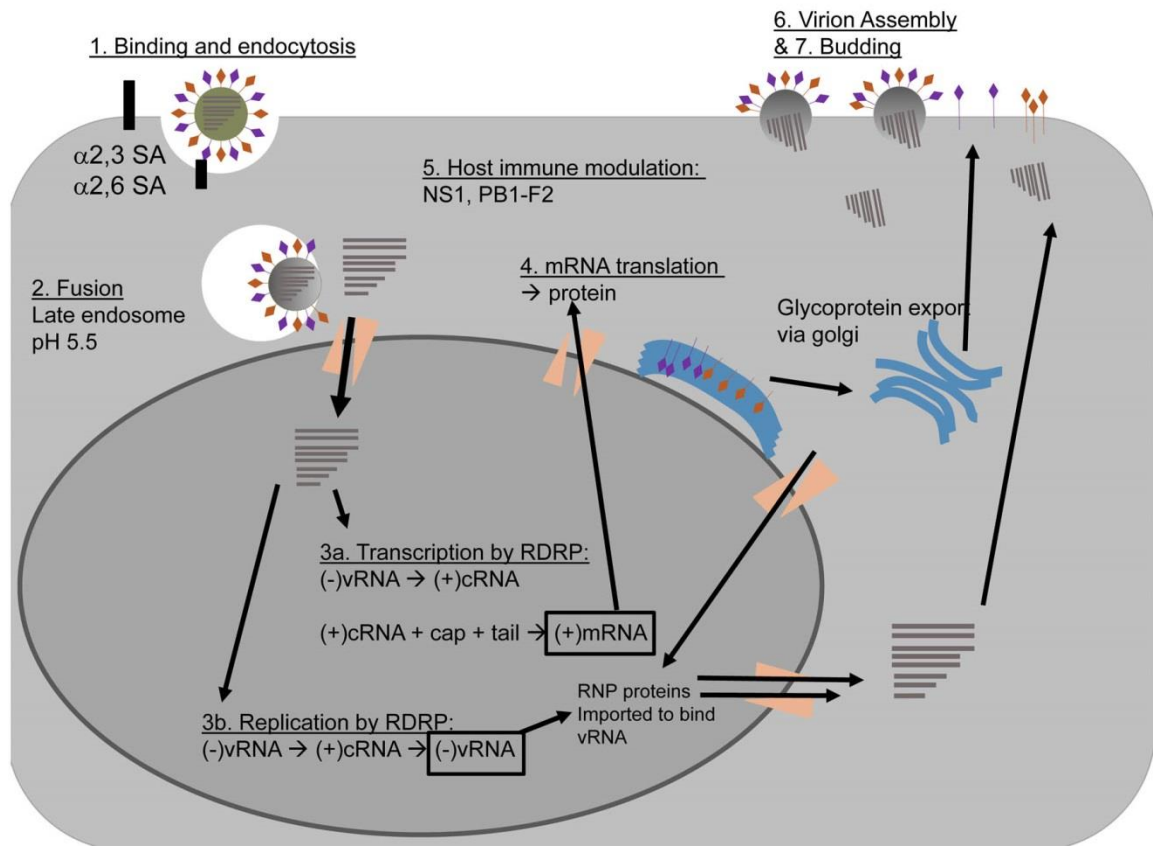
Figure 1.3 Influenza A virus life cycle diagram.

Seven major steps in the influenza A virus life cycle include: (1) binding to host cells via sialic acid residues (SA) and entry into cells via clathrin mediated endocytosis; (2) fusion to host cell membrane allows release of viral genome into cytoplasm and import into nucleus; (3) viral genome transcription (3a) and replication (3b) occur in the nucleus by the viral RNA-dependent RNA polymerase (RDRP); (4) mRNA is exported for translation by host ribosomes; (5) some proteins modify the host immune response, glycoproteins are exported to the cell membrane through the Golgi body and proteins that form the ribonucleoprotein (RNP) are imported back to the nucleus to bind to new vRNA, which is exported from the nucleus (6) to the plasma membrane where virions are assembled and (7) bud out from the host plasma membrane.

Animal Models of Influenza A Virus Infection

	Mouse	**Ferret**
Signs/Symptoms	Weight Loss Viral replication in respiratory tract Lethality (LD_{50}) Seroconversion	
	Ruffled fur, Hunched posture, Hypothermia	Sneezing, Coughing Rhinorrhea, Lethargy Fever
Advantages	Inexpensive Well-characterized genetics Abundance of reagents Inbred strains	Similar to humans in: receptor distribution clinical symptoms pathology in resp. tract
Disadvantages	Not a natural host Lack clinical symptoms No virus transmission Mouse strain-dependent	Expensive USDA/special housing No standardized methods No immunological reagents Outbred

Figure 1.4 Animal models of influenza A virus infection

Mice and ferrets are commonly used animal models to study influenza A virus pathogenesis. Advantages and disadvantages are listed for each species.
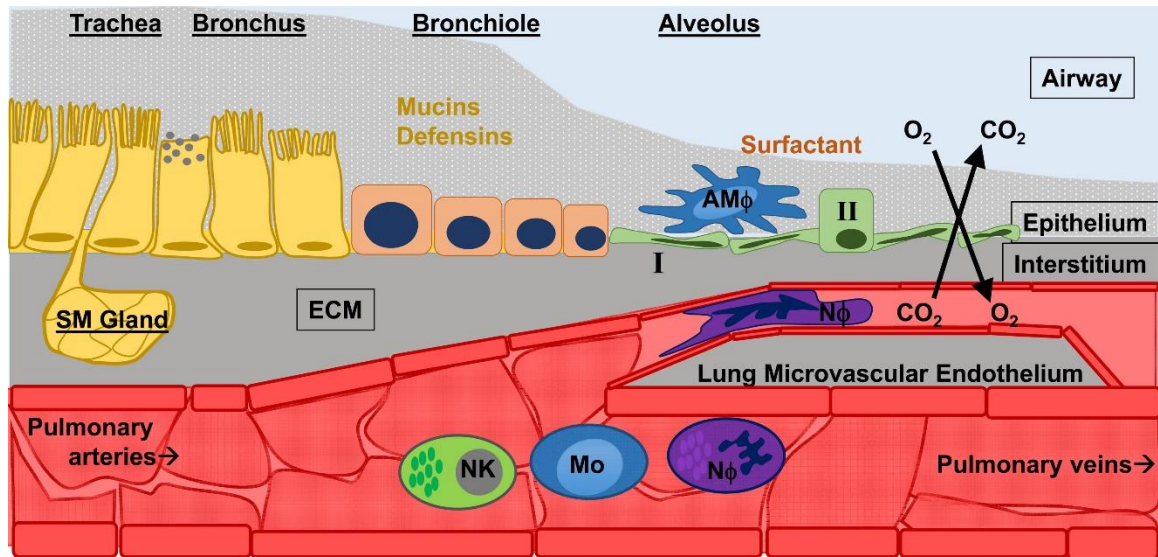
Figure 1.5 Cartoon diagram of normal human airways

The upper airways are on the left, consisting of ciliated pseudostratified epithelium with occasional secretory cells and submucosal (SM) secretory glands embedded within the extracellular matrix (ECM). In the lung, the airways branch into bronchioles and end in alveoli, which are made of type I (I) and type II (II) pneumocytes which are in near-constant contact with alveolar macrophages (AMϕ). The alveoli are the site of gas exchange, working in close proximity to the lung microvascular endothelium to expel carbon dioxide (CO2) from the pulmonary arteries and carry oxygen (O2) through the pulmonary veins back through the heart and into circulation. The airway epithelium is lined with mucus containing mucins, defensins; and the alveoli contain surfactant proteins that aid in surface tension and innate immune defenses. Because the entire blood volume passes through the lungs, innate immune cells (such as natural killer cells, NK; monocytes, Mo; and neutrophils, Nϕ) are transient through the lungs and must navigate the capillary beds near the alveoli.
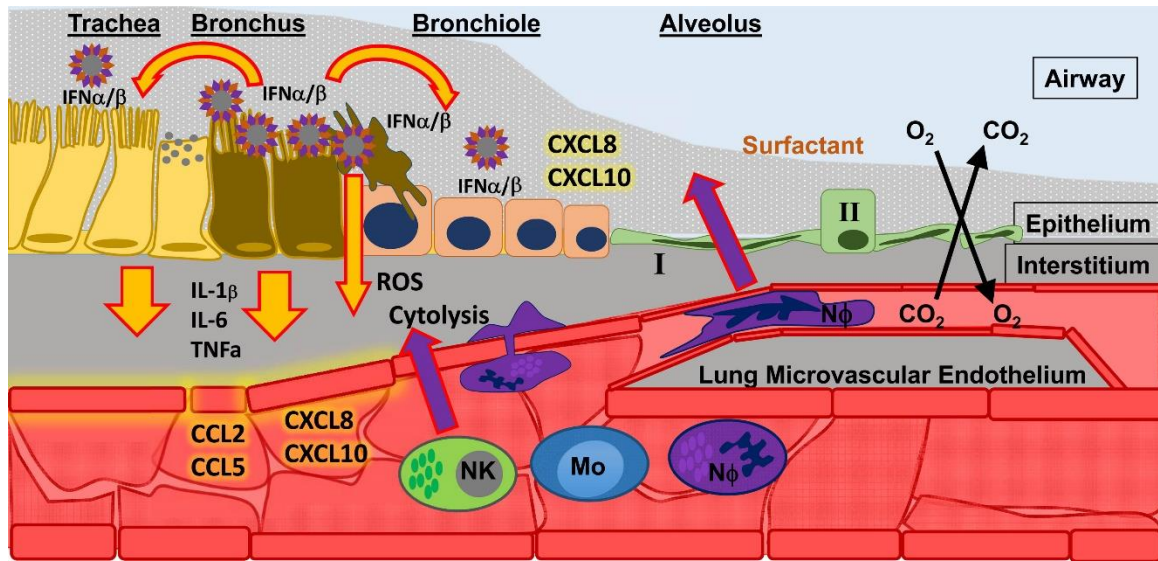
Figure 1.6 A cartoon diagram of IAV infection in the human respiratory tract.

Infection of epithelial cells in the bronchus results in the release of type I interferons

(IFNα/β) which signal to nearby cells. The result of IAVα/β signaling is the release of

proinflammatory cytokines (e.g., IL-1β, IL-6, TNFα) that signal to endothelial cells,

which help spread inflammatory signals (chemokines such as CCL2, CCL5, CXCL8,

CXCL10) throughout the blood to recruit innate immune cells to the site of infection.

Recruited of innate immune cells (such as natural killer cells, NK; monocytes, Mo; and

neutrophils, Nϕ) must interact with activated endothelium to leave the blood stream and

crawl towards the site of infection. There they can perform effector functions to control

infection, such as releasing reactive oxygen species (ROS) and directly killing infected

cells (cytolysis).

Table 1.1 Effect of cytokine knockout mice infected with IAV on neutrophils

Mouse Model	Virus	Leth?	Dose	Effect on Lung Neutrophils	Effect on Disease Phenotype compared to wt	Ref
IL-1β$^{-/-}$	H3N2 A/Taiwan/3446/2002	No	5×10^5 PFU	Same as wt	Same as wt	(428)
IL-1β$^{-/-}$	H3N2 A/TW/3446/02 with PA gene from A/VN/1194/04	No	5×10^5 PFU	Same as wt	Delayed pathology	(428)
IL-1β (Casp 1$^{-/-}$)	H3N2 A/Taiwan/3446/2002	No	5×10^5 PFU	Same as wt	Same as wt	(428)
IL-1β (Casp 1$^{-/-}$)	H3N2 A/TW/3446/02 with PA gene from A/VN/1194/04	No	5×10^5 PFU	Increased	Weight loss, delayed pathology	(428)
IL-1β (Casp 1$^{-/-}$)	H1N1 A/PR/8/1934	70% Survival	6×10^4 PFU with 0.1% alum	Reduced	Increased Lethality	(426)
IL-1β (Casp 1$^{-/-}$)	H1N1 A/PR/8/1934	70-80% Survival	8000 EID$_{50}$	Reduced	Increased Lethality	(535)
IL-6$^{-/-}$	H5N1 A/Hong Kong/483/1997	Yes	10^3 MID$_{50}$	n/c	Same as wt	(430)
IL-6$^{-/-}$	H5N1 A/Hong Kong/486/1997	No	10^3 MID$_{50}$	n/c	Same as wt	(430)
IL-6$^{-/-}$	H5N1 A/Vietnam/1203/04	Yes	10^3 EID$_{50}$	n/c	Same as wt	(536)
IL-6$^{-/-}$	H1N1 A/PR/8/1934	No	3000 EIU	Decreased	Features of chronic infection, delayed viral clearance	(463)
TNF$^{-/-}$	H5N1 A/Vietnam/1203/04	Yes	10^3 EID$_{50}$	n/c	Same as wt	(536)
IL-18$^{-/-}$	H3N2 X31 (A/PR/8/1934)	No	10^4 PFU	Increased	Increased virus in lungs early, cleared virus same as wt	(362)

Leth? = "yes" means it is a lethal model of disease; wt refers to wild-type mice; Casp 1 = caspase 1; PFU = plaque forming units; EID$_{50}$ = 50% egg infectious dose; MID$_{50}$ = 50% mouse infectious dose; EIU = egg infectious units, n/c = no change.

Table 1.2 Effect of cytokine receptor knockout mice infected with IAV on neutrohils

Mouse Model	Virus	Leth?	Dose	Effect on Lung Neutrophils	Effect on Disease Phenotype compared to wt	Ref
IFNαβR$^{-/-}$	H1N1 A/PR/8/1934*	Yes	6.7 LD$_{50}$	Same as wt	Same as wt	(380)
IFNαβR$^{-/-}$	H3N2 X31 (A/PR/8/1934)	Yes	800 TCID$_{50}$	Reduced	Protection	(65)
IFNαβR$^{-/-}$	H1N1 A/California/04/2009	Yes	330 TCID$_{50}$	Reduced	Protection	(65)
IFNαβR$^{-/-}$	H1N1 A/PR/8/1934	LD$_{50}$	10000 PFU	Increased	Increased lethality	(70)
IL-1R1$^{-/-}$	H5N1 A/HK/483/1997**	Yes	10^3 MID$_{50}$	Increased	Delayed Death	(429)
IL-1R1$^{-/-}$	H5N1 A/HK/483/1997	Yes	10^3 MID$_{50}$	Increased	Delayed Death	(429)
IL-1R1$^{-/-}$	H5N1 A/HK/483/1997	Yes	10^3 MID$_{50}$	Same as wt	Same as wt	(430)
IL-1R1$^{-/-}$	H5N1 A/HK/486/1997	No	10^3 MID$_{50}$	Slightly less (n.s.)	Reduced Weight loss	(430)
IL1-R1$^{-/-}$	H1N1 A/PR/8/1934	No	100 PFU	Reduced	Increased Lethality	(397)
IL1-R1$^{-/-}$	H1N1 A/PR/8/1934	No	100 PFU	Reduced	Increased Lethality	(397)
IL1-R1$^{-/-}$	H1N1 r1918	Yes	10^6 PFU	Same as wt	Increased Complement Gene Expression	(427)
IL-6R$^{-/-}$	H1N1 A/PR/8/1934	No	3000 EUI	n/c	Increased Lethality	(463)
IL-17RA$^{-/-}$	H1N1 A/PR/8/1934	Yes	1 LD$_{90}$	Reduced	Protection	(399)
TNF-R1$^{-/-}$	H5N1 A/Hong Kong/483/1997	Yes	10^3 MID$_{50}$	Reduced	Delayed Death	(429)
TNF-R1$^{-/-}$	H5N1 A/Hong Kong/483/1997	Yes	10^3 MID$_{50}$	n/c	Reduced leukopenia	(430)
TNF-R1$^{-/-}$	H5N1 A/Vietnam/1203/04	Yes	10^3 EID$_{50}$	n/c	Same as wt	(536)
TNF-R1$^{-/-}$ TNF-R2$^{-/-}$	H5N1 A/Vietnam/1203/04	Yes	10^3 EID$_{50}$	n/c	Increased survival (n.s.)	(536)
TNF-R1$^{-/-}$ TNF-R2$^{-/-}$	H1N1 r1918	Yes	10^6 PFU	Reduced	Delayed death	(427)
TNF-R1$^{-/-}$ TNF-R2$^{-/-}$ IL1R$^{-/-}$	H5N1 A/Hong Kong/483/1997	Yes	10^3 MID$_{50}$	Reduced	Delayed Death	(429)

Leth? = "yes" means it is a lethal model of disease; wt refers to wild-type mice; Casp 1 = caspase 1; PFU = plaque forming units; EID$_{50}$ = 50% egg infectious dose; MID$_{50}$ = 50% mouse infectious dose; EIU = egg infectious units, n/c = no change. *PR = Puerto Rico, ** HK = Hong Kong.

Table 1.3 Effect of chemokine receptor knockout mice infected with IAV on neutrophils

Mouse Model	Virus	Leth?	Dose	Effect on Lung Neutrophils	Effect on Disease Phenotype compared to wt	Ref
CCR2$^{-/-}$	H1N1 A/PR/8/1934	No	3.3 PFU	Increased	Increased lung CCL2, CCL3, CCL4, CXCL1, CXCL2, CXCL10	(379)
CCR2$^{-/-}$	H1N1 A/PR/8/1934	70-80% Survival	5 HAU	Increased, delayed	Reduced lethality, increased virus in lung, increased CCL2, CXCL10 in lung	(537)
CCR5$^{-/-}$	H1N1 A/PR/8/1934	70-80% Survival	5 HAU	Increased	Increased lethality, increased virus in lung, , increased CCL2, CCL5, CXCL10 in lung	(537)
CCR2$^{-/-}$ CCL3$^{-/-}$	H1N1 A/PR/8/1934	70-80% Survival	5 HAU	n/c	Reduced lethality, increased virus in lungs	(537)
CXCR2$^{-/-}$	H1N1 A/PR/8/1934	No	10-100 PFU	Reduced	Increased lung macrophages Decreased T cell recruitment	(538)
CXCR3$^{-/-}$	H1N1 A/PR/8/1934	No	3.3 PFU	Reduced	Same as wt	(539)
CXCR3$^{-/-}$	H1N1 A/PR/8/1934	Yes	6.7 LD$_{50}$	Reduced	Increased Survival	(380)

Leth? = "yes" means it is a lethal model of disease; wt refers to wild-type mice; Casp 1 = caspase 1; PFU = plaque forming units; EID$_{50}$ = 50% egg infectious dose; MID$_{50}$ = 50% mouse infectious dose; EIU = egg infectious units, n/c = no change.

Table 1.4 Effect of chemokine knockout mice infected with IAV on neutrophils

Mouse Model	Virus	Leth?	Dose	Effect on Lung Neutrophils	Effect on Disease Phenotype compared to wt	Ref
CCL2$^{-/-}$	H5N1 A/Vietnam/1203/04	Yes	10^3 EID$_{50}$	n/c	Same as wt	(536)
CCL3$^{-/-}$	H5N1 A/Hong Kong/483/1997	Yes	10^3 MID$_{50}$	n/c	Same as wt	(430)
CCL3$^{-/-}$	H5N1 A/Hong Kong/486/1997	No	10^3 MID$_{50}$	n/c	Same as wt	(430)
CCL5$^{-/-}$	H1N1 A/PR/8/1934	No	3.3 PFU	Same as wt	Same as wt	(539)
CXCL10$^{-/-}$	H1N1 A/PR/8/1934	Yes	6.7 LD$_{50}$	Reduced	Increased Survival	(380)

Leth? = "yes" means it is a lethal model of disease; wt refers to wild-type mice; Casp 1 = caspase 1; PFU = plaque forming units; EID$_{50}$ = 50% egg infectious dose; MID$_{50}$ = 50% mouse infectious dose; LD$_{50}$ = 50% mouse lethal dose, n/c = no change. PR = Puerto Rico.

Table 1.5 Effect of neutrophil effector knockout mice on IAV infection

Mouse Model	Virus	Leth?	Dose	Effect on Lung Neutrophils	Effect on Disease Phenotype compared to wt	Ref
Cybb[tm1] Mice (gp91[phox] deficient)	H3N2 X31 (A/PR/8/1934)	No	50 HAU	Increased	Increased lung cellularity, Decreased lung consolidation, Increased TNFa, IL6, CCL2, Decreased virus in lung	(439)
Elane^{-/-}	H3N2* A/Memphis/1/1971 Written as H3N1 in pub.	No	$10^{4.5}$ PFU	Same as wt	Same as wt	(434)
NETs (PAD4^{-/-})	H1N1 A/WSN/33	50% Survive	1 LD_{50}	Same as wt	Same as wt	(457)

Leth? = "yes" means it is a lethal model of disease; wt refers to wild-type mice; Casp 1 = caspase 1; HAU = hemagglutinating units; PFU = plaque forming units; LD_{50}= mouse 50% lethal dose, n/c = no change.

Table 1.6 (-) sense RNA respiratory viruses that cause increased neutrophil infiltration during infection

Virus Family	Virus species	Host/ model	Primary cell target	Pathology	N	Ref
Orthomyxoviridae (-)	Influenza A virus	Hu,NHP, Mo,Fe,Sw	epithelial cells (URT, LRT)	Mild: necrotic rhinitis and tracheitis; Moderate: necrotic bronchiolitis and alveolitis; Severe: diffuse alveolar damage, hypercytokinemia (HPAI)	(+++)	(87, 473, 474)
Paramyxoviridae (-)	Human respiratory syncytial virus	Hu	epithelial cells (URT,LRT)	Severe: necrotic bronchiolitis and alveolitis, obstructed bronchioles and giant cell formation	(+++)	(485, 486)
Paramyxoviridae (-)	Human metapneumovirus	Hu			(+)	(493, 494)
Paramyxoviridae (-)	Measles virus	Hu, Mo	Resident myeloid cells of the lung	Severe: bronchiolitis obliterans	(++)	-492
Paramyxoviridae (-)	Hendrah/Nipah virus	Hu			(++)	-491
Paramyxoviridae (-)	Human parainfluenza virus	Hu	Ciliated epithelium	Bronchiolitis and alveolitis	No?	-495
Bunyaviridae (-)	New World hantavirus	Hu	Lung microvascular endothelium	Hantavirus Pulmonary Syndrome, endothelial inflammation and focal antigen-positive sites in lung	(+)	-504

Families and species of (-)-sense RNA respiratory viruses for which the presence or absence of neutrophils in the respiratory tract has been documented. Also listed are: the host species (Human, Non-Human Primate, Mouse, Ferret, Swine) in which neutrophils have been known to be increased following infection; the primary site of infection (URT = upper and LRT = lower respiratory tract); the typical pathology associated with increased neutrophils; the relative amount of neutrophil infiltration; and references.

Table 1.7 (+) sense RNA and DNA respiratory viruses that cause increased neutrophil infiltration during infection.

Virus Family	Virus species	Host/ model	Primary cell target	Pathology	N	Ref
Picornaviridae (+)	Human rhinovirus	Hu	Epithelial cells	Mild to moderate: neutrophilic rhinitis; Severe: acute LRT, bronchiolitis and alveolitis	(+++)	-87
Adenoviridae (DNA)	Human adenovirus (HAdv3, HAdv7)	Hu		Bronchitis and alveolitis		-502
Coronaviridae (+)	Human coronavirus (NL-63 or OC43)	Hu			(+/-)?	
Coronaviridae (+)	Severe acute respiratory syndrome coronavirus	Hu, Fe	Epithelial cells	Alveolitis, ARDS, hypercytokinemia	(++)	-23
Coronaviridae (+)	Middle east respiratory syndrome coronavirus	Hu, Fe	Epithelial cells	Alveolitis, ARDS, hypercytokinemia	(++)	-24
Filoviridae (+)		NHP		Experimental aerosolized infection; hemorrhagic fever, associated with antigen and necrosis in lungs, neutrophilia	(+)	(540, 541)

Families and species of (-)-sense RNA respiratory viruses for which the presence or absence of neutrophils in the respiratory tract has been documented. Also listed are: the host species (Human, Non-Human Primate, Ferret) in which neutrophils have been known to be increased following infection; the primary site of infection (URT = upper and LRT = lower respiratory tract); the typical pathology associated with increased neutrophils, including Acute Respiratory Distress Syndrome and notes on the circumstances in which neutrophils were increased; the relative amount of neutrophil infiltration; and references.

CHAPTER II

PHENOTYPIC DIFFERENCES IN VIRULENCE AND IMMUNE RESPONSE IN

CLOSELY RELATED CLINICAL ISOLATES OF INFLUENZA A 2009 H1N1

PANDEMIC VIRUSES IN MICE

Overview

To capture the possible genotypic and phenotypic differences of the 2009 influenza A

virus H1N1 pandemic (H1N1pdm) strains circulating in adult hospitalized patients, we

isolated and sequenced nine H1N1pdm viruses from patients hospitalized during 2009-

2010 with severe influenza pneumonia in Kentucky. Each viral isolate was characterized

in mice along with two additional H1N1 pandemic strains and one seasonal strain to

assess replication and virulence. All isolates showed similar levels of replication in nasal

turbinates and lung, but varied in their ability to cause morbidity. Further differences

were identified in cytokine and chemokine responses. IL-6 and KC were expressed early

in mice infected with strains associated with higher virulence. Strains that showed lower

pathogenicity in mice had greater IFNγ, MIG, and IL-10 responses. A principal

component analysis (PCA) of the cytokine and chemokine profiles revealed 4 immune

response phenotypes that correlated with the severity of disease. A/KY/180/10, which

showed the greatest virulence with a rapid onset of disease progression, was compared in

additional studies with A/KY/136/09, which showed low virulence in mice. Analyses

comparing a low (KY/136) versus a high (KY/180) virulent strain showed a significant

difference in the kinetics of infection within the lower respiratory tract and immune responses. Notably by 4 DPI, virus titers within the lung, bronchoalveolar lavage fluid (BALf), and cells within the BAL (BALc) revealed that the KY/136 replicated in BALc, while KY/180 replication persisted in lungs and BALc. In summary, our studies suggest four phenotypic groups based on immune response that result in different virulence outcomes in H1N1pdm strains with a high degree of genetic similarity. *In vitro* studies with two of these isolates suggested that the more virulent isolate, KY/180, replicates productively in macrophages and this may be a key determinant in tipping the response toward a more severe disease progression.

Introduction

The 2009 pandemic H1N1 influenza virus (H1N1pdm) arose through reassortment of two preexisting swine influenza viruses, a Eurasian avian-like virus and a North American triple reassortant virus (44, 127, 542). The risk factors associated with human cases of H1N1pdm mirrored those of seasonal influenza (543). As observed with seasonal influenza, the most common underlying chronic conditions among hospitalized patients were respiratory disease, asthma, cardiac disease, and diabetes (6, 30, 543-546). However, in contrast to seasonal influenza, a greater proportion of severe and fatal cases had a pre-existing chronic illness. A second notable difference was the age distribution of hospitalized and severe cases. Children less than 17 years old had the greatest rates of hospitalization per capita and adults over 64 had the greatest rates of mortality per capita. Retrospective clinical studies focused on surveillance H1N1pdm sequences present in ICU admissions suggest that pre-existing medical conditions may be a more important

factor in severity rather than particular viral variants (547). However, this does not explain why a greater proportion of persons with pre-existing medical conditions had more severe disease than typically observed for seasonal influenza. Further, previously unreported comorbidities such as morbid obesity have been widely suggested for H1N1pdm for increased risk for admission to the ICU and death (548). At this time, it is difficult to rule out the contribution of viral variants to the resulting illness observed with the various comorbidities. Nonetheless, the course of illness and the progression to more severe disease are most likely due to the combined interplay of the individual's health, the intrinsic phenotype of the infecting viral variant and the treatment regime.

In contrast to seasonal influenza viruses, the H1N1pdm viruses replicate well and show greater pathogenicity with viral antigen in the bronchiolar epithelia and the alveolus by day 3 post-infection (DPI) (127, 247, 542). In the BALB/c mouse, A/California/04/09 and other H1N1pdm viruses show lethality, but only at the highest dose of $10^{6.5}$ plaque forming units (PFU) (247, 542). Studies of infection of BALB/c with several different 2009 H1N1pdm virus isolates show high virus titers in nasal turbinates (NT) and lung tissues by 3 DPI. Virus titers show a slight decrease by 6 DPI in lung and NT although the decrease varies among strains, too. Proinflammatory cytokines and chemokines were elevated for most mice in whole lung specimens at 3DPI for KC, IL-6, IL-12(p40), G-CSF, M-CSF, MCP-1 MIG, MIP-1β, and LIF. By 6 DPI, IL-10 was present, albeit low, whereas some of the cytokines were reduced (e.g., MIP-2, IL-6), but most remained elevated (247, 542). The levels of cytokines and chemokines in humans or mice do not suggest hypercytokinemia common to H5N1 and 1918 viruses (46, 142, 222).

The overall genetic distance among H1N1pdm isolates remained low with 7 distinct clades in the first wave of the pandemic, while in the second wave a single viral lineage dominated (107). Molecular surveillance, while important, will not confirm potential phenotypic differences *in vivo* resulting from amino acid changes associated with viral variants in newly emerging strains or the potential for mixed infections and the genetic diversity of the intrahost viral populations (549). Animal studies can complement molecular surveillance in monitoring the potential pathogenicity and immunogenicity of circulating strains. Further, such studies have potential to reveal the efficacy of treatment regimes. Herein we report the isolation, sequence, and characterization of nine H1N1pdm influenza A viruses from adult patients hospitalized in Kentucky during the second pandemic wave, September 2009 and April 2010. Four of the nine patients died and all of the patients for whom data was available had an underlying chronic condition. This group of clinical isolates, with high genetic similarity, was characterized for virus load, virulence, and host immune response in mice. Immune responses in the lungs suggest four distinct immunological phenotypes that correlate with the observed mortality in mice. This study underscores the potential variability in the virulence of 2009 H1N1 influenza A strains circulating in Kentucky during the pandemic. These data suggest the hypothesis that the high severity of disease seen in certain hospitalized patients may be related to infection with H1N1pdm viral variants that, due to cell tropism and replication levels, may exacerbate certain types of disease associated with comorbidity.

Results

Isolation and sequence analyses of H1N1pdm isolates from hospitalized patients

H1N1pdm strains were isolated from nasopharyngeal swab samples obtained from nine de-identified patients enrolled in the Severe Influenza Pneumonia Surveillance (SIPS) project, a clinical study of hospitalized patients with severe community-acquired pneumonia in Kentucky from December 2008 – December 2011 (Table 2.1). Hospitals included in the SIPS project included two rural areas of Kentucky, one in the east and one in the midwest, and one in an urban area (Louisville). The midwest is active in agriculture and one of the highest livestock producers of hogs and pigs. The age of the patients ranged from 31 to 58 and included five females and 4 males. Many of those patients had underlying comorbidities commonly associated with severe influenza disease such as obesity, diabetes and chronic obstructive pulmonary disorder (COPD) (Table 2.S1) Four of the nine patients died.

Viruses were isolated by passage through both Madin-Darby canine kidney (MDCK) cells and eggs and virus isolates were designated according to a tracking number that contains no patient identifier information. Herein, isolates will be referred to by the tracking number and virus isolation method (*e.g.,* A/Kentucky/180/2010 egg-passaged isolate will be referred to as "KY/180E"). Viruses were amplified and the virus titers were determined by 50% tissue culture infectious dose ($TCID_{50}$), plaque forming units (PFU) and hemagglutination assays in Madin-Darby canine kidney (MDCK) cells (data not shown). Viral titers measured in $TCID_{50}$ and PFU assays were similar for MDCK-

adapted viruses and egg-adapted isolates (e.g., median titer $\sim10^7$). Some viruses (A/KY/96/09, A/KY/99/09, A/KY/108/09, A/KY/180/10) showed a 10-100 fold higher titers in MDCK cell culture than in egg, but some (A/KY/80/09, KY/110/09, KY/136/09) did not. Egg-adapted viruses that were not recovered included A/KY/104/09 and A/KY/190/10. Hemagglutination titers were generally lower from egg-adapted viruses and showed variability among isolates (data not shown).

Universal and gene-specific primers were designed and used to amplify and sequence full-length cDNAs of all viral segments from each isolate. The amino acid sequences encoded by each gene were deduced and compared. All of the isolates have stop codons in PB1-F2 at positions 12, 58, and 88 (data not shown) (550). Amino acids that showed polymorphisms are listed for each viral protein for the majority of genes (Table 2.S2). The most amino acid changes were observed in HA1 and acidic polymerase (PA) with 18 and 9 mutations collectively across the 7-8 the KY isolates (not all isolates were completely sequenced). Neuraminidase and the two basic polymerase subunits (NA, PB1 and PB2) each had 4-5 mutations while the nonstructural protein 1 (NS1) and HA2 showed 3 mutations collectively. In contrast, matrix (M1), nucleoprotein (NP) had only 1 mutation and there were none in M2, NS2 or PA-X. Of the mutations only a few have been previously studied functionally to our knowledge. For example, in the HA1/HA2 of KY/180E we noted changes in D222G, S83P, S183P, and E374K. E374K was identified as a vaccine escape mutation (551). The S183P and the Q293H mutations in HA1 (found in KY/180E and KY/96E, respectively) have been reported by others (552-555), and have

been associated with alterations in receptor binding and increases in disease severity in humans (106, 134).

Differential progression of virus replication and disease in mice infected with H1N1pdm strains

To make an initial assessment of the levels of replication and virulence potential of each of the clinical H1N1pdm isolates, groups of six DBA2 mice were intranasally-infected and monitored daily for clinical signs and body weight. In addition to the nine clinical isolates, we included two pandemic strains (A/CA/07/09 and A/NY/18/09) and a seasonal H1N1 strain (A/BN/59/07). On days three and six, three mice each were euthanized and analyzed for viral load and antibody titers (Table 2.2). All mice infected with influenza strains showed weight loss (Table 2.2). Mice infected with KY/96M, KY/80M, KY/180E, KY/80E, and NY/18E showed the greatest weight loss in this short study (Table 2.2). Mice infected with the seasonal influenza strain BN/59E showed the least weight loss (about 9%). All other mice infected with H1N1pdm influenza isolates (KY/136M, KY/99M, KY/136E, KY/110E, CA/07E, KY/108M, KY/110M, KY/104M, and KY/108E) showed weight loss averages ranging from 13% to 26%, respectively.

The mortality rates for mock- and virus-infected groups were expressed as a percentage of lethal infections (Table 2.2). BN/59, CA/07, KY/110 and KY/136 showed no lethality and low morbidity; whereas KY/190 and KY/180 showed the greatest lethality and substantial weight loss. Both KY/80 and NY/18 showed lethality and weight loss. On 3

and 6 days post-infection (DPI), three animals were sacrificed and the lung tissues were collected for virus titration analysis ($TCID_{50}$ assay of lung tissue homogenate using MDCK cells). Virus titers of lungs from each mouse-infected group showed relatively little difference between the various isolates on 3 and 6 DPI ($p > 0.05$ using pairwise Wilcoxon Rank-Sum test without correction for multiple comparisons, Table 2.2). Mice infected with egg-adapted viruses showed a higher mortality than several of the corresponding MDCK isolates (*e.g.*, see KY/96, KY/99, KY/108). However, both egg and MDCK-adapted KY/80 and KY/180 showed lethality in mice.

The influenza-specific serum IgG antibody responses in mice were measured at 6 DPI by ELISA using antigen prepared from inactivated NY/18 virus (Table 2.2) and reciprocal endpoints were determined. Strains KY/80E, KY/180, and KY/190 had no detectable IgG antibody by 6 DPI. The seasonal strain and all other pandemic strains produced detectable IgG antibody; the highest endpoint titers were collected from BN/59, KY/108E, NY/18E, KY99M, KY/136, and KY/110M. In some cases, these numbers reflect a small numbers of animal remaining at 6 DPI.

Cytokine and chemokines responses in H1N1pdm isolates show four distinct phenotypic profiles

Mouse cytokine and chemokine panels were employed to gain a broad overview of the immune response at 3 and 6 DPI in the lungs and sera of mice infected with each of the viral isolates (Figures 2.1 and 2.2). No significant difference was seen between egg- and

MDCK-passaged isolates; therefore, the combined data are presented in these two figures. There was an overall increase in proinflammatory cytokines (TNFα, IL-1β, IL-6 and KC) albeit different levels were noted. The levels of TNFα and IL-1β were greater in the lungs on day 3 in viral isolates with greater lethality (*e.g.*, KY/180, KY/190) as compared to those with no lethality (*e.g.*, KY/136, $p < 0.05$). These same cytokines were higher in the mice with no lethality on day 6 as compared to those showing lethality. A similar temporal pattern was noted with some chemokines (*e.g.,* RANTES, Figure 2.2). Interferon-gamma (IFNγ) and IL-10, an anti-inflammatory cytokine, were present on day 6 in mice infected with all but the most lethal strains, KY/180, KY/190 (Figure 2.1, $p < 0.05$).

With the exception of isolate KY/110 and KY/104, the chemokines CCL2 (MCP-1), CCL3 (MIP1α), CXCL9 (MIG), and CXCL10 (IP-10) displayed similar levels in all isolates on 3 DPI followed by a relative increase in animals infected with nonlethal versus a decrease in animals infected with lethal isolates at 6 DPI (Figure 2.2 and Table 2.2). IFNγ stimulates both IP-10 and MIG, and as expected the IFNγ levels were low in lethal isolates as compared to nonlethal isolates at 6 DPI. Cytokines and chemokines that showed limited response in mice with any viral infection included Eotaxin, GM-CSF, IL-1a, M-CSF, IL-2, IL-3, IL-4, IL-5, IL-7, IL-9, IL-12p40, IL-13, IL-15, IL-17, MIP2, LIX, MIP1β, RANTES, IL-12p70, and VEGF (data not shown).

A principal components analysis (PCA) was performed using 11 cytokine/chemokine measurements from the lungs of mice infected with each virus (Figure 2.S1). The

cytokines and chemokines included in the analysis were selected because they were determined to be the most significantly different between isolates on 3 and 6 DPI by generalized linear model fitness testing (data not shown). The first two components explained 72% of the variance (Figure 2.S1) and the third component explained an additional 10% (data not shown). CCL3, TNFα, IL-10, IL1β, and IFNγ were all highly correlated with the first component dimension (>80%), meaning these cytokines were principally important in differentiating the isolates. CXCL10, KC and G-CSF were similarly highly correlated with the second component (>70%), and CXCL9 was highly correlated with the third component dimension (83%, data not shown). The remaining variables, IL-6 and CCL2, were not highly correlated with the components used in this model, although they were significantly different between isolates on 3 and 6 DPI. The mean for each isolate on 3 and 6 DPI are plotted according to the coordinates of the first two components in Figure 2.3 (and Figure 2.S1).

The method used for computing this PCA is similar to k-means cluster analysis, and therefore we expected to observe the isolates to group according to their cytokine/chemokine signatures. To better visualize these clusters, we connected each isolates' 3 DPI coordinate to its 6 DPI coordinate with an arrow (Figure 2.3). According to this method of using a "time-resolved" PCA, the isolates were observed to cluster clearly into four groups representing various trajectories of disease.

The first three groups of isolates could be differentiated by their immunogenicity and low to moderate lethality. The first group includes isolates with a low lethality in mice, and

was exemplified by infection with the seasonal strain BN/59, and 2009 pandemic strains CA/07, KY/80 and KY/136. The second group (KY/96, KY/99, and KY/104) included those strains with moderate lethality in the mouse model, and was similar to the first group in course of disease, but was characterized by increased inflammatory cytokines (e.g., IL-6, KC-like, and G-CSF) and chemokines (e.g., CXCL9). In contrast to the first group, these had a higher level of the anti-inflammatory cytokine IL-10 later in disease, as well as increased IFNγ at 6 DPI. The third group of influenza strains (KY/108 and KY/110) was the most immunogenic compared to the other isolates, and differed from the two groups above in that they show the highest levels of inflammatory cytokines late in infection (e.g., IL-6, TNF-α, IL-1β) but were similar to Group 2 in terms of lethality. They showed the highest level of chemoattractant chemokines, particularly CCL2, CCL3, and CXCL10, and produced the highest levels of IL-10 and IFNγ detected in this study.

Finally, the fourth group of isolates, consisting only of KY/180, KY/190, and NY/18, were the most lethal of the viruses screened in mice. Their proinflammatory cytokines were elevated throughout the course, but not different from 3 DPI in Group 1 isolates. Most notably, these isolates failed to produce any IFNγ or IL-10 by 6 DPI. In Figure 3, the trajectory of these isolates point in an opposite direction from all other isolates, perhaps indicating a different course of disease. In summary (see Table 2.S5), the immune responses of the virus isolates clustered similar to other phenotypic markers of virulence and lethality (Table 2.2).

In-depth comparison of the temporal progression of survival, viral load and immune responses of two clinical isolates, KY/136E and KY/180E, with low and high virulence, respectively.

KY/136E and KY/180E were selected from the nine H1N1pdm clinical isolates for further characterization as representatives of lower and higher virulence based on the apparent disease in mice. These isolates had similar concentrations of lung cytokines and chemokines on 3 and 6 DPI compared to other isolates and clustered together in the PCA. However, the time-resolved PCA revealed that the isolates differed in the progression of immune responses in the course of infection. To gain additional insight, we first assessed dose response to infection in DBA/2 mice. Mice were infected with 10^0, 10^2 or 10^5 TCID$_{50}$ of KY/180E or KY/136E and examined daily for clinical signs. Each day, mice were weighed and data from each dose group are presented in Figure 4A (KY/136E) and Figure 4B (KY/180E). The Kaplan-Meier survival curves of mice infected with KY/180E or KY/136E (Figure 2.4C and 2.4D, respectively) confirmed the observations reported above in terms of the general lethality of each virus, although KY/136E did show lethality in 1-2 mice on 10 DPI (Figure 2.4C). Mice infected with KY/180E succumbed to infection starting at 3 DPI at the high dose and on 6 DPI for the middle dose (Figure 2.4D). Animals were humanely euthanized upon showing a moribund state or upon a 25% loss in body weight as described in the materials and methods.

The levels of infectious virus present in the upper and lower respiratory tracts, nasal turbinates (NT) and lung, respectively, were measured at 1, 3 and 5 DPI at the three

different doses (10^0, 10^2 or 10^5 pfu per mouse) of KY/180E or KY/136E (Table 2.S3).

As expected, levels of virus were greatest in mice with higher doses of infection. Mice

infected with KY/180E persisted at higher levels of virus over the 5 day period as

compared to KY/136E which had approximately 2-3 logs lower virus in the lungs and

had virus levels that decreased from 3 to 5 DPI. The infectious dose (ID_{50}) and lethal

dose (LD_{50}) were $<10^0$ $TCID_{50}$/mouse and $10^{1.2}$ $TCID_{50}$ per mouse, respectively, for

KY/180E (data not shown).

To further dissect the immune responses of these two viruses, multiplex

cytokine/chemokine bead arrays were employed to insight into the temporal patterns for

the key cytokine and chemokine profiles responses noted in the broad survey of all the

isolate. Mice (5 per group/per day) were infected with each of the isolates and humanely

euthanized on 1, 3, and 5 DPI (Figure 2.5 and 2.6). There was an overall increase in

proinflammatory cytokines (TNFα, IL-1β, IL-6 and KC) in the lungs of all mice,

however, there were much higher levels of all cytokines in lungs of mice infected with

KY/180E. Further the responses were much earlier and correlated with the high levels of

infection noted in the lung. In contrast with KY/180E, KY/136E-infected mice showed a

gradual progression in immune response, however, the overall responses on 6 DPI of

KY/136E remained low. Interferon-alpha (IFNα) and IL-12p70 levels were higher in the

lungs of KY/180E-infected mice as compared to KY/136E-infected mice (Figure 2.S2).

Virus-infected mice that recovered from KY/136E infection showed a high IL-10

response by 6 DPI whereas KY/180E-infected mice showed no response (Figures 1 and

5, $p < 0.05$). As expected, and also shown in Figure 1, the IFNγ levels were low in the

lethal KY/180E isolate as compared to the robust response observed in the nonlethal

KY/136E isolates at 6 DPI (no statistically significant difference).

Mice infected with the middle dose of KY/180E that survived after 6 DPI, and produced

high concentrations of IFNγ, eventually became moribund with all but one euthanized by

Day 10. These data suggest that the immune response differences between the two

isolates are due to the high levels of infection in the lung by KY/180E. The levels of

cytokines and chemokines in the lung support this observation (Figures 2.S3-2.S6),

showing a dose response for both isolates on 1, 3, and 5 DPI in mouse lung homogenate.

Notably, a dose of 10^2 pfu/mouse of KY/180E showed a progressive increase in

chemotactic chemokines to 5DPI whereas a higher dose (10^5 pfu/mouse) began declining

in concentration of these analytes after 3DPI (Figure 2.S3). Similar patterns were seen

for proinflammatory cytokines in the lung (Figure 2.S5) and cytokines involved in

adaptive immunity initiation, IFNγ and IL12p70 (Figure 2.S6). The endpoint titer IgG

responses of the mice for the low and middle doses were similar for both viruses (Figure

2.7; all significantly different from control using Student's t-test, $p < 0.05$). Further, the

HI titers were also very similar except for the lower dose, which was about 2-fold higher

in mice infected with KY/180E (Figure 2.7).

The leukocyte chemoattractant chemokines CCL2, CXCL10, KC (CXCL8-like), and G-

CSF were greater and earlier in the lungs of mice infected with high doses of KY/180E

than with a similar dose of KY/136E (Figure 2.6, $p < 0.05$). As expected, cytospins of

BAL revealed that KY/180E contained more neutrophils and monocytes on Day 4

74

compared to KY/136E (Figure 2.8A,B, $p < 0.05$). Additionally, we observed a higher

proportion of macrophages in the lungs in the low dose group of KY/136E compared to

the higher dose group ($p < 0.05$, Figure 2.8C). Despite there being a greater number of

infiltrating leukocytes in the lungs of KY/180E-infected mice, these mice had a delayed

clearance of virus in the lung.

Given the apparent clearance of virus from the lungs of KY/136E (Table 2.S4), we were

interested in whether the apparent differences in lethality of the two viruses could be due

to the site of virus replication. We tested virus titers from bronchoalveolar lavage fluid

(BALf), from the cellular pellet of the BALc (BALc) of the mice, and from the

homogenized lung after lavage using TCID$_{50}$ assay. Samples were collected on 3 and 4

DPI because we began to see decreases in viral titer in the lungs of KY/136E-infected

mice after 3DPI. In our earlier studies (Table 2.S4), the virus titer in lung reflects lung,

BALf, and BAL cells combined and we observed a nearly 3 log difference between

KY/136E and KY/180E. When BAL is collected before isolation of lung tissue, we found

the majority of infectious KY/136E virus present in lungs of mice was localized in the

cellular fraction of the BAL (Figure 2.9). In contrast to KY/180E, no infectious KY/136E

virus was present in the BALf by 4 DPI. Flow cytometric analysis revealed that the

influenza NP-positive cells in the BAL from both isolates were also Gr1-positive (clone

RB6-8C5), a marker of mouse phagocytic leukocytes, *i.e.*, Ly6C/Ly6G positive (Figure

2.8D).

Infection and replication of H1N1pdm viruses in macrophage cell lines

Given the differences noted within the levels of virus in BALf and BALc, we used a

BALB/c mouse macrophage cell line (RAW264.7) and a C57BL/6 mouse macrophage

cell line (NR-9465) to test for the ability of KY/136E and KY/180E to infect and

replicate in macrophage cells. Confocal microscopy at 24 hours post-infection showed

that both viruses were able to infect macrophage cell lines (Figure 2.10). However,

KY/180E was more efficient at replication, reaching 10-fold higher virus titers that

persisted longer in both cell culture systems (Figure 2.11 and Figure 2.S7). Although the

cell culture supernatant was positive at 24 hours post-infection for both viruses *in vitro*,

KY/180E was the only isolate detected from the cellular component in BAL (Figure 2.8;

$p < 0.05$ at 24 and 48 hours post-infection). These observations agree with our findings

in the DBA/2 mouse model and suggest that KY/180 is more successful *in vivo* in

replication and production of infectious virus in macrophages (Figure 2.8).

Discussion

Herein we present data characterizing several isolates of H1N1pdm influenza virus taken

from human patients with severe pneumonia in Kentucky, USA. Clinical surveillance

from foci around the world showed that the majority of human cases of H1N1pdm were

mild (36, 556). Severe disease from H1N1pdm infection was more likely to be seen in

patients with pre-existing chronic illness (557). It was initially observed that antigenic

and genetic variation in circulating pdmH1N1 2009 influenza viruses was less than what

is seen during seasonal human influenza A (H1N1) (38). Similarly, the isolates listed

here show relatively low variation, differing at only 43 amino acid positions. Each

isolate contained from 2 to 12 unique non-synonymous mutations from the consensus sequence.

Three of the 4 lethal cases occurred in western Kentucky, and 1 of these lethal cases (KY/180) contained a virus isolate with the avian-like HA RBS (G222). The D222 is most commonly associated with human H1 strains while the G222 is common in avian strains. The HA 222 position, D222G/N/S/E/Y, was a common polymorphism in severe cases of influenza in human patients, which is within the HA receptor binding site, RBS (547, 558-561). Additionally, the D222G has been associated with increased pathogenesis in some animal models possibly due to increased replication of the virus (125, 129, 131, 558, 559, 562, 563). The aspartic acid functions in binding of the receptor and as a calcium antigenic site. Each of these amino acids will give rise to a specific binding affinity to the α2-6-sialic acid receptor with the D222G increasing α2-3-sialic acid receptor binding specificity (125, 224, 563). However, it is clear that other amino acids constellations at positions 183, 186, 187, 216 and 224 will also influence these interactions (127), and may result in different overall outcomes. Additional amino acid signatures in closely related H1N1pdm isolates have also been implicated in differences in virulence in animal models. For example, in a study in a cynomolgus macaque model of two highly similar strains of H1N1pdm, A/Mexico/4487 and A/Mexico/4108, showed notable heterogeneity in virulence (137). The amino acid variations responsible for the differences noted in these studies have not yet been reported. The HA1 of KY/180E also has a P183 (noted as 186 in (552)) rather than a S183 at the Sb antigenic site, which also has been noted to affect receptor specificity ((553-555)). This site, independently or

77

together with the D222G mutation, is thought to allow binding to α-2,3 linked sialic acid residues. This substitution may allow the virus to more efficiently enter and replicate in the lower airway epithelium (276, 555, 564, 565).

Other mutations observed in the HA gene of the Kentucky isolates have also been reported by others. Belser, *et al.* (2010) published data that showed A/CA/04/09 also has the S83P mutation in HA (as in KY/180E), although this mutation is not a known pathogenicity determinant (247). Ilyushina, *et al.* (2010) found the S183P (as seen in KY/180E) mutation arose from serial passage of A/CA/04/09 in mice and resulted in increased pathogenicity (553). Xu, *et al.* (2011) report isolates from China show similar variability and share some of our mutations in HA (S83P, T203S, and V321I; seen in KY/180E, KY/96E, and KY/80E, respectively), as well as mutations in NS1 (V123I, seen in KY/99E) and PA (V14I, seen in KY/180E) (566). Melidou *et al.* have data that suggest V321I mutation in HA may be associated with increased disease severity (134). Finally, HA1 amino acid mutation Q293H, identified in KY/96E, has been associated with increased severity of disease observed in human cases during the pandemic (106, 134). We include a summary of those mutations that correlate with virulence in humans and mice (Table 2.S6). An understanding of these and other signatures associated with more virulent phenotypes will benefit insight into the biology of the virus, patient management and public health responses.

In total, KY/180E contains mutations that differ from KY/136E in seven amino acid sites in the HA protein, four sites in PA, two sites in NA, PB1 and PB2, and one site in each of M1, NS1, and NP. Comparison of the CA/07/09, NY/18, NL/602 isolates with the KY isolates showed additional variation among all isolates (Table 2.S2). Specifically, CA/07/09, NY/18, NL/602 were similar to the KY consensus in M, HA2, PA, PB1 and PB2, In HA1, a Q223R occurred in NY/18 only. In NA, a D248N changed occurred in CA/07 and NL/602. In NS1, a D247N was noted for KY/110, CA/07, NY/18, and NL/602. Most additional changes were conserved hydrophobic changes such as Val to Iso or Met to Leu. No differences were observed among the KY, CA/07/09, NY/18, NL/602 isolates in M2 or NS2 (Table 2.S2). Despite the small apparent genomic variation between H1N1pdm isolates, we and others have shown that there exists substantial variation in the course of disease, pathogenicity, and immune response in human patients, in animal models, and in primary cell culture (106, 135, 137, 566, 567). As virulence determinants of influenza viruses typically involve the genes encoding the HA, NA, and polymerase proteins, we would expect changes in these genes to be of future interest for biological function (568). Addition genome diversity that might give rise to unique phenotypes during infection may be revealed be deep sequencing or isolation of clones that sample the population of the virus (549).

To gain insight into the potential phenotypic variability inferred from the genotypic variability each virus was screened in DBA2 mice. All IAV tested so far, H1N1pdm, 1918 H1N1, and seasonal influenza A H1N1 virus, infect DB2 with varying levels of lethality without adaptation (569), and express comparatively high levels of

proinflammatory cytokines and chemokines (570, 571). Herein all DBA2 mice showed

high levels of infection with all isolates similar to infection of BALB/c mouse with

H1N1pdm viruses (247, 542) with relatively little difference between the various isolates

on 3 and 6 DPI ($p > 0.05$ using pairwise Wilcoxon Rank-Sum test without correction for

multiple comparisons, Table 2.2). However, the isolates did show three groupings in

lethality (lethal, moderately lethal and not lethal) in DBA2 mice with KY/180, KY190

and KY/96 showing the highest lethality. Using a statistical method, PCA, we asked if

based on these differences in lethality we might be able to cluster cytokine and

chemokine responses across the H1N1pdm isolates. To our knowledge, this is the first

time this method (a "time-resolved" PCA) has been used to discriminate phenotypic

characteristics of viruses. Classically PCA is used as a method to reduce multivariate

data so that they are better suited for a predictive statistical model. The most common

contemporary usage of PCA in microbiology is during the analysis of gene expression

arrays to check reproducibility of replicates. We chose to use the PCA method because

of its similarity to common clustering algorithms (specifically, k-means clustering), and

therefore its potential to elucidate clusters of the immune response of mice after infection

with genetically similar influenza isolates. Our approach relied on two defined time

points to detect differences between virus isolates using expression of multiple immune

markers. Although some of the markers used in this analysis may be redundant in a virus

model (*e.g.,* pro-inflammatory IL-6 and CXCL10), subtle differences that may go

unnoticed are seen using this multivariate approach, particularly in the timing of these

responses (and not necessarily the magnitude). Therefore, using indicators of adaptive

immune priming (IFNγ) and reduction of inflammation (IL-10) were critical to the

successful implementation of this strategy. More data of this kind from other influenza

isolates and other respiratory virus infections may assist in the development of this

method, and may reduce the number of soluble immune markers needed for analysis in a

clinical setting.

Analyses of our data suggest that there are at least two main trajectories of H1N1

influenza infection in these mice: one that successfully resolves infection, and one that

does not. The majority of the isolates followed a trajectory that led to resolution and

clearance of the virus from the lungs. These isolates could be further clustered into three

subgroups, and these subgroups differ according to the overall immunogenicity of the

isolates (*i.e.,* the levels of cytokines/chemokines in the lung). In general, the isolates

showing the least mortality in DBA2 mice share in common a trajectory of disease that is

characterized by a gradual increase, then decrease, in inflammatory cytokines and

leukocyte chemoattractant chemokines, and concomitant increase in anti-inflammatory

cytokines and IFNγ. The isolates causing the highest lethality in the DBA2 mouse

(KY/180E, KY/180M, and KY/190M) showed an early rise in the proinflammatory

cytokines and chemokines, and a delayed or absent rise in IL-10 and IFNγ. The lethal

isolates were clearly differentiated using the time-resolved PCA in that they showed a

trajectory that was opposite of all other isolates. The small sample size of human patient

data and their confounding comorbidities limit the inferences that can be made

connecting locale, age, sex, and length of hospital stay with genotype and pathogenicity

of the isolates in the human patients. Recent data suggest that human polymorphisms in

genes that restrict virus infection (e.g., *Ifitm3* gene) may also play an important role in outcome (572). A final challenge is there are no relevant scoring systems for influenza pneumonia. A pneumonia severity index (PSI) is commonly used in hospitals by clinicians for community acquired pneumonia, but the comorbidities (e.g. high BMI, diabetes) complicate interpretation.

Selecting two isolates, KY/180E and KY/136E we sought to better define two of these trajectories in DBA2 mice. We initially observed KY/136E had a low level of immunogenicity in mice, which included an increase in IL-10 and IFNγ by day 6. Although mice infected with KY/136E are similar to KY/180E in concentration of IFNα, G-CSF, CCL2, KC, IL-6, CXCL10, and other inflammatory cytokines and chemokines in the lung, the isolates differ in the timing of these responses. Increases in these cytokines and chemokines are typically seen during infections with H1N1pdm influenza isolates (112, 395, 542). For example, some studies show that IL-6 is released in response to influenza infection and that levels of IL-6 in the upper respiratory tract and in blood correlate with symptoms (101, 393, 573).

Type-I interferons are known to initiate the anti-viral response to influenza virus infection. One hypothesis to explain a more severe course of illness is that the virus is capable inhibiting the effect of type-I interferon signals via NS1 protein (298, 306). The NS1 protein from KY/136E differs from KY/180E in a single amino acid at site 112 (112M versus 1121I, respectively). By day 1 post-infection, mice infected with KY/180E

had a higher level of IFNα in the lung. Despite an increased IFNα and IL12-p70 response, mice infected with KY/180 failed to produce IFNγ, IL-10, and serum antibodies by 6 DPI. This most closely resembles the type of aberrant immune response seen during infections with the pandemic 1918 Influenza A (H1N1) (574, 575) and with severe seasonal influenza isolates (71). Others have shown similar patterns of inflammation with isolates of pandemic 2009 H1N1 influenza (135, 560, 576).

Cytokines and chemokines such as CCL2 (MCP-1), CCL3 (MIP1α), CCL5 (RANTES), and CXCL10 (IP10) are responsible for activating leukocytes and attracting them to the lung compartment to clear infection (337). Indeed, there were a higher number of leukocytes, including elevated numbers of neutrophils and monocytes, seen in the lungs of KY/180E-infected mice on days 3 and 4 post-infection. It is known that certain pathogenic H1N1 strains, such as the 1918 H1N1 strain, causes the increased neutrophil recruitment to the lung due to increased chemokine responses (577, 578), which was seen with KY/180E. Neutrophils are important for assisting in clearing influenza-infected cells from the lungs directly and indirectly (579, 580), but the precise mechanisms remain to be discovered (78, 86, 577). Although important to the resolution of influenza virus infection, neutrophils contain cytotoxic granules that may cause severe pathology, and may contribute to morbidity and mortality (84). An increase in neutrophils late in disease confers the pathogenicity seen in highly pathogenic strains of influenza viruses (86).

Natural Killer (NK) cells are known to be potent innate immune cells that recognize influenza hemagglutinin (581). Classically, NK cell effector functions include release of IFNγ and direct cytotoxicity to influenza-infected cells by granule exocytosis (*e.g.,* granzyme B and perforin). Mice infected with KY/180E have higher numbers of peripheral NK cells at 3 DPI compared to KY/136E using flow cytometry (data not shown). Consistent with this finding, CCL5 (RANTES) was increased in the lungs and serum of mice infected with KY/180E compared to KY/136E (Figure 2.2). NK cell deficiency in mouse models of influenza infection leads to increased pathogenicity (582, 583). Despite the increase in NK cells in KY/180E-infected mice, it has been shown that some influenza isolates may counteract this effector response, causing lysosomal degradation of the ζ chain, which is a critical component of the NK-activating receptor (584). Additionally, DBA2 mice lack the NKG2A activating receptor that is responsible for recognizing the down-regulation of MHC-I that typically occurs with a viral infection (585). Therefore, KY/180E may be able to exacerbate this deficiency by decreasing NK cell effector function. It has been shown that NK cells also contribute to immune pathology in response to influenza and other respiratory virus infections (586).

Finally, this study and others have shown that some strains of influenza virus are capable of infecting macrophages (587-590), and may alter their functionality in response to infection (591, 592). During influenza infection, alveolar macrophages are critical in clearing virus from the lungs and are key producers of IFNγ to stimulate the adaptive immunity (321, 353, 378, 577, 578, 586, 593-595). Upon infection, influenza viruses

may interfere with their normal function (341, 595, 596). Of the two isolates tested here, mice infected with KY/136E showed clearance of virus from the lung by day 4. (341, 595, 596). Our *in vitro* data using mouse macrophage cell lines indicates that KY/180E was able to produce infectious virus better than KY/136E. Additionally, mice infected with KY/180E had a higher number of Gr-1 positive infiltrating cells into the lungs by day 4, a delayed IL-10 production, and very low levels of IFNγ resulting in a deficient virus clearance. Both our *in vivo* and *in vitro* data show that KY/180E can infect macrophages, which may affect the cell's ability to release IFNγ and explain the increase pathogenicity observed with this virus compared to KY/136E. Future studies will focus on understanding the mechanism(s) involved in the virus-induced deregulation of macrophage function *in vitro* and *in vivo*. Understanding the genetic basis for the differences in the interaction between the virus and macrophages as well as other pulmonary and immune cells will contribute to understanding the course of influenza infection in patients, and assist in predicting potential virulence during future outbreaks.

Materials and Methods

Detection of influenza in clinical nasopharyngeal swab specimens

Nasal swab samples were provided by the SIPS project. A nasopharyngeal swab was taken from all patients meeting the case definition, which was defined as a patient admitted to an intensive care unit with the physician diagnosis of community-acquired pneumonia. The University of Louisville Institutional Review Board Human Subject Protection Program Office (HSPPO) approved this study prior to any data collection (#08.0399). Informed consent was waived because it was a retrospective chart review and

the data were analyzed anonymously. The nasopharyngeal swabs were taken as part of 'standard of care' diagnosis. Detection of influenza virus was accomplished using the Luminex Respiratory Viral Panel (RVP) detection kit, recently approved for *in vitro* diagnostics by the FDA. The RVP is a reverse-transcriptase, real-time PCR assay which is multiplexed to detect 12 viral targets in a single reaction well. Those targets include Influenza A, Influenza A-subtype H1, Influenza A-subtype H3, Influenza B, RSV-A, RSV-B, Parainflunza 1, Parainfluenza 2, Parainfluenza 3, human metapneumovirus, Rhinovirus and Adenovirus. Nasal swabs were collected from each patient and placed in Universal Transport Media (Copan Diagnostics, Inc, Murietta, CA). A 5.0 µl aliquot was combined with 20 µl of RVP mastermix and processed through several rounds of amplification, including a single-tube multiplex reverse-transcriptase PCR, followed by a multiplex target-specific primer extension protocol, a bead-hybridization step, and finally a data acquisition step in the Luminex reader. Results are qualitative and read-outs are Positive, Negative or a No Call (equivalent).

Viruses and virus isolation

The viruses CA/07, NY/18, and BN/59 were kindly provided by the Centers for Disease Control and Prevention, Virus Surveillance and Diagnosis Branch, Influenza Division. Viruses from clinical cases from KY present in nasopharyngeal swab specimens were isolated and propagated in the chorioallantoic cavity of 10-day-old embryonated chicken eggs and MDCK cell line purchased from ATCC (CCL-34). The allantoic fluid containing infectious particles or MDCK supernate was harvested 72 h after inoculation. MDCK cells were infected in DMEM virus culture medium (DMEM containing 2%

BSA, 1% PEN/STREP, and 2 μg/mL of Trypsin-TPCK). The infectious virus titer of the resulting seed stock was determined by $TCID_{50}$ and the titer calculated by Reed and Muench (597), and confirmed by plaque assay on MDCK cells. Egg passage E2 was used for the studies involving KY/180E and KY/136E reported herein.

RNA isolation and sequencing

To sequence each of the gene segments of each H1N1pdm isolate, we followed the method described by Inoue et al (598) with minor modifications. In brief, total RNA was isolated with MagMAX AI/ND Viral RNA isolation kit (Ambion) from each virus seed stock solutions. Five μL of RNA was used to synthesize cDNA with SuperScriptase III (Invitrogen) using the FWuni12 and RVuni13 primers based on those reported by Inoue et al (598) and the cDNAs were PCR-amplified based with Accuprime (Invitrogen) The amplified products were separated by agarose gel electrophoresis and the DNA bands corresponding to the size of each segment were purified using the Wizard SV gel Clean-Up System (Promega). The purified DNAs were used as templates for automated dideoxy sequencing with BigDye 3.1 cycle sequencing kit (Applied Biosystems). To sequence the entire gene we used approximately 500 bp overlapping gene-specific primers in both directions. For the sequencing of HA gene, we used FWuni12, RVuni13, HA462_f (5′-GACTCGAACAAAGGTGTAACGG-3′) and HA1202_r (5′-GTCAATGGCATTCTGTGTGCTC-3′) as sequencing primers. For the sequencing of NA gene, we used FWuni12, RVuni13, NA_521r (5′-TGACCAAGCGACTGACTCAA-3′), NA376_f (5′-CCCTTGGAATGCAGAACCTT-3′) and NA905_f (5′-CGTGGGTGTCTTTCAACCAGAA-3′). The sequences were assembled with the

SeqScape™ program (Applied Biosystems). Alignments of nucleic and amino acid sequences were completed to identify polymorphisms with other H1N1pdm isolates and sequences for all isolates were submitted through the Influenza Research Database and uploaded into the GenBank (accession numbers provided in Table S4).

Ethics statement for animal studies

Mice studies were approved by the University of Louisville Institutional Animal Care and Use Committee with Veterinary Medicine tasked to monitor and support all animal experiments. Research was conducted in compliance with the Animal Welfare Act and other federal statutes and regulations relating to animals and experiments involving animals and adheres to principles stated in the *Guide for the Care and Use of Laboratory Animals*, National Research Council, 1996. The facilities where this research was conducted in a fully accredited by the Association for Assessment and Accreditation of Laboratory Animal Care International.

Mice studies

Six to nine-week-old female DBA/2 mice were purchased from Jackson Laboratories (Bar Harbor, ME) and housed in the vivarium managed by UofL at the Research Resource Center or at the Regional Biocontainment Laboratory. The mice received food and water *ad libitum,* and all experiments were conducted in accordance with rules of the Institutional Animal Control and Use Committee of UofL. Mice were anaesthetized by isofluorane inhalation and infected intranasally with in a total volume of 30 µl at the dose as outlined in the figure legends and text. Viruses were adjusted to the dose required in

PBS (pH 7.2). Animals were observed daily for morbidity and measured for weight loss. All mice showing more than 25% body weight loss were considered to have reached the experimental end point and were euthanized humanely.

Mice were euthanized on the days noted in the results and on figure legends and blood, nasal turbinates and lung tissues were collected and stored appropriately until analyses. For collection of BAL after euthanasia, the neck and thoracic area were disinfected by soaking with 70% ethanol, and the trachea exposed by dissection. An 18G catheter needle was inserted into upper trachea, the needle removed, and the outer catheter sheath moved into the lower trachea. A 3 mL syringe filled with 1 mL of DPBS was used to carefully inject DPBS into the lungs, and aspirate BAL fluid. Collected fluids were transferred to an ice-cold, sterile 15 mL conical tube on ice and repeated once more as above. BAL fluids were immediately centrifuged at 500g for 10 minutes to separate fluids and cells. After centrifugation, supernatants are separated and kept separately at -80°C freezer until used for TCID$_{50}$ assay. Cells pellets were washed once by adding 2 mL ice-cold DPBS and centrifuged again at 500g for 10 min. Cells were resuspended in 1 mL DPBS and kept at -80°C until used.

TCID$_{50}$ assay for viral load in tissues and bronchial lavage fluid

Tissues were homogenized in ice-cold virus culture medium (DMEM containing 2% BSA, 1% PEN/STREP) within a biosafety cabinet. Tissue homogenates were clarified by centrifugation (4000g for 20 min at 4°C) prior to storage at -80°C, and later analyzed by TCID$_{50}$ or Luminex cytometric bead array (next section). For measurement of the level of infectious virus present in tissue samples, the titers of the virus were determined by

TCID$_{50}$ assay by titration of the clarified tissue homogenates or BALf on MDCK cells. The limit of virus detection was typically $10^{1.5}$ TCID$_{50}$/ml or as indicated in each figure. Virus titers were calculated by the method of Reed and Muench (597), and are expressed as the mean log$_{10}$ TCID$_{50}$ per milliliter. Tissues in which no virus was detected were given a value of $10^{1.0}$ TCID$_{50}$/ml for calculation of the mean titer.

Quantification of cytokine and chemokine levels in lungs

Sera and lungs from mice euthanized on days as noted in figure legends and text were analyzed by using Luminex® xMAP® technology-based assay kit (Millipore) according to the manufacturer's protocol. The final reaction plate was read with a Luminex 100 or FlexMAP 3D machine and specific concentrations were calculated from a standard using Luminex xPONENT software.

Statistics and PCA

R (version 2.13.0) base statistical package and GraphPad software package were used in the analysis of data and generation of figures. Generalized linear models were constructed using each analyte included in the initial screen of Kentucky isolates in DBA/2 mice as a response variable (cytokine/chemokine concentrations) and isolate, DPI, and egg vs. MDCK stock, were used as predictors. The stock designation of the virus was removed from the model after it was seen that it did not contribute to explain significant proportion of the variance. Log likelihood ratios were used to compare the relative fit of each model, and the top 12 models showing the highest parameter estimates for the isolates were chosen for inclusion into the PCA (*i.e.,* the cytokines/chemokines

that were the most different between isolates, controlling for DPI, selected from the best-fit models). The R package "FactoMineR" (version 1.14) was used to perform the PCA. Statistically significant differences between multiple groups was assessed using Kruskal-Wallis tests followed by *post hoc* tests using pairwise Wilcoxon Rank Sum tests unless otherwise noted. Multiple comparisons were adjusted according to Holm's method and a *p*-value < 0.05 is considered significant.

Cytospin and flow cytometry

BAL cells were centrifuged at 300g for 5 min and washed twice in PBS. Cells were resuspended in 0.4 mL PBS and loaded into Shandon Cytospin™ centrifuge funnels. The cytocentrifuge chambers were spun at 1000 rpm for 5 min. Slides were air dried in a BSC and then were fixed and stained with Eosin and Methylene Blue (Kwik-Diff, Thermo Scientific). Slides were inspected under a light microscope.

For flow cytometry analysis, BAL cells were washed in PBS as above and stained with antibodies specific to mouse CD3 (500A2 Pacific Blue, BD Biosciences), Gr-1 (RB6-8C5 phycoerythrin, eBioscience), and CD49b (DX5 phycoerythrin-Cy7, eBioscience). Cells were then washed and fixed in 4% paraformaldehyde for 15 minutes at room temperature, followed by permeabilization with 0.2% saponin in 2% BSA for 20 minutes. Cells were then stained intracellularly for influenza nucleoprotein using a fluorescein isothiocyanate conjugated antibody (NP-FITC, AbCam #ab20921) for 30 minutes. Cells were washed and analyzed on a FACSAria II flow cytometer (BD).

Mouse macrophages experiments

RAW264.7 cells (ATCC #TIB-71) were seeded onto glass chamber slides (LabTek) and allowed to rest overnight. The cells were gently washed in PBS and virus was added at 1.0 MOI. The cells were washed and fixed at 24 hours post-infection and permeabilized with 0.2% saponin in 10% FBS. Cells were stained for intracellular influenza nucleoprotein as above, and a nuclear counter stain was included for the final 10 minutes (TO-PRO3, Molecular Probes). Cells were washed, mounted under a coverslip with ProLong Antifade media (Invitrogen), and visualized using a Zeiss LSM/710 confocal microscope. Kinetics of infection were determined by infecting mouse macrophage cell lines, RAW264.7 or BEI Resources #NR9456 (NIAID, NIH), in triplicate wells of a 24-well plate in DMEM supplemented with 0.2% BSA, 1% Pen/Strep, 2.5% L-glutamine, and 25 mM HEPES. Supernatants were taken and centrifuged prior to performing a TCID50 assay using MDCK cells. Virus titers were confirmed at 24 hours using a plaque assay.
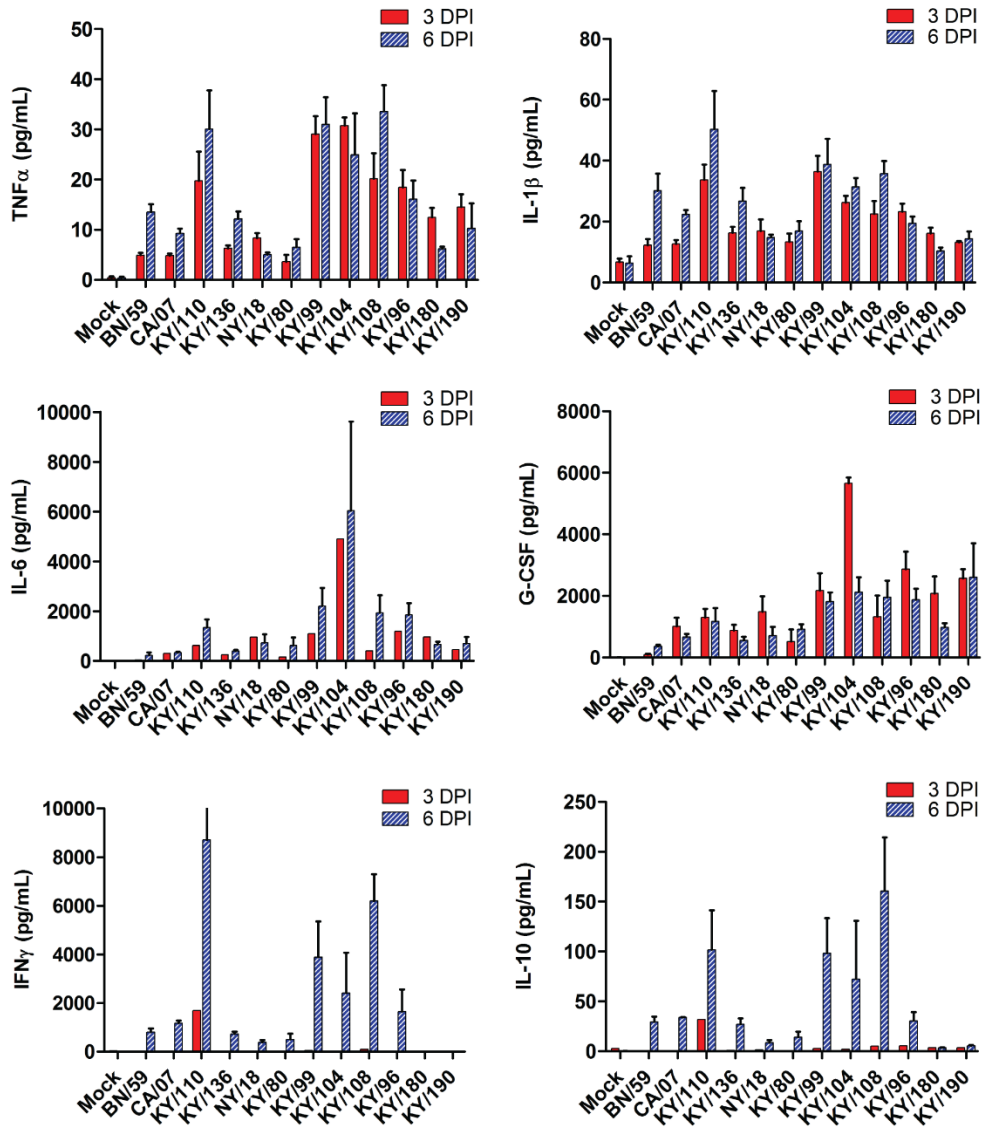
Figure 2.1 Cytokine levels in mice infected with pandemic and seasonal H1N1 influenza viruses.

Six to eight week old DBA/2 mice were infected intranasally with 10^5 TCID$_{50}$ with a seasonal virus isolate (BN/59), Kentucky (KY/80, KY/136, KY/96, KY/99, KY/104, KY/108, KY/108, KY/110, KY/180, KY/190) or other H1N1 pandemic isolates (CA/07, NY/18) from 2009. Cytokine levels were measured at 3 and 6 DPI as described in the materials and methods and presented as mean +/- SEM (n=6 per group, although fewer animals were available for lethal isolates).
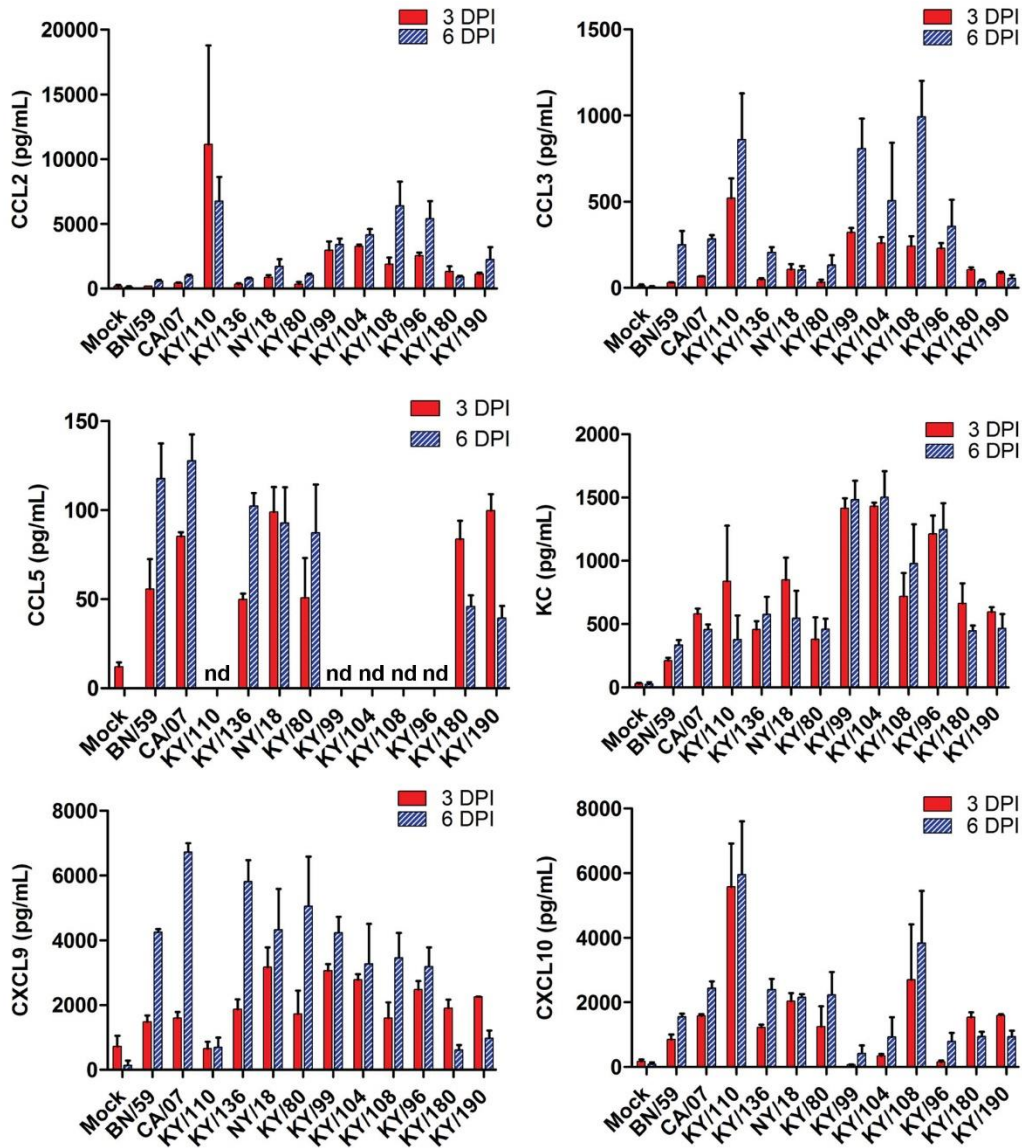
Figure 2.2 Chemokine levels in mice infected with pandemic and seasonal H1N1 influenza viruses.

Six to eight week old DBA/2 mice were infected intranasally with 10^5 TCID$_{50}$ with a seasonal virus isolate (BN/59), Kentucky (KY/80, KY/136, KY/96, KY/99, KY/104, KY/108, KY/108, KY/110, KY/180, KY/190) or other H1N1 pandemic isolates (CA/07, NY/18) from 2009. Chemokine levels were measured at 3 and 6 DPI as described in the materials and methods and presented as mean +/- SEM (n=6 per group when possible).
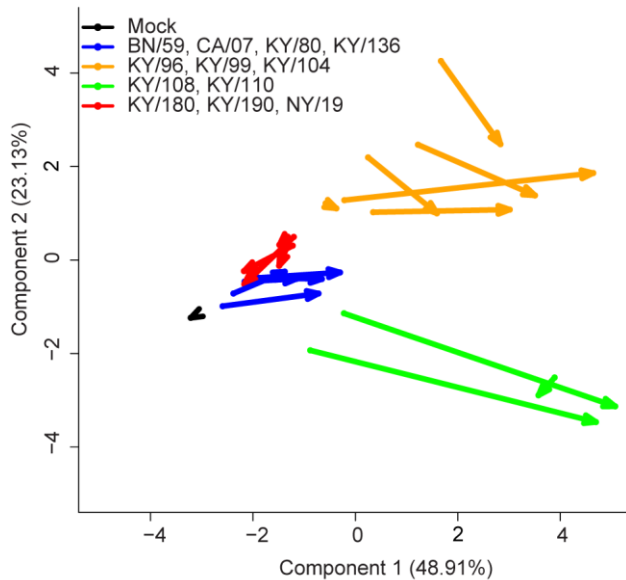
Figure 2.3 Principal components analysis of immune responses in lungs of mice to infection with pandemic and seasonal influenza viruses.

A principal components analysis was performed using the 14 cytokines/chemokines analytes shown to be the most significantly different across all isolates from days 3 and 6 (determined by generalized linear model fitness testing, data not shown). The data were normalized and scaled (zero mean-centered) cytokine responses after influenza infection at 3 and 6 DPI for all viruses. The ordinate and abscissa represent the first and second components from the PCA, which explain approximately 72% of the variance. Each arrow represents the mean of a virus isolate tested in mice. Arrow tails represent day 3 components and arrow heads represent day 6 components. Using this tool to visualize the immune response, the arrows depict the trajectory of disease of the various influenza isolates as tested in DBA/2 mice. Additionally, the 12 virus isolates clustered into four distinct patterns: Group 1, BN/59, CA/07, KY/80, KY/136; Group 2, KY/96, KY/99, KY/104, KY/108; Group 3, KY/108, KY/110; Group 4, KY/180, KY/190, NY/18 (See Table 2.S5).
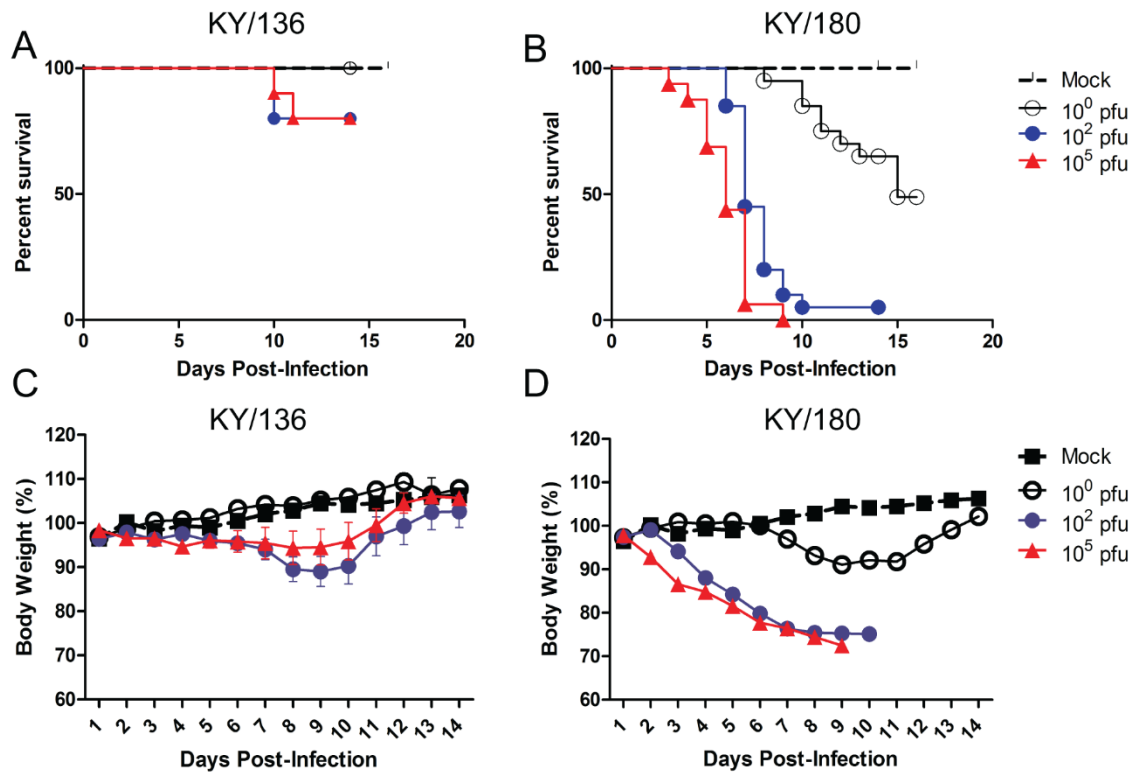
Figure 2.4 Weight loss and Kaplan-Meier curve of mice infected with KY/136 and KY/180.

Mean weight change (+/- SEM) after six to eight week old DBA/2 mice were infected intranasally with 10^0, 10^2 and 10^5 TCID$_{50}$ with KY/136E (A) or KY/180E (B). Mice were examined daily for clinical signs and weighed (n=10 mice per virus group). Kaplan-Meier Survival curves for these mice show KY/136E to have low lethality (C) compared to KY/180E (D).
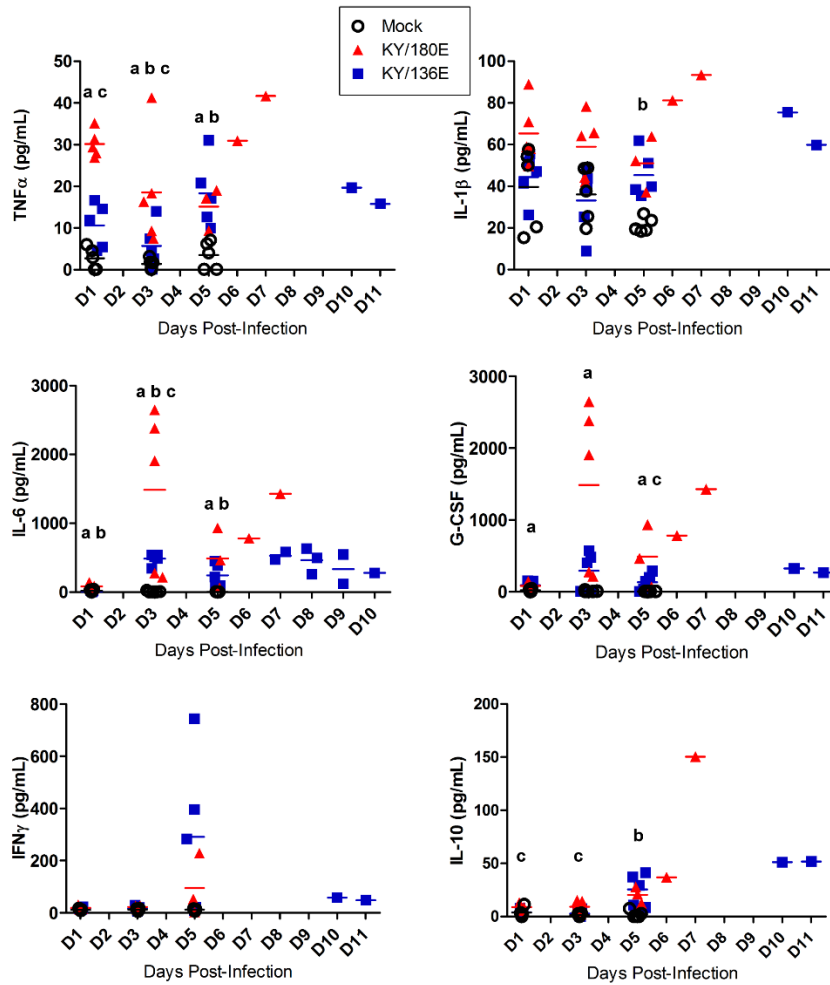
Figure 2.5 Cytokine levels in mice infected with KY/136 or KY/180.

The levels of notable cytokine responses are shown for 1, 3 and 5 DPI in six to eight

week old DBA/2 mice that were infected intranasally with 10^5 TCID$_{50}$ of KY/180E or

KY/136E (n=10 mice per virus group per time point).   Statistical significance was

determined by day using Kruskal-Wallis test followed by pairwise Wilcoxon Rank Sum

post hoc test with Holm's adjustment for multiple comparisons. P-values < 0.05 are

indicated by the following method: "a" = KY/180 is significantly different from mock;

"b" = KY/136 is significantly different from mock; "c" = KY/180 is significantly

different from KY/136.
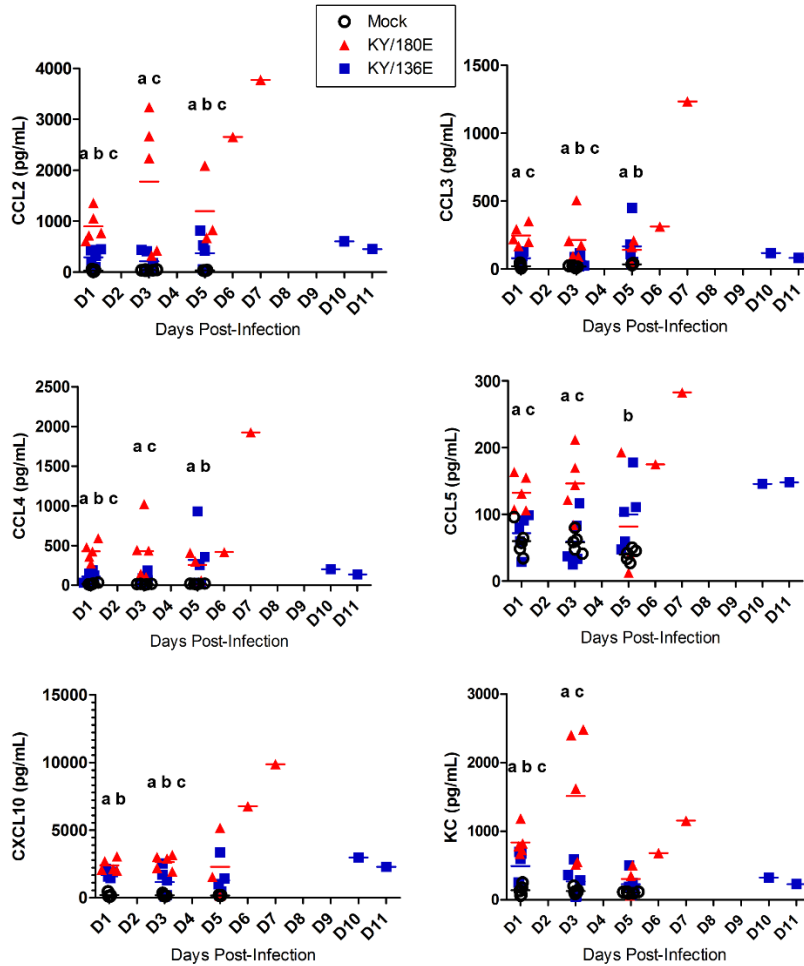
Figure 2.6 Chemokine levels in mice infected with KY/136 or KY/180.

The levels of notable chemokine responses are shown for 1, 3 and 5 DPI in six to eight week old DBA/2 mice that were infected intranasally with 10^5 TCID$_{50}$ of KY/180E or KY/136E (n=10 mice per virus group per time point). Statistical significance was determined by day using Kruskal-Wallis test followed by pairwise Wilcoxon Rank Sum post hoc test with Holm's adjustment for multiple comparisons. P-values < 0.05 are indicated by the following method: "a" = KY/180 is significantly different from mock; "b" = KY/136 is significantly different from mock; "c" = KY/180 is significantly different from KY/136.
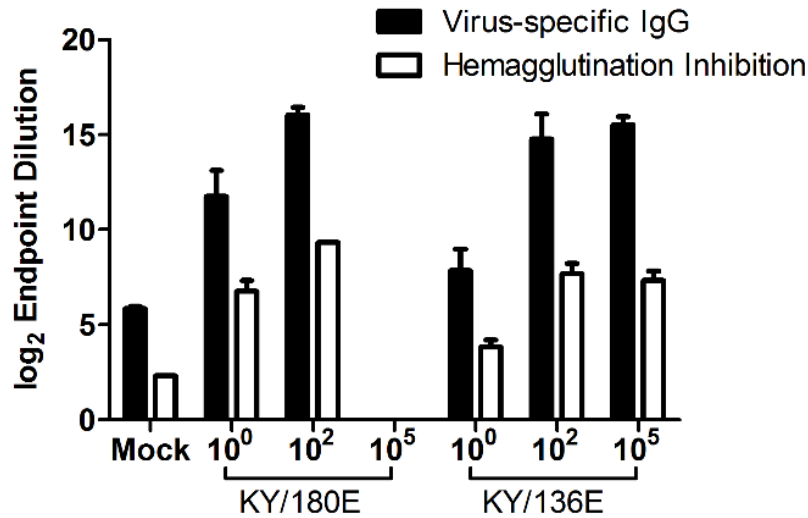
Figure 2.7 IgG responses of mice infected with different doses of KY/136 or KY/180.
Serum from day 20 post-infection was taken from six to eight week old DBA/2 mice that
were infected intranasally with 10^0, 10^2 and 10^5 $TCID_{50}$ of KY/180E or KY/136E (n=10
mice per virus group per time point). Influenza-specific (A/NY/18/09 BPL-inactivated
whole viral antigen) IgG titers were measured by ELISA and presented as average log2
endpoint titers (+/-SEM). No mice survived to day 20 at the high dose of KY/180. All
endpoint titers for animals infected with influenza virus isolates were significantly
different from mock ($p < 0.05$). Endpoint titers for both IgG and HI from animals
infected with KY/180 were significantly different from the same dosage amount of
KY/136 ($p < 0.05$).
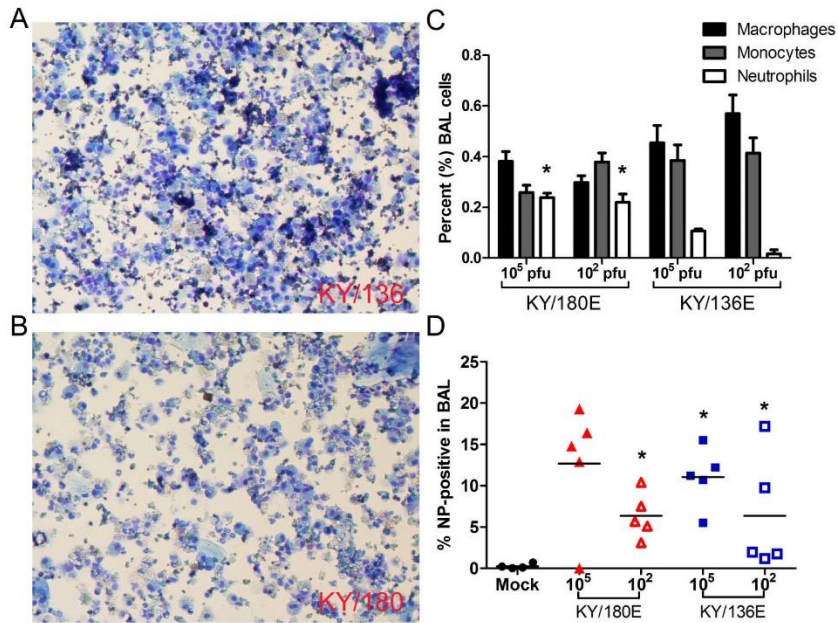
Figure 2.8 Cells within bronchial lavage fluid of mice infected with KY/136 or KY/180.
The cells within the bronchoalveolar lavage fluid (BALf) at 4 DPI from DBA/2 mice
infected with 10^5 TCID$_{50}$ of KY/136E (A) or KY/180E (B) (n=5 mice per virus group per
time point) were affixed to slides by cytospin centrifuge and stained (Kwik-Diff).
Microscopic images from three fields per slide were counted by three blinded,
independent observers. (C) The average number of macrophages, non-specific
monocytes, and neutrophils are presented as a percent of the total cell count (+/- SEM).
There were significantly more neutrophils in the BALf of mice infected with KY/180E
virus ($p < 0.05$, indicated by asterisks). (D) Cells in the BALf were fixed, permeabilized,
and stained with anti-influenza nucleoprotein (NP)-FITC antibody conjugate and
analyzed by flow cytometry. There were significantly more NP-positive cells in mice
infected with KY/180 at a dose of 10^2 TCID$_{50}$, and in mice infected with KY/136
compared to mock-infected controls ($p < 0.05$, indicated by asterisks). 80% of NP-
positive cells were Gr-1 positive (macrophage or neutrophil).
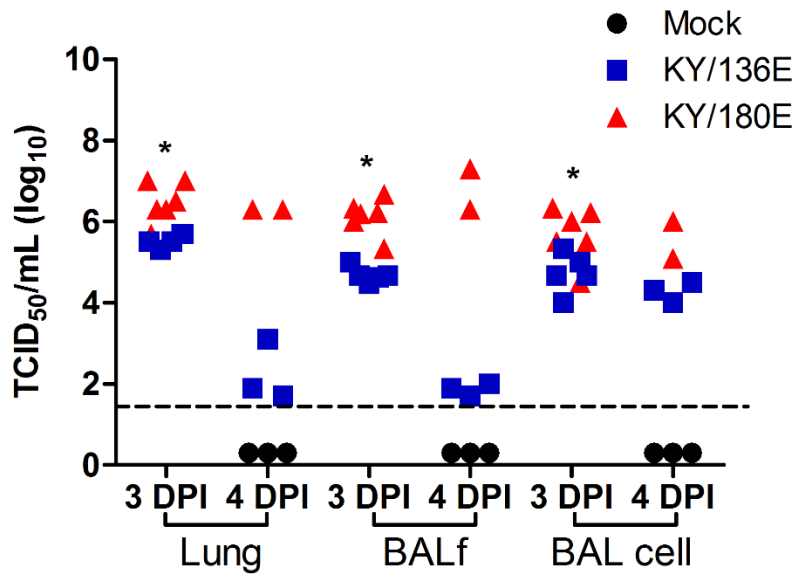
Figure 2.9 Virus titer the in lung compartments of mice infected with KY/136 or
KY/180.

Bronchoalveolar lavage was taken from six to nine week old DBA/2 mice that were
infected with 10^5 TCID$_{50}$ KY/136E or KY/180E on days 3 and 4 post-infection. Cells
were separated from the lavage fluid by centrifugation and the fluid (BALf), cellular
(BAL cell), and whole lung homogenate were tested separately for virus by TCID$_{50}$ assay
on MDCK cells. Lung compartments taken from mice infected with KY/180 had
statistically higher virus titers at 3 DPI than from mice infected with KY/136 ($p < 0.05$,
indicated by asterisks on the figure). It is not possible to compute statistical differences
from 4 DPI, as there were only two mice infected with KY/180 in that experiment that
survived to 4 DPI.
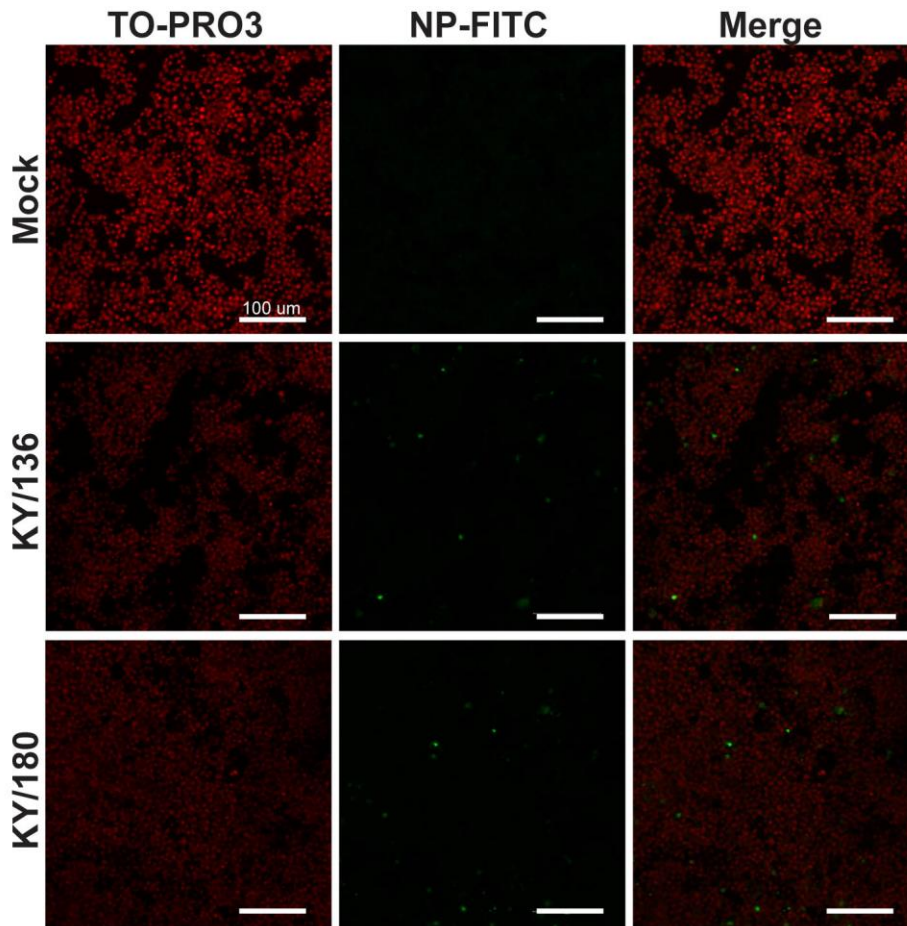
Figure 2.10 Detection of influenza in mouse macrophage cell lines.

Mouse macrophage cell line, RAW264.7, was infected in vitro with MOI=1 of each

influenza isolate (high pathogenic isolate, KY/180, and low pathogenic isolate, KY/136)

on chambered microscopy slides. At 24 hours post-infection cells were fixed,

permeabilized, and stained using a FITC antibody conjugate specific for influenza A

(H1N1) nucleoprotein (green). Cells were counterstained with a nuclear dye (TO-PRO3,

Molecular Probes, red), and visualized on a Zeiss LSM710 confocal microscope. Both

isolates tested were observed to infect macrophages. Scale bars indicate 100 microns.
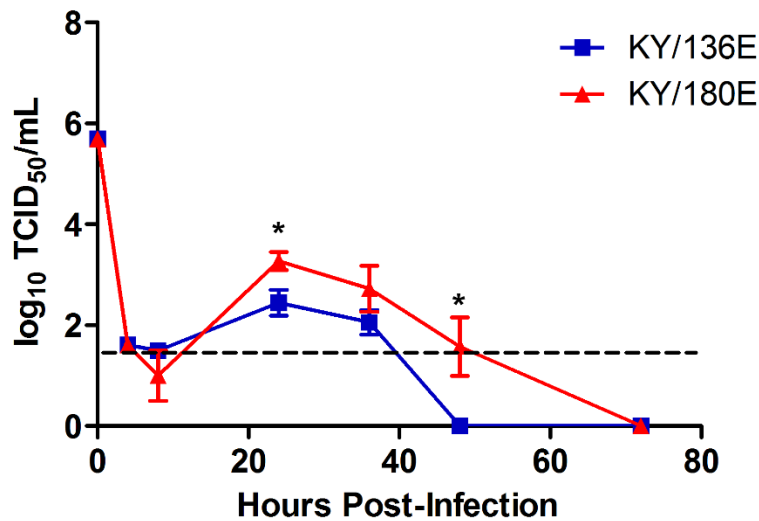
Figure 2.11 Replication of KY/180E and KY/136E in mouse macrophage cell lines.
Mouse macrophage cell line, RAW264.7, was infected in vitro with the influenza isolates
on a 24-well plate at an MOI = 1.0. After one hour of incubation, the cells were washed
and returned to the incubator. Cell culture supernatants were collected over time and
virus titer was determined by TCID50 assay. Both KY/180E and KY/136E replicate in
mouse macrophage cell lines. KY/180E had significantly higher titers of virus detected
at 24 and 48 hours post-infection ($p < 0.05$, indicated by asterisks on the figure).
Pathogenic isolate KY/180E was able to replicate better in mouse macrophages compared
to the low pathogenic isolate, KY/136E.
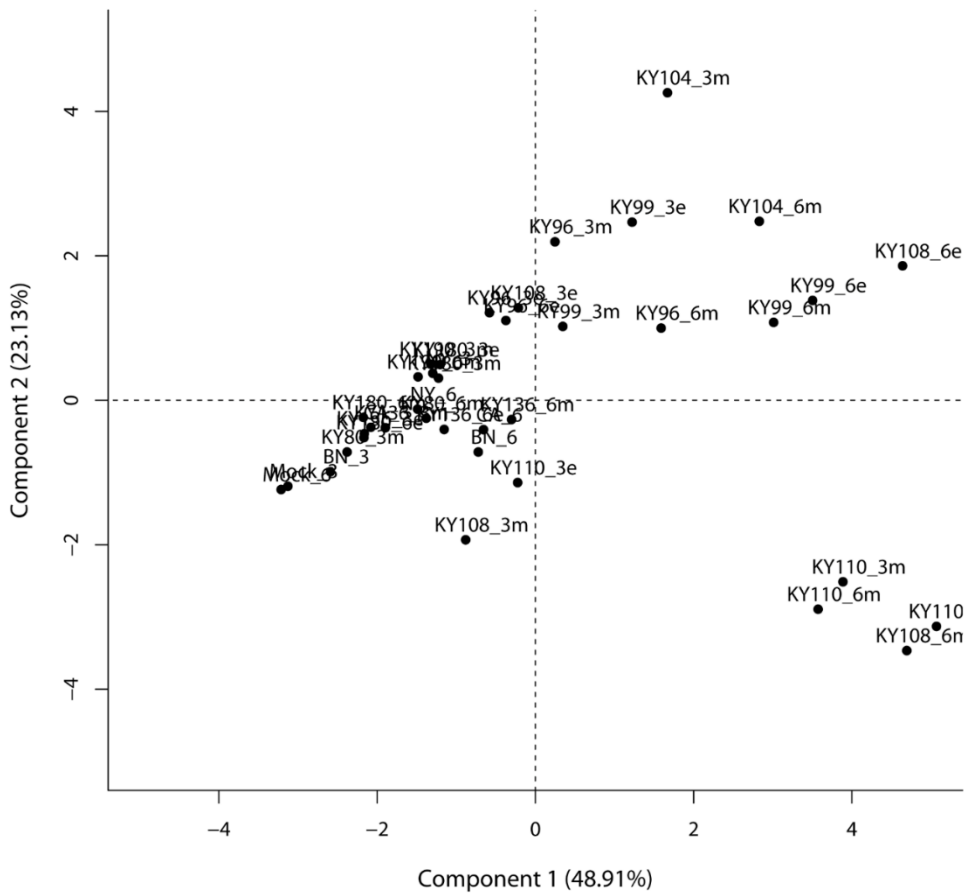
Figure 2.S1 Principal components cnalysis (PCA) of mouse lung cytokine and chemokine expression after challenge with clinical influenza A (H1N1) virus isolates from Kentucky, 2009.

Standardized mean values for each cytokine/chemokine are plotted from Day 3 and Day 6 post-infection (n=3, each) against the first two principal components, accounting for 72% of the variation in the analysis.
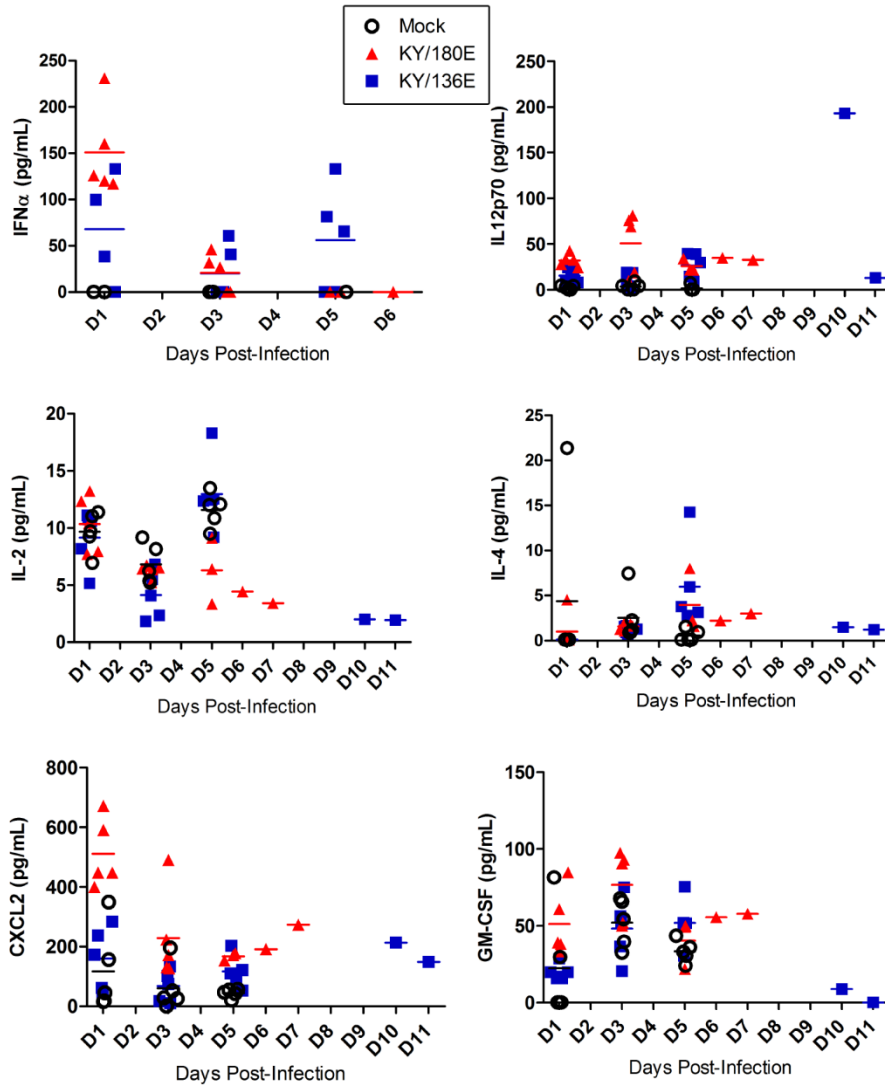
Figure 2.S2 Cytokine and chemokine profiles from mouse lung homogenate.

DBA/2 mice were infected with KY/180E, KY/136E (10^5 pfu), or mock-infected with

PBS. The mice were sacrificed 1, 3, and 5 days post-infection (n=5 mice per group-day).

Samples from moribund mice taken after Day 5 post-infection were also analyzed when

available. Bars indicate mean concentration.
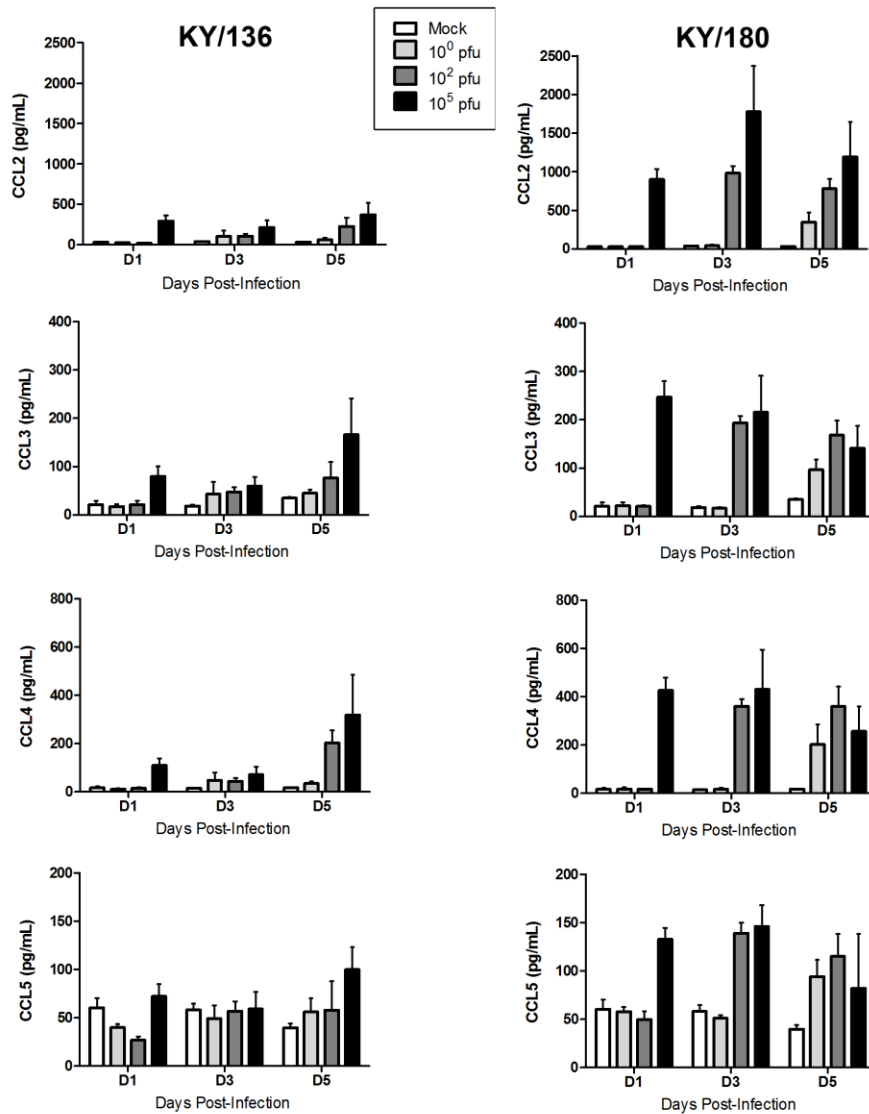
Figure 2.S3 Dose response of chemokines in the lungs of mice infected with KY/136 or KY/180 influenza A (H1N1) virus isolates.

Mice were infected with 10^0, 10^2, or 10^5 pfu of virus and samples were collected upon euthanasia on days 1, 3, or 5 post-challenge (D1, D3, and D5, respectively). n = 5 mice per dose-day for all groups except for mice infected with 105 pfu of KY/180 where only 2/5 mice survived to D5.
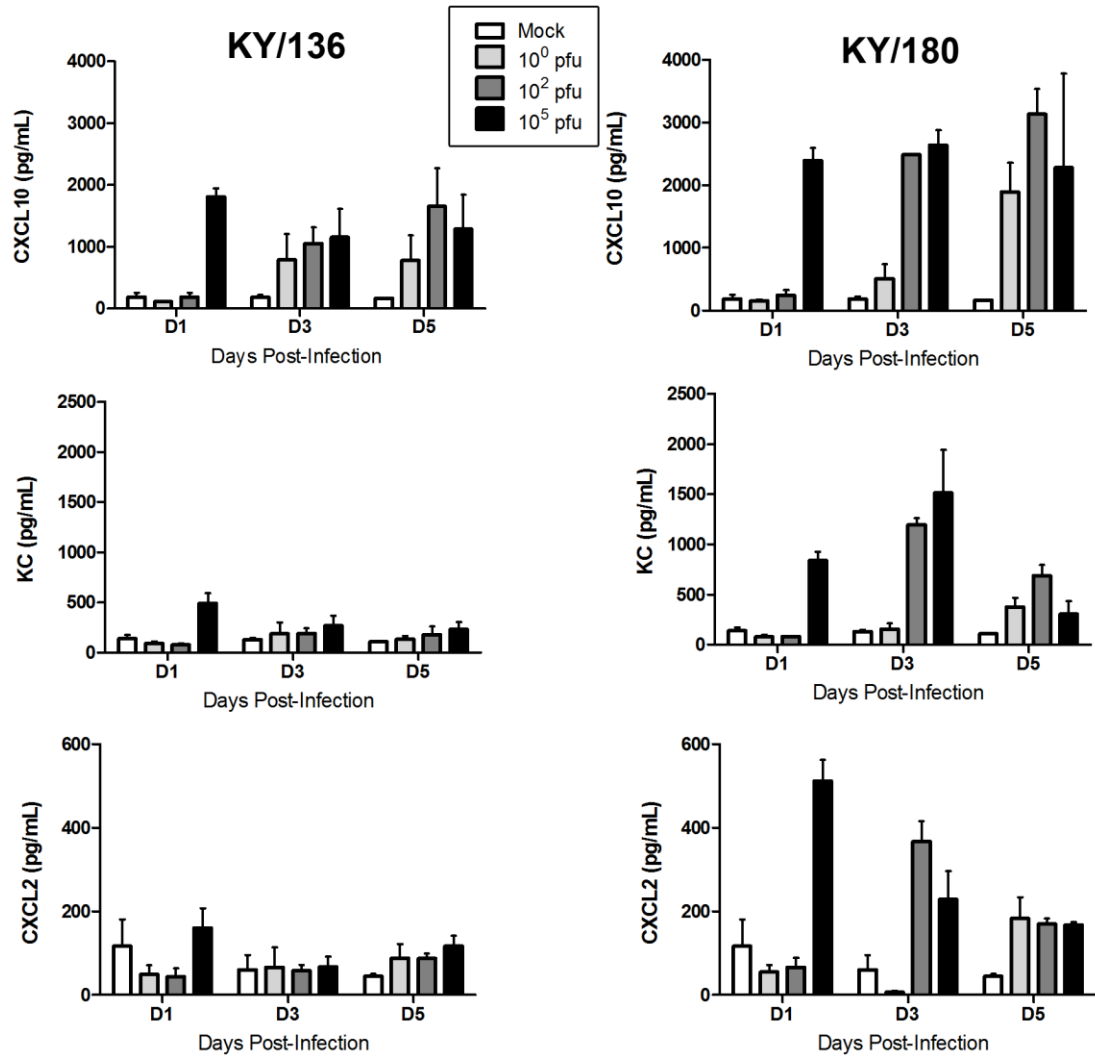
Figure 2.S4 Dose response of chemokines in the lungs of mice infected with KY/136 or KY/180 influenza A (H1N1) virus isolates.

Mice were infected with 10^0, 10^2, or 10^5 pfu of virus and samples were collected upon euthanasia on days 1, 3, or 5 post-challenge (D1, D3, and D5, respectively). $n = 5$ mice per dose-day for all groups except for mice infected with 10^5 pfu of KY/180 where only 2/5 mice survived to D5.
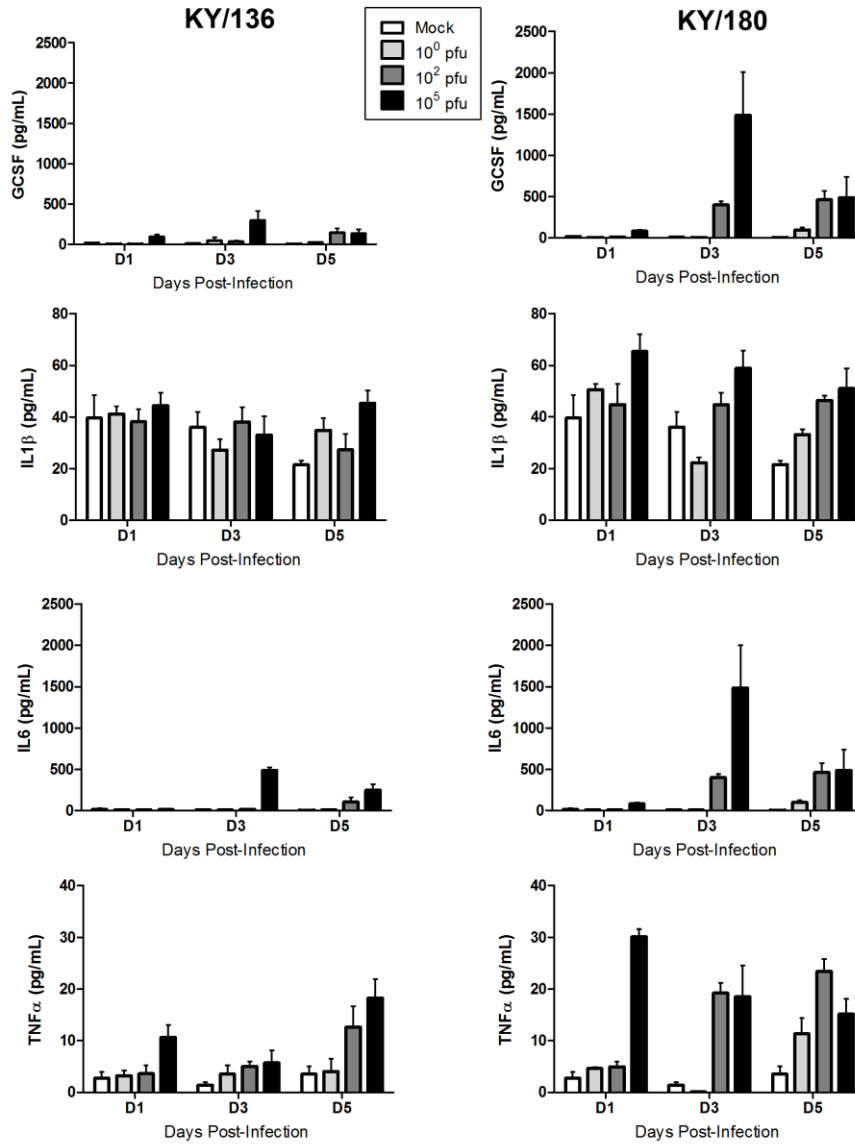
Figure 2.S5 Dose response of cytokines in the lungs of mice infected with KY/136 or KY/180 influenza A (H1N1) virus isolates.

Mice were infected with 10^0, 10^2, or 10^5 pfu of virus and samples were collected upon euthanasia on days 1, 3, or 5 post-challenge (D1, D3, and D5, respectively). n = 5 mice per dose-day for all groups except for mice infected with 105 pfu of KY/180 where only 2/5 mice survived to D5.
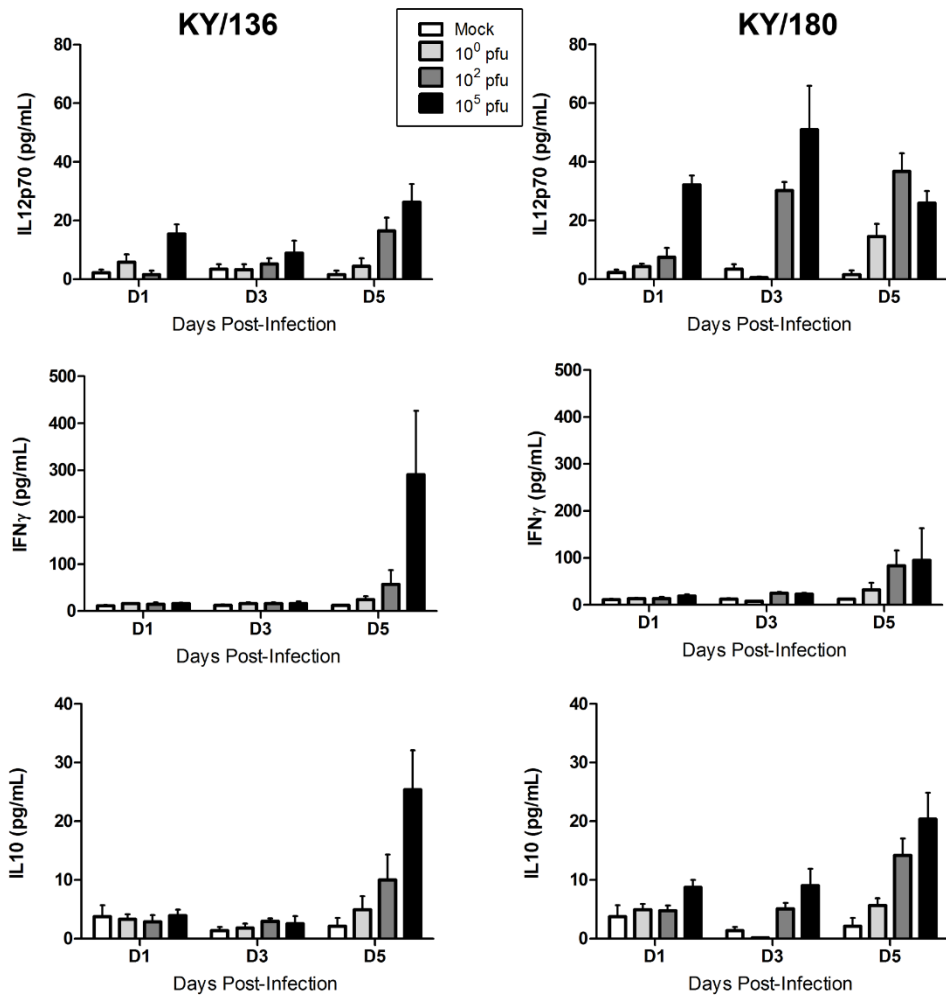
Figure 2.S6 Dose response of cytokines in the lungs of mice infected with KY/136 or KY/180 influenza A (H1N1) virus isolates.

Mice were infected with 10^0, 10^2, or 10^5 pfu of virus and samples were collected upon euthanasia on days 1, 3, or 5 post-challenge (D1, D3, and D5, respectively). n = 5 mice per dose-day for all groups except for mice infected with 105 pfu of KY/180 where only 2/5 mice survived to D5.

C57BL/6 Macrophages
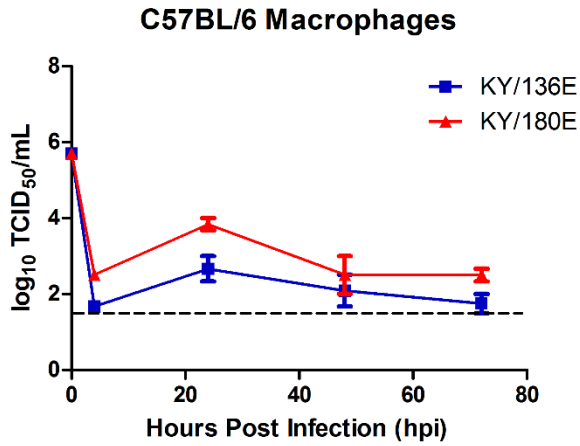
Figure 2.S7 Replication kinetics of KY/180E and KY/180E isolates in C57BL/6 mouse macrophages.

The macrophage cell line, BEIR #NR-9465, was infected at 1.0 MOI (two independent experiments at n=3 per experiment) and clarified supernatants were taken at 4, 24, 48, and 72 hour post-infection. Virus titers were measured by TCID50 assay on MDCK cells.

Table 2.1 General patient data for nasal swabs used for virus isolation.

Sample ID/ Locality Code*	Patient Age/Sex	Hospital Admission Date	Nasal Swab Sample Date	LOS$^\Psi$ (Days)	Comorbidity	Mortality
80/3	31/F	9/30/2009	9/30/2009	10	COPD, MRSA, BMI=123.6	Died
96/2	51/M	10/24/2009	10/26/2009	4	ND	Survived
99/3	35/F	10/28/2009	10/29/2009	3	ND	Survived
104/2	58/M	10/30/2009	11/4/2009	2	ND	Died
108/6	57/F	11/2/2009	11/3/2009	19	COPD, Diabetes Renal Disease, BMI= 79.7	Survived
110/6	54/F	11/3/2009	11/4/2009	3	Diabetes	Survived
136/3	46/M	12/10/2009	12/11/2009	8	Diabetes, MRSA	Survived
180/2	53/M	3/24/2010	4/1/2010	19	COPD, Renal Disease	Died
190/2	55/F	4/10/2010	4/15/2010	12	ND	Died

*locality, 2=western Kentucky (KY); 3=eastern KY; 6=Louisville metro; $^\Psi$LOS, Length

of stay in hospital; MRSA, methicillin-resistant Staphylococcus aureus; COPD, chronic

obstructive pulmonary disease; BMI- body mass index; ND, none determined.

Table 2.2 Summary of viral titers, lethality of H1N1pdm isolates in DBA2 mice.

Inoculum	DPI	Virus titer (Lung)	Lethality
Mock	3	<1.5 *	0.0
	6	<1.5 *	0.0
KY/80M	3	7.2 ± 0.5	0.0
	6	6.4 ± 0.9	33.3
KY/80E	3	7.6 ± 0.1	0.0
	6	7.0 ± 0.3	33.3
KY/96M	3	7.0 ± 0.5	0.0
	6	7.2 ± 0.5	0.0
KY/96E	3	7.3 ± 0.4	0.0
	6	7.4 ± 0.4	100.0
KY/99M	3	6.4 ± 0.2	0.0
	6	5.8 ± 0.7	0.0
KY/99E	3	7.4 ± 0.9	0.0
	6	7.3 ± 0.3	33.3
KY/104M	3	6.6 ± 0.9	0.0
	6	6.9 ± 0.5	33.3
KY/108M	3	7.5 ± 0.6	0.0
	6	6.6 ± 0.4	0.0
KY/108E	3	6.5 ± 0.5	0.0
	6	6.4 ± 0.8	33.3
KY/110M	3	5.9 ± 0.4	0.0
	6	6.2 ± 0.9	0.0
KY/110E	3	5.9 ± 0.2	0.0
	6	6.8 ± 0.7	0.0
KY/136M	3	5.3 ± 0.3	0.0
	6	5.8 ± 0.9	0.0
KY/136E	3	5.8 ± 0.4	0.0
	6	5.2 ± 0.5	0.0
KY/180M	3	6.8 ± 0.3	0.0
	6	5.7 ± 0.7	100.0
KY/180E	3	6.9 ± 0.4	33.3
	6	6.4 ± 0.1	66.7
KY/190M	3	6.8 ± 0.5	0.0
	6	6.3 ± 0.3	100.0
NY/18E	3	6.9 ± 0.6	0.0
	6	6.8 ± 1.0	33.3
CA/07E	3	7.2 ± 0.6	0.0
	6	6.9 ± 0.8	0.0
BN/59E	3	6.7 ± 0.0	0.0
	6	5.9 ± 0.1	0.0

Legend: Virus titer (log10 TCID$_{50}$/mL at a limit of detection = $10^{1.5}$ TCID$_{50}$ / mL)

Table 2.S1 Comorbidities associated with severe, hospitalized influenza pneumonia patients.

ID	Gender	BMI	Tamiflu Therapy	PSI	PSI Class	COPD	Diab	Cancer	Other Infect	Invasive Vent Fail
80	Female	123.6	Tamiflu 75 mg Q12H x 7 days	61	II	yes	no	no	MRSA	yes
96	Male	21.9	No	91	IV	no	no	no	None	yes
99	Female	76.90	No-Flu vaccine only	54	II	no	no	no	None	0
104	Male	26.63	Tamiflu 75mg x2 doses	123	IV	no	yes	no	*Proteusspp.*	yes
108	Female	79.71	Tamiflu 75 mg daily x 5 days	106	IV	yes	yes	no	None	no
110	Female	21.40	Tamiflu 75 mg daily x 5 days	73	III	no	yes	no	None	no
136	Male	24.4	Tamiflu 150mg daily x 5 days	76	III	no	yes	yes	MRSA	yes
180	Male	49.4	Tamiflu	93	IV	yes	no	no	None	yes
190	Female	56.4	Tamiflu	75	III	yes	yes	no	none	no

Legend: BMI, body mass index; PSI, pneumonia severity index; COPD, Chronic obstructive pulmonary syndrome; MRSA, Methicillin-resistant Staphylococcus aureus; Inf, infection; vent, ventilation failure

Table 2.S2 Variants noted in amino acid sequence alignments of H1N1pdm clinical isolates.

	M1	HA1													
A.A.	30	39	83	83	84	97	116	121	137	147	183	186	199	200	203
A.A. Change	S→G	G→E	S→P	S→F	S→N	D→N	I→M	S→G	P→T	N→S	S→P	A→T	V→A	F→L	T→S
CA/07	A	G	**C**	C	G	G	A	**A**	C	A	T	G	T	T	**T**
NY/18	A	G	T	C	G	G	A	A	C	A	T	G	T	T	A
NL/602	A	G	T	C	G	G	A	A	C	A	T	G	T	T	**T**
KY/80	A	G	T	C	G	G	A	**G**	C	A	T	G	T	T	A
KY/96	A	G	T	C	G	G	A	A	C	A	T	G	T	T	**T**
KY/99	A	G	T	C	G	G	**G**	A	C	A	T	G	**C**	T	A
KY/104	A	G	T	C	G	**A**	A	A	C	A	T	G	T	T	A
KY/110	A	**A**	T	C	G	G	A	A	**A**	A	T	G	T	T	A
KY/136E	A	G	T	**T**	G	G	A	A	C	A	T	G	T	T	A
KY/180E	**G**	G	**C**	C	**A**	G	A	A	C	A	**C**	**A**	T	T	A
KY/180M	NA	G	**C**	C	**A**	G	A	A	C	**G**	**C**	**A**	T	T	A
KY/190	NA	G	**C**	C	**A**	G	A	A	C	**G**	T	G	T	**C**	A

	HA	HA2							PA						
A.A.	222	223	234	293	321	374	440	499	14	387	465	471	538	581	610
A.A. Change	D→G	Q→R	V→I	Q→H	V→I	E→K	S→L	E→K	V→I	V→I	I→T	N→S	E→K	M→L	E→D
CA/07	A	A	G	G	**A**	G	C	G	G	G	T	A	G	**C**	A
NY/18	A	**R**	G	G	G	G	C	G	G	G	T	A	G	A	A
NL/602	A	A	G	G	G	G	C	G	G	G	T	A	G	**C**	A
KY/80	A	A	G	G	**A**	G	C	G	G	G	T	A	G	A	A
KY/96	A	A	G	**T**	G	G	C	**A**	G	**A**	T	A	G	A	A
KY/99	A	A	G	G	G	G	C	G	G	G	T	**G**	G	A	A
KY/104	A	A	G	G	G	**A**	C	G	G	G	T	A	**A**	A	A
KY/110	A	A	G	G	G	G	C	G	NA	NA	NA	NA	NA	A	NA
KY/136E	A	A	**A**	G	G	G	C	G	G	G	**C**	A	G	A	A
KY/180E	**G**	A	G	G	G	**A**	C	G	**A**	G	T	A	G	A	**T**
KY/180M	**G**	A	G	G	G	**A**	C	G	NA	NA	NA	NA	NA	NA	NA
KY/190	A	A	G	G	G	**A**	**T**	G	NA	NA	NA	NA	NA	NA	NA

	PA			PB1							PB2				
A.A.	647	654	716	14	196	215	83	563	662	736	33	176	183	340	584
A.A. Change	N→D	Q→E	K→Q	V→I	E→G	P→Q	A→G	R→G	T→K	K→G	K→R	I→T	L→M	K→N	V→I
CA/07	A	C	A	G	**G**	C	C	G	C	A	A	T	C	A	G
NY/18	A	C	A	G	A	C	C	G	C	A	A	T	C	A	G
NL/602	A	C	A	G	A	C	C	G	C	A	A	T	C	A	G
KY/80	A	C	A	G	A	C	C	G	C	A	A	T	C	A	G
KY/96	A	C	A	G	A	**A**	C	G	C	A	**G**	T	**A**	A	G
KY/99	**G**	**S**	A	G	A	C	C	G	C	A	A	T	C	A	G
KY/104	A	C	A	G	A	C	C	**A**	C	A	A	T	C	A	G
KY/110	NA	NA	NA	G	A	C	C	G	**A**	A	A	**C**	C	A	G
KY/136E	A	C	A	G	A	C	**G**	G	C	A	A	T	C	**T**	G
KY/180E	A	C	**C**	**A**	A	C	C	G	C	**G**	A	T	C	A	**A**

Table.s.S2 cont'd

A.A.	NA								NP			NS1		
	79	106	108	150	220	248	396	407	100	181	373	112	123	154
A.A. Change	S→P	I→V	I→V	K→R	R→K	D→N	I→K	V→I	I→V	A→D	T→I	I→M	V→I	G→R
CA/07	T	**G**	A	A	G	**A**	T	G	**G**	C	C	A	G	G
NY/18	T	A	A	A	G	G	T	G	A	C	C	A	G	G
NL/602	T	A	**G**	A	G	**A**	T	**A**	**G**	C	**T**	A	G	G
KY/80	T	A	A	A	G	G	T	G	A	C	C	A	G	G
KY/96	**C**	A	A	A	G	G	**A**	G	A	C	C	A	**A**	G
KY/99	T	A	A	A	G	G	T	G	A	C	C	A	G	G
KY/104	T	A	A	A	G	G	T	G	A	C	C	A	G	G
KY/110	T	A	A	A	G	G	T	G	A	C	C	A	G	**A**
KY/136/E	T	A	A	**G**	G	G	T	G	A	**A**	C	**G**	G	G
KY/180/E	T	A	A	A	**A**	G	T	G	A	C	C	A	G	G

*NA = not yet sequenced; for KY/190 only the HA gene has been sequenced.

Table 2.S3 GenBank accession numbers of H1N1pdm isolates.

10Virus ID	HA	M	NA	NP	NS	PA	PB1	PB2
A/Kentucky/190/10/E	JX875013	*	*	*	*	*	*	*
A/Kentucky/180/10/E	CY099332	JX875027	CY099333	JX875032	JX875031	JX875030	JX875028	JX875029
A/Kentucky/180/10/M	JX875056	*	*	*	*	*	*	*
A/Kentucky/136/10/E	CY099330	JX87521	CY099331	JX875026	JX875025	JX875024	JX875022	JX875023
A/Kentucky/110/09/E	JX875054	JX875049	JX875052	JX875055	JX875053	*	JX875050	JX875051
A/Kentucky/104/09/E	JX875047	JX875041	JX875044	JX875048	JX875046	JX875045	JX875042	JX875043
A/Kentucky/99/09/E	JX875019	JX875014	JX875016	JX875020	JX875018	JX875017	*	*
A/Kentucky/96/09/E	JX875039	JX875033	JX875036	JX875040	JX875038	JX875037	JX875034	JX875035
A/Kentucky/80/09/E	JX875011	JX875005	JX875008	JX875012	JX875010	JX875009	JX875006	JX875007
A/Netherlands/602/09	CY039527	CY046944	CY039528	CY046943	CY046945	CY046942	CY046941	CY046940
A/NewYork/18/09	GQ232064	FJ984348	FJ984350	FJ984352	GQ232063	FJ984354	FJ984353	FJ984351
A/California/07/09	FJ969540	FJ966975	FJ969536	FJ969528	FJ969528	FJ966977	FJ969531	FJ984387

* not yet sequenced

116

Table 2.S4 Virus titers ($TCID_{50}$/ml*) on 1, 3, and 5 days post-infection in lungs and nasal turbinates of DBA/2 mice infected with KY/180E and KY/136E.

		Lung			NT		
	Dose	**1 DPI**	**3 DPI**	**5 DPI**	**1 DPI**	**3 DPI**	**5 DPI**
KY/136E	10^0	< 1.5*	2.86 ± 2.15	0.68 ± 1.52	< 1.5	< 1.5	< 1.5
	10^2	1.42 ± 1.95	3.78 ± 2.23	2.50 ± 0.00	< 1.5	< 1.5	1.94 ± 1.89
	10^5	5.04 ± 0.86	3.64 ± 2.17	< 1.5	< 1.5	3.64 ± 0.76	2.92 ± 0.29
KY/180E	10^0	0.50 ± 1.12	2.76 ± 2.61	4.40 ± 2.47	< 1.5	< 1.5	< 1.5
	10^2	4.86 ±1.77	6.54 ± 0.36	6.42 ± 0.44	0.50 ± 1.12	5.22± 0.54	5.32 ± 0.75
	10^5	7.54 ± 0.34	6.18 ± 0.46	6.38 ± 0.30	5.40 ± 0.26	4.80 ± 0.45	4.96 ± 0.36

Legend: Dose = pfu/mouse. Values in mean $\log_{10}$ $TCID_{50}$/mL ± S.D. (n = 5 mice per dose-day); * Limit of detection = $10^{1.5}$ $TCID_{50}$ / mL.

Table 2.S5 Relative magnitude of immune responses of H1N1pdm isolates in mice in groups revealed by principal component analysis clustering.

Cytokine/ Chemokine	Function	DPI	Group 1	Group 2	Group 3	Group 4
IL-6	Inflammation	3	+	+++	+	+
		6	+	++++	+++	+
TNFα	Inflammation	3	+	+++	+++	++
		6	+	+++	++++	+
KC	PMN attraction	3	+	+++	++	++
		6	+	+++	++	+
G-CSF	PMN proliferation	3	+	+++	++	+++
		6	+	++	++	++
CXCL9 (MIG)	T-cell chemoattractant	3	+++	++++	++	+++
		6	++++	+++	++	+
CCL2 (MCP-1)	Monocyte chemoattractant	3	+	+++	++++	++
		6	++	+++	++++	++
IL-1β	Inflammation	3	+	++	++	+
		6	++	++	+++	+
CXCL3 (MIP1α)	PMN attraction	3	+	++	+++	+
		6	++	+++	++++	+
CXCL10 (IP10)	Chemoattractant	3	++	-	++++	++
		6	+++	+	++++	+
IFNγ	Adaptive immunity	3	-	-	+	-
		6	+	++	+++	-
IL-10	Anti-inflammation	3	-	-	+	-
		6	+	++	+++	-

Legend: Group 1, BN/59, CA/07, KY/80, KY/136; Group 2, KY/96, KY/99, KY/104, KY/108; Group 3, KY/108, KY/110; Group 4, KY/180, KY/190.

Table 2.S6 Summary of references to mutations in influenza A (H1N1) isolates with observed virulence.

Gene product	Mutation	Source	Citation
HA1	S83P	mouse, *in vitro*	3, 12
HA1	S183P	mouse	21, 22, 93, 94
HA1	T203S	mouse	44
HA1	D222G	human, mouse, macaque	10, 30, 31, 32, 34, 36, 38, 37, 43, 89
HA1	Q293H	mouse	44
HA1	V321I	mouse	3, 24, 44
HA2	E374K	human	95
NA	I106A	mouse	44
NS1	V123I	mouse	44
PA	V14I	mouse	44
PB2	K340N	human	95

CHAPTER III

MOLECULAR IMAGING REVEALS A PROGRESSIVE PULMONARY

INFLAMMATION IN LOWER AIRWAYS IN FERRETS INFECTED WITH 2009

H1N1 PANDEMIC INFLUENZA VIRUS

Overview

Molecular imaging has gained attention as a possible approach for the study of the

progression of inflammation and disease dynamics. Herein we used [^{18}F]-2-deoxy-2-

fluoro-D-glucose ([^{18}F]-FDG) as a radiotracer for PET imaging coupled with CT (FDG-

PET/CT) to gain insight into the spatiotemporal progression of the inflammatory

response of ferrets infected with a clinical isolate of a pandemic influenza virus, H1N1

(H1N1pdm). The thoracic regions of mock- and H1N1pdm-infected ferrets were imaged

prior to infection and at 1, 2, 3 and 6 days post-infection (DPI). On 1 DPI, FDG-PET/CT

imaging revealed areas of consolidation in the right caudal lobe which corresponded with

elevated [^{18}F]-FDG uptake (maximum standardized uptake values (SUVMax), 4.7-7.0).

By days 2 and 3, consolidation (CT) and inflammation ([^{18}F]-FDG) appeared in the left

caudal lobe. By 6 DPI, CT images showed extensive areas of patchy ground-glass

opacities (GGO) and consolidations with the largest lesions having high SUVMax (6.0-

7.6). Viral shedding and replication were detected in most nasal, throat and rectal swabs

and nasal turbinates and lungs on 1, 2 and 3 DPI, but not on day 7, respectively.

In conclusion, molecular imaging of infected ferrets revealed a progressive consolidation on CT with corresponding [^{18}F]-FDG uptake. Strong positive correlations were measured between SUVMax and bronchiolitis-related pathologic scoring (Spearman's $\rho = 0.75$). Importantly, the extensive areas of patchy GGO and consolidation seen on CT in the ferret model at 6 DPI are similar to that reported for human H1N1pdm infections. In summary, these first molecular imaging studies of lower respiratory infection with H1N1pdm show that FDG-PET can give insight into the spatiotemporal progression of the inflammation in real-time.

Introduction

In March of 2009, an outbreak of a novel variant of H1N1 influenza A virus was reported in cases of influenza illness in Mexico (35). By June 11, the World Health Organization raised the pandemic alert level to its highest level, declaring the first influenza pandemic in over 40 years (35). Unlike seasonal influenza viruses, this novel H1N1 pandemic strain (H1N1pdm) tended to affect younger healthier populations and had an increased risk of morbidity and mortality (37, 39, 40) with 12-30% of the population developing clinical influenza, 4% of those requiring hospital admission, and 1 in 5 requiring critical care (599). In general, however, infection of the H1N1pdm was relatively mild in most persons, although a fatal viral pneumonia with acute respiratory distress syndrome occurred in approximately 18,000 cases.

In contrast to seasonal influenza in human cases, H1N1pdm infections showed a tropism for the lung similar to H5N1 (30). The ability of H1N1pdm viruses to infect the lower

respiratory track has been attributed to a broader specificity in the binding of the viral

hemagglutinin (HA) to □2-3- in addition to □2-6-linked sialic acid (SA) receptors (284,

336). It is reasonable that the lung tropism of the H1N1pdm contributed to the severity of

disease in those individuals with preexisting complications such as asthma and chronic

obstructive pulmonary disease (COPD) (6, 30, 544-546). Data from limited human

autopsies and animal studies of various pandemic strains also suggest contribution of the

host innate immune response and the virus in the progression of disease (46, 394, 600,

601).

Molecular imaging can potentially play a strong role in basic infectious disease research

and clinical response by providing a noninvasive, spatiotemporal measurement of viral

infection and host inflammation (602, 603). To explore the potential utility of molecular

imaging in influenza infection, we chose the ferret (*Mustela putorius furo*) model. Ferrets

have been used as an animal model of influenza infection and pathogenesis since 1934,

when they were reported to develop an acute respiratory tract illness when exposed to

influenza viruses from humans and swine (149). In contrast to mice, the ferret can be

infected by human isolates without adaptation and display signs and symptoms of

infection such as sneezing and nasal secretions that are similar to what is seen in humans

(43, 47, 49, 256). The ferret is an attractive model for imaging influenza pulmonary

infections given the ferret's long trachea, large lung capacity, and bronchiolar branching.

These anatomical features can potentially bridge imaging with histopathologic

evaluation. Finally, the ferret more closely mimics humans in distribution of sialic acid

(SA) receptors in the respiratory tract with higher α-2-6 SA in the upper respiratory tract and α 2-3 SAs- in the lower (228).

Historically, plain film (x-ray) radiography and computed tomography (CT) have been useful for clinical assessments of influenza disease severity in clinical cases (41, 604). These imaging modalities are limited by characterizing only anatomic changes in the lung parenchyma, such as ground-glass opacity (GGO) and consolidations, which represent different degrees of interstitial and alveolar filling by cells, edema, and inflammatory exudate (605). In contrast, positron emission tomography (PET) imaging with the radiotracer [^{18}F]-2-fluoro-2-deoxy-D-glucose ([^{18}F]-FDG) can provide data on metabolic activity of cells by measuring sites of increased glycolysis from leukocyte chemotaxis and accumulation, and provide increased sensitivity in detection of cells during inflammation. [^{18}F]-FDG, an analog of glucose that is moved into cells via facilitated transport, is commonly used in PET imaging as a radiotracer in clinical and basic science research. Recent studies have demonstrated the utility of [^{18}F]-FDG in assessment of infectious disease burden in animal models of schistosomiasis and tuberculosis (606-608). PET/CT has been used in the assessment of one hospitalized H1N1pdm patient and revealed an intense inflammatory response (609). The uptake of [^{18}F]-FDG in humans and animals suggests the predominant presence of activated neutrophils (610-613). In studies of mice infected with influenza A virus, neutrophils play a critical role in protection and recovery from infection, and participate in the process of adaptive immunity to the virus (78). Coupled with molecular virology and pathology, molecular imaging with important probes of disease has enormous potential to reveal early critical

factors that contribute to the clinical progression of illness as well as accelerate screening, the efficacy and mechanistic studies of vaccines and antiviral therapies (602, 603).

To test the hypothesis that FDG-PET/CT imaging could reveal the spatiotemporal nature of H1N1pdm inflammation and disease progression, we chose the ferret model of H1N1pdm influenza infection. Further, for these studies we chose a low passage clinical isolate, A/Kentucky/180/2010 or KY/180, herein, which has a change in the HA1 gene, D222G, which correlates with increased severity of disease in patient cases from several countries (558, 559, 562, 563). In mice, infection with H1N1pdm engineered to include this change show increased viral titers and pathology, however, in ferrets there do not seem to be any major differences in clinical signs, transmissibility or pathogenicity (125, 614). Our results show for the first time, the spatiotemporal progression of inflammation with CT and PET using [^{18}F]-FDG in ferrets infected with H1N1pdm in conjunction with histopathology and viral titers over a seven day period. Importantly, the extensive areas of patchy GGO and consolidation seen in the ferret model at 6 days post-infection (DPI) are similar to that reported for human H1N1pdm infections (609). In vivo imaging with these modalities for anatomic (CT) and molecular (PET) data suggests increased pulmonary inflammation as the amount of circulating virus becomes undetectable. These results suggest that molecular imaging will be a great asset in gaining insight into the temporal and spatial progression of the inflammatory process caused by influenza virus infection.

Results

Characterization of KY/180 in female ferrets

Due to the size of the Siemens Trimodal gantry for PET/CT imaging we chose four month old females rather than male ferrets. The pandemic H1N1 isolate KY/180 employed in these studies was isolated from nasal swab sample provided by the Severe Influenza Pneumonia Surveillance project, a clinical study of hospitalized patients with influenza pneumonia in Kentucky. The patient had a severe course of influenza disease and died after 19 days. Sequencing of the HA1 gene from this isolate revealed the D222G mutation, which has been associated with severe disease in human cases (558, 559, 562, 563). The second passage of the KY/180 seed was employed in the characterization of infection in the female ferrets. The 50% infectious dose in female ferrets was determined to be $10^{0.07}$ TCID$_{50}$ (data not shown). In group 1, six ferrets were mock infected with PBS. In group 2, six ferrets were infected intranasally (i.n.) with KY/180 with a 0.5 ml dose of 0.5 x $10^{5.7}$ TCID$_{50}$ per naris. Ferrets were monitored for temperature for 10 DPI, and for body weight and clinical symptoms for 28 DPI. Two animals in each group were euthanized on days 2, 14 and 18 to determine virus and HI titers in blood, lung and several additional organs at 2 DPI.

In figure 3.1A, the body weight changes are shown for mock- and KY/180-infected ferrets. Body weight showed a drop on day 2 where the weight remained for the remainder of the study. Figure 3.1B shows the average temperatures of the mock- and KY/180-infected ferrets for the first 10 DPI. Temperature peaked on days 1 and 5 for KY/180 infected animals with a mean temperature of 103.4ºF (SD=1.71ºF) and 103.2ºF

(SD=0.52 °F), respectively. The average hemagglutination-inhibiting (HI) serum antibody titer in the blood on day 14 was 540 reciprocal dilution and the average total serum influenza-specific IgG by ELISA was 7610 reciprocal dilution (Fig. 3.1C). In studies to determine the infectious dose, additional tissues were taken from animals infected at with KY/180 with a 0.5 ml dose of $0.5 \times 10^{4.7}$ TCID$_{50}$ per naris. On day 2, viral titers were the highest in the nasal turbinates ($10^{6.25}$ TCID$_{50}$/g) followed by the caudal lung ($10^{6.0}$ TCID$_{50}$/g) and trachea ($10^{3.75}$ TCID$_{50}$/g). The lowest levels of virus were observed in the cranial lobe of the lung ($10^{3.2}$ TCID$_{50}$/g). Viral titers were measured by TCID$_{50}$ in nasal turbinates, trachea, right cranial lobe of the lung, right caudal lobe, brain, liver, spleen, kidney, duodenum, jejunoilieum, colon and rectum. KY/180 was detected in jejunum in one animal ($10^{2.0}$ TCID$_{50}$/g), but was not detected in any other tissues (data not shown).

FDG-PET/CT imaging of the H1N1pdm-infected ferrets show progressive inflammation

Female Fitch ferrets were divided into five groups, with two per group of animals that were mock-infected with PBS (group 1) or intranasally infected with KY/180 (groups 2-5), in a 0.5 ml dose of $0.5 \times 10^{6.0}$ TCID$_{50}$ per naris, on day 0 (Table 1). Group 5 was the only group that was imaged each day; while groups 2-4 were imaged and sacrificed on days 1, 2 and 3 post-infection. This study design permitted evaluation of the progression of imaging with infection and pathology in two animals each day as well as continuous imaging of the lungs in one cohort over the seven-day time-period.

FDG-PET and CT images of the H1N1pdm-infected and mock-infected ferrets were successfully obtained and fused for two ferrets on days 1, 2, 3 and 6 (Fig. 3.2 and 3.3). Volumes of interest (VOI) and corresponding maximum standardized uptake values (SUVMax) were generated for any metabolically active lesions in the lung as well as background activity in the lungs, liver, heart, thymus, and thoracic lymph nodes. Baseline imaging prior to infection showed no focal areas of lung consolidation on CT and background standard uptake values (SUVMax) of the [^{18}F]-FDG levels ranged from 0.7-1.0 for PET (Fig. 3.2A and Fig. 3.3A). Each figure shows the one two-dimensional coronal plane that were standardized across days to provide a similar orientation and do not necessarily represent the SUVMax as that plane may be out of view.

By 1 DPI, an area of consolidation was identified on CT in the right caudal lobe with corresponding radiotracer uptake on PET (Fig. 3.2B, SUVMax of 4.7). Consolidative areas in the right caudal lobe increased by day 2, with a persistently elevated SUVMax of 3.1(data not shown). By day 3, the consolidation increased in the right caudal lobe (Fig. 3.2C and Fig. 3.3C, SUVMax of 3.7 and 4.4, respectively) and also appeared in the left caudal lobe (SUVMax of 3.2) of ferret 2214 (Fig. 3.3C). By 6 DPI, there were widespread areas of patchy consolidation on CT with multiple areas of increased radiotracer uptake in both ferrets in caudal and cranial lobes (Fig. 3.2D and Fig. 3.3D, SUVMax of 6.0 and 7.6 on the right, 4.2 and 4.6 on the left, respectively). These results suggest that inflammation progresses into the lower respiratory airways after infection into the upper part of the lower respiratory system. A ferret from the uninfected cohort was also imaged on day 6, with no focal appearance of consolidation on CT and no

evidence of increased [^{18}F]-FDG uptake on PET (image not shown, background SUV of 0.6).

Viral shedding and replication of the nasal turbinates and lung tissues

To measure viral shedding, each day each ferret was swabbed in the nasal, throat and fecal passages and the viral titer was measured by TCID$_{50}$ (Table 2). The highest levels of viral shedding were measured in the throat swabs. Nasal swabs also showed viral shedding for most animals, while the presence of virus in rectal swabs was low although detectable in a few animals.

Replication of H1N1pdm in nasal turbinates and lungs were determined post-mortem from the right caudal lobe of the lung taken on euthanasia (Table 3.3). Four sections were taken per lobe to provide greater insight into the spread of the virus in the tissue (Fig. 3.4). High levels of virus were detected in all nasal turbinate samples at 1, 2, and 3 DPI (95% C.I. = 5.43 +/- 1.00 TCID$_{50}$/mL). Virus was also detected in a majority of lung sections from 1, 2, and 3 DPI. It was absent in the lung sections from one animal on 2 DPI, although it was present in the ferret's nasal turbinates, suggesting that the timing of infection in this animal was slower than the others. Of note, this same animal had a focus of consolidation on CT and radiotracer uptake on PET. This observation also suggests that, while the virus may have been undetectable by TCID$_{50}$, low levels of virus had entered the lower respiratory system. No animals on day 7 post-infection had detectable virus in the nasal turbinates or the sampled lung tissue. Virus was not detected in nasal, throat and fecal passages or the sampled lung tissue from ferrets in any of the controls.

Histopathology of H1N1pdm-infected and mock-infected ferrets

Upon necropsy, all but the right caudal lobe of the ferret lung was fixed with paraformaldehyde. Following fixation, sections were taken for histopathology from the right and left cranial lobes, left caudal lobe and the middle accessory lobe. Representative photographs from slides of the left caudal lobe are shown in figure 3.5. The ferrets in the control group had intact bronchiolar walls with very minimal infiltration by neutrophils with the exception of the left caudal lobe from control animal 2206 sacrificed on Day 1. Possible causes of this pattern of change may be an underlying systemic vasculopathy which is typically confirmed by evaluation of other organs that were not collected (e.g., kidney, spleen, liver).

In general pulmonary lesions associated with influenza infection were roughly comparable at Days 1 and 2 and consisted of variable suppurative or necrosuppurative bronchiolitis and mixed cell alveolitis at minimal to moderate severity levels. By 1 DPI, there were some small foci of inflammation without much infiltration of the bronchi or bronchioles. There was an increased severity of inflammatory findings in lung lobes from infected ferrets on day 3. Specifically, more extensive infiltration of neutrophils can be seen within the bronchiolar lumen, along with necrosuppurative bronchiolitis and mixed cell alveolitis. At Day 7, lesions observed in the lung lobes continued to exhibit an increased severity compared to the majority of lung lesions seen at 1 and 2 DPI. Bronchiolar epithelial hyperplasia and cytokaryomegaly were noted in addition to bronchiolitis.

FDG-PET/CT and histopathology show positive correlation during infection

To evaluate potential correlations between PET/CT with histopathology, the SUVMax of lesions in the right and left lung of each ferret were compared with the cumulative histopathology scores assigned by the veterinary pathologist (Fig. 3.6). On average, the SUVMax was higher in the right lung than the left lung but the slopes and Spearman's correlation coefficients (ρ) were similar between the two sides. The highest correlation was seen between the cumulative bronchiolitis score and SUVMax (ρ of 0.71 and 0.75 on the right and left, respectively). The next highest was between the cumulative bronchitis score and SUVMax (ρ of 0.69 on the right and 0.67 on the left). A weaker positive correlation was seen between the cumulative alveolitis score and SUVMax (ρ of 0.47 on the right and 0.57 on the left).

<u>Discussion</u>

Herein, we show for the first time the feasibility of utilizing [^{18}F]-FDG PET coupled with CT imaging of H1N1pdm in ferret to track the progression of pulmonary disease in real-time. We chose a low passage clinical isolate, KY/180, which has a change in the HA1 gene, D222G. The D222G change in H1N1pdm correlates with increased severity of disease in patient cases from several countries (558, 559, 562, 563). The patient from which we obtained the KY/180 isolate also had a severe course of influenza illness over a period of 19 days that resulted in death. Recently, studies in mice and ferrets infected with pandemic influenza viruses A/California/04/2009 and A/Netherlands/602/2009 engineered with the D222G mutation have shown that the D222G mutation are lethal in

mice, but not ferret (125, 614). The lethality in mice, but not ferrets, has been attributed to the greater abundance of α2-3-SA in the mouse model (125, 230). All of these viruses have an affinity for α2,6-SAs associated with attachment to and replication in cells of the upper respiratory tract as shown by the high levels of viral replication in the nasal turbinates. Thus, infection of ferrets with these H1N1pdm isolates engineered with D222G and our clinical isolate have not correlated with clinical findings in patients. These results in ferrets are not surprising given that 80% of the fatal cases of H1N1pdm had underlying medical conditions and bacterial infections (30). Discovery of the molecular components of the host response that may promote pathogenesis will be critical for defining new treatments.

Noninvasive imaging can provide real-time in vivo monitoring of the progression of infection, inflammation and disease that may give insight into the mechanisms that modulate disease progression. Recently, Veldhuis Kroeze *et al*., presented data on the monitoring of pulmonary lesions of H1N1pdm influenza virus-infected ferrets with CT scanning which correlated with disease progression and severity (615). As those studies demonstrate, CT is a powerful tool, but it will not give the molecular details that can be provided by PET or SPECT imaging of probes that target critical host responses such as neutrophil invasion. In our study we coupled CT scanning with the [^{18}F]-FDG radiotracer and show infection and inflammation of influenza infection in the lower respiratory system with foci of increased [^{18}F]-FDG uptake corresponding to areas of lung opacity on CT, with underlying inflammation on necropsy. In comparison to human CT imaging studies of influenza, the molecular images in the ferret show strong similarity. CT

findings in patients with confirmed influenza infection show patchy ground-glass

opacities in segmental multifocal distributions, mixed with areas of consolidation in the

lung (6, 41, 616). Moreover, the few case reports of human influenza in which lungs were

imaged by [^{18}F]-FDG PET demonstrate areas of high uptake in these ground-glass

opacities and consolidation (609). Our study similarly demonstrates this pattern in the

ferret model, also showing patchy opacities on CT with high uptake of radiotracer on

PET, with necroscopy-based confirmation of inflammation in the left caudal lobe.

Specifically, we show the ferret lung demonstrated progressive consolidation on CT and

FDG uptake on PET predominantly in the right caudal lobe, which progressed to the left

caudal lobe by day 3 p.i.. By day 6, the diffuse metabolically active lesions seen on

PET/CT were similar to what has been reported in the human literature during the 2009

H1N1 pandemic (609).

Histopathologic evaluation of the lungs confirmed the progressive nature of the

pulmonary lesions and corroborated the radiologic data. Suppurative and

necrosuppurative bronchiolitis seen on days 1 and 2 became progressively worse by days

3 and 7 post-infection. The inflammation tended to be patchy or multifocal and an entire

lung lobe was never uniformly affected, corresponding to the multiple patchy lesions

seen on PET/CT by the end of the study. This also agreed with the analyses of the viral

titers in various sections of the right caudal lobe and the PET/CT imaging. Our analyses

of viral titers in the four representative sections suggest different levels of infiltration of

the lobe. The histopathologic scoring for bronchiolitis correlated the best with the

SUVMax of the lesions seen in the right and left lungs on PET. In general, the severity of

infection and inflammation on imaging can be represented by (1) the volume of affected lung (i.e. the percentage of diseased lung relative to total lung capacity), and (2) the extent of parenchymal destruction (disruption of pulmonary architecture) and inflammatory cell migration. Our study first aims to correlate FDG uptake measurements with histology, thereby analyzing the extent of parenchymal destruction and cellular infiltrates.

It should be considered that there can be variation in matching FDG uptake with histologic severity because more severe architectural distortion can lead to necrosis with more dead cells, therefore showing less uptake of radiotracer among metabolically inactive dead cells and nonviable tissue. Our study, however, shows that progressing inflammatory infiltrates on histology in the studied time period after acute influenza infection corresponds to radiologic trends. Additionally, our study demonstrates spatial progression with increased size and number of abnormal foci in the lung parenchyma during acute infection.

Ultimately, utilizing these new imaging tools, we envision a number of future experiments to delineate potential differences in the course of H1N1pdm and H5N1 isolates infection in ferrets. We also plan to explore additional radiotracers that might reveal potential differences in host responses in the immune system and the process of acute injury in the lung. Future studies will assess differences in presentation of those who recover from infection versus those who eventually succumb to infection such as with more lethal isolates such as H5N1. This model should be valuable in rapid

assessment of the effect of various treatments on pulmonary inflammation and damage.

Finally, these first PET/CT imaging approaches could be extended to a number of other

important pulmonary infections caused by pathogens such as hantaviruses, respiratory

syncytial virus, and SARS CoV, to gain further insight into the spatiotemporal *in vivo*

dynamics of disease progression (603).

Materials and Methods

Virus and cells

The influenza H1N1pdm virus, A/Kentucky/180/2010, (KY/180; GenBank CY99332 and

CY99333) was isolated from the nasal swab of a severe hospitalized case (hospitalized in

March 2010) provided by the Severe Influenza Pneumonia Surveillance project, an

ongoing clinical study of hospitalized patients with influenza pneumonia in Kentucky

(courtesy of Dr. Julio Ramirez). The virus was isolated and passaged in the allantoic

cavity of ten-day-old embryonated hens' eggs at 37°C. The allantoic fluid was harvested

72 h after inoculation, pooled and stored in stored in aliquots at -80C until use. The

infectious virus titer of the resulting seed stock was determined by $TCID_{50}$ (50% tissue

culture infectious dose) and the titer calculated by Reed and Muench (597) and confirmed

by plaque assay on MDCK cells. Passage E2 was used for the studies reported herein.

Ferrets

Ferret studies were approved by the University of Louisville Institutional Animal Care

and Use Committee. University of Louisville has Veterinary Medicine tasked to monitor

and support all animal experiments. Research was conducted in compliance with the

Animal Welfare Act and other federal statutes and regulations relating to animals and experiments involving animals and adheres to principles stated in the *Guide for the Care and Use of Laboratory Animals*, National Research Council, 1996. The facility where this research will be conducted is fully accredited by the Association for Assessment and Accreditation of Laboratory Animal Care International.

All female Fitch ferrets were obtained from Triple F Farms (Sayre, PA). Ferrets were selected after screening blood samples for the presence of influenza antibodies using a hemagglutination inhibition assay (HI). Ferrets that were seronegative for seasonal and pandemic viruses were shipped directly to the University of Louisville Regional Biocontainment Laboratory and acclimated for seven days prior to initiation of the studies. Animals were fed Teklad Laboratory Diet #2072 (Harlan/Teklad, Madison, WI) and water *ad libitum.*

For the characterization of the progression of infection of the KY/180 clinical isolate we utilized four month old, female ferrets. Prior to infection with virus, ferrets were anesthetized with 0.05 mg/kg atropine, 5.0 mg/kg ketamine, and 0.08 mg/kg dexmedetomidine intramuscularly. Subsequently, six animals were inoculated intransally (i.n.) with 0.5 mL of infectious virus per naris as a bolus, which was diluted to $10^{5.7}$ $TCID_{50}$/mL in phosphate buffered saline (PBS). Six additional animals were inoculated by i.n. with 0.5 mL of infectious virus per naris as a bolus with PBS (mock). Anesthesia was reversed with 0.4 mg/kg atipamezole. Ferrets were monitored daily for temperature and clinical symptoms. On day 2 post-infection, two ferrets were taken to measure viral

titers in blood, lung, brain, trachea, nasal turbinates, spleen, kidney, thymus, liver, duodenum, jejuno-ileum, large intestine, and rectum. Gross pathology was defined during necropsy for the lung. At 14 and 28 days post-infection two additional ferrets from each group were analyzed for viral titers and pathology in the lung.

For molecular imaging studies, twelve, four-month-old female Fitch ferrets were utilized. Animals were fed food and water *ad libitum* except 4 h prior to and during CT/PET imaging. On day 0, ferrets were anesthetized prior to inoculation with virus or PBS with ketamine, dexmedetomidine and atropine. Eight animals were inoculated i.n. with 0.5 mL of infectious virus per naris as a bolus, which was diluted to $10^{6.0}$ TCID$_{50}$/mL in phosphate buffered saline (PBS). Four ferrets were inoculated i.n. with 0.5 mL PBS per naris as a mock-infected control. For imaging, on days 0, 1, 2, 3 and 6, anesthetic induction and maintenance were achieved with 1-3% isoflurane. Blood glucose levels were checked prior to administration of the radiolabeled tracer to ensure that they were within normal limits, which typically range from 62-134 mg/dL in ferrets (617). Glucose was provided to animals to compensate for body fluids lost during imaging. Typically 30 mls of Lactated Ringer's solution (Hospira) was administered subcutaneously (s.q.) following completion of the imaging. Animals were monitored for body temperature and vital signs during imaging.

CT and PET imaging

Imaging was performed on 0, 1, 2, 3, and 6 days post-infection (DPI). Each day, four ferrets were imaged with CT and PET on hardware designed for preclinical animal

studies, including microCT and microPET, respectively. Two ferrets were euthanized the

each day and necropsied to obtain tissue samples for virologic and histopathologic

analyses (please see study design Table 1). Image acquisition was conducted with a

Siemens Inveon Trimodal Scanner (Siemens Preclinical, Knoxville, TN), which is a small

animal imaging platform that combines microPET, microCT, and microSPECT

modalities within one unit. This combination facilitated co-registration of PET and CT

images as the study subject was kept in a uniform position on the scanner bed,

minimizing potentially large motion artifacts as a result of repositioning the animal

between each scan. The Inveon microCT scanner features a variable-focus tungsten X-

ray source with an achievable resolution of 20 μm and a detector with a maximum field

of view (FOV) of 8.4 cm x 5.5 cm. The source-to-object distance was 263.24 mm and

the source-to-detector distance was 335.67 mm. The Inveon PET detector provided an

axial field of view (FOV) of 12.7 cm with a spatial resolution of 1.44 mm. PET images

were reconstructed using a 2D-filtered backprojection algorithm with attenuation

correction provided by microCT imaging. For the microCT scan, the following imaging

settings were used: two bed positions, 80 kVp, 500 μA, 500 ms exposure time, and 4 x 4

binning. After each ferret underwent microCT imaging, the bed position was reset and

microPET imaging with 18F-FDG (PETNET, Louisville, KY) began immediately. For

each ferret, 2 mCi of 18F-FDG was administered (i.p.) with a 60-90 min uptake period.

Radioactive dose was confirmed with an Atomlab 500 Dose Calibrator (Biodex Medical

Systems Inc., NY).

Image processing and analyses

All imaging data were processed with PMOD software (v3.1; PMOD Technologies Ltd.,

Zurich, Switzerland). MicroCT data were received from the Inveon platform as DICOM

files and PET data as microPET files. Scans were imported into the program's local SQL

database with the units for the PET radiotracer in kBq/cc. PET images were co-registered

with the CT images with re-slicing done as necessary to facilitate later calculations. For

analysis of 18F-FDG levels, the standardized uptake value (SUV) was used. SUV is a

widely used semi-quantitative measure that normalizes radiotracer uptake in a given

region of interest based on body weight, and calculated for this study as follows:

$$SUV = \frac{Tissue\ Concentration\ \frac{9kBq}{mL}}{Injected} Dose\ (kBq) * Body\ Weight\ (g) \qquad Eq.\ 1$$

For all calculations, animal weights were expressed in kilograms and FDG activity in

megabecquerels. For each image series, SUVs for each voxel were calculated using an

external filter in PMOD, with the radionuclide half-life set at 6586.2 sec for 18F-FDG.

For each pulmonary lesion, an ellipsoid volume of interest (VOI) was generated that

encompassed the structure. Then, automatic isocontour detection was used to refit the

VOI by setting a threshold of 50-60% of the difference between the maximum and

minimum intensity SUVs in the ellipsoid VOI such that $0.5*(SUV_{max}-SUV_{min})$. In cases

where the automated threshold included contiguous structures in the VOI, manual

refitting in conjunction with the co-registered CT scan was used to exclude those

surrounding structures. For all VOIs, maximum SUV (SUV_{Max}) and average and

standard deviation of all pixels in the volume ($SUV_{Mean} \pm SD$) were calculated.

For CT analysis, image interpretation was performed by a radiologist (in consultation

with the scientific team) having more than ten years of diagnostic experience along with

formal certifications by the American Board of Radiology (ABR) and the American Board of Nuclear Medicine (ABNM). Lesions on CT were identified using conventional criteria and terminology; Ground-glass opacity (GGO) is defined in this study as hazy increased lung opacity, with discernible underlying lung architecture such as visible bronchial and vascular structures, representing partial displacement of air in interstitial and alveolar airspaces; Consolidation is defined in this study as high density lung lesions (more dense than GGO) in which vascular and bronchial margins are obscured, representing complete displacement of alveolar air (605).

Viral titers in swabs and tissues

On days 1, 2, 3 and 6 and prior to euthanasia, swabs were taken from each ferret from nasal, throat and rectal regions. Following scheduled euthanasia, the nasal turbinates and the right caudal lobe of the lung from each ferret, which was divided laterally into four segments, were isolated. All swab and tissue samples were snap-frozen in liquid nitrogen and stored at -80°C until analyzed for virus titer by $TCID_{50}$. Frozen tissues were weighed and diluted 10% weight per volume into cold DMEM with 1% penicillin/streptomycin and 0.2% BSA before being homogenized and centrifuged to remove debris. Tissue homogenate and swabs were serially diluted 10-fold in DMEM with 2 μg/mL TPCK-Trypsin, 0.2% BSA, 4.5 g/L glucose, 1% penicillin/streptomycin, 2 mM L-glutamine, and 25 mM HEPES. Each sample was analyzed in quadruplicate following incubation in 96-well plates with Madin-Darby canine kidney (MDCK) cell monolayers at 37°C in 5% CO_2 for three days. Supernates were collected from each well were assayed for hemagglutination activity using 0.5% turkey red blood cells as an indicator of infection.

Viral titers were expressed as $\log_{10}$ TCID$_{50}$ / mL and were calculated using the Reed-Muench method (618).

Hemagglutination inhibition assay (HI)

The HI test quantitates serum antibody to influenza virus which can prevent agglutination of turkey RBCs (Fitzgerald Industries International Inc., MA). Heat-inactivated serum samples were treated with receptor-destroying enzyme (Sigma-Aldrich) for removing nonspecific inhibitors (followed by RBC adsorption) and were diluted 2- fold serially from initial dilution of 1:10. HA antigen (8 HA units in 25 µL) were added onto each well and incubated for 1 h at RT. Following antigen-antibody reaction, 50 µL of 0.5% turkey RBC were added to each well and incubated for 1 h at RT. HI negative wells were scored based upon a diffuse sheet of agglutinated RBCs covering the bottom. HI positive wells were scored if they showed a well circumscribed button of nonagglutinated RBCs.

Histopathology

Lungs were inflated and stored in 10% neutral-buffered formalin. Three lung sections were placed into cassettes per lung section (right cranial, left cranial, left caudal, and right middle lobe) until they were trimmed, paraffin-embedded, and sectioned. Sections were mounted on glass slides and stained with hematoxylin and eosin for microscopic evaluation at Experimental Pathology Laboratories, Inc. by a veterinary pathologist. Sections were examined for the presence of abnormal findings including supprative and necrosupprative inflammation; epithelial hyperplasia and cytokaryomegaly; and fibrinous and exudative changes. Changes were graded with a standardized scale of 0-5, with 0

classified as "not present", 1 as "minimal", 2 as "slight / mild", 3 as "moderate", 4 as "moderately severe", and 5 as "severe / high." For each ferret, a composite score for pathological changes was generated based on the locations in the respiratory tract (alveoli, bronchioli, bronchi) for statistical evaluation.

Statistical analyses

All statistics were performed using R version 2.13.0 and GraphPad Prism 5. For each image, mean SUVMax and standard deviations were obtained. For each ferret, SUVMax values were correlated with histopathologic scoring using Spearman's Rho (ρ).
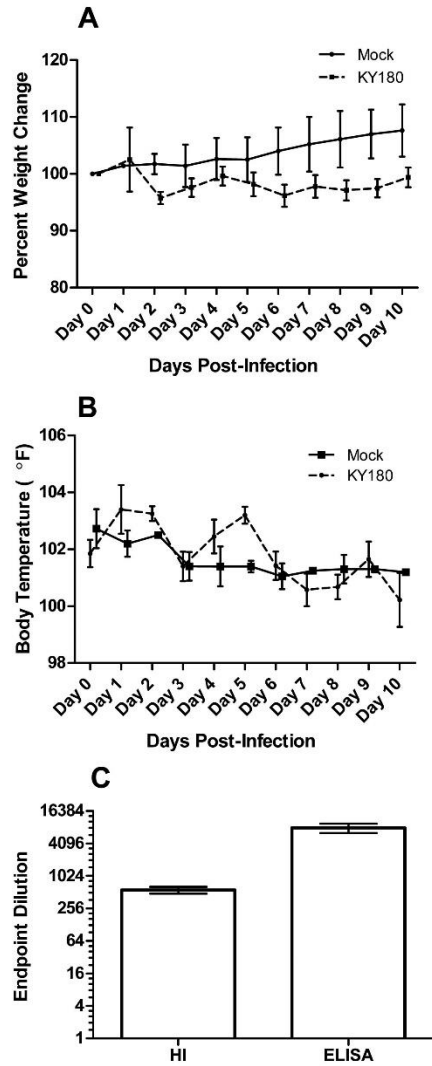
Figure 3.1 Characterization of KY/180 in female ferrets.

A cohort of six control and six KY/180-infected ferrets were examined for A) body

weight and B) temperature over a period of 10 days. C) Blood was examined for the

presence of HI and antibody titers at 14 days.

Figure 3.2 18F-FDG PET, CT, and PET/CT fusion images of the thorax in H1N1pdm-infected ferret 2213.

A) Day 0 shows background activity in the lung with minimal uptake in the mediastinal and subcarinal lymph nodes. B) Day 1 post-infection demonstrates an area of developing consolidation in the right caudal lobe corresponding to increased radiotracer uptake. C) By day 3, the consolidation appears in the right caudal lobe and into the left caudal lobe. D) By day 6, there are multiple lesions in the lung parenchyma bilaterally with intense radiotracer uptake.
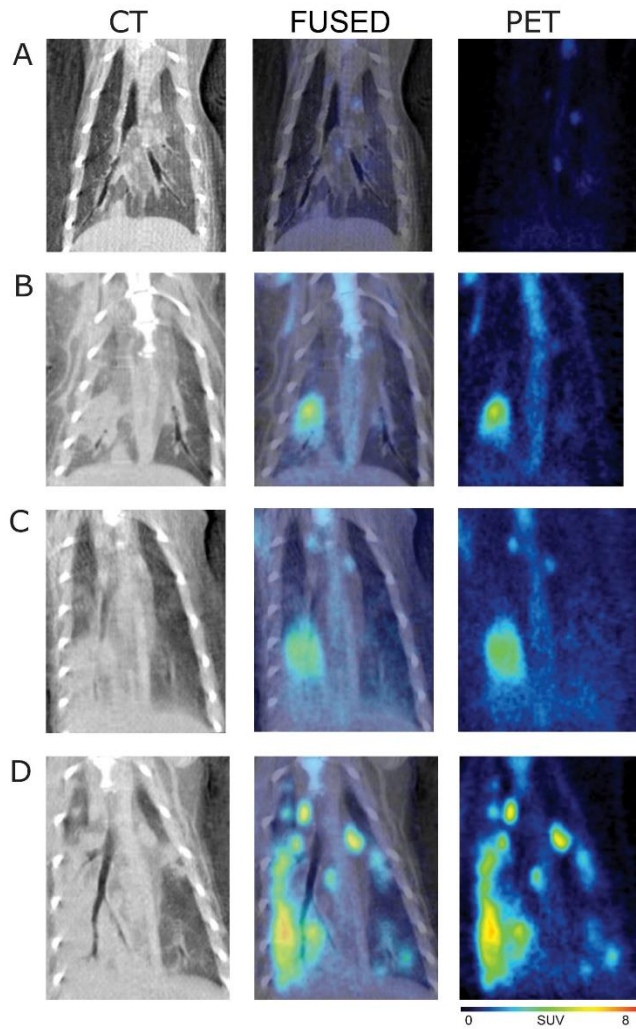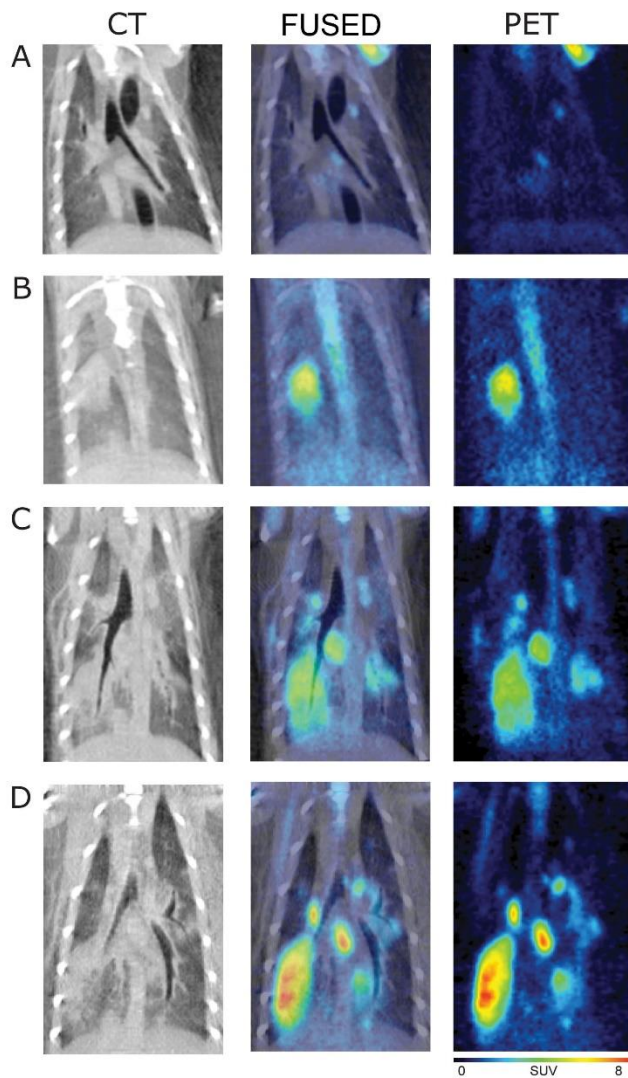
Figure 3.3 18F-FDG PET, CT, and PET/CT fusion images of the thorax in H1N1pdm-infected ferret 2214.

A) Day 0 shows background activity in the lung with minimal uptake in the mediastinal and subcarinal lymph nodes. B) Day 1 post-infection demonstrates an area of developing consolidation in the right caudal lobe corresponding to increased radiotracer uptake. C) By day 3, the consolidation has spread in the right caudal lobe and into the left caudal lobe. D) By day 6, there are multiple lesions in the lung parenchyma bilaterally with intense radiotracer uptake.

Figure 3.4 Right caudal lobe of ferret.

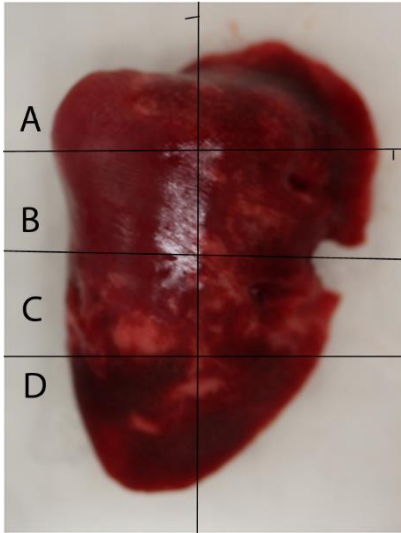The right caudal lobe of each ferret was divided into 4 sections, A (top), B (middle), C

(middle-lower) and D (bottom) for measurement of viral replication. Please refer to table

3.3 for viral replication titers measured from each tissue section.
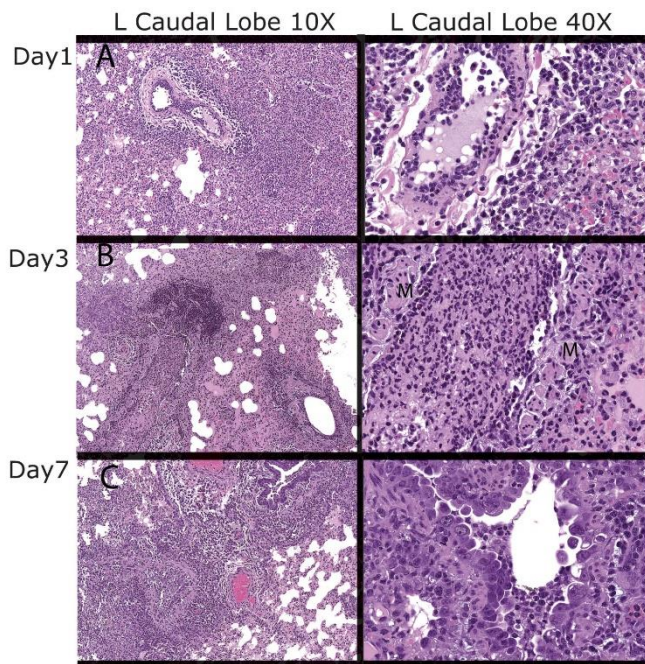
Figure 3.5 Histopathologic evaluation of the lung caudal lobe in H1N1 infected ferrets.
A) On day 1, there are small foci of inflammation (10X) in animal 2208. A higher 40X
magnification of the bronchiole (shown in the 10X magnification with a box) exhibits
neutrophils within the lumen with loss of part of the epithelial layer. Mixed cell alveolitis
surrounds the bronchiole. B) On day 3, a bronchiole with necrosupprative exudate is
highlighted at 10X for animal 2212. In the 40X magnification (from the region in the 10X
magnification with a box), muscle (M) defines the bronchiole from which the epithelium
has been sloughed and the lumen is filled with neutrophils (necrosuppurative
bronchiolitis). C) On day 7, a bronchiole with necrosuppurative exudate is surrounded by
an extensive area of mixed cell alveolitis. Cytokaryomegaly is depicted by the variable
large size and shape of the epithelial cells with piling up of the bronchiolar epithelium
(hyperplasia) as shown in 10X image, and also visible in this bronchiole from another
section of the left caudal lung lobe from animal 2214 (40X image).
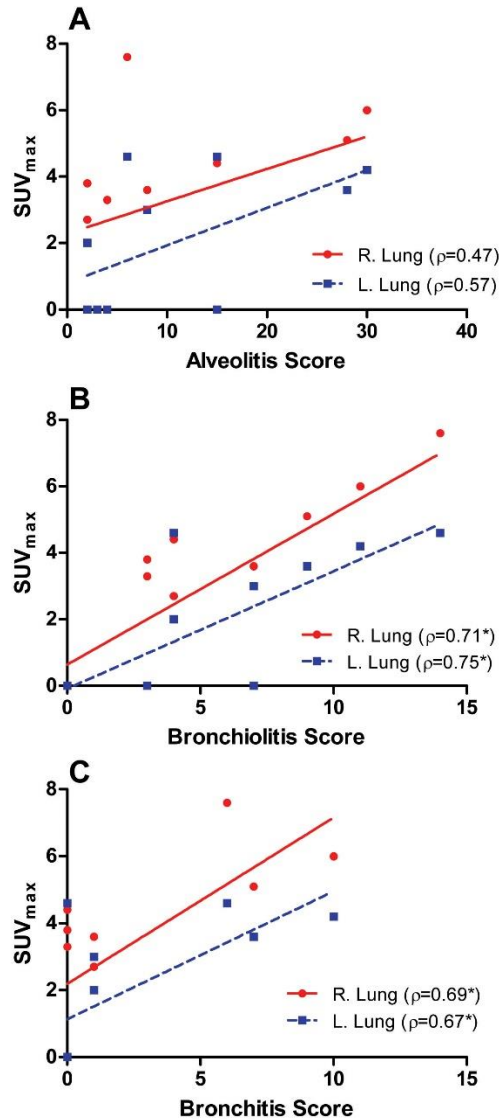
Figure 3.6 Correlations between SUVMax of lung lesions on FDG-PET versus histopathologic severity scores.

A) SUVMax versus cumulative alveolitis severity shows minimal positive correlations in the right (red) and left (blue) lung. B) SUVMax versus cumulative bronchiolitis severity shows high positive correlation in both lungs. C) SUVMax versus cumulative bronchitis severity demonstrates moderate correlation.

Table 3.1 Study design for ferret imaging and sample collection*

Group	Animal ID	Day 0	Day 1	Day 2	Day 3	Day 6	Day 7
1	2206/2207	£	†	†			
	2203/2210				†		†
2	2208		£†				
	2209		£†				
3	2202			£†			
	2204			£†			
4	2211				£†		
	2212				£†		
5	2213	£	£	£	£	£	†
	2214	£	£	£	£	£	†

†Date for necropsy; £ Date for imaging; *Swab samples were collected for viral

shedding daily and upon necropsy

Table 3.2 Viral shedding.

Group	Animal ID	Area	Day 1	Day 2	Day 3	Day 7
1	2206	Nasal	0*			
		Throat	0			
		Rectal	0			
	2207	Nasal		0		
		Throat		0		
		Rectal		0		
	2210	Nasal			0	
		Throat			0	
		Rectal			0	
	2203	Nasal				0
		Throat				0
		Rectal				0
2	2208	Nasal	0			
		Throat	4.7			
		Rectal	2.2			
	2209	Nasal	4.7			
		Throat	5.3			
		Rectal	0			
3	2202	Nasal	3.0	3.5		
		Throat	3.5	3.5		
		Rectal	1.2	0		
	2204	Nasal	0	3.0		
		Throat	3.5	3.5		
		Fecal	0	0		
4	2211	Nasal	0	0	0	
		Throat	3.8	4.7	4.3	
		Rectal	1.0	0	0	
	2212	Nasal	0	3.5	0	
		Throat	4.5	4.3	3.5	
		Rectal	1.0	0	0	
5	2213	Nasal	3.8	4.3	3.5	1.5
		Throat	5.5	2.7	5.0	2.0
		Rectal	0	0	0	0
	2214	Nasal	4.0	3.7	3.3	0
		Throat	6.7	3.7	5.3	0
		Rectal	2.7	0	2.3	0

*Numerical values are log base 10 $TCID_{50}/g$

Table 3.3 Distribution of H1N1pdm in right caudal lung and nasal turbinates

Day		Animal ID	RC A	RC B	RC C	RC D	NT
1		2208	6.7*	6.5	5.0	5.7	5.7
		2209	0	6.5	0	1	6.8
2		2202	0	4.4	3.3	4.5	5.0
		2204	0	0	0	0	4.5
3		2211	4.2	0	0	2.8	6.0
		2212	5.8	6.5	3.5	6.3	4.7
7		2213	0	0	0	0	0
		2214	0	0	0	0	0

*Numerical values represent log base 10 $TCID_{50}/g$; Abbreviation: right caudal (RC) lung

lobe divided into sections A through D as illustrated in figure 3.4, nasal turbinate (NT)

CHAPTER IV

LOWER RESPIRATORY TRACT INFECTION OF THE FERRET BY PANDEMIC

INFLUENZA A(H1N1)2009 VIRUS TRIGGERS BIPHASIC, SYSTEMIC AND

LOCAL NEUTROPHIL RECRUITMENT

Overview

Infection of the lower respiratory tract by influenza A viruses results in an increase in inflammation and immune cell infiltration in the lung. The dynamic relationships among the lung microenvironments, the lung and systemic host responses during infection remain poorly understood. Herein, we used an extensive systematic histologic analysis coupled with live imaging to gain access to these relationships in ferrets infected with the pandemic A(H1N1)2009 virus [H1N1pdm]. Neutrophil levels rose in lungs of H1N1pdm-infected ferrets 6 hours post-infection and became concentrated at areas of H1N1pdm-infected bronchiolar epithelium by 1 dpi (days post-infection). In addition, neutrophils were increased throughout the alveolar spaces during the first 3 dpi, and returned to baseline density by 6 dpi. Histochemical staining revealed neutrophil infiltration in the lungs occurred in two waves, at 1 and 3 dpi, and gene expression within microenvironments suggested two types of neutrophils. Specifically, CCL3, but not CXCL8/IL-8, levels were greater within discrete lung microenvironments, and coincided with increased infiltration of neutrophils in the lung. We used live imaging of ferrets to monitor host responses within the lung over time with ^{18}fluorodeoxyglucose (FDG).

Sites within the H1N1pdm-infected ferret lung with high FDG had high levels of proliferative epithelium. In summary, neutrophils invaded the H1N1pdm-infected ferret lung, globally, and focally, at sites of infection. The microenvironments with increased neutrophils, did not correlate with FDG, and hence, FDG-uptake may reflect prior infection and inflammation that has experienced damage as reflected by bronchial regeneration of tissues in the lungs at sites of high FDG.

Importance

Severe influenza disease is characterized by an acute infection of the lower airways that may rapidly progress to organ failure and death. Well-developed animal models that mimic human disease are essential to understanding the complex relationships of the microenvironment, organ and system in controlling virus replication, inflammation, and disease progression. Employing the ferret model of H1N1pdm infection, we used live imaging and comprehensive histological analyses to address specific hypothesis regarding spatial and temporal relationships that occur over the progression of infection and inflammation. We show the general invasion of neutrophils at the organ level (lung), but a distinct pattern of localized accumulation within the local microenvironment at the site of infection. Moreover, we show that these responses were biphasic within the lung. Finally, live imaging revealed an early and sustained host metabolic response at sites of infection that may reflect damage and repair of tissues in the lungs.

Introduction

The annual impact of seasonal influenza A viruses (IAV) on public health is fairly predictable and is mostly preventable in normal, healthy populations with currently available vaccine strategies (619-621). However, novel IAV variants arising from antigenic shift in zoonotic reservoirs are not predictable and may not be immediately preventable with contemporary vaccines (622-624). In the last 100 years, IAV have emerged with high transmissibility and virulence (1918 H1N1), high transmissibility and moderate virulence (2009 H1N1 pandemic), and low transmissibility and high virulence (H5N1, H7N9) (122, 625, 626). Virulence factors of IAV have been attributed to specific mutations in the hemagglutinin (HA) and polymerase (PB2) viral proteins (627, 628). Moreover, the specific sialic acid-binding affinity of the HA determines the cell types infected in the respiratory tract and hence the location of infection (i.e., upper versus lower) (116, 281). In general, IAV strains that are able to infect the lower respiratory tract cause more inflammation and have greater lethality (52, 281, 294, 629).

Controlled inflammation is required for resolution of IAV infection, yet increased inflammation is correlated with more severe influenza disease, and a dysregulated immune response to infection with highly pathogenic avian IAV (HPAI, *e.g.,* H5N1) may be fatal (9, 253). Seasonal H3N2 and H1N1 IAV typically infect only the upper respiratory tract and result in mild inflammation of the nasopharynx and trachea. Infection and increased inflammation in the lung was observed in cases of the 2009 pandemic H1N1 IAV (H1N1pdm), which caused increased mortality compared to seasonal strains (6, 30, 42, 127, 132, 630). Studies in humans and ferrets show that

highly pathogenic avian influenza (HPAI) viruses (*e.g.*, H5N1) and the H1N1pdm viruses infect and replicate well in the lower respiratory tract (95, 629), yet cases of H1Npdm virus had much lower lethality compared to H5N1 and did not cause severe immune dysregulation. Thus, the precise relationship between location of infection and location of inflammation is complex, and pathogenesis may depend on other specific immune responses to certain IAV isolates.

We know very little about how most respiratory viral infections, and the resulting immune responses, progress in real-time within the local microenvironments of the upper and/or lower respiratory tract in humans or in animal models. Live, whole body imaging of pathogens or host responses may offer a bridge to gain insight into these dynamics (603). During the 2009 H1N1pdm outbreak, molecular imaging of patients revealed that FDG (fluorodeoxyglucose) increases and becomes concentrated in sites of consolidation and ground-glass opacities within the lung (6, 42, 602, 609). This motivated our exploration of live, FDG-imaging in the ferret model of IAV infection (631). The ferret serves as a critical animal model to ask questions regarding IAV disease progression given the similarity in its clinical signs and disease with those in humans (266, 272, 631, 632). Similar to those observations in human cases of H1N1pdm disease, H1N1pdm-infected ferrets have a focal pattern of FDG uptake in the lungs that correlated with bronchiolitis and bronchitis histopathology scores (631).

We and others have shown that IAV infection initiates in discrete foci of the respiratory tract (285, 631, 633). Viral replication triggers inflammation in the form of cytokines,

chemokines, and the infiltration of innate immune cells in the lungs (30, 135, 360).

Cellular uptake of FDG in acute lung injury correlates with inflammatory cell infiltration

(612, 634). We and others have hypothesized that cellular uptake of FDG in the lung

following infection may be due to inflammatory cell infiltration, *e.g.,* neutrophils and

monocytes (631, 635, 636). Neutrophils are among the first to respond to many types of

inflammation, particularly bacterial infection (16, 18, 60). Neutrophils perform many

functions during bacterial infection (*e.g.,* phagocytosis, release of anti-bacterial proteases,

reactive oxygen species) yet very little is known about their contributions to viral

infections (472). In mild and severe human cases of influenza, neutrophils and neutrophil

chemoattractant signals are elevated in blood and nasal lavage and are independent of

bacterial co-infection (6-8, 30, 99, 105). In mouse models of influenza, depletion of

neutrophils results in increased virus replication and increased disease severity (84, 577,

637, 638). However, it is known that neutrophils are increased in the lungs of mice during

severe IAV infection (85, 253, 294, 363, 639).

Currently, we know very little about the timing and spatial distribution of neutrophils as

they infiltration the lungs following viral infection, and importantly, how they function in

disease resolution or exacerbation. Herein, we used an extensive systematic histologic

analysis coupled with live imaging to probe the temporal dynamics of virus distribution

and inflammation within microenvironments of lungs of ferrets infected with a clinical

H1N1pdm isolate. Given their importance early in infection, we focused on neutrophils

and hypothesized that neutrophils would migrate to sites of IAV infection preferentially,

creating an inflammatory microenvironment (16, 80, 472, 636). IAV distribution,

neutrophil accumulation and selected immune gene expression profiles were measured within discrete sections of a lung lobe. We show that recruitment of neutrophils to the lung following infection occurs in two waves, coincides with chemokine gene expression, and may reflect two different states of neutrophil activation. Using extensive histological sampling, we show that neutrophilic inflammation correlates with the temporal and spatial distribution of IAV in the lungs of infected ferrets. Importantly, the neutrophil recruitment and accumulation occurs at the tissue level (*i.e.,* the whole lung) and at sites of IAV infection. Finally, we show that FDG uptake in the infected lungs is not due to neutrophilic infiltrates, but correlates with epithelial cell proliferation and regeneration following infection.

Materials and Methods

Virus and viral titers.

Ferrets were infected with a clinical isolate of IAV H1N1pdm (A/Kentucky/180/2010) taken from a fatal case of H1N1pdm (130) that has been previously described in ferret (631), DBA/2 mouse (130) and human primary cell culture (331) models. Virus was grown in 10-day old embryonated hen eggs and diluted in phosphate buffered saline (PBS). The concentration of virus stock was determined using 50% tissue culture infectious dose assay (TCID$_{50}$) in Madin-Darby canine kidney cells as described previously (631) .

Ferrets, ferret virus challenge, and ethics statement.

Four month old (16-20 weeks) female Fitch ferrets were obtained from Triple F Farms

(Sayre, PA, USA). Ferrets were determined to be seronegative for A/Uruguay/716/2007

(H3N2), seasonal A/Brisbane/59/2007 (H1N1), and A/Kentucky/180/2010 (H1N1pdm)

subtypes of IAV by hemagglutination inhibition assay (631). Animals were housed for

an acclimation period of at least one week at the University of Louisville Regional

Biocontainment Laboratory prior to virus challenge (this research facility is fully

accredited by the Association for Assessment and Accreditation of Laboratory Animal

Care International). Animals were maintained on a 12-hour light/dark cycle and provided

Teklad Laboratory Diet #2072 (Harlan/Teklad, Madison, WI) and water *ad libitum*. The

research described herein complied with federal statutes and regulations relating to

animal experimentation, including the Animal Welfare Act, and adhered to principles

stated in the Guide for the Care and Use of Laboratory Animals, published by the

National Research Council, 1996. Experiments involving ferrets were approved by the

University of Louisville Institutional Animal Care and Use Committee.

Ferrets were inoculated with 10^6 TCID$_{50}$ influenza A/Kentucky/180/2010 (H1N1pdm) as

a 1 mL bolus. To prepare animals for infection with virus, ferrets were sedated with

intramuscular 0.05 mg/kg atropine, 5.0 mg/kg ketamine, and 0.08 mg/kg

dexmedetomidine. Sedated ferrets were scruffed and held with their nose pointing

upwards and neck extended while 0.5 mL of virus or PBS was given per naris. Following

intranasal (i.n.) inoculation, animals were held in place for 1 min before anesthesia was

reversed with 0.4 mg/kg atipamezole. Following infection, ferrets were measured daily

for temperature and weight and monitored twice daily for clinical signs (dyspnea, nasal and ocular discharge, loss of appetite, neurological signs, sneezing, lethargy, anorexia, diarrhea, and other abnormalities) through study completion. Body temperatures were measured via subcutaneous implanted microchip IPTT transponder (BioMedic Data Systems, Inc.). Right caudal lung tissues were snap frozen on liquid nitrogen and stored -80°C until homogenized and stored in TRIzol® reagent (Invitrogen). Blood was taken in sodium-ethylenediaminetetraacetic acid tubes and stored in TRIzol®. Other lung tissues were taken for immunohistochemistry (IHC) as described below.

Analysis of gene expression levels by RT-PCR.

Previously, the right caudal lung lobe of each ferret was divided into four sections and each section was homogenized for quantification of virus by determining the $TCID_{50}$ (631). Following homogenization, a portion of the lung tissue was placed in TRIzol® reagent and stored at -80°C. Herein, total RNA was extracted from these samples and 1 µg RNA was used to make cDNA using Superscriptase III. Ferret mRNA gene-specific primers were generated using published ferret sequences (Table 1). Primers were designed to span exons when possible by comparing to known human and canine splice sites. Primers were chosen to identify cell type-specific targets (*e.g.*, granulocyte colony stimulating factor receptor [G-CSFR, *Csf3r* gene], myeloperoxidase [MPO, *Mpo* gene], and neutrophil elastase [ELANE, *Ela2* gene] transcripts which are specific to neutrophils; monocyte colony stimulating factor receptor [M-CSFR, *Csf1r* gene] which is used as a macrophage/monocyte marker; NCR1 [*Ncr1* gene] which is a natural killer cell receptor; and CD11b [*Itgam* gene] which is an integrin expressed on inflammatory leukocytes), as

well as soluble inflammatory signals (interleukin-6 [IL-6, *Il6* gene], CXCL8 [also known as interleukin-8, *Il8* gene], interferon-beta [IFN-β, *Ifnb1* gene], CCL2 [also known as monocyte chemotactic protein 1, *Ccl2* gene], CCL3 [also known as monocyte inducible protein 1 alpha, *Ccl3* gene], and tissue necrosis factor-alpha [*Tnf*]). Real time-polymerase chain reaction was performed using SYBR Green dye on a ViiA™ 7 real time PCR machine (Applied Biosystems). Primers were validated using mitogen-stimulated whole blood from donor ferrets (Marshall Farms; data not shown). Transcript fold-increase measurements were compared to housekeeping genes (glyceraldehyde 3-phosphate dehydrogenase [*Gapdh*]) and average mock-infected animals using the delta-delta-cycle threshold method ($\Delta\Delta Ct$); the fold change is expressed here as the $2^{-\Delta\Delta Ct}$ value.

Histology.

Lungs were inflated with 10% neutral-buffered formalin and fixed for 48 h. Lungs were trimmed, placed into cassettes, dehydrated through ethanol to Limonene-D, paraffin-embedded, and sectioned at 5 μm. For systematic sampling of the lungs, the right and left caudal lung lobes (RCa and LCa, respectively) were trimmed into four consecutive transverse slices approximately 0.5-cm thick moving from the lung hilum to the posterior of the lobe, as illustrated in Fig. 1. Sections (1, 2, 3) followed the main bronchus to approximately the lower-middle of the lung, as shown on Fig. 1 (left panels). The sections were paraffin-embedded and two serial 5 μm sections were mounted onto each glass slide (Fig. 1, middle panel). Slides were dewaxed in 3 xylene washes, and rehydrated in decreasing ethanol gradients to water for IHC, and regions of the slides were photographed and analyzed (*e.g.*, square regions on Fig. 1, right panel).

159

IHC and tissue staining.

For detection of IAV nucleoprotein (NP), antigen was retrieved with 1% Pronase in CaCl$_2$ solution and was detected with a primary monoclonal antibody (HB65 clone EVS238 from East Coast Bio, Inc.)(640) and avidin-biotin complex amplification (Vector Labs) was used to visualize the antibody with diaminobenzidine (DAB) peroxidase substrate. The slides were dehydrated through increasing ethanol gradients, cleared in xylenes, and mounted under coverglass with toluene solution. Neutrophils were stained pink with a 30 min incubation in naphthol AS-D chloroacetate esterase (NACE) at 37°C according to manufacturer's instructions (Sigma-Aldrich) and one serial section was counterstained with hematoxylin to identify anatomical features. Slides were mounted with coverglass under an aqueous mounting medium (Vectamount AQ, Vector Labs). For each NACE-stained slide, the next consecutive slide was similarly stained for IAV antigen. Rehydrated tissue slides were incubated in 3% hydrogen peroxide and avidin/biotin blocking buffer (Vector Labs) for 15 min each at room temperature before blocking in 5% fetal calf serum for 1 h at room temperature. For both NACE and NP staining, one section per slide was counterstained with hematoxylin for anatomical reference, and a second unstained section was used for image processing as described below. Antigen retrieval for Ki-67 and histone-3 was performed by heating rehydrated slides in a 72°C water bath overnight in target retrieval buffer (Dako). A monoclonal antibody cross-reactive to ferret Ki-67 (Dako, clone MIB-1) was used as above to stain with DAB peroxidase substrate, and rabbit polyclonal anti-human histone-3 antibody (Abcam) was stained red with alkaline phosphatase substrate Vector Red (Vector Labs).

Sirius red staining was performed by incubating rehydrated tissue slides for 30 min in saturated picric acid containing 0.1% Sirius Red and 0.1% Fast Green, then dehydrating and mounting under Permount (Fisher Scientific).

IHC analyses.

Images from IHC slides were analyzed with the "Threshold Colour" plug-in of the FIJI package of ImageJ software (641). Briefly, pixels of a certain hue and saturation (bright pink for NACE-stained neutrophils, red for Sirius Red, and brown for DAB-stained NP-positive or Ki-67-positive cells) were selected and the percentage of total pixels was calculated for each image. The percent consolidation was calculated for each image by converting each image to high contrast 8-bit (black-and-white) and calculating the percentage of black pixels (*i.e.*, the number of pixels containing tissue, eliminating airspace). A Java computer language script (available upon request) was generated to analyze all images in the same way using validated settings. Neutrophil density is reported here as the percent NACE-positive pixels divided by percent consolidation in a single image. To validate this measurement, two independent observers counted the number of NACE-positive neutrophils in 50 images and there was a 95% correlation between the automated method and visual inspection (data not shown).

Comprehensive, systematic sampling of the caudal lung lobes was performed by a blinded observer choosing four regions per NACE-stained tissue section and photographing three images per region at 20X magnification (squares in right panels of Fig 1). To correlate the amount of neutrophils with foci of IAV infection, NP antigen-

positive areas were photographed and their anatomical locations were recorded (i.e.,

bronchial epithelium, bronchiolar epithelium, submucosal epithelium, alveolar region).

The same site was located on the NACE-stained slides and photographed (i.e., a serial

section of tissue no greater than 15 μm away from the NP-positive site). IAV NP

antigen-negative regions were anatomically site-matched to NP-positive focus and

located in the same general regions (e.g., a region of bronchiolar epithelium that was

antigen-negative was selected on a slide where bronchiolar epithelium was antigen-

positive, and therefore was always < 0.5 cm from the original antigen-positive focus).

NACE-positive neutrophils, IAV NP-positive cells, and Sirius Red-stained collagen were

measured using automated image analysis as described above. The number of Ki-67-

positive cells per slice was estimated by two observers using a scoring index (642, 643).

Ferret molecular imaging.

Ferrets were anesthetized by isoflurane induction and 2 mCi of FDG was administered

intraperitoneally as previously described (631, 644). The dose was confirmed before and

after injection with an Atomlab 500 Dose Calibrator; Biodex Medical Systems Inc., NY.

Ferrets were kept warm under sedation with isoflurane for 1 h prior to intubation and

during imaging using the Siemens Trimodal as described previously (631, 644).

Following imaging, ferrets were removed from isoflurane, given intramuscular ketamine

(5 mg/kg) and dexmedetomidine (0.08mg/kg), and immediately euthanized by cardiac

exsanguination.

PET-CT Image Analysis.

After PET and CT images were acquired from the Trimodal scanner, PET images are aligned to CT anatomical reference space in order to provide one-to-one voxel correspondence between anatomical and functional images. Since pathology on CT (*e.g.,* consolidation) can confound true lung volume and boundary estimation, the lungs were segmented from CT images using a robust algorithm (*i.e.,* interactive region growing) proposed in (645) by which users had chance to correct any mis-segmented lung portion interactively if necessary. Then, significant uptake regions were segmented using affinity propagation PET delineation algorithm (646). Once all the metabolically active lesions were identified and delineated, maximum standard uptake values (SUVmax) and maximum intensity values were calculated as an evaluation metric for the FDG uptake. These measurements were taken from regions coinciding with histopathology slices, locating the slices on the registered and segmented PET-CT scans manually. The alignment between histology and PET-CT was ensured by processing 9-parameter affine registration and using prior knowledge about the anatomy, particularly the airway structures and the lung lobes. For airway structure extraction, we used the hybrid algorithm for delineation of the airway tree as proposed in (647). Due to the 2D nature of the histopathology slices, registration operations were all done in 2D. After alignment of the histopathology slices into PET-CT scans were satisfied, *in vivo* imaging correlation with histopathology slices was explored.

Statistical analyses.

All statistics were performed using R version 2.13.0 and GraphPad Prism 5. In general, nonparametric statistical tests were used as stated in the results, even when sample size was large non-independent measurements within the same ferret made parametric analyses undesirable. Pairwise *post hoc* tests were adjusted for multiple comparisons using Bonferroni's method. For generalized linear modeling of neutrophil density, variables such as time post-infection, individual ferret, lung lobe within ferret, and sample region within lung lobe approximated a nested block design with repeated measures within ferrets, and within lobes within ferrets. The fully factorial model was reduced using stepwise regression to find the best fitting model as determined by significant reduction in Akaike information criterion. For all statistical tests, the Type-I error rate was set to $\alpha = 0.05$; although values $p < 0.1$ are given consideration here due to sample size limitation and pseudoreplication as discussed below.

Results

Previously we have shown that infection of ferrets with H1N1pdm (A/Kentucky/180/2009) causes moderate disease, evidenced by the brief febrile period, low weight loss, and clinical signs recorded during infection (*i.e.,* lethargy, rhinorrhea) (631). Virus was detected from nasal swabs, throat swabs, nasal turbinates, and right caudal lung lobes on 1, 2, and 3 dpi, but was undetectable by 7 dpi (one animal had low amounts of virus in nasal and throat swabs on 7 dpi) (631). Histopathology revealed a focal bronchitis and bronchiolitis characterized by infiltration of leukocytes (neutrophils and exudate macrophages) during H1N1pdm infection (631). Cellular uptake of FDG

correlates with leukocytic infiltration in certain model systems (612, 635, 636). In this ferret model, we have observed progressive increase of FDG uptake in distinct foci of the H1N1pdm-infected ferret lung (631). Therefore, herein, we tested the overarching hypothesis that FDG uptake during ferret IAV infection was due to infiltrating neutrophils and macrophages. We first determined which leukocytes were likely to be increased in these regions by measurement of immune gene expression profiles within discrete lung microenvironments.

Lung microenvironments of IAV infection have increased CCL2 and CCL3 gene expression

First, the expression of signature immune genes was analyzed in the right caudal lobe of one mock and two H1N1pdm-infected ferrets on 1, 2, 3, and 7 dpi. As stated above, the right caudal lobe had the greatest levels of FDG uptake following infection (631). Primers for IAV HA and inflammatory cytokines and chemokines were used to confirm the presence of virus and the host immune response to infection. Genes were chosen to detect cytokines and chemokines that are known to be increased during the acute phase of influenza infection and are important for leukocyte activation and chemoattraction (*e.g.*, IFNβ, TNFα, IL-6, CCL2, CCL3, and CXCL8). First, IAV HA mRNA was detected at 1, 2 and 3 dpi, but not 7 dpi, and was not uniformly distributed within the right caudal lobe (data not shown). This matched the pattern of IAV infection as measured by $TCID_{50,}$ previously reported from the same ferret lung sections (631). The fold-change in gene expression of inflammatory cytokines (IFNβ, TNFα, IL-6) and chemokines (CCL2, CCL3, CXCL8) in sections were compared to mock-infected controls. No significant

165

change in inflammatory expression levels was detected in the blood (data not shown). In some lung sections, the cytokines IL-6 and TNFα (not shown) were elevated at 2 dpi, but not in all sections from infected ferrets. Other inflammatory signals (*e.g.,* IFN-β, CXCL8) were not elevated above mock-infected animals (data not shown). Gene expression levels of CCL2 and CCL3 were both slightly increased at 1 dpi and significantly increased on 3 dpi ($p < 0.05$, Fig. 2). Both CCL2 ($p = 0.01$) and CCL3 ($p = 0.04$) were significantly increased in all lung sections expressing viral HA gene mRNA (compared to all HA-negative sections, including those within the same ferret; Mann-Whitney $U = 105$ & 73, respectively for CCL2 and CCL3).

Neutrophil-specific gene expression is detected in lung microenvironments

Primers for leukocyte-specific genes which encode cell surface receptors and other cell-specific proteins were used to determine the presence of neutrophils (G-CSFR, MPO, ELANE, CD11b), macrophages (M-CSFR, CD11b), and natural killer cells (NCR1, Granzyme A, CD11b) in the lung. The monocyte/macrophage specific gene, *Csf1r* (M-CSFR), was increased slightly at 2 and 3 dpi, and increased expression of the natural killer cell receptor, *Ncr1* (NCR1), was detected in some sections at 2 and 3 dpi (data not shown). Some lung sections had increased expression of the leukocyte cell surface integrin, CD11b, and the median expression value of CD11b in HA-positive sections was significantly increased above mock (median = 2.6, $p = 0.01$, Wilcoxon test, data not shown). Expression of the neutrophil growth factor receptor gene, *Csf3r* (G-CSFR), was increased in lung sections at 3 dpi ($p < 0.05$) (Fig. 3A). Expression of *Csf3r* was not significantly increased in tissue sections that were positive for HA gene expression

compared to HA-negative sections (Mann-Whitney *U* test). Neutrophil specific granule

genes (*e.g.*, *Mpo*, *Elane*) were not significantly upregulated compared to the mock-

infected animals (data not shown).

Neutrophils have biphasic infiltration into the lungs of IAV-infected ferrets

The major inflammatory signals in the right caudal lung sections were the neutrophil-

specific gene *Csf3r* and the leukocyte chemoattractants CCL2 and CCL3. To confirm the

temporal pattern of neutrophils detected by gene expression in the lungs of these ferrets,

NACE staining was used to label neutrophil specific granules. One histological

preparation per lung lobe (except right caudal lobe which was used for gene expression,

above) from H1N1pdm-infected and mock-ferrets were stained and inspected for

neutrophils. To estimate the number of neutrophils within the stained histological

sections, image analysis software was used to determine the amount of NACE-positive

pixels per unit of tissue in an image (20X objective) of the NACE stained lung, as

described in the methods (expressed as the estimated "neutrophil density"). Image

analysis of sites chosen haphazardly within each tissue slice revealed that the overall

density of neutrophils in the lung was biphasic, showing a maximum at 1 dpi ($p < 0.05$)

with another peak at 3 dpi (n.s.) following a decrease at 2 dpi (Fig. 3B). Thus, the major

peak of neutrophils did not correspond to the major peak of neutrophil-specific gene

expression in the lung. The other lung lobes showed a wide range of neutrophil density,

similar to the gene expression data, suggesting there were foci of neutrophil infiltration

throughout the lungs.

167

Neutrophils may hone to specific sites of IAV infection in the lungs

To determine the precise distribution of IAV within the lungs, IHC was used to detect NP antigen in paraffin-embedded sections of the remaining lung lobes (except of right caudal lobe). Infection was detected in bronchial, submucosal, and bronchiolar epithelial cells (Fig. 4A-D), but not alveolar epithelium (not shown). IAV NP was detected from all infected ferrets at 1 and 3 dpi, and from one animal at 2 dpi; but was not detected from infected animals 7 dpi. H1N1pdm infection was highly focal in the lung, and was primarily restricted to sites in bronchioles and bronchi (Fig. 4A-D). Similarly, the pattern of antigen positivity matched the IAV mRNA expression, the pattern of chemokine and neutrophil-specific gene expression and the pattern of NACE staining. Counterstaining NP-labeled sections with hematoxalin allowed the identification of increased numbers of inflammatory macrophages and neutrophils, some of which were antigen-positive (Fig. 4D), at foci of infection in the bronchioles. Therefore, neutrophils appeared to hone to the sites of infection in specific anatomic regions.

Comprehensive sampling of the lung lobes for neutrophil infiltration

he preliminary data suggested that neutrophils infiltrate the lungs and hone to sites of IAV infection, driven by chemokine gradients (*e.g.,* CCL3). However, the data were correlative because the sampling was not comprehensive and data were obtained from different lobes (*i.e.,* gene expression from the right caudal lobe, neutrophil and NP staining from the four remaining lung lobes). Therefore, we performed a second ferret study to confirm these observations using a systematic histological sampling of the lung. Six female ferrets were infected with 10^6 TCID$_{50}$ of H1N1pdm (plus 2 mock-infected)

and 2 animals were euthanized per time-point at times that were established to have peak

neutrophil infiltration (1 dpi and 3 dpi) as well as an early time post-infection (0.25 dpi).

Left and right caudal lung lobes were formalin-fixed, then sectioned into four 0.5 cm

cross-sections from the hilum moving posteriorly, embedded in paraffin, and prepared for

histology (three cross-sections shown in Fig. 1). Tissue slices were NACE-stained and

photographed to quantify neutrophils. To establish factors important neutrophil

distribution in the lung, a methodical sampling was performed to provide data for a

generalized linear model. Four regions from each slice were chosen blindly, and three

non-overlapping images were taken from each region to quantify the number of NACE-

positive pixels as a function of total tissue (excluding airways) per image using ImageJ

(Fig. 1). This established a 3-D grid of sampling locations within the caudal lung lobes,

wherein three images are taken from locations within each caudal lung lobe ($n = 48$

images per lung lobe).

Neutrophils infiltrate the right caudal lobe at early times after infection

Step-wise model testing of the generalized linear model revealed that the best-fitting

model included time post-infection, lung lobe (left versus right), and the distance from

the lung hilum. *Post hoc* analyses confirmed that neutrophils were significantly

increased at 1 dpi and at 3 dpi as in the previous study (Fig. 5A, $p < 0.001$ in the left and

right caudal lobes), however increased neutrophil density was measured in the lungs of

infected animals above mock as early as 0.25 dpi (Fig. 5A, $p < 0.05$ in the left caudal

lobe, n.s. in the right caudal lobe). The distribution of neutrophils was highest in the right

caudal lobes at 0.25 and 1 dpi (Fig. 5A, $p < 0.001$) compared to the left, but not at other

169

time points. Additionally, it is important to note that a range of neutrophil density was observed, yet, in general, infected animals had higher baseline levels of neutrophils in either lobe at 0.25 dpi, 1 dpi, and 3 dpi. Thus, neutrophils appeared to be focally distributed throughout the lung, and these observations (*e.g.,* increased right caudal lung) suggest that they are driven by IAV infection.

Neutrophils are increased at sites of IAV infection.

To test the hypothesis that neutrophils were increased at foci of IAV-infected epithelial cells, IHC staining for IAV NP was performed in serial sections of the NACE-stained tissues taken from right and left caudal lobes as described above and Fig. 4. Using NP-stained serial sections as a reference, images were taken from three areas of NACE-stained tissue slices defined by their distance from NP-positive. First, three non-overlapping images were taken from each antigen-positive site. For each antigen-positive site, two other sites were chosen and three non-overlapping images were analyzed: sites < 1cm from antigen-positive sites (within the same histology slice), and sites > 1 cm from antigen-positive sites (other histology slices within the same lobe). These three groups of images were also compared to images taken of NACE-stained mock-infected controls, and image analysis software was used to calculate the estimated neutrophil density as described above. There was no linear relationship between distance from focus of infected cells and density of neutrophils, *i.e.,* neutrophils were increased in all sites relative to mock-infected control animals (Fig. 5B, $p < 0.01$). However, a pattern was revealed by resolving the spatial distribution over time: neutrophil density was significantly greater at NP-positive sites and at sites <1 cm from known NP-positive sites

at 1 dpi (Fig. 4, 5B, $p < 0.01$). There was no difference in spatial distribution at 3 dpi, and neutrophil density remained increased relative to mock-infected controls (Fig. 5B, $p < 0.01$).

Neutrophils are increased at specific locations of IAV infection.

To test the hypothesis that anatomical location explained the distribution of neutrophils after infection, sites of IAV-positive bronchi (*e.g.,* Fig. 4A), seromucinous glands (*e.g.,* Fig. 4B), and bronchioles (*e.g.,* Fig. 4C, 4D) were identified (no antigen-positive alveolar epithelial cells were detected). These sites and antigen-negative sites within the same ferret (matched to a similar anatomic region) were located on NACE-stained serial sections, imaged (Fig. 4E-G), and analyzed using image analysis software to calculate the estimated neutrophil density as described above. There was a significantly higher density of neutrophils in IAV-positive bronchioles compared to controls (Figs. 4C, 4D, 4G, 4H, and 5C, $p < 0.01$). Neutrophils were not increased in bronchi or seromucinous glands above antigen-negative regions (Figs. 4E, 4F, and 5C). Furthermore, neutrophils were increased in bronchioles and alveoli where there was no IAV-positive antigen present by IHC (Fig. 5C). Interestingly, certain areas containing neutrophils in the lumen of bronchioles near IAV-positive epithelial cells had extracellular Histone H3 staining (data not shown), an indicator of neutrophil extracellular trap formation (NETosis). However, there were insufficient sites of NETosis and a lack of available reagents for the ferret model to pursue investigation of this phenomenon further at this time.

Approach to analyze PET- FDG images to achieve direct spatial correspondence with histology

We have previously reported that molecular imaging of ferrets using FDG-PET showed progressive increase in inflammation following infection with H1N1pdm (correlated with bronchiolitis and bronchitis pathology scores) that was greatest in the right caudal lobe but also focally distributed throughout the other lung lobes (631). We hypothesized that this may be due to increased inflammatory cell infiltration at sites after infection (612, 631, 635, 636). Therefore, we injected infected ferrets with FDG and imaged them with PET-CT prior to euthanasia on 0.25, 1, and 3 dpi (Fig. 6). Using the same ferrets in the second study, we analyzed PET-CT data similar to histological data (*i.e.,* a 3D grid) and achieve direct spatial correspondence between the histology and imaging. Automated airway segmentation of CT images was first performed to extract the lungs and airways from the images (Fig. 6). Then, stacked 3D image constructions were used to locate the exact positions of tissues taken for IHC using anatomical features as references (such as branching of bronchi, location of the heart, and bone structure) as well as gross anatomical photographs taken during necropsy to ensure accurate correspondence between CT and IHC. Next automated registration of PET-CT images was performed to ensure PET-CT were aligned, which then allowed us to measure the uptake of FDG at sites taken for histology (Fig. 6).

FDG uptake did not match the pattern of neutrophil infiltration

We tested whether FDG uptake was associated with sites of increased neutrophil infiltration. The stacked CT images were used to locate the regions from which NACE

172

image analysis had been performed, and FDG uptake (SUVmax) was determined on PET images from these same regions. There was an early increase in FDG SUVmax at 0.25 dpi, which immediately decreased below mock levels before gradually increasing to 3 dpi (Fig. 6). For both left and right caudal lobes, uptake in mock-infected animals was significantly greater than uptake at 1 dpi ($p < 0.05$, Fig. 7A). Temporally, this did not align with the pattern of neutrophil infiltration (Fig. 5A). Due to differences in resolution between the two modalities (PET-CT and IHC) we averaged the three non-overlapping images from each region measured by IHC and this compared to a single SUVmax from that region. Over all time-points, there was no association between FDG uptake and the neutrophil density (data not shown). However there was a significant linear association between SUVmax and neutrophil density at 1 dpi, although the association was comparatively weak ($R^2 = 0.26$) and was likely due to outliers (non-zero slope, $p < 0.001$, data not shown). This finding was very surprising, therefore we attempted to identify what was responsible for the FDG uptake using this data set for which we had confidence in our correspondence between PET-CT and histology.

FDG uptake did not match sites of IAV infection

We tested the hypothesis that FDG uptake occurs in sites of H1N1pdm infection in ferret lungs. Using a similar approach to the one above for NACE-stained sections, we measured FDG-PET uptake (SUVmax) at sites of IAV-positive cells determined by IHC. We also measured SUVmax at two other sites based on distance from IAV-positive cells: < 1 cm from any known IAV-positive area, and < 1 cm from any known IAV-positive area, both were measured from regions within the same ferret lobe. There was

significantly less FDG uptake at sites of IAV-positive cells compared to mock-infected animals ($p < 0.01$ for all regions compared to mock, Fig. 7B). Because this approach was also potentially confounded by the disparity in resolution between PET-CT and microscopic imaging modalities, we tested whether IAV infection may increase the uptake of glucose *in vitro* by infecting immortalized cell lines with several IAV isolates. We experimentally infected several human cells and cell lines (e.g., A549 and well-differentiated human bronchial epithelial cells line, 16HBEo-), and we observed slightly increased uptake of FDG in some but not all treatments (data not shown). Thus, we may infer that increased FDG uptake in infected ferrets was not associated with IAV infection directly.

FDG uptake measured proliferation in the lungs following IAV infection

We then tested the hypothesis that proliferating cells were responsible for the increased FDG uptake in lung tissues by detecting Ki-67 protein with IHC. Ki-67 is a nuclear protein that is present in high amounts during cellular proliferation. In order to estimate the amount of proliferating cells, we used a Ki-67 proliferation index (Fig. 8, images show examples of each score, 0-3) which is an established method for grading tumors clinically (642). No significant regions of proliferating epithelium were detected in the ferrets imaged at 0.25 dpi, 1 dpi, and 3 dpi; therefore we included histological samples from the previous study described above (*i.e.,* two infected ferrets and one mock ferret were taken at each of 1, 2, 3, and 7 dpi, the right caudal lobe is excluded from these sections) (631). Three non-overlapping images were taken haphazardly from each of three anatomical regions per tissue slice and were scored by two independent observers in

a blinded fashion. Both alveolar and bronchiolar regions had baseline levels of proliferating cells and there was no difference between lung tissues taken from mock and infected animals in these anatomical regions (not shown). However, there was an increase over time in the amount of proliferating cells in the bronchi, which peaked at 7 dpi ($p < 0.01$; Fig. 8).

Discussion

The pathology of human infection with IAV is often only known from lethal endpoints, taken at autopsy (6-9). In humans, severe IAV infection affects the LRT, and results in the massive infiltration of neutrophils (6, 42). Similarly, severe IAV disease in ferrets is characterized by early infiltration of neutrophils (123, 253). With respect to neutrophils in the lungs during IAV infection, pathology reports from lethal, human influenza pneumonia typically state the presence of suppurative necrosis, mixed cellular infiltrates, or neutrophilic infiltration (6-8, 30, 272, 630). However, few studies have directly addressed simple questions about the relationship between neutrophils and IAV infection. For example: when do neutrophils arrive in the lungs following IAV infection? What is the pattern of neutrophil infiltration, *i.e.*, is it specific to anatomical locations? Is it specific to sites of IAV? Or is it specific to sites of damage and necrosis? How important are the various inflammatory signals released in viral microenvironments to the activation and chemoattraction of neutrophils during IAV infection? Answers to these questions will provide a basis for answering more important questions, such as how does the severity of disease affect neutrophil infiltration (or vice versa)? Severe IAV infection often results in a form of acute lung injury and the formation of ARDS, and neutrophils

are implicated as both contributing to and recovering from this syndrome (16, 18, 60).

Based on mouse studies, the role of neutrophils during IAV infection show importance in

protection from lethal disease, however much remains unknown about their relationship

in the ferret model (84, 85, 577, 637, 639).

Despite the importance of the ferret model in the study of IAV pathogenesis, and despite

it being used for nearly 80 years for this, the ferret model is challenging. For example,

there are no ferret-specific commercially available reagents, and the cross-reactive

antibodies are unverified (279, 280). To overcome the limitations in availability of

immunological reagents, we have explored the use of molecular imaging as a tool to

study the pathogenesis of IAV in the ferret lung (631). Molecular imaging modalities,

such as PET, rely on the *in vivo* accumulation of injectable non-species-specific

radioisotope-labeled probes that can be imaged in 3-dimensions, and images can be fused

with CT images to provide anatomical references (645, 648). Their use in infectious

disease imaging is quickly developing (635, 645), and preliminary data provides the

foundation for the use of FDG-PET imaging in diagnosis or prognosis of clinical cases of

IAV (42, 609, 631). To further develop this tool, and to expand the tools available for the

use of ferret model, we established a model of FDG-PET during ferret infection with

H1N1pdm (631, 644). To complement the comprehensive 3-D nature of the images

provided by PET-CT fusion, we chose a systematic sampling of the lung to measure

infiltrating neutrophils in ferrets. Our sampling approach differed from methods

previously used to determine the spatial and temporal dynamics of IAV infection in the

ferret (123, 132, 270), which typically focus measurements to the site of infection and/or

lung lesions. Additionally we relied on gene expression in discrete sections of tissue to test changes in the viral microenvironment because antibody-based staining of tissues (e.g., IHC) or cells (e.g., flow cytometry) is currently unavailable. In doing so, we were able to test many hypotheses about neutrophil infiltration following H1N1pdm infection.

Neutrophils migrate into the lungs early and accumulate in sites of infected bronchioles. The increase of neutrophil density in the lungs until 1 dpi may be due to the increase in chemokine transcription within specific lung microenvironments (649, 650). Leukocyte chemoattractant chemokines such as CXCL8, CCL2, and TNFα are known to be present at sites of infection following experimental human IAV infection (99), and levels are increased in patients with H1N1pdm compared to seasonal IAV (105, 112). Previously we and others have shown increased secretion of leukocyte chemoattractant chemokines (TNFα, CCL2, CCL3, and CXCL8) following *in vitro* infection of well-differentiated normal human bronchial epithelial cell culture with H1N1pdm compared to seasonal IAV infection (331, 334). In IAV-infected ferrets, we and others have shown increased gene expression of other leukocyte chemoattractants (CCL2, CCL3, and CXCL10) as well as leukocyte-specific genes (G-CSFR, M-CSFR, CD11b, and CTSB) in the blood (126, 516, 600). Therefore, it is likely that neutrophils infiltrate the lungs following H1N1pdm infection following chemokine gradients to the site of infection. Moreover, we observed that the distribution of neutrophils was higher in the right caudal lobes at 1 dpi, which matched our observations and others' that i.n. and aerosol challenge of ferrets with IAV shows a preference for infection of the right caudal lobe (272, 285, 631).

It remains unknown what specific signal drives neutrophil chemoattraction in ferrets during IAV infection. Herein, we demonstrate that CCL3 was upregulated in discrete locations within the lung that were correlated with the presence IAV HA mRNA, neutrophils and a neutrophil-specific gene (G-CSFR) (Figs. 2 and 3). The significant increase in gene expression for CCL3 occurred at 3 dpi, which indicates another chemoattractant may be more important for early recruitment at 1 dpi (Fig. 2). Similarly, depletion of neutrophils from a mouse model of influenza infection decreased the amount of CCL3, suggesting that neutrophils may also be a source of this chemokine (577). In this study, we found that ferrets did not upregulate CXCL8 following infection with H1N1pdm. CXCL8 is the major chemoattractant chemokine for neutrophils during many human infections (651). It is known that neutrophil chemoattraction is somewhat species specific, and some mammals do not possess CXCL8. For example, in mice the chief neutrophil chemoattractant chemokines are CXCL1 and CXCL2 (652). In humans, neutrophils display the chemokine receptors CCR1 and CCR5, which are important for their chemotaxis and oxidative burst in response to CCL3. The ferret genome contains orthologs for these gene sequences (NCBI Gene ID: 101693329 and 101692743, respectively) (649, 653), however it is not known if these are similarly expressed on ferret neutrophils. Additionally, neutrophil chemoattractants not commonly associated with viral infection, such as eicosanoid molecules (leukotriene) and complement, were not measured (472). In general, sectioning the lung lobe revealed the highly focal nature of inflammatory gene expression in the lungs, which matched the focal nature of viral distribution in this ferret model. Although not shown, the increased expression of IL6

and TNF in certain sections but not others indicates a complex relationship between infection and immune response.

We measured the focal nature of infection in two ways: sampling discrete sections of a single lung lobe for gene expression and virus titration, as well as an unbiased semi-comprehensive histological analysis of two lung lobes. Using NACE-stained tissues, the latter showed a range of neutrophil densities that was greater in infected animals compared to mock-infected. By resolving the distance from NP-positive cells over time, we show that neutrophils become greatly enhanced at specific viral foci by 1 dpi (Fig. 5B). We observed occasional neutrophil NETosis at sites of IAV-infected cells, but we were unable to make any further statistical correlation to spatial or temporal aspects of disease without further sampling. Together, these observations indicate that neutrophils migrate to sites of IAV infection, and perform functions there. Thus, we conclude that inflammation caused by IAV was focal and driven by the presence of IAV-infected cells, yet the entire lung experiences increased infiltration as a result of infection. This may be due to the specific migratory patterns of neutrophils through the lung to sites of inflammation (654). The increased "background" neutrophil infiltration in infected animals (*i.e.,* before and after 1 dpi and at 1 dpi away from foci) was not obvious by standard hematoxalin and eosin IHC - neutrophils were uniformly distributed throughout the lung at a density that was quantifiably greater than mock-infected controls.

We detected two waves of neutrophils following H1N1pdm infection using the histochemical stain, NACE. As discussed above the peak of the first wave occurred at 1

dpi, and was concentrated at sites of influenza infection. A second wave of neutrophils was detected a 3 dpi, by both NACE staining and gene expression signatures. This biphasic pattern of neutrophils following H1N1pdm infection has been reported elsewhere (123). Neutrophil-specific transcriptional markers were only detected in lung microenvironments at 3 dpi (*e.g.*, G-CSF receptor [*Csf3r*], and *Itgam*, the alpha-m subunit of the Mac-1 integrin leukocyte activation marker, CD11b) (Fig. 3). Thus, there appears to be two different pools of neutrophils invading the lung following infection which differ in their gene expression status, and the second may be responding to or producing CCL3. Currently, it is thought that steady-state neutrophils are mature, terminally differentiated cells with limited cell-specific gene regulation, *e.g.,* mature neutrophils have pre-formed granules, but neutrophils themselves are capable of gene transciption in response to certain stimuli (655, 656). This may explain why gene expression of neutrophil granule contents were not detected (MPO, ELANE, CTSB). We hypothesize that the first wave at 1 dpi consists of mature neutrophils, and the second at 3 dpi represents a more immature population, perhaps as a result of emergency granulopoiesis, that have been recruited to the lung from the bone marrow as a direct result of IAV infection and systemic inflammation, and thus contain mRNA for the neutrophil growth factor receptor, G-CSFR (472, 657). Additionally, these gene signatures provide support for the biphasic infiltration of neutrophils observed in other lung lobes, showing a relationship between systemic activation and recruitment of neutrophils and their subsequent concentration at specific viral microenvironments. These observations should be studied further, as this may indicate distinct functions of these two pools of neutrophils.

The lung is a known reservoir of steady-state neutrophils, perhaps due to the large blood volume of the lung capillaries (62, 472, 658). An early increase in airway and circulating blood neutrophils is a feature of IAV infection in humans (7, 8), and is common in experimental IAV infection in mice (130, 253, 363) and ferrets (123, 266, 659). We show this happens as early as 6 hours post-infection (Fig. 5A,B). However, increased numbers of neutrophils in the lower airways has been correlated with increased influenza disease severity (85, 123, 132, 253, 600), and fewer neutrophils are found in the lungs of ferrets infected with virus isolates causing less severe influenza disease (123, 659). Excessive neutrophil infiltration may contribute to acute lung injury by causing alveolar-capillary damage (577, 578, 639). Conversely, neutrophils are essential to the recovery from IAV infection as part of the innate immune response as well as the adaptive immune response (84, 319, 637, 638). For example, depleting mice of neutrophils prior to IAV infection leads to increased viral replication and increased clinical disease (85). This suggests that the balance between damage from excessive neutrophil infiltration and the generation of controlled immune responses during IAV-infection is a critical determinant of disease outcome. This study shows a unique pattern of neutrophils and suggests they are honing to specific sites of infection and inflammation during H1N1pdm-infection. It is not known how these patterns of infiltration will change in response to a more severe IAV infection or to infection with a HPAI which causes immune dysregulation.

As it pertains to our findings, a majority of neutrophil research has been centered on their relationship to acute injury (particularly acute lung injury) and bacterial infection

(reviewed in (16),(18), and (60)). Indeed, pulmonary bacterial co-infections are clinically

common during and following IAV infection and are thought to represent the major risk

factor for mortality from an IAV infection. Bacterial co-infection was not evident in any

of the ferrets examined by histopathology. No further effort was made to detect bacteria

(*e.g.*, PCR, IHC, or direct culture) since commensal bacteria are known to exist

throughout the respiratory tract, and any pathogenic bacterial infection would be

distinctive on histopathology. Further, our methodology for ferret husbandry and i.n.

infection is in line with contemporary standards, and we would not expect bacterial co-

infection to occur in this controlled laboratory model. Previous studies have shown that

neutrophils are capable of recognizing IAV and IAV-infected cells (660-663), although

disagreements in data suggest that neutrophil responses to IAV are dependent on the viral

strain (661-664). The role of neutrophils in viral disease remains a topic that is quickly

growing (80, 456, 471, 665) and deserves further research.

We have hypothesized that increases in FDG uptake following infection is due to

increases in inflammatory cell infiltration in the lungs (612, 631, 635, 636). Large FDG

lesions (SUVmax > 3) begin to be detected in the lungs of IAV-infected ferrets at 3 dpi

and increase (SUVmax $\geq$ 5) until 7 dpi (631). However, the density of neutrophils in the

lung did not match the temporal or spatial pattern of FDG uptake in the lung. We

previously reported greater uptake of FDG in the right caudal lung where we and others

have measured increased viral replication and neutrophilic infiltration (272, 285, 631).

Another hypothesis to explain increased FDG uptake is that IAV increases cellular

glucose metabolism (666). We found that infection with IAV isolates caused an increase

182

in FDG uptake by immortalized human epithelial cell lines (A549) *in vitro*, but not by

differentiated human bronchial epithelial cells (16HBEo-) (data not shown) (331, 631).

Increased glucose promotes the acidification of cellular endosomal compartments, a step

required for IAV infection of cells (666, 667). In hospital clinics, FDG is used to detect

metabolically active tumors throughout the body, including the lungs, as it is taken into

cells through glucose transporters and accumulates (648, 668, 669). In this study, we did

not detect an increase in gene expression of GLUT1 (*Slc2a1*) or GLUT4 (*Slc2a4*) in lung

tissues (data not shown). Thus, we could not detect IAV-dependent increased glycolysis

in vivo via uptake of FDG at the times tested in this study (Fig. 7). We have reported

gradually increasing FDG uptake until 7 dpi (SUVmax scores >5) (631) which is after

IAV is cleared from the lungs. Therefore we cannot support the hypotheses that FDG

uptake is related to neutrophil infiltration nor inflammation directly within the IAV-

infected microenvironment.

We tested the hypothesis that FDG uptake was related to lung regeneration and repair

after IAV-induced injury and inflammation. IHC staining for the nuclear antigen, Ki-67,

detects cells undergoing proliferation (*i.e.*, cells in S, G2, and M phase of the cell cycle)

(670) and is used on biopsy tissue as a diagnostic tool to confirm tumor diagnosis or the

presence of neoplastic tissue (671). In lung cancer, Ki-67 staining is known to be

correlated with FDG uptake measured by PET imaging (672, 673). We found a low

background of cell proliferation in the lungs, especially in bronchioles, but higher in

alveolar spaces. There was marked increase in the proliferation of cells within the

bronchial epithelium up to seven dpi with IAV (Fig. 8). This matches the timing of FDG

uptake in ferrets seen previously (631), and corresponds to the increase in bronchiolitis and the presence of bronchiolar cytonecrosis, which was replaced by metaplastic bronchiolar epithelium beginning as early as 3 dpi and detected fully at 7 dpi. It is still unknown if proliferating cells contribute to the early FDG uptake (< 3 dpi) in infected ferrets. Small foci of FDG are often seen in locations within the thorax soon after infection. This may indicate the initiation of an adaptive immune response (*e.g.*, within lymph nodules by migratory dendritic cells, stimulated with IFN signaling from NK cells).

The often extensive cytonecrosis of the airway epithelium, followed by metaplasia of pneumocytes and large airway epithelium (depending on the severity of disease), is a common feature of infection by many IAV subtypes, including H1N1pdm (6, 8). Normally, lung cells are quiescent and only enter the cell cycle after infection and injury as part of the regeneration process (reviewed in (674)). We have reported a significant enrichment of genes associated with cellular proliferation in primary human bronchial epithelial cell culture after IAV infection and found reduced virus replication in undifferentiated versus well-differentiated bronchial epithelial cells (331). Others have shown that ferrets infected with mild seasonal viruses, but not HPAI, also show significant enrichment of genes involved in cellular growth and proliferation (675). Recently, IAV has been used to elucidate the method by which the distal airways rebuild from basal-like stem cells, a process which may continue for up to one month post-infection (676). Our studies suggest FDG could be used to probe the recovery of the

lungs after infection. Such data could be valuable for screening compounds that assist repair and regeneration of the lungs during this sensitive time.

Conclusions

The microenvironmental dynamics of IAV infection are important for controlling virus replication, inflammation and disease progression (52, 95, 126, 281, 660), however processes of inflammation extend beyond the site of infection (9, 85, 253, 360). Whereas *in vitro* experimental approaches are important for defining cellular and subcellular effects of virus infection, well-defined relevant animal models are essential for understanding how these cellular interactions define organ and organismal responses to infection (52, 600, 629, 632). These data support the importance of the whole organ response to infection, as well as immunological changes that occur at viral foci. Neutrophils migrate into the lungs early and accumulate in sites of infected bronchioles, potentially responding to chemokines released by IAV-infected cells. A second wave of neutrophils is detected a 3 dpi, which have altered gene expression profiles suggesting differences in maturation/phenotype. Live imaging of infected ferrets suggested increased uptake of FDG at sites of cellular proliferation, and not necessarily at sites of leukocytic infiltration. Future studies should address several questions raised by the data herein, such as the site-specific actions of neutrophils; the mechanism behind the biphasic temporal distributions; and the phenomenon of epithelial regeneration in the context of the entire lung or entire organism during infection.
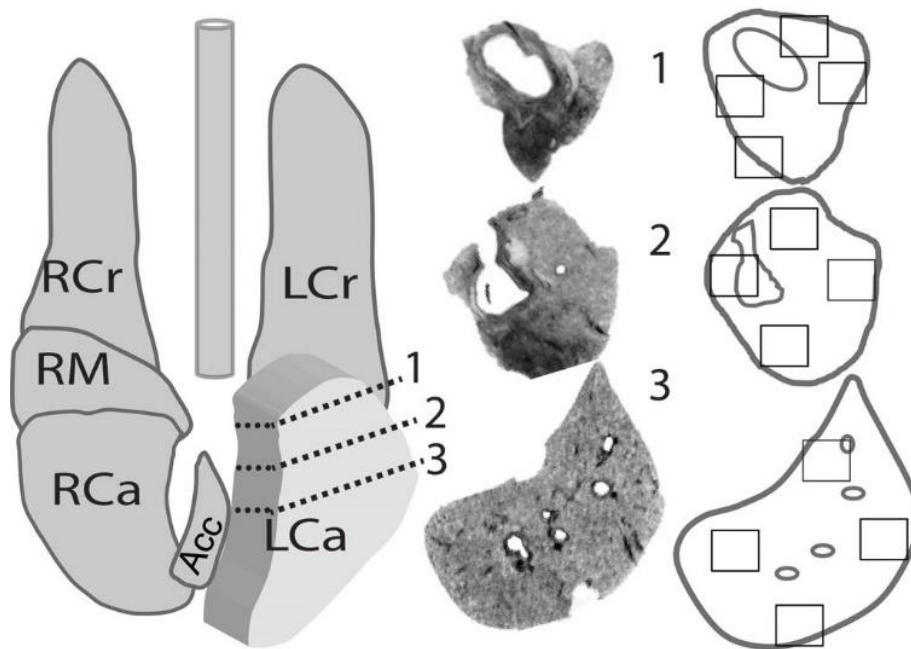
Figure 4.1. Sampling scheme for experiments on the temporal and spatial distribution of inflammation and infection in ferrets after H1N1pdm challenge.

A comprehensive histological sampling of ferret lungs was performed at time points following intranasal infection of ferrets with 10^6 TCID$_{50}$/ferret H1N1pdm virus (A/Kentucky/180/10). Samples were taken at 0.25, 1, and 3 dpi from 2 infected ferrets per time point, and 2 mock-infected ferrets at 3 dpi, immediately following PET-CT imaging. The diagram of a ferret lung (left) shows the method by which the left caudal lobe was divided (dashed lines on expanded lobe) for histology. The right caudal lobe (cuts not shown) similarly was divided into at least 4 cross-sections along the main branching bronchus. The resulting cross-sections of tissues are shown in the center column as black-and-white photos of histological slides, numbered according to locations on the lung diagram. To the right, outlines of the tissues were given to a blinded observer to select four regions for IHC analysis (black squares on the right). This sampling scheme for IHC was used to analyze the pattern of neutrophil infiltration, as well as

186

computed tomography and positron emission tomography images. Ferret lung lobes are labeled as follows: RCr, right cranial lobe; LCr, left cranial lobe; RCa, right caudal lobe; RM, right middle lobe; Acc, accessory lobe.
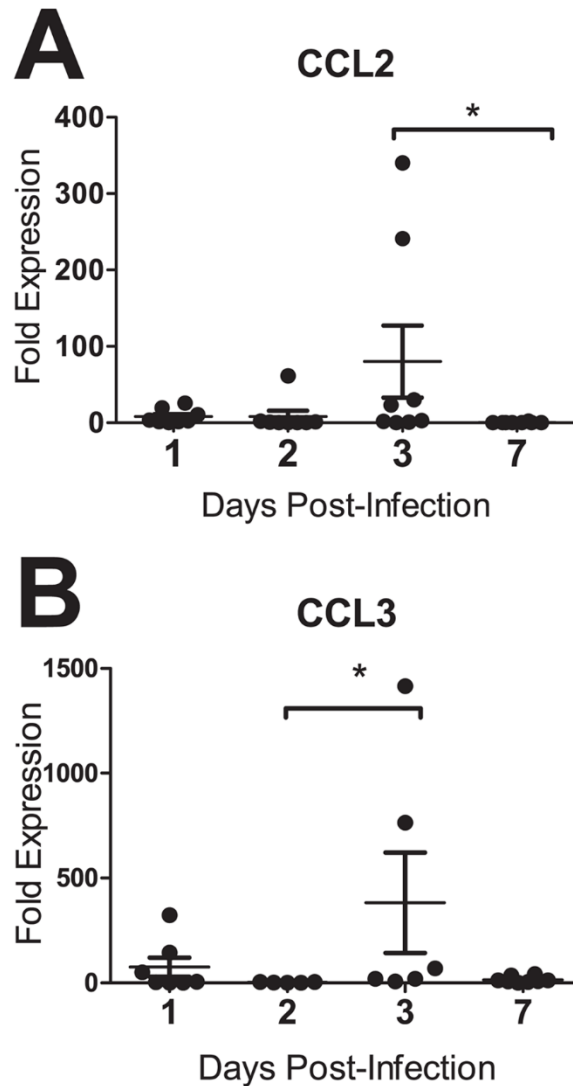
Figure 4.2. Inflammatory cytokine and chemokine gene expression in the ferret lung after infection with influenza A virus (H1N1pdm).

Female ferrets were infected with 10^6 $TCID_{50}$ per ferret of H1N1pdm virus, A/Kentucky/180/2010 ($n = 2$ ferret per timepoint). The right caudal lung lobe from each H1N1pdm-infected and mock-infected ferrets ($n = 1$ ferret per timepoint) was taken upon euthanasia on days 1, 2, 3, and 7 post-infection and divided into four sections. Each section was homogenized separately and cDNA synthesis was prepared for gene expression analysis. Ferret gene-specific primers were developed to cross exons and RT-

PCR was performed to identify gene expression of leukocyte chemoattractant chemokines (A) CCL2 and (B) CCL3. Fold expression is compared to expression of housekeeping controls (GAPDH) and mock-infected animals using the delta-delta Ct method. Asterisks indicate significant differences between days by nonparametric statistical tests, corrected for multiple comparisons..
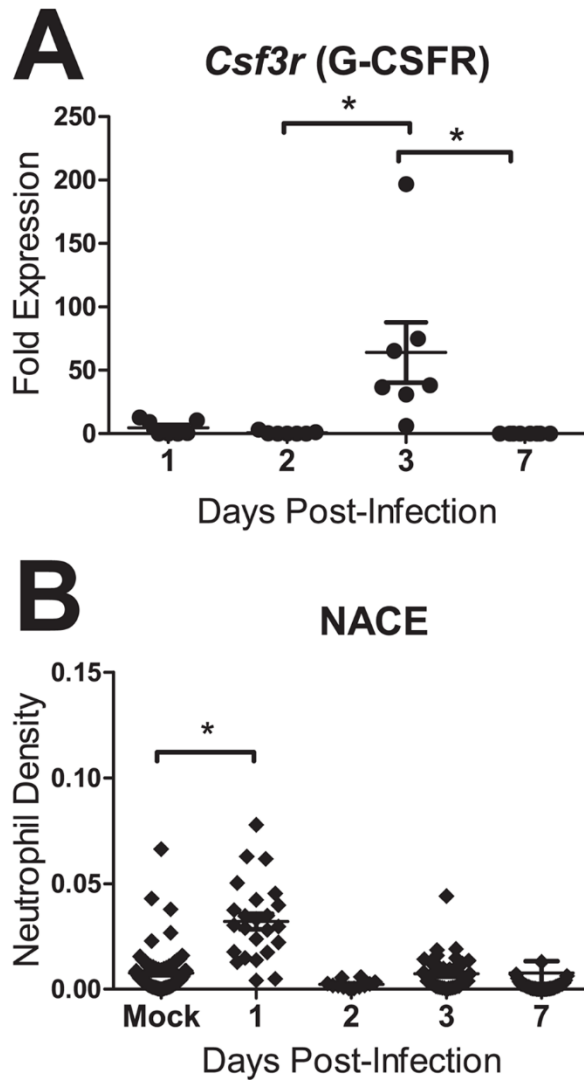
Figure 4.3. Neutrophils were detected in ferret lung sections after infection with influenza A virus (H1N1pdm).

Female ferrets were infected with 10^6 TCID$_{50}$ per ferret of H1N1pdm virus, A/Kentucky/180/2010 ($n = 2$ ferret per timepoint). (A) The right caudal lung lobe from H1N1pdm-infected and mock-infected ferrets ($n = 1$ ferret per timepoint) was taken upon euthanasia on days 1, 2, 3, and 7 post-infection and divided into four sections. Each section was homogenized separately and cDNA synthesis was prepared for gene expression analysis. Ferret gene-specific primers were developed to cross exons and RT-

PCR was performed to identify gene expression of a neutrophil-expressed gene (*Csf3r*/G-CSFR) relative to housekeeping controls and mock-infected animals. Asterisks indicate significant differences between days by nonparametric statistical tests, corrected for multiple comparisons. (B) Other lung lobes (left cranial, right cranial, left caudal, and middle) taken from each ferret were prepared for IHC, and one slice from each was stained for neutrophils (NACE). Neutrophils were quantified in 20X images taken from 3 regions on each of the NACE-stained slides using ImageJ image analysis software. The number of NACE-pixels divided by the number of total tissue-containing pixels are presented as the "neutrophil density". Asterisk indicates significant difference in distribution compared to mock-infected ferrets using non-parametric statistical tests.
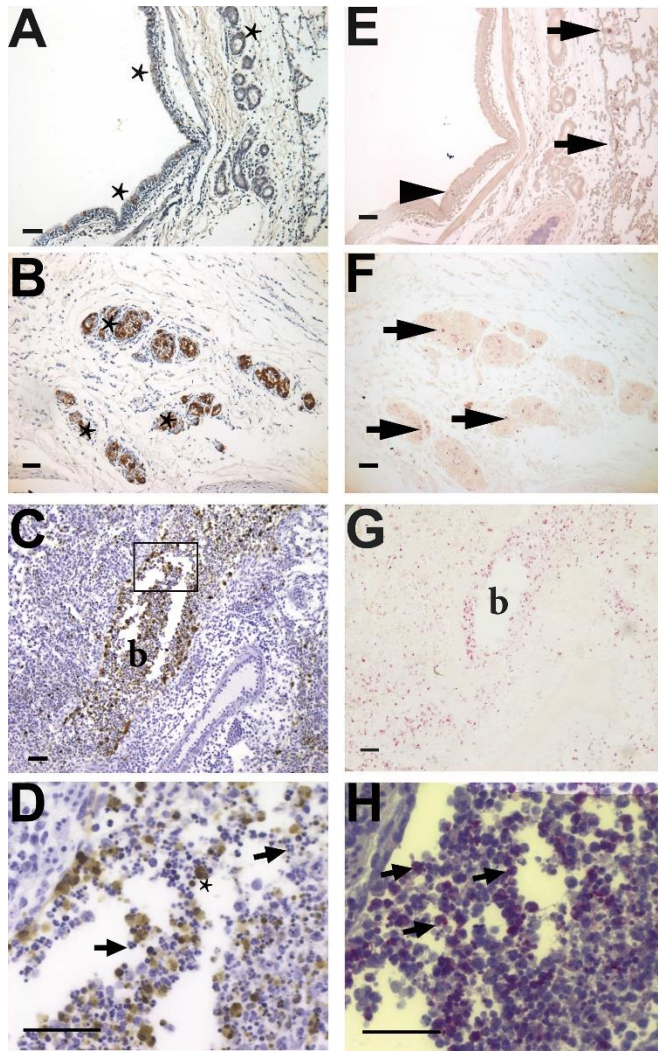
Figure 4.4. Immunohistochemical staining of influenza nucleoprotein and neutrophils in ferret lungs.

Histological preparations from the right caudal lobe of a female ferret 1 day post-infection with 10^6 TCID$_{50}$ of an H1N1pdm virus isolate (A/KY/180/2010). On the left panels (A-D), influenza antigen (nucleoprotein, NP) is stained brown with hematoxalin (blue) counterstain. On the right panels (E-H) neutrophils are stained pink with naphthol AS,D chloroacetate esterase (NACE) in a serial section of the same region of lung as the IHC NP stain (A-D) (without counterstain in E-F to show bright pink NACE stain, blue hematoxalin counterstain in F). (A) Influenza-infected cells (stars) in the pseudostratified

columnar epithelium of the bronchus of a ferret 2 days post-infection. (B) Infected

seromucinous glands (three are marked with stars but more are visible). (C) Infection of

the bronchiolar epithelium (lumen marked "b") was more common than other sites, and

antigen can be seen within luminal cells. (D) Magnification of the indicated region in (C)

shows that many NP-positive cells (star) are macrophages, and the lumen of the

bronchiole is filled with polymorphonuclear neutrophils (arrows show two but many

more are visible). (E) Few neutrophils are present within the epithelial layer of the

bronchus at sites of influenza-infected epithelial cells (arrowhead), but more are present

within the alveolar spaces adjacent to this site (arrows). (F) Inflammatory cells within the

infected submucosal glands are neutrophils (three areas are indicated with arrows but

more are present in each gland). (G) Extensive neutrophil infiltration in the bronchiolar

lumen ("b"). (H) Magnification of a serial section of (G) that is stained for NACE and

counterstained with hematoxalin to show the morphological features defining neutrophils

(arrows show three but many more are visible). Panels A-C and E-G were taken with

10X objective, D and H were taken with 40X objective. Horizontal black bars in all
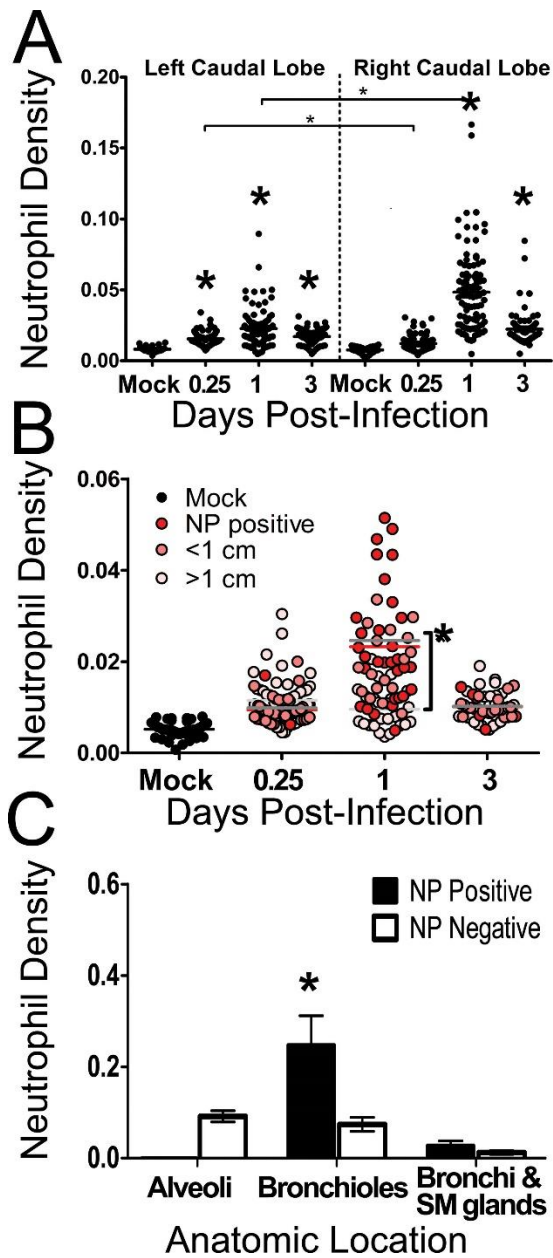
panels are 50 μm long.

Figure 4.5. Neutrophils in the lungs of ferrets after infection with influenza A virus (H1N1pdm).

Ferrets were infected with 10^6 TCID$_{50}$ of an H1N1pdm virus isolate (A/KY/180/2010), and lung tissues were taken upon euthanasia and processed for histology. Caudal lung lobes, taken from two infected ferrets per day (0.25, 1, and 3 days post-infection, dpi), were systemically divided and prepared for histology. Neutrophils were quantified from

histochemical staining with napthol AS,D choroacetate esterase (NACE) using image analysis software, and data are presented as neutrophil density - the number neutrophil-positive pixels per total tissue pixels on each image. (A) Neutrophil density is quantified over time, dividing data by lobe. Asterisks indicate significant differences from mock-infected animals, and significant comparisons between lobes are shown as bars with asterisks above (nonparametric statistical tests, $p < 0.05$). (B) Influenza nucleoprotein (NP) was identified on histological sections with IHC. The neutrophil density was calculated from the serial NACE-stained section, grouped according to distance from known NP-positive cells and matching sites of IAV-positive cells to distant sites within the same ferret (red, pink, and white dots to indicate NP-positive, < 1 cm from NP-positive, and > 1 cm from NP-positive sites, respectively) to mock-infected animals (black dots). Data are plotted over time, and means within a given timepoint are shown colored according to distance (red, pink, and grey lines for NP-positive, <1 cm rom NP-positive, and > 1 cm from NP-positive sites, respectively). Asterisk indicates significant difference between sites within a given timepoint. (C) Neutrophil density was calculated from pictures taken at sites of known influenza infection (NP-positive) and grouped by anatomic region (alveoli, bronchioles, and bronchi with submucosal [SM] glands). These images were site-matched within the same ferret (< 1 cm from known IAV-positive sites) to anatomic regions that had no IAV-positive cells (NP-negative). *N.B.,* NP-positive cells at alveolar sites were leukocytes; and mock-infected animals are not shown on this panel, but are shown above. Asterisks indicate significant difference between NP-positive and NP-negative sites.
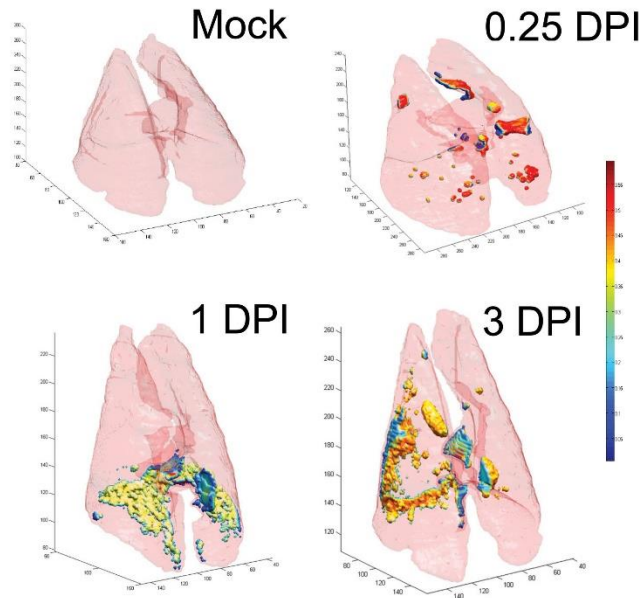
Figure 4.6. Rendering of PET-CT images of ferret lungs at different time points post-infection with H1N1pdm.

Stacked whole lung images give a 3-dimensional view of ferrets at three timepoints following infection with 10^6 TCID$_{50}$ H1N1pdm virus (A/KY/180/2010); only one ferret shown per time point, including a mock-infected shown at 3 days post-infection (DPI). Ferrets were injected with an intraperitoneal dose of radio-labeled [^{18}F]-fluorodeoxyglucose (FDG) and imaged using PET-CT one hour later. For each image, the light pink surface corresponds to the border of the lung which was segmented from CT images by an automated CT analysis. PET-CT fusion images were used to define the uptake of FDG within the segmented lung space, and the intensity of FDG uptake is illustrated as small colored volumes within the lung borders. Regions of FDG uptake are colored according to voxel intensity within the FDG-PET image as shown on the color scale on the right (from <0.05 in blue to >0.5 in dark red).
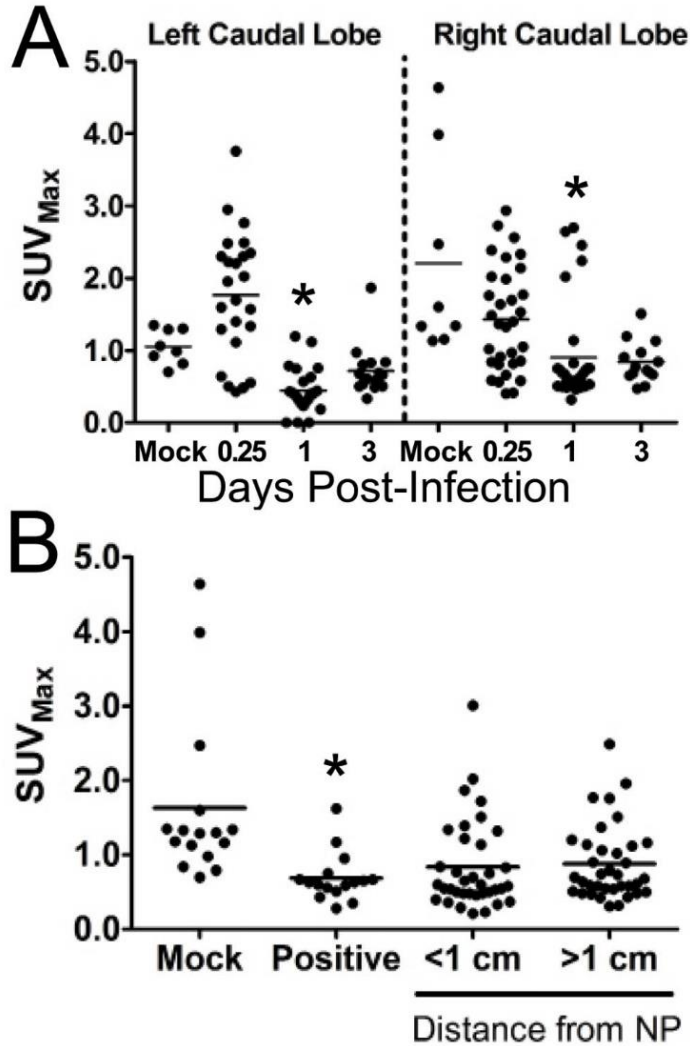
Figure 4.7. Distribution of cellular uptake of radiolabeled FDG during influenza infection in ferrets.

Female ferrets were infected with 10^6 $TCID_{50}$ of H1N1pdm virus (A/KY/180/2010). A radiolabeled glucose analog ($[^{18}F]$-fluorodeoxyglucose, FDG) was injected at 0.25, 1, and 3 days post-infection and ferrets were imaged 1 h later ($n = 2$ per time point). Ferrets were euthanized immediately after imaging and lung tissues were prepared for histology. (A) The temporal distribution of FDG uptake (maximum standard uptake value, SUVmax, within a defined volume) was measured in images taken by positron emission tomography after locating histology slices using anatomical references in registered

computed tomography images. These areas matched areas analyzed for neutrophil

infiltration, and approximate a 3-D grid of each ferret caudal lung lobe. (B) The spatial

distribution of FDG uptake at sites in the ferret lung grouped by distance from IAV

nucleoprotein (NP)-positive cells within the lungs. The presence of H1N1pdm was

measured with immunohistochemistry staining for viral nucleoprotein. Asterisks indicate

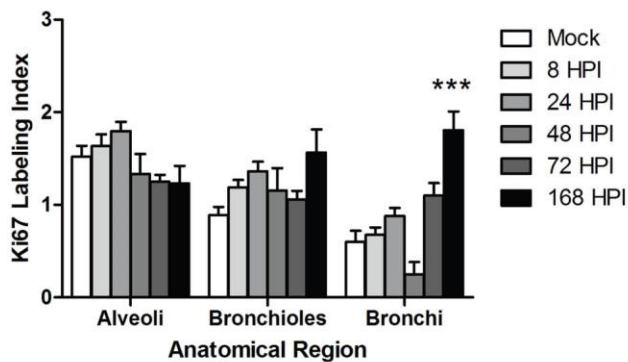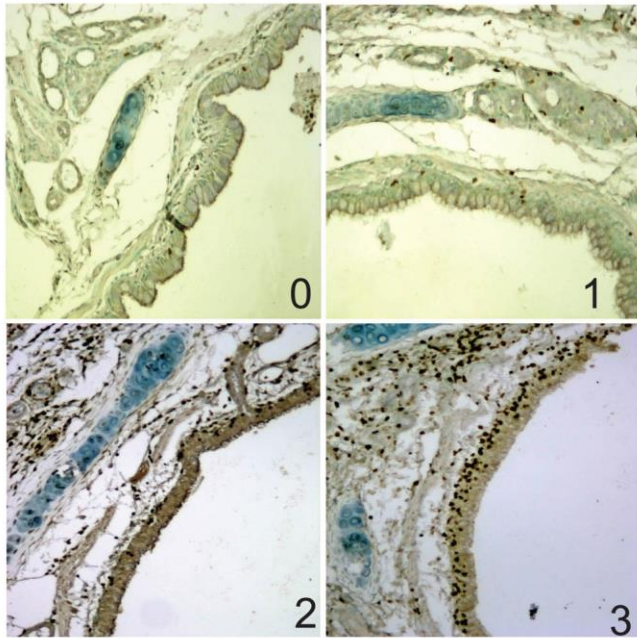statistically significant differences from mock-infected animals.

Figure 4.8. Proliferation of lung epithelial cells measured by Ki-67 labeling index.

The top four images are representative of the scoring system used to grade (labeling

index values of 0-3) the extent of lung cellular proliferation (Ki-67 antigen positivity) in

immunohistochemical sections taken from ferrets infected with 10^6 $TCID_{50}$ H1N1pdm

virus (A/KY/180/2010). The left and right cranial, left caudal, and middle lobes were

taken at necropsy (at 8, 24, 48, 72, and 168 hours post-infection, HPI) and prepared for

histology. Various anatomical locations were analyzed in one lobe of each ferret per

timepoint, including bronchi, bronchioles, and alveolar spaces. The images were grouped

anatomically and scored by two independent observers for the amount of Ki-67 positive cells using the guides above. The bottom figure shows the mean proliferation index per anatomic region over time. For reference of scale, the height of the numbers is 50 μm in the images. Asterisks indicate significant difference from mock within each anatomical region (***, $p < 0.01$) using nonparametric statistical tests.

Table 4.1. Primers used to identify ferret leukocyte-specific and inflammatory genes.

Gene	Forward Primer (5'-3')	Reverse Primer (5'-3')
ELANE	GCTGCTGAATGACATCGTG	CACGTTCCTGTTGATGGTG
CCL2	CAGAAGTGGGTCCGGGATTC	TTCATGGCTTTGCAGTTTGGG
CSF3R	AGAGCTGGAAGATGGAGCAT	TAGAGCTGAAAGGGCCTGAT
CCL3	GGTCTTCTCTGCACCATTTG	CTTGCGTGTAATCTGCTTGG
MMP9	AGCGAGAGACTCTTCACCCA	CAGTGGTGCAGGTGGAGTAA
CSF1R	ATGGAGACACCAAGCTCACA	CATCTTGGAAGCCTACGTGA
CD11B	CTGGAGCTGCCTGTGAAATA	ATAATGCGGCTGGTCTTCTC
TNFA	CCAGATGGCCTCCAACTAAT	CAGCTTCAGGGTTTGCTACA
IL6	ACCGGTCTTCAGGAGTTTCA	AAGAACTGGAGCAGGTGTTTG
IFNB	TCCCAGAAGTTCCAGAAGGA	TCGACAATGCTCTCATTCCA
IL8	GTGAAGCTGCAGTTCTGACG	GGGCCACTGTCAATCACTCT
SLC2A1	CTGCTGAGCGTCATCTTCAT	TTCTTCAGCACACTCTTGGC
NCR1	GCACCGAGAAGCAGAATCTT	GCTGGTACTTCACAGCCTCA
GZMA	AGCTCACTGTGTCCTGAACAA	TCAAAGCACGGATAAGGAAA
MPO	TCCCTGAGGAGGAAGAGATG	GCTGGTGTCAGCATGTCAGT
GAPDH	AGCTGAATGGGAAGCTCACT	CTGCTTCACCACCTTCTTGA
IAV HA	CACCAGTCCACGATTGCAATA	ATGGGAGGCTGGTGTTTATAGC

CHAPTER V

CONCLUSIONS

Influenza A viruses (IAV) may cause severe respiratory disease, and emergent strains

with increased virulence have the potential to infect the world's population within a short

time frame. These points have been illustrated in just in the last fifteen years with the

emergence of H5N1 in 2003, the re-emergence of a swine-origin H1N1 resembling the

1918 Spanish influenza in 2009, and the emergence of avian-origin H7N9 in 2013.

Fortunately, in the aftermath of each virus outbreak, none had both the virulence and

transmissibility that is feared of the next IAV pandemic. Importantly, these events have

resulted directly or indirectly in increased surveillance and increased funding into IAV

research, and valuable data has been collected. To date, few infectious diseases have

received more attention than the 2009 H1N1 "pandemic" IAV (Figure 5.1). This

dissertation uses H1N1pdm infection of mouse and ferret animal models to investigate

the timing and magnitude of general and specific host immune responses to IAV viruses.

In conclusion, the findings from the experiments presented herein are summarized in the

context of very recent publications in the field of IAV research, highlighting the benefits

and limitations of animal models for understanding IAV pathogenesis in humans.

The timing of an IAV infection

The earliest responses to IAV. The studies presented here help establish a temporal-spatial course of disease for H1N1pdm and provide a model to test determinants of lethality (Figure 5.2). Shortly following H1N1pdm infection, the virus enters cells and begins to replicate its genome. The ferret model provided information that neutrophils arrive in the lungs as early as 6 hpi (Figure 5.2). This coincides with the gene expression of type I IFN and release of ISG products, such as CXCL10, from *in vitro* infection of human primary epithelial cell culture with H1N1pdm at 6 hpi (331, 332, 334, 335). Others have shown that virus detection and inflammatory response genes, such as IL-6, CXCL8, and CCL5, are upregulated as early as 3 hpi following *in vitro* infection of human primary bronchial epithelial cells with both seasonal H1N1 and H1N1pdm (330, 333). Detectable secretion of these products into cell culture media is detected by 24 hpi (330-332, 334, 335).

The expanding inflammation. Host responses within the viral microenvironment are important determinants of influenza pathogenesis; however these effects are transmitted systemically (360, 363). The systemic amplification of these signals, which influence the recruitment of inflammatory cells during IAV infection, is determinants in the outcome of IAV disease (9, 14, 94). This amplification occurs through endothelial cells, which are also important for leukocyte recruitment to the site of infection (20, 60, 64, 360, 472, 538). In mouse models, it has been suggested that increased inflammation and increased inflammatory leukocytic infiltration in the lungs contributes to the increased

pathogenicity of IAV (85, 86, 130, 136, 139, 247, 253, 323, 363, 375, 379, 430, 539).

What remains unclear is the connection between inflammation at the site of infection and

how this amplification of inflammation systemically affects disease outcome, specifically

with regard to innate leukocyte recruitment and activation.

The severity of disease is related to the quality of the "signal." The fidelity of this

immune signal – the timing and the context – is critical to the responses of recruited

white blood cells to a localized virus infection in order to contain the infection. We have

established the recruitment of neutrophils to sites of inflammation and infection is very

specific in space and time during a non-lethal H1N1pdm infection of ferrets (Chapter IV).

Infiltrating leukocytes respond to the IAV-infected lung viral microenvironment by

releasing effectors, such as ROS or additional chemoattractants, to additionally shape the

microenvironment (441, 442). An abundance of activating signals for infiltrating

leukocytes may contribute to the creation of an unrestricted "macroenvironment," one

that results in unmanageable inflammation for the host (86, 253, 380, 381, 396).

Increased inflammation (due to viral determinants or chronic inflammatory disease in the

host) may alter critical timing of the recruitment of immune cells, which may not be able

to respond appropriately (e.g., recruited immature neutrophils do not have type I IFN

receptors (530)). Moreover, IAV strains which alter specific signals, such as suppression

of type I IFN production from infected cells (69, 199) or disabling neutrophil responses

(421, 422, 431, 440), increase disease severity in ferrets and mice, respectively. In these

scenarios, the absence of a typical "viral" lung microenvironment restricts valuable information to needed to elicit an appropriate response.

The importance of macrophages in the immune response to IAV infection

Airway macrophages are also capable of responding quickly to IAV infection, as shown by experiments which infected primary human macrophages in cell culture (74, 341, 342, 374, 377, 595, 677). Macrophages infected with H1N1pdm are able to secrete CXCL10, TNFa, IL6 as early as 8 hpi (74), and increased secretion by 24 hpi (75, 342, 359, 377, 678) (Figure 5.2). More importantly, experiments using co-culture systems have shown that these interactions may regulate epithelial apoptosis within a viral microenvironment during IAV infection via TRAIL-DR5, and CD40-CD40L, and therefore may be important mediators of mucosal barrier integrity during severe infection (61, 65, 312, 341, 343, 344, 347, 352, 353, 373). These experiments have shown that type I IFNs are extremely important signals regulating these responses and therefore establish the viral microenvironment. Thus, multiple *in vitro* systems have indicated that the response of specific cell types to IAV infection is immediate, gene expression can be detected as early as 3 hpi, and secretion of immune mediators can be detected within the first 24 hours following infection. However, more research should focus on the use of coculture systems to reveal the importance of cellular interactions at the site of infection since these are physiologically relevant to the establishment of the viral microenvironment.

While co-culture models of infection and immune response are essential to establish a role for macrophages in IAV pathogenesis, it remains to be demonstrated whether IAV modulates the *in vivo* macrophage response to infection. Thus far, demonstrating viral replication within airway or exudate macrophages provides valuable background to support mechanistic studies of the affect infection has on the functions of macrophages during IAV infection (73, 74, 359, 375). Apart from their role as pathogen sensors and inflammatory signalers, resolution of infection (and inflammation) relies in part on the phagocytic functions of macrophages to clear debris and necrotic cells within these microenvironments (61, 79, 459, 679). This causes the release of anti-inflammatory cytokines which, in the case of increased inflammation, may not be sufficient to tip the balance towards recovery (61, 79, 459, 679). Indeed, the most severe form of IAV in humans causes a hypercytokinemia, which is characterized by both pro- and anti-inflammatory signals simultaneously expressed (9, 10, 14, 94). Much remains to be discovered about these critical fine-scale interactions at IAV viral foci. As we demonstrate, the ferret is an excellent model in which to pursue these questions.

Animal models for the study of influenza A virus pathogenicity in humans

Clinically, severe respiratory disease, including IAV, progresses in one of four ways: early or late recovery, and early or late death (680). Children and young adults (<65 years of age) were at increased risk for hospitalization from H1N1pdm infection during the first two waves of the outbreak in 2009-2010 (133, 681, 682). Additionally, patients with certain comorbidities experienced a more severe disease (*e.g.,* obesity, chronic lung

disease)(133, 682). It was important to establish whether the variability in human response to H1N1pdm virus was solely host comorbidity or if viral variants contributed to differential pathogenicity. The laboratory mouse is genetically homogeneous, and therefore variability in disease outcome following H1N1pdm infection is driven by virus-specific factors. Using the mouse model, we and others have shown that the variability in human responses to H1N1pdm infection may have been due, in part, to circulating genetic variants of H1N1pdm (130, 136, 247, 683-686). Importantly, key differences in disease between mice infected with closely related IAV strains was the timing and quantity of chemokines in the lungs and the resulting recruitment of inflammatory cells such as neutrophils (130, 136, 685, 687). Moreover, genetically similar H1N1pdm viruses produced variable host responses in outbred animal models as well including ferrets and macaques (127, 130, 132, 247, 683, 686). Animal models were essential to understanding these very basic features of the 2009 H1N1 global pandemic, when only genetic information and patient reports were available (127, 132). Therefore, it is important to understand the benefits and limitations in animal models, which currently offer the best information for inferring human IAV disease severity.

Testing the limits of the mouse model: host determinants of pathogenicity

In nature, there is no such thing as "mouse influenza" (as far as we know, and there is limited interest in understanding IAV pathogenesis in mice for the benefit of mice). It is known that IAV virulence determinants are mouse strain-specific, further illustrating the need for caution in using mouse models (136, 250, 683, 684). Thus, our discovery of

three-to-four distinct mouse immune responses to H1N1pdm infection, although a useful

tool to understand differences between H1N1pdm isolates (viral determinants), may not

offer great insight into pathogenicity in humans (host determinants). One group has

recently demonstrated that the variability among genetically similar H1N1pdm isolates is

only observable in certain mouse strains, indicating that our discovery may not even

extend to mice other than DBA/2J mice (130, 136). However, certain aspects of IAV

infection of the respiratory tract seem to be similar for many mammalian species. In

humans, increased cytokines and chemokines in the blood and respiratory samples (e.g.,

nasal lavage) during H1N1pdm infection were correlated with increased disease severity

(105, 112). Cytokines and chemokines such as IL-6, TNFa, CCL2, CXCL8, and

CXCL10 were also higher during infection with a more lethal H1N1pdm virus isolate in

macaques (*e.g.*, (686)), ferrets (*e.g.*, (71)), and mice (*e.g.*, (130, 683)). It has been

demonstrated that release of these chemokines are related to the increased recruitment of

inflammatory leukocytes to the site of IAV infection in mice (85, 86, 130, 247, 294, 323,

363, 539, 683). However, the precise relationship between increased cytokines and

chemokines and disease severity remains unclear, and this may be where the limit of a

mouse model is drawn.

Testing the limits of the mouse model: viral determinants of pathogenicity

While interpretation of host determinants of increased IAV pathogenicity must require

strict prudence, is the same true for the interpretation of data showing viral determinants

of increased pathogenicity in the mouse? Does pathogenicity of emergent IAV hold true

for all mammals? Are there species-specific determinants of pathogenicity and how are

they linked to host response? This is an interesting problem in the field.

<u>Preliminary data linking viral traits and immune response</u>

Using the advances in reverse genetics, it possible to test hypotheses regarding the

contribution of specific amino acid constellations in viral proteins that affect the timing

and magnitude of specific immune responses. For example, in we (chapter III) and others

have observed that H1N1pdm viruses possessing an HA with an alpha 2,3-linked SA

binding affinity are lethal in DBA/2 mice (*e.g.*, a D222G mutation in HA (125, 129, 131,

685)), which supports the hypothesis that receptor binding drives pathogenicity in mice

(50, 125, 230, 247). In preliminary studies currently underway, we have used reverse

genetics to create a virus with this HA molecule on the background of another H1N1pdm

virus that is lethal in mice but does not have alpha 2,3-linked SA affinity

(A/Netherlands/602/2009 [= "NL602"] differs from KY180 HA at 6 amino acid

positions). Materials and methods for these experiments were similar to those in chapter

II (*e.g.*, 6-8 week old female DBA/2 mice were infected intranasally with 30 μL virus).

There were no differences in lethality or morbidity (weight loss) between KY180- and

NL602-infected mice (10^2 TCID$_{50}$/mouse), indicating that NL602 has increased virulence

independent of alpha 2,3-linked SA binding (Figure 5.3). Moreover, we did not observe

differences in virus in the bronchoalveolar lavage (BAL) at 3 dpi, nor in cytokine and

chemokine secretion in the BAL at 3 dpi between mice infected with either wildtype

viruses or the reassortant virus (10^5 TCID$_{50}$/mouse) (Figure 5.4). However, at this

dosage, mice infected with viruses possessing an alpha 2,3-linked SA binding HA had

reduced lung cellularity and an altered balance between airway macrophages and

neutrophils following infection (Figure 5.5). Thus, for H1N1 viruses in mice, specific

mutations in HA may be traced to surprising effects beyond receptor tropism, and these

effects are related to the interaction between systemic and local inflammatory responses

(254, 688, 689).

Host adaptation approach to identify virulence determinants

As mentioned previously, this specific polymorphism in HA (D222G/N/S) was also

associated with increased virulence in humans (125, 547, 558, 559, 561-563, 690, 691).

Thus, perhaps we can infer that increased affinity to avian-type SA linkages is a common

virulence determinant for mice and humans. To attempt to identify additional viral

variants that have increased virulence in humans for which mice can be used to study

pathogenicity, we may try a reverse approach. Adaptation of IAV (and many other

viruses) within a host species typically leads to attenuation of the virus upon coevolution

over many cycles of continued transmission (682). Perhaps we can identify viral variants

that have disappeared from the H1N1pdm gene pool following for prolonged

transmission between humans and ask: were these were associated with increased

pathogenicity in humans, and were these associated with increased pathogenicity in

mice? Researchers in the United Kingdom divided sequenced human H1N1pdm isolates

into first/second/third wave to show human adaptation (692). Elderfield, *et al.* showed

that third wave H1N1pdm isolates induced less type I IFN in human cells *in vitro*, had

distinct mutations in HA which increased tropism for alpha 2,6-linked SA, and increased

polymerase activity within mammalian cell culture (692). More to the point, these

mutations were less lethal in mice (136).

A similar analysis is presented in Table 5.1, comparing the circulating polymorphisms of

H1N1pdm in humans taken three years after the 2009 emergence of H1N1pdm in the

United States to those circulating during 2009 (*i.e.*, during the first two waves of the

H1N1pdm). The HA, PA, and PB2 genes are compared, since these are established

virulence factors for many IAVs and mutations within these genes are known to

contribute to virulence differences (177, 251, 275, 294). For simplicity, polymorphisms

are compared to two Kentucky H1N1pdm sequences of known lethality in mice (130). In

general, the results suggest that increased pathogenicity was associated with rare variants

that were likely not adapted to mammals.

Polymerase proteins: For example, 3 of the 4 polymorphic sites in PA have mutations in

2009 that disappear from the circulating human viruses by 2012 (Table 5.1). Therefore,

PA I14, PA D610, and PA Q716 are likely avian-adapted mutations, and they may

contribute to altered fitness and/or virulence in mammals. This is not surprising since it is

known that the PA and PB2 both came from avian-adapted ancestors (1). Therefore,

reverse genetics approaches that focus on the contribution of these mutations to virulence

in the mouse model may be beneficial to understanding human pathogenicity.

Hemagglutinin: Interestingly, only one of the selected sites in the HA protein shows potential adaptation to mammals (HA2 E47K). The lysine at position 47 of HA2 went from 20% of the circulating viruses to 100%. This polymorphism was shown to be involved in stability of the virion, and specifically the pH stability of the HA (287). This type of change is a known avian-to-mammalian host-adaptation, and it is important for fusion and entry of the virus into the host cell (693, 694). Using syncytium formation assays and erythrocyte lysis assays (common assays to determine pH of fusion for viral hemagglutinin proteins), we determined that there was no difference in pH of fusion for this viral polymorphism alone (HA2 E374K, unpublished data). This is further supported by the finding by others that an additional mutation is needed to alter pH of fusion for H1N1pdm viruses (287). The other polymorphisms in HA show limited evidence of human adaptation. Therefore, the isolate with decreased mouse lethality had the dominant variants (>90% of 998 isolates analyzed) in human cases of H1N1pdm isolated in the U.S. in 2012. HA is under many selective pressures, including herd immunity as well as host adaptations, and thus variants identified here may not necessarily indicate attenuation (or increased virulence). However, one of these variants was extremely well-studied (D222G/N/S/Y), and illustrates the type of evidence needed to connect viral genotype with phenotype in humans using animal models.

HA1 D222G, a case in point

Mice typically are not susceptible to infection with human isolates of IAV, and therefore it is common practice to adapt H1N1 and H3N2 IAV to mice by serial passage (249).

The immediate result is an IAV that replicates well in the respiratory tract of mice and causes increased lethality in mice (255, 695). Some of the variants isolated from Kentucky patients during the first and second waves of H1N1pdm had mutations in HA that have arisen from mouse adaptation and these mutations, alone, are known to increase the lethality in mice: D222G and S183P (255, 685). The mutation D222G, near the SA binding site in the head of the HA molecule, was also discovered from reconstructed samples of the 1918 Spanish flu, and was responsible for increased transmission of the virus between ferrets (276). This specific mutation, a glycine at position 222, is a virulence determinant in macaques (689) and in ferrets (125), and results in altered receptor tropism in human cell culture (563) and on glycan array (125). The G222 substitution is thought to allow the HA increased binding to alpha 2,3-linked SA while maintaining alpha 2,6-linked SA tropism, whereas the D222 virus has affinity to only alpha 2,6-linked SA (125, 276, 563, 689). Therefore, again, increased binding to avian-type receptors is an important virulence determinant considering the distribution of receptors in the host, particularly when there is an increase in avian-type receptors in the lower respiratory tract.

A fascinating study showed that the HA D222 mutation may function as a site for diversifying viral population (696). Memoli, *et al.* found this pattern of adaptation within a single patient with H1N1pdm over time, where the dominant D222 variant switched to a G222 dominant population. They turned to the ferret model to test the virulence of these populations, since the ferret is more similar to humans with respect to the

relationship of virus tropism and virulence. Ferrets were infected with a population of 100% D222 variants HA, a population where G222 was the major variant (8% D222), or a plaque-purified 100% G222 IAV population. They found that only the plaque-purified isolate (100% G222) had increased pathogenicity, but also led to the greatest diversity of the quasispecies group after infection (127, 132). This illustrates the implications of how viral quasispecies can affect the course of IAV disease, and how quasispecies can complicate testing hypotheses for a specific viral variant. Ultimately, it is important to frame these types of questions in the context of understanding human disease. Two additional studies ($n = 7$ and 357) showed that the D222 mutant was significantly associated with mild human cases of H1N1pdm, and the G222 mutant (or more specifically the D/G222 quasispecies) was associated with more severe cases of H1N1pdm (690, 691). In all, this well-studied mutation from H1N1pdm shows the level of evidence required to make a convincing argument for HA position 222 as a viral determinant of pathogenicity, and the utility of animal models for establishing this. Interestingly, both D222G and S183P emerged from a single passage within a BALB/c mouse model, perhaps eluding to the fact that more than one variant contributes to differential pathogenicity of quasispecies (138).

Future directions

We showed that increased H1N1pdm replication in mouse macrophage cell culture was associated with the isolate that caused increased lethality. This increased replication was not seen in human monocyte-derived macrophages (Gerlach, *et al*. unpublished).

However, viruses with increased lethality in mice may show differences in human monocyte-derived macrophage immune signaling (Gerlach, *et al*. unpublished). It is not known if this is true for mouse macrophages, or what the implications are of this in humans. Additionally, we observed increased neutrophils in the bronchoalveolar lavage (BAL) of mice infected with a lethal isolate compared to a non-lethal isolate of H1N1pdm (130). Because very little is known about neutrophils and IAV infection, we turned to the ferret model to validate this finding (Chapter IV). The ferret model showed that neutrophils are, indeed, recruited to the lungs and may become concentrated at sites of H1N1pdm infected epithelium. This establishes a foundation for further research into their role in IAV pathogenicity. Much more is known about neutrophils in mice, in general, and therefore cautious research on IAV and neutrophils may move back into the mouse model.

For both ferrets and mice, an important part of the neutrophil story is missing: the role of viral determinants of increased pathogenicity. What drives the increased lethality in mice? And is the increase in neutrophils related to the increased lethality in mice? Perhaps a proof-in-principle would be to make a virus that increases neutrophils in the lungs of mice without causing increased pathogenicity. These approaches to these questions in mouse models of H1N1pdm rely on the use of reverse genetics. For IAV, plasmid-based reverse genetics systems allow genetic manipulations of the viral genome – site directed mutagenesis, (limited) insertion of genes, or knock-out of certain gene functions – to study IAV pathogenicity (150, 697, 698). Currently, the best technique

involves simultaneously co-transfecting 8 plasmids into 293T cells (an easily

transfectable cell line) and Madin-Darby canine kidney (MDCK) cells (for IAV, an easily

"infect-able" cell line). The plasmids, one for each virus gene segment, contain bi-

directional mammalian promoters to make both viral mRNA (for viral protein production

necessary to make infectious virions) as well as minus-sense viral nucleic acid. Viruses

are rescued and passaged in hen eggs or in MDCK cells to make virus stocks.

The Kentucky clinical isolates of H1N1pdm published in Camp, *et al*. (2013) provide

unique tool to study IAV pathogenesis (130). There are 50 known polymorphisms

among all 8 isolates, 22 between the lethal and non-lethal isolates which were focused on

for publication (130). With the exception of D222G, none have been convincingly

studied for their role in increased lethality. However, Camp, *et al*. (2013) show that

lethality is not necessarily the only endpoint available; it may be possible to identify

mutant viruses that increase lung neutrophilia, for example. (This may not be probable,

as the host response is similarly complicated and inter-related.) It is fairly well

established that mutations that affect receptor binding determine the pathogenicity in

humans, mice, ferrets, and macaques; however, it has been shown that this is not always

the case. Recently, experimental manipulation of H1N1pdm viruses to purposefully alter

their receptor binding preference (*i.e.*, their affinity for only alpha 2,3-linked or only

alpha 2,6-linked specificity) did not show altered replication or virulence in the ferret

(688). Perhaps this binary paradigm for receptor specificity and virulence (i.e., high

versus low virulence is due to avian versus mammalian SA distribution in the LRT versus

URT, respectively) is more complicated, and perhaps differences in the frequency and distribution of complex sialic acid linkages within a specific host's respiratory tract is most important for understanding virulence (688), or perhaps it is just the remnants of a viral quasispecies in this specific experiment masking effects of specific viral variants (690, 691, 696). Again, this illustrates the fascinating complexities of understanding viral determinants of pathogenicity, and the importance of animal models to test hypotheses about IAV pathogenesis.

Influenza A viruses are looming and carry a potential to infect every human on the planet. The study of influenza A viruses is fascinating and complex, owing to their impressive variability. As a tool, they will continue to provide important insights into immune functions important for human disease.
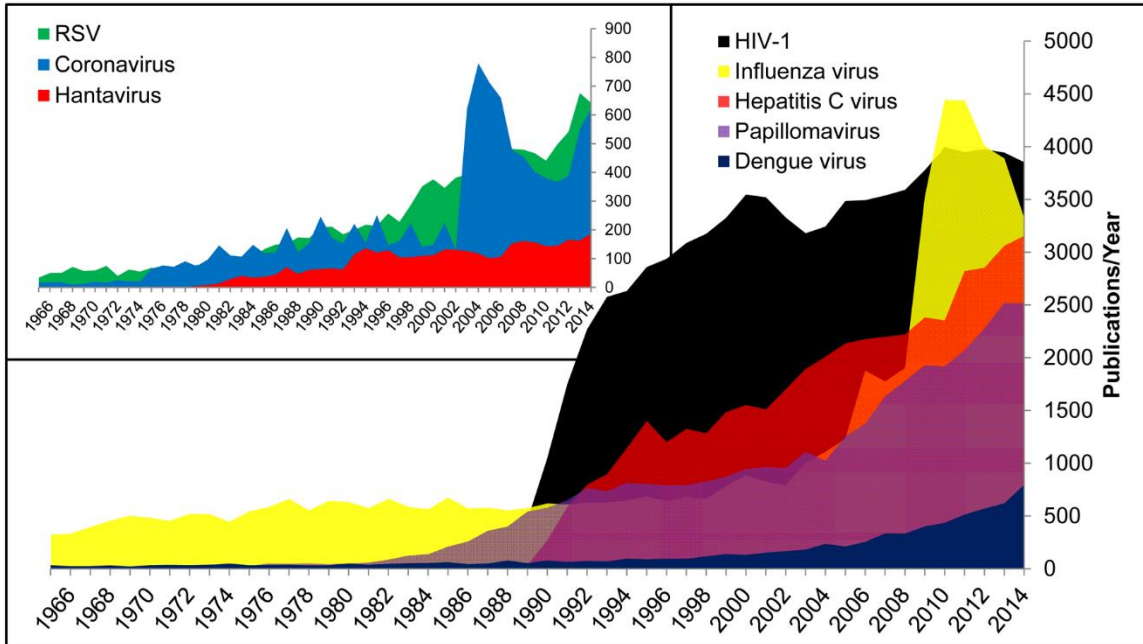
Figure 5.1 Research interest in viruses affecting humans.

The relative amount of scientific research devoted to each of 5 selected viruses is measured by the number of publications per year over the last 50 years (inset shows 3 additional viruses on a different scale over the same time frame). Source: NCBI PubMed searches for given terms; RSV = Respiratory syncytial virus; HIV-1, human immunodeficiency virus type 1.
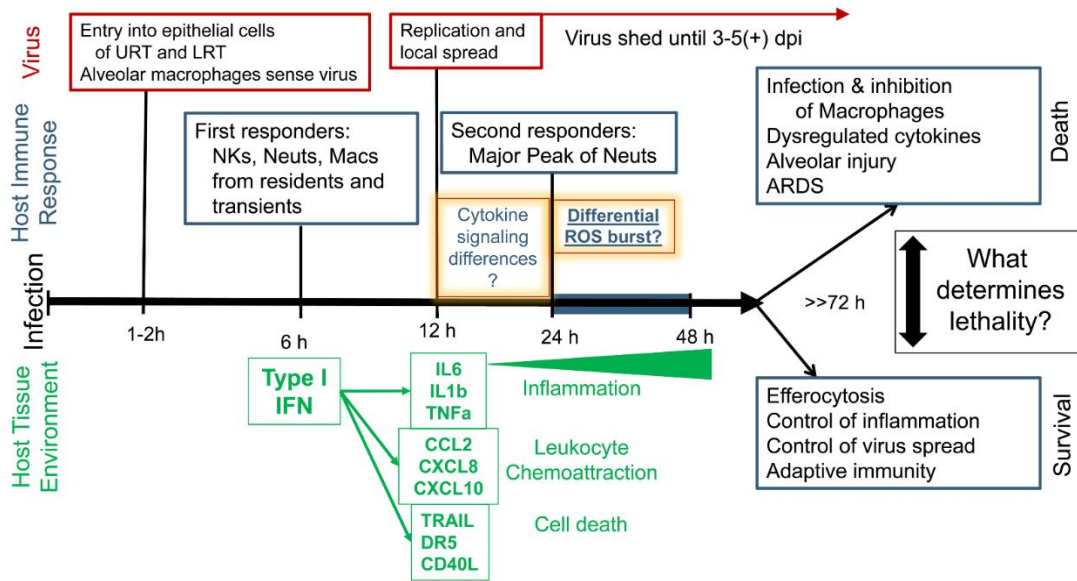
Figure 5.2 A course of disease following influenza A virus infection.

This figure is a prototype course of disease following infection with influenza A virus.

Shown are major events in the viral replication cycle (red), the host immune response

(blue), and the effects on the host tissue environment (green). A critical points for the

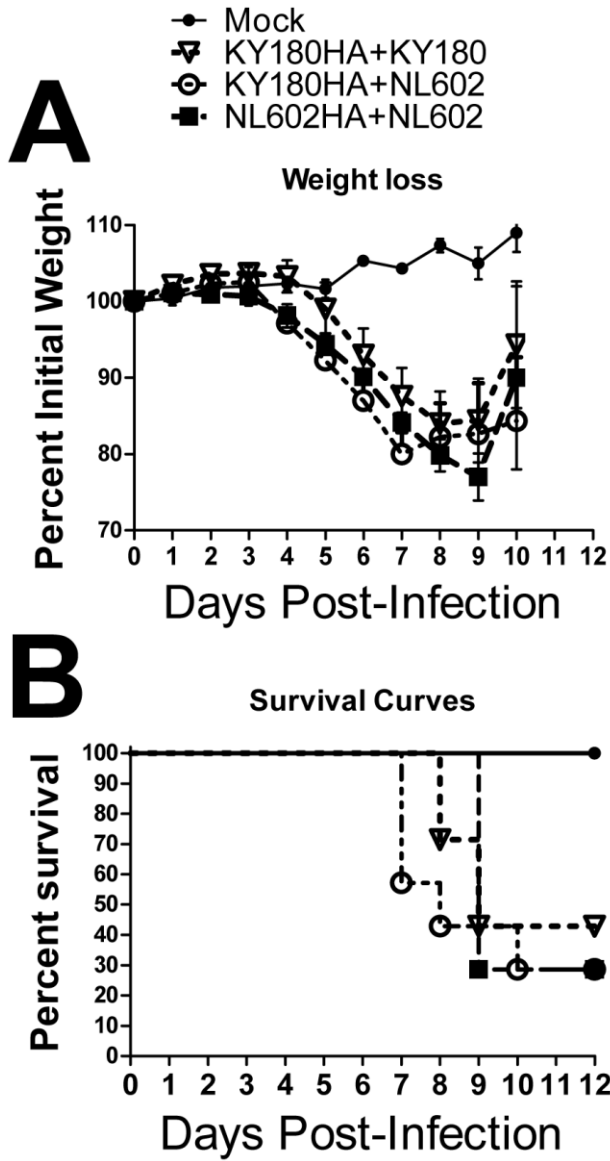formation of severe disease is established following 48 hours.

Figure 5.3 Weight loss and survival of mice infected with wild type and reassortant influenza A(H1N1)pdm09 viruses.

Mice were infected with human clinical isolates of influenza A(H1N1)pdm09 (H1N1pdm) viruses to test the hypothesis that the alpha 2,3-linked sialic acid (SA) binding is a major virulence determinant for mouse infection. It is known that

A/Kentucky/180/2010 (KY180) is lethal in DBA/2 mice, and the hemagglutinin (HA) binds alpha 2,3-linked SA. The A/Netherlands/602/2009 (NL602) isolate is also lethal in DBA/2 mice, however it does not possess an alpha 2,3-linked SA affinity. We used reverse genetics to create a reassortant virus that had the hemagglutinin (HA) of KY180 with the remaining gene segments from NL602 and infected mice intranasally with 10^2 TCID$_{50}$ of each virus. (A) All viruses caused weight loss following infection and (B) the infection was 70%-80% lethal for all viruses.
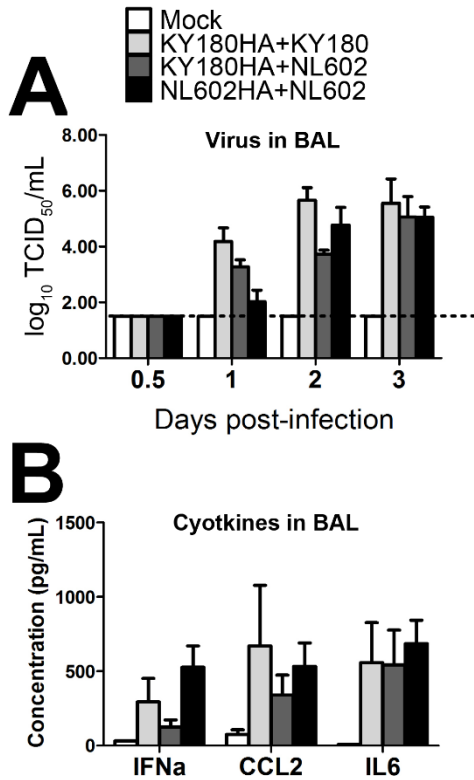
Figure 5.4 Virus replication and immune response in the lungs of mice infected with wild type and reassortant influenza A(H1N1)pdm09 viruses.

DBA/2 mice were infected with human clinical isolates of influenza A(H1N1)pdm09 (H1N1pdm) viruses: A/Kentucky/180/2010 (KY180) or A/Netherlands/602/2009 (NL602). Both isolates are lethal in DBA/2 mice, however the hemagglutinin (HA) from KY180 possesses alpha 2,3-linked SA binding affinity. We used reverse genetics to create a reassortant virus that had the HA of KY180 with the remaining gene segments from NL602 (KY180HA+NL602) and infected mice intranasally with 10^5 TCID$_{50}$ of each virus. (A) All viruses were detected at similar titers in the bronchoalveolar lavage (BAL) and (B) the interferon alpha (IFNa), interleukin-6 (IL6), and CCL2 were present in similar concentrations in the BAL at 3 dpi.
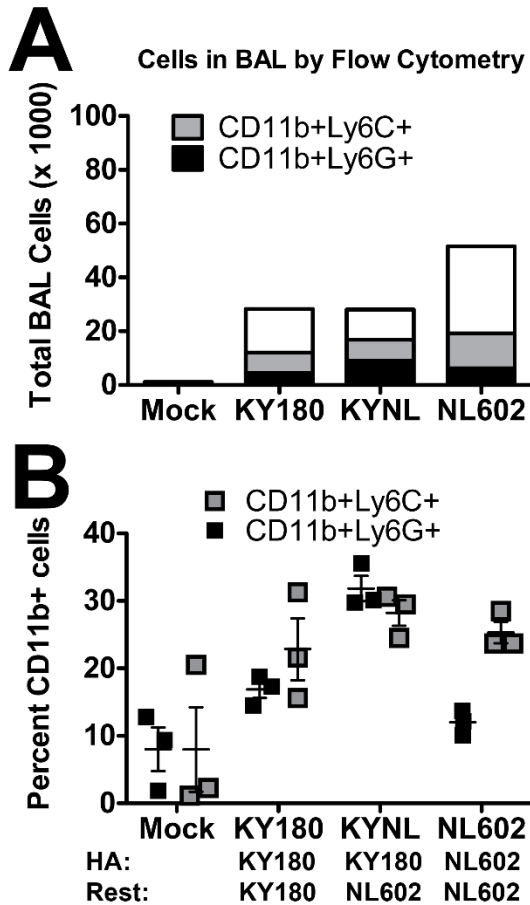
Figure 5.5 Cellular infiltration into the lungs of mice infected with wild type and reassortant influenza A(H1N1)pdm09 viruses.

DBA/2 mice were infected with human clinical isolates of influenza A(H1N1)pdm09 viruses: A/Kentucky/180/2010 (KY180) or A/Netherlands/602/2009 (NL602). Both isolates are lethal in DBA/2 mice, however the hemagglutinin (HA) from KY180 possesses alpha 2,3-linked SA binding affinity. We used reverse genetics to create a reassortant virus that had the HA of KY180 with the rest of the seven gene segments from NL602 (KY180HA+NL602) and infected mice intranasally with 10^5 TCID$_{50}$ of each virus. (A) Flow cytometry was used to measure the population of cells within the

bronchoalveolar lavage (BAL) at 3 dpi. The total number of CD11b+ cells was counted

and the number of CD11b+Ly6G+ and CD11b+Ly6C+ cells are shown stacked within

the total number of CD11b+ cells. The animals infected with viruses containing

KY180HA had reduced overall lung cellularity compared to NL602-infected mice. (B)

The percentage of Ly6G+ (neutrophils) cells and Ly6C+ (macrophages) cells relative to

all CD11b+ cells in the BAL show that there are proportionately fewer neutrophils in the

BAL of mice infected with the virus possessing the NL602HA at 3 dpi.

Table 5.1: Variants in influenza A(H1N1)pdm virus in the human population.

Polym.	PA:14		PA:465		PA:610		PA:716		PB2:340		PB2:584	
Virul.	Low	High	Low	High	Low	High	Low	High	Low	High	Low	High
A.A.	V	I	T	I	E	D	K	Q	N	K	V	I
2009	87%	13%	0%	99%	99%	1%	87%	13%	3%	97%	100%	0%
2012	99%	1.2%	0%	100%	99%	0%	100%	0%	1%	98%	100%	0%
Total	86%	14%	0.2%	99%	99%	0.6%	86%	13%	3%	97%	100%	0%

HA	HA1:84		HA1:183		HA1:186		HA1:222		HA1:234		HA2:47	
Virul.	Low	High	Low	High	Low	High	Low	High	Low	High	Low	High
A.A.	S	N	S	P	A	T	D	G	E	V	E	K
2009	100%	0%	100%	0%	98%	2%	96%	1%	0%	100%	80%	20%
2012	93%	2%	98%	1%	96%	3%	97%	1%	0%	90%	0%	100%
Total	97%	1%	99%	1%	96%	4%	96%	1%	0%	97%	48%	51%

Hemagglutinin (HA, top), and two polymerase subunit proteins (PA & PB2, bottom) of H1N1pdm viruses isolated from patients in the United States in 2009 and 2012. Frequency of specific amino acid (A.A.) mutations at each site (top row) expressed as a percentage of the total known polymorphisms at each site for each year. The variants are divided into low virulence and high virulence (Virul.) based on the lethality of two viruses in DBA/2J mice.

REFERENCES

1. **Smith GJ, Vijaykrishna D, Bahl J, Lycett SJ, Worobey M, Pybus OG, Ma SK, Cheung CL, Raghwani J, Bhatt S, Peiris JS, Guan Y, Rambaut A.** 2009. Origins and evolutionary genomics of the 2009 swine-origin H1N1 influenza A epidemic. Nature **459:**1122-1125.
2. **Webster RG, Bean WJ, Gorman OT, Chambers TM, Kawaoka Y.** 1992. Evolution and ecology of influenza A viruses. Microbiol Rev **56:**152-179.
3. **Russell CA, Jones TC, Barr IG, Cox NJ, Garten RJ, Gregory V, Gust ID, Hampson AW, Hay AJ, Hurt AC, de Jong JC, Kelso A, Klimov AI, Kageyama T, Komadina N, Lapedes AS, Lin YP, Mosterin A, Obuchi M, Odagiri T, Osterhaus AD, Rimmelzwaan GF, Shaw MW, Skepner E, Stohr K, Tashiro M, Fouchier RA, Smith DJ.** 2008. The global circulation of seasonal influenza A (H3N2) viruses. Science **320:**340-346.
4. **Olsen B, Munster VJ, Wallensten A, Waldenstrom J, Osterhaus AD, Fouchier RA.** 2006. Global patterns of influenza a virus in wild birds. Science **312:**384-388.
5. **Cox NJ, Subbarao K.** 2000. Global epidemiology of influenza: past and present. Annu Rev Med **51:**407-421.
6. **Gill JR, Sheng ZM, Ely SF, Guinee DG, Beasley MB, Suh J, Deshpande C, Mollura DJ, Morens DM, Bray M, Travis WD, Taubenberger JK.** 2010. Pulmonary pathologic findings of fatal 2009 pandemic influenza A/H1N1 viral infections. Arch Pathol Lab Med **134:**235-243.
7. **Kuiken T, Taubenberger JK.** 2008. Pathology of human influenza revisited. Vaccine **26 Suppl 4:**D59-66.
8. **Taubenberger JK, Morens DM.** 2008. The pathology of influenza virus infections. Annu Rev Pathol **3:**499-522.
9. **de Jong MD, Simmons CP, Thanh TT, Hien VM, Smith GJ, Chau TN, Hoang DM, Chau NV, Khanh TH, Dong VC, Qui PT, Cam BV, Ha do Q, Guan Y, Peiris JS, Chinh NT, Hien TT, Farrar J.** 2006. Fatal outcome of human influenza A (H5N1) is associated with high viral load and hypercytokinemia. Nat Med **12:**1203-1207.
10. **Peiris JS, Yu WC, Leung CW, Cheung CY, Ng WF, Nicholls JM, Ng TK, Chan KH, Lai ST, Lim WL, Yuen KY, Guan Y.** 2004. Re-emergence of fatal human influenza A subtype H5N1 disease. Lancet **363:**617-619.
11. **Yuen KY, Chan PK, Peiris M, Tsang DN, Que TL, Shortridge KF, Cheung PT, To WK, Ho ET, Sung R, Cheng AF.** 1998. Clinical features and rapid viral diagnosis of human disease associated with avian influenza A H5N1 virus. Lancet **351:**467-471.

12. **Gao HN, Lu HZ, Cao B, Du B, Shang H, Gan JH, Lu SH, Yang YD, Fang Q, Shen YZ, Xi XM, Gu Q, Zhou XM, Qu HP, Yan Z, Li FM, Zhao W, Gao ZC, Wang GF, Ruan LX, Wang WH, Ye J, Cao HF, Li XW, Zhang WH, Fang XC, He J, Liang WF, Xie J, Zeng M, Wu XZ, Li J, Xia Q, Jin ZC, Chen Q, Tang C, Zhang ZY, Hou BM, Feng ZX, Sheng JF, Zhong NS, Li LJ.** 2013. Clinical findings in 111 cases of influenza A (H7N9) virus infection. N Engl J Med **368:**2277-2285.

13. **Gao R, Cao B, Hu Y, Feng Z, Wang D, Hu W, Chen J, Jie Z, Qiu H, Xu K, Xu X, Lu H, Zhu W, Gao Z, Xiang N, Shen Y, He Z, Gu Y, Zhang Z, Yang Y, Zhao X, Zhou L, Li X, Zou S, Zhang Y, Li X, Yang L, Guo J, Dong J, Li Q, Dong L, Zhu Y, Bai T, Wang S, Hao P, Yang W, Zhang Y, Han J, Yu H, Li D, Gao GF, Wu G, Wang Y, Yuan Z, Shu Y.** 2013. Human infection with a novel avian-origin influenza A (H7N9) virus. N Engl J Med **368:**1888-1897.

14. **To KF, Chan PK, Chan KF, Lee WK, Lam WY, Wong KF, Tang NL, Tsang DN, Sung RY, Buckley TA, Tam JS, Cheng AF.** 2001. Pathology of fatal human infection associated with avian influenza A H5N1 virus. J Med Virol **63:**242-246.

15. **Rello J, Pop-Vicas A.** 2009. Clinical review: primary influenza viral pneumonia. Crit Care **13:**235.

16. **Abraham E.** 2003. Neutrophils and acute lung injury. Crit Care Med **31:**S195-199.

17. **Burns AR, Smith CW, Walker DC.** 2003. Unique structural features that influence neutrophil emigration into the lung. Physiol Rev **83:**309-336.

18. **Grommes J, Soehnlein O.** 2011. Contribution of neutrophils to acute lung injury. Mol Med **17:**293-307.

19. **Lowe DM, Redford PS, Wilkinson RJ, O'Garra A, Martineau AR.** 2012. Neutrophils in tuberculosis: friend or foe? Trends Immunol **33:**14-25.

20. **McDonald B, Kubes P.** 2011. Cellular and molecular choreography of neutrophil recruitment to sites of sterile inflammation. J Mol Med (Berl) **89:**1079-1088.

21. **Smith PK, Wang SZ, Dowling KD, Forsyth KD.** 2001. Leucocyte populations in respiratory syncytial virus-induced bronchiolitis. J Paediatr Child Health **37:**146-151.

22. **Nicholls JM, Poon LL, Lee KC, Ng WF, Lai ST, Leung CY, Chu CM, Hui PK, Mak KL, Lim W, Yan KW, Chan KH, Tsang NC, Guan Y, Yuen KY, Peiris JS.** 2003. Lung pathology of fatal severe acute respiratory syndrome. Lancet **361:**1773-1778.

23. **Tse GM, To KF, Chan PK, Lo AW, Ng KC, Wu A, Lee N, Wong HC, Mak SM, Chan KF, Hui DS, Sung JJ, Ng HK.** 2004. Pulmonary pathological features in coronavirus associated severe acute respiratory syndrome (SARS). J Clin Pathol **57:**260-265.

24. **van den Brand JM, Smits SL, Haagmans BL.** 2015. Pathogenesis of Middle East respiratory syndrome coronavirus. J Pathol **235:**175-184.

25. **Matthay MA, Ware LB, Zimmerman GA.** 2012. The acute respiratory distress syndrome. J Clin Invest **122:**2731-2740.

26. **Hufford MM, Richardson G, Zhou H, Manicassamy B, Garcia-Sastre A, Enelow RI, Braciale TJ.** 2012. Influenza-infected neutrophils within the infected lungs act as antigen presenting cells for anti-viral CD8(+) T cells. PLoS One **7:**e46581.

27. **Sprenger H, Meyer RG, Kaufmann A, Bussfeld D, Rischkowsky E, Gemsa D.** 1996. Selective induction of monocyte and not neutrophil-attracting chemokines after influenza A virus infection. J Exp Med **184:**1191-1196.

28. **Calore EE, Uip DE, Perez NM.** 2011. Pathology of the swine-origin influenza A (H1N1) flu. Pathol Res Pract **207:**86-90.

29. **Gu J, Xie Z, Gao Z, Liu J, Korteweg C, Ye J, Lau LT, Lu J, Gao Z, Zhang B, McNutt MA, Lu M, Anderson VM, Gong E, Yu AC, Lipkin WI.** 2007. H5N1 infection of the respiratory tract and beyond: a molecular pathology study. Lancet **370:**1137-1145.

30. **Shieh WJ, Blau DM, Denison AM, Deleon-Carnes M, Adem P, Bhatnagar J, Sumner J, Liu L, Patel M, Batten B, Greer P, Jones T, Smith C, Bartlett J, Montague J, White E, Rollin D, Gao R, Seales C, Jost H, Metcalfe M, Goldsmith CS, Humphrey C, Schmitz A, Drew C, Paddock C, Uyeki TM, Zaki SR.** 2010. 2009 pandemic influenza A (H1N1): pathology and pathogenesis of 100 fatal cases in the United States. Am J Pathol **177:**166-175.

31. **Webster RG.** 1997. Predictions for future human influenza pandemics. J Infect Dis **176 Suppl 1:**S14-19.

32. **Webster RG.** 1997. Influenza virus: transmission between species and relevance to emergence of the next human pandemic. Arch Virol Suppl **13:**105-113.

33. **Webster RG, Shortridge KF, Kawaoka Y.** 1997. Influenza: interspecies transmission and emergence of new pandemics. FEMS Immunol Med Microbiol **18:**275-279.

34. **Webster RG.** 1998. Influenza: an emerging disease. Emerg Infect Dis **4:**436-441.

35. 2009. Outbreak of swine-origin influenza A (H1N1) virus infection - Mexico, March-April 2009. MMWR. Morbidity and mortality weekly report **58:**467-470.

36. **Cao B, Li XW, Mao Y, Wang J, Lu HZ, Chen YS, Liang ZA, Liang L, Zhang SJ, Zhang B, Gu L, Lu LH, Wang DY, Wang C.** 2009. Clinical features of the initial cases of 2009 pandemic influenza A (H1N1) virus infection in China. N Engl J Med **361:**2507-2517.

37. **Donaldson LJ, Rutter PD, Ellis BM, Greaves FE, Mytton OT, Pebody RG, Yardley IE.** 2009. Mortality from pandemic A/H1N1 2009 influenza in England: public health surveillance study. BMJ **339:**b5213.

38. **Garten RJ, Davis CT, Russell CA, Shu B, Lindstrom S, Balish A, Sessions WM, Xu X, Skepner E, Deyde V, Okomo-Adhiambo M, Gubareva L, Barnes J, Smith CB, Emery SL, Hillman MJ, Rivailler P, Smagala J, de Graaf M, Burke DF, Fouchier RA, Pappas C, Alpuche-Aranda CM, Lopez-Gatell H, Olivera H, Lopez I, Myers CA, Faix D, Blair PJ, Yu C, Keene KM, Dotson PD, Jr., Boxrud D, Sambol AR, Abid SH, St George K, Bannerman T, Moore AL, Stringer DJ, Blevins P, Demmler-Harrison GJ, Ginsberg M, Kriner P, Waterman S, Smole S, Guevara HF, Belongia EA, Clark PA, Beatrice ST,**

Donis R, Katz J, Finelli L, Bridges CB, Shaw M, Jernigan DB, Uyeki TM, Smith DJ, Klimov AI, Cox NJ. 2009. Antigenic and genetic characteristics of swine-origin 2009 A(H1N1) influenza viruses circulating in humans. Science **325:**197-201.

39. Jain S, Kamimoto L, Bramley AM, Schmitz AM, Benoit SR, Louie J, Sugerman DE, Druckenmiller JK, Ritger KA, Chugh R, Jasuja S, Deutscher M, Chen S, Walker JD, Duchin JS, Lett S, Soliva S, Wells EV, Swerdlow D, Uyeki TM, Fiore AE, Olsen SJ, Fry AM, Bridges CB, Finelli L. 2009. Hospitalized patients with 2009 H1N1 influenza in the United States, April-June 2009. N Engl J Med **361:**1935-1944.

40. Libster R, Bugna J, Coviello S, Hijano DR, Dunaiewsky M, Reynoso N, Cavalieri ML, Guglielmo MC, Areso MS, Gilligan T, Santucho F, Cabral G, Gregorio GL, Moreno R, Lutz MI, Panigasi AL, Saligari L, Caballero MT, Egues Almeida RM, Gutierrez Meyer ME, Neder MD, Davenport MC, Del Valle MP, Santidrian VS, Mosca G, Garcia Dominguez M, Alvarez L, Landa P, Pota A, Bolonati N, Dalamon R, Sanchez Mercol VI, Espinoza M, Peuchot JC, Karolinski A, Bruno M, Borsa A, Ferrero F, Bonina A, Ramonet M, Albano LC, Luedicke N, Alterman E, Savy V, Baumeister E, Chappell JD, Edwards KM, Melendi GA, Polack FP. 2010. Pediatric hospitalizations associated with 2009 pandemic influenza A (H1N1) in Argentina. N Engl J Med **362:**45-55.

41. Agarwal PP, Cinti S, Kazerooni EA. 2009. Chest radiographic and CT findings in novel swine-origin influenza A (H1N1) virus (S-OIV) infection. AJR Am J Roentgenol **193:**1488-1493.

42. Mollura DJ, Asnis DS, Crupi RS, Conetta R, Feigin DS, Bray M, Taubenberger JK, Bluemke DA. 2009. Imaging findings in a fatal case of pandemic swine-origin influenza A (H1N1). AJR Am J Roentgenol **193:**1500-1503.

43. Neumann G, Noda T, Kawaoka Y. 2009. Emergence and pandemic potential of swine-origin H1N1 influenza virus. Nature **459:**931-939.

44. Peiris JS, Poon LL, Guan Y. 2009. Emergence of a novel swine-origin influenza A virus (S-OIV) H1N1 virus in humans. J Clin Virol **45:**169-173.

45. Perez-Padilla R, de la Rosa-Zamboni D, Ponce de Leon S, Hernandez M, Quinones-Falconi F, Bautista E, Ramirez-Venegas A, Rojas-Serrano J, Ormsby CE, Corrales A, Higuera A, Mondragon E, Cordova-Villalobos JA, Influenza IWGo. 2009. Pneumonia and respiratory failure from swine-origin influenza A (H1N1) in Mexico. N Engl J Med **361:**680-689.

46. Woo PC, Tung ET, Chan KH, Lau CC, Lau SK, Yuen KY. 2010. Cytokine profiles induced by the novel swine-origin influenza A/H1N1 virus: implications for treatment strategies. J Infect Dis **201:**346-353.

47. Belser JA, Katz JM, Tumpey TM. 2011. The ferret as a model organism to study influenza A virus infection. Dis Model Mech.

48. Smith H, Sweet C. 1988. Lessons for human influenza from pathogenicity studies with ferrets. Rev Infect Dis **10:**56-75.

49. **Barnard DL.** 2009. Animal models for the study of influenza pathogenesis and therapy. Antiviral Res **82:**A110-122.

50. **Belser JA, Szretter KJ, Katz JM, Tumpey TM.** 2009. Use of animal models to understand the pandemic potential of highly pathogenic avian influenza viruses. Adv Virus Res **73:**55-97.

51. **van den Brand JM, Haagmans BL, van Riel D, Osterhaus AD, Kuiken T.** 2014. The pathology and pathogenesis of experimental severe acute respiratory syndrome and influenza in animal models. J Comp Pathol **151:**83-112.

52. **van Riel D, Munster VJ, de Wit E, Rimmelzwaan GF, Fouchier RA, Osterhaus AD, Kuiken T.** 2007. Human and avian influenza viruses target different cells in the lower respiratory tract of humans and other mammals. Am J Pathol **171:**1215-1223.

53. **Watanabe T, Kawaoka Y.** 2011. Pathogenesis of the 1918 pandemic influenza virus. PLoS Pathog **7:**e1001218.

54. **Cameron CM, Cameron MJ, Bermejo-Martin JF, Ran L, Xu L, Turner PV, Ran R, Danesh A, Fang Y, Chan PK, Mytle N, Sullivan TJ, Collins TL, Johnson MG, Medina JC, Rowe T, Kelvin DJ.** 2008. Gene expression analysis of host innate immune responses during Lethal H5N1 infection in ferrets. J Virol **82:**11308-11317.

55. **Lu X, Tumpey TM, Morken T, Zaki SR, Cox NJ, Katz JM.** 1999. A mouse model for the evaluation of pathogenesis and immunity to influenza A (H5N1) viruses isolated from humans. J Virol **73:**5903-5911.

56. **Zitzow LA, Rowe T, Morken T, Shieh WJ, Zaki S, Katz JM.** 2002. Pathogenesis of avian influenza A (H5N1) viruses in ferrets. J Virol **76:**4420-4429.

57. **Ware LB, Matthay MA.** 2000. The acute respiratory distress syndrome. N Engl J Med **342:**1334-1349.

58. **Abraham E, Matthay MA, Dinarello CA, Vincent JL, Cohen J, Opal SM, Glauser M, Parsons P, Fisher CJ, Jr., Repine JE.** 2000. Consensus conference definitions for sepsis, septic shock, acute lung injury, and acute respiratory distress syndrome: time for a reevaluation. Crit Care Med **28:**232-235.

59. **Aherne W, Bird T, Court SD, Gardner PS, McQuillin J.** 1970. Pathological changes in virus infections of the lower respiratory tract in children. J Clin Pathol **23:**7-18.

60. **Craig A, Mai J, Cai S, Jeyaseelan S.** 2009. Neutrophil recruitment to the lungs during bacterial pneumonia. Infect Immun **77:**568-575.

61. **Herold S, Mayer K, Lohmeyer J.** 2011. Acute lung injury: how macrophages orchestrate resolution of inflammation and tissue repair. Front Immunol **2:**65.

62. **Lien DC, Wagner WW, Jr., Capen RL, Haslett C, Hanson WL, Hofmeister SE, Henson PM, Worthen GS.** 1987. Physiological neutrophil sequestration in the lung: visual evidence for localization in capillaries. J Appl Physiol (1985) **62:**1236-1243.

63. **Rubenfeld GD, Caldwell E, Peabody E, Weaver J, Martin DP, Neff M, Stern EJ, Hudson LD.** 2005. Incidence and outcomes of acute lung injury. N Engl J Med **353:**1685-1693.

64. **Reutershan J, Basit A, Galkina EV, Ley K.** 2005. Sequential recruitment of neutrophils into lung and bronchoalveolar lavage fluid in LPS-induced acute lung injury. Am J Physiol Lung Cell Mol Physiol **289:**L807-815.

65. **Davidson S, Crotta S, McCabe TM, Wack A.** 2014. Pathogenic potential of interferon alphabeta in acute influenza infection. Nat Commun **5:**3864.

66. **Garcia-Sastre A, Biron CA.** 2006. Type 1 interferons and the virus-host relationship: a lesson in detente. Science **312:**879-882.

67. **Le Bon A, Tough DF.** 2002. Links between innate and adaptive immunity via type I interferon. Curr Opin Immunol **14:**432-436.

68. **Stetson DB, Medzhitov R.** 2006. Type I interferons in host defense. Immunity **25:**373-381.

69. **Meunier I, von Messling V.** 2011. NS1-mediated delay of type I interferon induction contributes to influenza A virulence in ferrets. J Gen Virol **92:**1635-1644.

70. **Seo SU, Kwon HJ, Ko HJ, Byun YH, Seong BL, Uematsu S, Akira S, Kweon MN.** 2011. Type I interferon signaling regulates Ly6C(hi) monocytes and neutrophils during acute viral pneumonia in mice. PLoS Pathog **7:**e1001304.

71. **Svitek N, Rudd PA, Obojes K, Pillet S, von Messling V.** 2008. Severe seasonal influenza in ferrets correlates with reduced interferon and increased IL-6 induction. Virology **376:**53-59.

72. **Cheung CY, Poon LL, Lau AS, Luk W, Lau YL, Shortridge KF, Gordon S, Guan Y, Peiris JS.** 2002. Induction of proinflammatory cytokines in human macrophages by influenza A (H5N1) viruses: a mechanism for the unusual severity of human disease? Lancet **360:**1831-1837.

73. **Cline TD, Karlsson EA, Seufzer BJ, Schultz-Cherry S.** 2013. The hemagglutinin protein of highly pathogenic H5N1 influenza viruses overcomes an early block in the replication cycle to promote productive replication in macrophages. J Virol **87:**1411-1419.

74. **Sakabe S, Iwatsuki-Horimoto K, Takano R, Nidom CA, Le M, Nagamura-Inoue T, Horimoto T, Yamashita N, Kawaoka Y.** 2011. Cytokine production by primary human macrophages infected with highly pathogenic H5N1 or pandemic H1N1 2009 influenza viruses. J Gen Virol **92:**1428-1434.

75. **Yu WC, Chan RW, Wang J, Travanty EA, Nicholls JM, Peiris JS, Mason RJ, Chan MC.** 2011. Viral replication and innate host responses in primary human alveolar epithelial cells and alveolar macrophages infected with influenza H5N1 and H1N1 viruses. J Virol **85:**6844-6855.

76. **Durbin JE, Fernandez-Sesma A, Lee CK, Rao TD, Frey AB, Moran TM, Vukmanovic S, Garcia-Sastre A, Levy DE.** 2000. Type I IFN modulates innate and specific antiviral immunity. J Immunol **164:**4220-4228.

77. **Sugamata R, Dobashi H, Nagao T, Yamamoto K, Nakajima N, Sato Y, Aratani Y, Oshima M, Sata T, Kobayashi K, Kawachi S, Nakayama T,**

Suzuki K. 2012. Contribution of neutrophil-derived myeloperoxidase in the early phase of fulminant acute respiratory distress syndrome induced by influenza virus infection. Microbiol Immunol **56:**171-182.

78. **Fujisawa H.** 2008. Neutrophils play an essential role in cooperation with antibody in both protection against and recovery from pulmonary infection with influenza virus in mice. J Virol **82:**2772-2783.

79. **Hashimoto Y, Moki T, Takizawa T, Shiratsuchi A, Nakanishi Y.** 2007. Evidence for phagocytosis of influenza virus-infected, apoptotic cells by neutrophils and macrophages in mice. J Immunol **178:**2448-2457.

80. **Jenne CN, Wong CH, Zemp FJ, McDonald B, Rahman MM, Forsyth PA, McFadden G, Kubes P.** 2013. Neutrophils recruited to sites of infection protect from virus challenge by releasing neutrophil extracellular traps. Cell Host Microbe **13:**169-180.

81. **Nathan C.** 2006. Neutrophils and immunity: challenges and opportunities. Nat Rev Immunol **6:**173-182.

82. **Tamassia N, Le Moigne V, Rossato M, Donini M, McCartney S, Calzetti F, Colonna M, Bazzoni F, Cassatella MA.** 2008. Activation of an immunoregulatory and antiviral gene expression program in poly(I:C)-transfected human neutrophils. J Immunol **181:**6563-6573.

83. **Tate MD, Brooks AG, Reading PC, Mintern JD.** 2012. Neutrophils sustain effective CD8(+) T-cell responses in the respiratory tract following influenza infection. Immunol Cell Biol **90:**197-205.

84. **Tate MD, Deng YM, Jones JE, Anderson GP, Brooks AG, Reading PC.** 2009. Neutrophils ameliorate lung injury and the development of severe disease during influenza infection. J Immunol **183:**7441-7450.

85. **Tate MD, Brooks AG, Reading PC.** 2008. The role of neutrophils in the upper and lower respiratory tract during influenza virus infection of mice. Respir Res **9:**57.

86. **Tate MD, Ioannidis LJ, Croker B, Brown LE, Brooks AG, Reading PC.** 2011. The role of neutrophils during mild and severe influenza virus infections of mice. PLoS One **6:**e17618.

87. **Turner RB.** 1990. The role of neutrophils in the pathogenesis of rhinovirus infections. Pediatr Infect Dis J **9:**832-835.

88. **Chandrasekaran A, Srinivasan A, Raman R, Viswanathan K, Raguram S, Tumpey TM, Sasisekharan V, Sasisekharan R.** 2008. Glycan topology determines human adaptation of avian H5N1 virus hemagglutinin. Nat Biotechnol **26:**107-113.

89. **Imai M, Watanabe T, Hatta M, Das SC, Ozawa M, Shinya K, Zhong G, Hanson A, Katsura H, Watanabe S, Li C, Kawakami E, Yamada S, Kiso M, Suzuki Y, Maher EA, Neumann G, Kawaoka Y.** 2012. Experimental adaptation of an influenza H5 HA confers respiratory droplet transmission to a reassortant H5 HA/H1N1 virus in ferrets. Nature **486:**420-428.

90. **de Graaf M, Fouchier RA.** 2014. Role of receptor binding specificity in influenza A virus transmission and pathogenesis. EMBO J **33:**823-841.

91. **Herfst S, Schrauwen EJ, Linster M, Chutinimitkul S, de Wit E, Munster VJ, Sorrell EM, Bestebroer TM, Burke DF, Smith DJ, Rimmelzwaan GF, Osterhaus AD, Fouchier RA.** 2012. Airborne transmission of influenza A/H5N1 virus between ferrets. Science **336:**1534-1541.

92. **Chan PK.** 2002. Outbreak of avian influenza A(H5N1) virus infection in Hong Kong in 1997. Clin Infect Dis **34 Suppl 2:**S58-64.

93. **Claas EC, Osterhaus AD, van Beek R, De Jong JC, Rimmelzwaan GF, Senne DA, Krauss S, Shortridge KF, Webster RG.** 1998. Human influenza A H5N1 virus related to a highly pathogenic avian influenza virus. Lancet **351:**472-477.

94. **Korteweg C, Gu J.** 2008. Pathology, molecular biology, and pathogenesis of avian influenza A (H5N1) infection in humans. Am J Pathol **172:**1155-1170.

95. **Nicholls JM, Chan MC, Chan WY, Wong HK, Cheung CY, Kwong DL, Wong MP, Chui WH, Poon LL, Tsao SW, Guan Y, Peiris JS.** 2007. Tropism of avian influenza A (H5N1) in the upper and lower respiratory tract. Nat Med **13:**147-149.

96. **WHO.** 2014. Influenza (Seasonal). World Health Organization.

97. **Hilleman MR.** 2002. Realities and enigmas of human viral influenza: pathogenesis, epidemiology and control. Vaccine **20:**3068-3087.

98. **Carrat F, Vergu E, Ferguson NM, Lemaitre M, Cauchemez S, Leach S, Valleron AJ.** 2008. Time lines of infection and disease in human influenza: a review of volunteer challenge studies. Am J Epidemiol **167:**775-785.

99. **Hayden FG, Fritz R, Lobo MC, Alvord W, Strober W, Straus SE.** 1998. Local and systemic cytokine responses during experimental human influenza A virus infection. Relation to symptom formation and host defense. J Clin Invest **101:**643-649.

100. **Skoner DP, Gentile DA, Patel A, Doyle WJ.** 1999. Evidence for cytokine mediation of disease expression in adults experimentally infected with influenza A virus. J Infect Dis **180:**10-14.

101. **Kaiser L, Fritz RS, Straus SE, Gubareva L, Hayden FG.** 2001. Symptom pathogenesis during acute influenza: interleukin-6 and other cytokine responses. J Med Virol **64:**262-268.

102. **Francis T, Stuart-Harris CH.** 1938. Studies on the Nasal Histology of Epidemic Influenza Virus Infection in the Ferret : I. The Development and Repair of the Nasal Lesion. J Exp Med **68:**789-802.

103. **Haff RF, Schriver PW, Stewart RC.** 1966. Pathogenesis of influenza in ferrets: nasal manifestations of disease. Br J Exp Pathol **47:**435-444.

104. **Walsh JJ, Dietlein LF, Low FN, Burch GE, Mogabgab WJ.** 1961. Bronchotracheal response in human influenza. Type A, Asian strain, as studied by light and electron microscopic examination of bronchoscopic biopsies. Arch Intern Med **108:**376-388.

105. **Lee N, Wong CK, Chan PK, Chan MC, Wong RY, Lun SW, Ngai KL, Lui GC, Wong BC, Lee SK, Choi KW, Hui DS.** 2011. Cytokine response patterns in severe pandemic 2009 H1N1 and seasonal influenza among hospitalized adults. PLoS One **6:**e26050.

106. **Glinsky GV.** 2010. Genomic analysis of pandemic (H1N1) 2009 reveals association of increasing disease severity with emergence of novel hemagglutinin mutations. Cell cycle **9:**958-970.

107. **Baillie GJ, Galiano M, Agapow PM, Myers R, Chiam R, Gall A, Palser AL, Watson SJ, Hedge J, Underwood A, Platt S, McLean E, Pebody RG, Rambaut A, Green J, Daniels R, Pybus OG, Kellam P, Zambon M.** 2012. Evolutionary dynamics of local pandemic H1N1/2009 influenza virus lineages revealed by whole-genome analysis. J Virol **86:**11-18.

108. **Zarychanski R, Stuart TL, Kumar A, Doucette S, Elliott L, Kettner J, Plummer F.** 2010. Correlates of severe disease in patients with 2009 pandemic influenza (H1N1) virus infection. CMAJ **182:**257-264.

109. **Louie JK, Acosta M, Winter K, Jean C, Gavali S, Schechter R, Vugia D, Harriman K, Matyas B, Glaser CA, Samuel MC, Rosenberg J, Talarico J, Hatch D, California Pandemic Working G.** 2009. Factors associated with death or hospitalization due to pandemic 2009 influenza A(H1N1) infection in California. JAMA **302:**1896-1902.

110. **Nguyen-Van-Tam JS, Openshaw PJ, Hashim A, Gadd EM, Lim WS, Semple MG, Read RC, Taylor BL, Brett SJ, McMenamin J, Enstone JE, Armstrong C, Nicholson KG, Influenza Clinical Information N.** 2010. Risk factors for hospitalisation and poor outcome with pandemic A/H1N1 influenza: United Kingdom first wave (May-September 2009). Thorax **65:**645-651.

111. **Rosen DG, Lopez AE, Anzalone ML, Wolf DA, Derrick SM, Florez LF, Gonsoulin ML, Hines MO, 3rd, Mitchell RA, Phatak DR, Haden-Pinneri K, Sanchez LA.** 2010. Postmortem findings in eight cases of influenza A/H1N1. Mod Pathol **23:**1449-1457.

112. **Hagau N, Slavcovici A, Gonganau DN, Oltean S, Dirzu DS, Brezoszki ES, Maxim M, Ciuce C, Mlesnite M, Gavrus RL, Laslo C, Hagau R, Petrescu M, Studnicska DM.** 2010. Clinical aspects and cytokine response in severe H1N1 influenza A virus infection. Crit Care **14:**R203.

113. **Kim YH, Kim JE, Hyun MC.** 2011. Cytokine response in pediatric patients with pandemic influenza H1N1 2009 virus infection and pneumonia: comparison with pediatric pneumonia without H1N1 2009 infection. Pediatr Pulmonol **46:**1233-1239.

114. **Takano T, Tajiri H, Kashiwagi Y, Kimura S, Kawashima H.** 2011. Cytokine and chemokine response in children with the 2009 pandemic influenza A (H1N1) virus infection. Eur J Clin Microbiol Infect Dis **30:**117-120.

115. **To KK, Hung IF, Li IW, Lee KL, Koo CK, Yan WW, Liu R, Ho KY, Chu KH, Watt CL, Luk WK, Lai KY, Chow FL, Mok T, Buckley T, Chan JF, Wong SS, Zheng B, Chen H, Lau CC, Tse H, Cheng VC, Chan KH, Yuen KY.** 2010. Delayed clearance of viral load and marked cytokine activation in severe cases of pandemic H1N1 2009 influenza virus infection. Clin Infect Dis **50:**850-859.

116. **Stevens J, Blixt O, Glaser L, Taubenberger JK, Palese P, Paulson JC, Wilson IA.** 2006. Glycan microarray analysis of the hemagglutinins from modern and

pandemic influenza viruses reveals different receptor specificities. J Mol Biol **355:**1143-1155.

117. **Morens DM, Taubenberger JK, Fauci AS.** 2008. Predominant role of bacterial pneumonia as a cause of death in pandemic influenza: implications for pandemic influenza preparedness. J Infect Dis **198:**962-970.

118. **Memoli MJ, Tumpey TM, Jagger BW, Dugan VG, Sheng ZM, Qi L, Kash JC, Taubenberger JK.** 2009. An early 'classical' swine H1N1 influenza virus shows similar pathogenicity to the 1918 pandemic virus in ferrets and mice. Virology **393:**338-345.

119. **Kobasa D, Jones SM, Shinya K, Kash JC, Copps J, Ebihara H, Hatta Y, Kim JH, Halfmann P, Hatta M, Feldmann F, Alimonti JB, Fernando L, Li Y, Katze MG, Feldmann H, Kawaoka Y.** 2007. Aberrant innate immune response in lethal infection of macaques with the 1918 influenza virus. Nature **445:**319-323.

120. **Tumpey TM, Basler CF, Aguilar PV, Zeng H, Solorzano A, Swayne DE, Cox NJ, Katz JM, Taubenberger JK, Palese P, Garcia-Sastre A.** 2005. Characterization of the reconstructed 1918 Spanish influenza pandemic virus. Science **310:**77-80.

121. **Wang SM, Liao YT, Hu YS, Ho TS, Shen CF, Wang JR, Lin YS, Liu CC.** 2014. Immunophenotype expressions and cytokine profiles of influenza A H1N1 virus infection in pediatric patients in 2009. Dis Markers **2014:**195453.

122. **Palese P.** 2004. Influenza: old and new threats. Nat Med **10:**S82-87.

123. **van den Brand JM, Stittelaar KJ, van Amerongen G, Reperant L, de Waal L, Osterhaus AD, Kuiken T.** 2012. Comparison of temporal and spatial dynamics of seasonal H3N2, pandemic H1N1 and highly pathogenic avian influenza H5N1 virus infections in ferrets. PLoS One **7:**e42343.

124. **van den Brand JM, Stittelaar KJ, van Amerongen G, Rimmelzwaan GF, Simon J, de Wit E, Munster V, Bestebroer T, Fouchier RA, Kuiken T, Osterhaus AD.** 2010. Severity of pneumonia due to new H1N1 influenza virus in ferrets is intermediate between that due to seasonal H1N1 virus and highly pathogenic avian influenza H5N1 virus. J Infect Dis **201:**993-999.

125. **Belser JA, Jayaraman A, Raman R, Pappas C, Zeng H, Cox NJ, Katz JM, Sasisekharan R, Tumpey TM.** 2011. Effect of D222G mutation in the hemagglutinin protein on receptor binding, pathogenesis and transmissibility of the 2009 pandemic H1N1 influenza virus. PLoS One **6:**e25091.

126. **Maines TR, Belser JA, Gustin KM, van Hoeven N, Zeng H, Svitek N, von Messling V, Katz JM, Tumpey TM.** 2012. Local innate immune responses and influenza virus transmission and virulence in ferrets. J Infect Dis **205:**474-485.

127. **Maines TR, Jayaraman A, Belser JA, Wadford DA, Pappas C, Zeng H, Gustin KM, Pearce MB, Viswanathan K, Shriver ZH, Raman R, Cox NJ, Sasisekharan R, Katz JM, Tumpey TM.** 2009. Transmission and pathogenesis of swine-origin 2009 A(H1N1) influenza viruses in ferrets and mice. Science **325:**484-487.

128. **Neumann G, Ozawa M, Kawaoka Y.** 2012. Reverse genetics of influenza viruses. Methods Mol Biol **865:**193-206.

129. **Abed Y, Pizzorno A, Hamelin ME, Leung A, Joubert P, Couture C, Kobasa D, Boivin G.** 2011. The 2009 pandemic H1N1 D222G hemagglutinin mutation alters receptor specificity and increases virulence in mice but not in ferrets. J Infect Dis **204:**1008-1016.

130. **Camp JV, Chu YK, Chung DH, McAllister RC, Adcock RS, Gerlach RL, Wiemken TL, Peyrani P, Ramirez JA, Summersgill JT, Jonsson CB.** 2013. Phenotypic differences in virulence and immune response in closely related clinical isolates of influenza A 2009 H1N1 pandemic viruses in mice. PLoS One **8:**e56602.

131. **Chutinimitkul S, Herfst S, Steel J, Lowen AC, Ye J, van Riel D, Schrauwen EJ, Bestebroer TM, Koel B, Burke DF, Sutherland-Cash KH, Whittleston CS, Russell CA, Wales DJ, Smith DJ, Jonges M, Meijer A, Koopmans M, Rimmelzwaan GF, Kuiken T, Osterhaus AD, Garcia-Sastre A, Perez DR, Fouchier RA.** 2010. Virulence-associated substitution D222G in the hemagglutinin of 2009 pandemic influenza A(H1N1) virus affects receptor binding. J Virol **84:**11802-11813.

132. **Itoh Y, Shinya K, Kiso M, Watanabe T, Sakoda Y, Hatta M, Muramoto Y, Tamura D, Sakai-Tagawa Y, Noda T, Sakabe S, Imai M, Hatta Y, Watanabe S, Li C, Yamada S, Fujii K, Murakami S, Imai H, Kakugawa S, Ito M, Takano R, Iwatsuki-Horimoto K, Shimojima M, Horimoto T, Goto H, Takahashi K, Makino A, Ishigaki H, Nakayama M, Okamatsu M, Takahashi K, Warshauer D, Shult PA, Saito R, Suzuki H, Furuta Y, Yamashita M, Mitamura K, Nakano K, Nakamura M, Brockman-Schneider R, Mitamura H, Yamazaki M, Sugaya N, Suresh M, Ozawa M, Neumann G, Gern J, Kida H, Ogasawara K, Kawaoka Y.** 2009. In vitro and in vivo characterization of new swine-origin H1N1 influenza viruses. Nature **460:**1021-1025.

133. **Jhung MA, Swerdlow D, Olsen SJ, Jernigan D, Biggerstaff M, Kamimoto L, Kniss K, Reed C, Fry A, Brammer L, Gindler J, Gregg WJ, Bresee J, Finelli L.** 2011. Epidemiology of 2009 pandemic influenza A (H1N1) in the United States. Clin Infect Dis **52 Suppl 1:**S13-26.

134. **Melidou A, Gioula G, Exindari M, Chatzidimitriou D, Diza E, Malisiovas N.** 2010. Molecular and phylogenetic analysis of the haemagglutinin gene of pandemic influenza H1N1 2009 viruses associated with severe and fatal infections. Virus Res **151:**192-199.

135. **Meunier I, Embury-Hyatt C, Stebner S, Gray M, Bastien N, Li Y, Plummer F, Kobinger GP, von Messling V.** 2012. Virulence differences of closely related pandemic 2009 H1N1 isolates correlate with increased inflammatory responses in ferrets. Virology **422:**125-131.

136. **Otte A, Gabriel G.** 2011. 2009 pandemic H1N1 influenza A virus strains display differential pathogenicity in C57BL/6J but not BALB/c mice. Virulence **2:**563-566.

137. **Safronetz D, Rockx B, Feldmann F, Belisle SE, Palermo RE, Brining D, Gardner D, Proll SC, Marzi A, Tsuda Y, Lacasse RA, Kercher L, York A, Korth MJ, Long D, Rosenke R, Shupert WL, Aranda CA, Mattoon JS, Kobasa D, Kobinger G, Li Y, Taubenberger JK, Richt JA, Parnell M, Ebihara H, Kawaoka Y, Katze MG, Feldmann H.** 2011. Pandemic swine-origin H1N1 influenza A virus isolates show heterogeneous virulence in macaques. J Virol **85:**1214-1223.

138. **Ye J, Sorrell EM, Cai Y, Shao H, Xu K, Pena L, Hickman D, Song H, Angel M, Medina RA, Manicassamy B, Garcia-Sastre A, Perez DR.** 2010. Variations in the hemagglutinin of the 2009 H1N1 pandemic virus: potential for strains with altered virulence phenotype? PLoS Pathog **6:**e1001145.

139. **Gubareva LV, McCullers JA, Bethell RC, Webster RG.** 1998. Characterization of influenza A/HongKong/156/97 (H5N1) virus in a mouse model and protective effect of zanamivir on H5N1 infection in mice. J Infect Dis **178:**1592-1596.

140. **Shortridge KF, Zhou NN, Guan Y, Gao P, Ito T, Kawaoka Y, Kodihalli S, Krauss S, Markwell D, Murti KG, Norwood M, Senne D, Sims L, Takada A, Webster RG.** 1998. Characterization of avian H5N1 influenza viruses from poultry in Hong Kong. Virology **252:**331-342.

141. **Chen Y, Liang W, Yang S, Wu N, Gao H, Sheng J, Yao H, Wo J, Fang Q, Cui D, Li Y, Yao X, Zhang Y, Wu H, Zheng S, Diao H, Xia S, Zhang Y, Chan KH, Tsoi HW, Teng JL, Song W, Wang P, Lau SY, Zheng M, Chan JF, To KK, Chen H, Li L, Yuen KY.** 2013. Human infections with the emerging avian influenza A H7N9 virus from wet market poultry: clinical analysis and characterisation of viral genome. Lancet **381:**1916-1925.

142. **Wong SS, Yuen KY.** 2006. Avian influenza virus infections in humans. Chest **129:**156-168.

143. **Fouchier RA, Schneeberger PM, Rozendaal FW, Broekman JM, Kemink SA, Munster V, Kuiken T, Rimmelzwaan GF, Schutten M, Van Doornum GJ, Koch G, Bosman A, Koopmans M, Osterhaus AD.** 2004. Avian influenza A virus (H7N7) associated with human conjunctivitis and a fatal case of acute respiratory distress syndrome. Proc Natl Acad Sci U S A **101:**1356-1361.

144. **Chen E, Chen Y, Fu L, Chen Z, Gong Z, Mao H, Wang D, Ni MY, Wu P, Yu Z, He T, Li Z, Gao J, Liu S, Shu Y, Cowling BJ, Xia S, Yu H.** 2013. Human infection with avian influenza A(H7N9) virus re-emerges in China in winter 2013. Euro Surveill **18**.

145. **Zhou J, Wang D, Gao R, Zhao B, Song J, Qi X, Zhang Y, Shi Y, Yang L, Zhu W, Bai T, Qin K, Lan Y, Zou S, Guo J, Dong J, Dong L, Zhang Y, Wei H, Li X, Lu J, Liu L, Zhao X, Li X, Huang W, Wen L, Bo H, Xin L, Chen Y, Xu C, Pei Y, Yang Y, Zhang X, Wang S, Feng Z, Han J, Yang W, Gao GF, Wu G, Li D, Wang Y, Shu Y.** 2013. Biological features of novel avian influenza A (H7N9) virus. Nature **499:**500-503.

146. **Shope RE.** 1935. The Infection of Mice with Swine Influenza Virus. J Exp Med **62:**561-572.

147. **Francis T, Jr., Magill TP.** 1935. Cultivation of Human Influenza Virus in an Artificial Medium. Science **82:**353-354.

148. **Smith W, Andrewes CH, Laidlaw PP.** 1933. A virus obtained from influenza patients. The Lancet **222:**66-68.

149. **Shope RE.** 1934. The Infection of Ferrets with Swine Influenza Virus. J Exp Med **60:**49-61.

150. **Pleschka S, Jaskunas R, Engelhardt OG, Zurcher T, Palese P, Garcia-Sastre A.** 1996. A plasmid-based reverse genetics system for influenza A virus. J Virol **70:**4188-4192.

151. **Palese P, Shaw M.** 2007. Orthomyxoviridae, p. 1647-1690. *In* Knipe DM, Howley PM (ed.), Fields virology 5th edition, vol. 2. Lippincott WIlliams & Wilkins, Philadelphia.

152. **McGeoch D, Fellner P, Newton C.** 1976. Influenza virus genome consists of eight distinct RNA species. Proc Natl Acad Sci U S A **73:**3045-3049.

153. **Ye Q, Krug RM, Tao YJ.** 2006. The mechanism by which influenza A virus nucleoprotein forms oligomers and binds RNA. Nature **444:**1078-1082.

154. **Klumpp K, Ruigrok RW, Baudin F.** 1997. Roles of the influenza virus polymerase and nucleoprotein in forming a functional RNP structure. EMBO J **16:**1248-1257.

155. **Zheng W, Tao YJ.** 2013. Structure and assembly of the influenza A virus ribonucleoprotein complex. FEBS Lett **587:**1206-1214.

156. **Arranz R, Coloma R, Chichon FJ, Conesa JJ, Carrascosa JL, Valpuesta JM, Ortin J, Martin-Benito J.** 2012. The structure of native influenza virion ribonucleoproteins. Science **338:**1634-1637.

157. **Sha B, Luo M.** 1997. Structure of a bifunctional membrane-RNA binding protein, influenza virus matrix protein M1. Nat Struct Biol **4:**239-244.

158. **Nayak DP, Balogun RA, Yamada H, Zhou ZH, Barman S.** 2009. Influenza virus morphogenesis and budding. Virus Res **143:**147-161.

159. **Skehel JJ, Wiley DC.** 2000. Receptor binding and membrane fusion in virus entry: the influenza hemagglutinin. Annu Rev Biochem **69:**531-569.

160. **Wilson IA, Skehel JJ, Wiley DC.** 1981. Structure of the haemagglutinin membrane glycoprotein of influenza virus at 3 A resolution. Nature **289:**366-373.

161. **Varghese JN, Laver WG, Colman PM.** 1983. Structure of the influenza virus glycoprotein antigen neuraminidase at 2.9 A resolution. Nature **303:**35-40.

162. **Palese P, Schulman JL.** 1976. Mapping of the influenza virus genome: identification of the hemagglutinin and the neuraminidase genes. Proc Natl Acad Sci U S A **73:**2142-2146.

163. **Elleman CJ, Barclay WS.** 2004. The M1 matrix protein controls the filamentous phenotype of influenza A virus. Virology **321:**144-153.

164. **Harris A, Cardone G, Winkler DC, Heymann JB, Brecher M, White JM, Steven AC.** 2006. Influenza virus pleiomorphy characterized by cryoelectron tomography. Proc Natl Acad Sci U S A **103:**19123-19127.

165. **Calder LJ, Wasilewski S, Berriman JA, Rosenthal PB.** 2010. Structural organization of a filamentous influenza A virus. Proc Natl Acad Sci U S A **107:**10685-10690.
166. **Rossman JS, Lamb RA.** 2011. Influenza virus assembly and budding. Virology **411:**229-236.
167. **Roberts PC, Lamb RA, Compans RW.** 1998. The M1 and M2 proteins of influenza A virus are important determinants in filamentous particle formation. Virology **240:**127-137.
168. **Rogers GN, Paulson JC, Daniels RS, Skehel JJ, Wilson IA, Wiley DC.** 1983. Single amino acid substitutions in influenza haemagglutinin change receptor binding specificity. Nature **304:**76-78.
169. **Russell RJ, Stevens DJ, Haire LF, Gamblin SJ, Skehel JJ.** 2006. Avian and human receptor binding by hemagglutinins of influenza A viruses. Glycoconj J **23:**85-92.
170. **Rust MJ, Lakadamyali M, Zhang F, Zhuang X.** 2004. Assembly of endocytic machinery around individual influenza viruses during viral entry. Nat Struct Mol Biol **11:**567-573.
171. **Sieczkarski SB, Whittaker GR.** 2002. Influenza virus can enter and infect cells in the absence of clathrin-mediated endocytosis. J Virol **76:**10455-10464.
172. **Bullough PA, Hughson FM, Skehel JJ, Wiley DC.** 1994. Structure of influenza haemagglutinin at the pH of membrane fusion. Nature **371:**37-43.
173. **Marsh M, Helenius A.** 1989. Virus entry into animal cells. Adv Virus Res **36:**107-151.
174. **Cross KJ, Langley WA, Russell RJ, Skehel JJ, Steinhauer DA.** 2009. Composition and functions of the influenza fusion peptide. Protein Pept Lett **16:**766-778.
175. **Skehel JJ, Cross K, Steinhauer D, Wiley DC.** 2001. Influenza fusion peptides. Biochem Soc Trans **29:**623-626.
176. **Kielian M.** 2006. Class II virus membrane fusion proteins. Virology **344:**38-47.
177. **Steinhauer DA.** 1999. Role of hemagglutinin cleavage for the pathogenicity of influenza virus. Virology **258:**1-20.
178. **Stieneke-Grober A, Vey M, Angliker H, Shaw E, Thomas G, Roberts C, Klenk HD, Garten W.** 1992. Influenza virus hemagglutinin with multibasic cleavage site is activated by furin, a subtilisin-like endoprotease. EMBO J **11:**2407-2414.
179. **Chen J, Lee KH, Steinhauer DA, Stevens DJ, Skehel JJ, Wiley DC.** 1998. Structure of the hemagglutinin precursor cleavage site, a determinant of influenza pathogenicity and the origin of the labile conformation. Cell **95:**409-417.
180. **Munster VJ, Schrauwen EJ, de Wit E, van den Brand JM, Bestebroer TM, Herfst S, Rimmelzwaan GF, Osterhaus AD, Fouchier RA.** 2010. Insertion of a multibasic cleavage motif into the hemagglutinin of a low-pathogenic avian influenza H6N1 virus induces a highly pathogenic phenotype. J Virol **84:**7953-7960.

181. **Klenk HD, Garten W.** 1994. Host cell proteases controlling virus pathogenicity. Trends Microbiol **2:**39-43.
182. **Wharton SA, Belshe RB, Skehel JJ, Hay AJ.** 1994. Role of virion M2 protein in influenza virus uncoating: specific reduction in the rate of membrane fusion between virus and liposomes by amantadine. J Gen Virol **75 (Pt 4):**945-948.
183. **Wang C, Takeuchi K, Pinto LH, Lamb RA.** 1993. Ion channel activity of influenza A virus M2 protein: characterization of the amantadine block. J Virol **67:**5585-5594.
184. **Martin K, Helenius A.** 1991. Nuclear transport of influenza virus ribonucleoproteins: the viral matrix protein (M1) promotes export and inhibits import. Cell **67:**117-130.
185. **Helenius A.** 1992. Unpacking the incoming influenza virus. Cell **69:**577-578.
186. **Mukaigawa J, Nayak DP.** 1991. Two signals mediate nuclear localization of influenza virus (A/WSN/33) polymerase basic protein 2. J Virol **65:**245-253.
187. **Davey J, Dimmock NJ, Colman A.** 1985. Identification of the sequence responsible for the nuclear accumulation of the influenza virus nucleoprotein in Xenopus oocytes. Cell **40:**667-675.
188. **Neumann G, Castrucci MR, Kawaoka Y.** 1997. Nuclear import and export of influenza virus nucleoprotein. J Virol **71:**9690-9700.
189. **O'Neill RE, Jaskunas R, Blobel G, Palese P, Moroianu J.** 1995. Nuclear import of influenza virus RNA can be mediated by viral nucleoprotein and transport factors required for protein import. J Biol Chem **270:**22701-22704.
190. **Deng T, Vreede FT, Brownlee GG.** 2006. Different de novo initiation strategies are used by influenza virus RNA polymerase on its cRNA and viral RNA promoters during viral RNA replication. J Virol **80:**2337-2348.
191. **Crow M, Deng T, Addley M, Brownlee GG.** 2004. Mutational analysis of the influenza virus cRNA promoter and identification of nucleotides critical for replication. J Virol **78:**6263-6270.
192. **Plotch SJ, Bouloy M, Krug RM.** 1979. Transfer of 5'-terminal cap of globin mRNA to influenza viral complementary RNA during transcription in vitro. Proc Natl Acad Sci U S A **76:**1618-1622.
193. **Bouloy M, Plotch SJ, Krug RM.** 1980. Both the 7-methyl and the 2'-O-methyl groups in the cap of mRNA strongly influence its ability to act as primer for influenza virus RNA transcription. Proc Natl Acad Sci U S A **77:**3952-3956.
194. **Daffis S, Szretter KJ, Schriewer J, Li J, Youn S, Errett J, Lin TY, Schneller S, Zust R, Dong H, Thiel V, Sen GC, Fensterl V, Klimstra WB, Pierson TC, Buller RM, Gale M, Jr., Shi PY, Diamond MS.** 2010. 2'-O methylation of the viral mRNA cap evades host restriction by IFIT family members. Nature **468:**452-456.
195. **Zust R, Cervantes-Barragan L, Habjan M, Maier R, Neuman BW, Ziebuhr J, Szretter KJ, Baker SC, Barchet W, Diamond MS, Siddell SG, Ludewig B, Thiel V.** 2011. Ribose 2'-O-methylation provides a molecular signature for the distinction of self and non-self mRNA dependent on the RNA sensor Mda5. Nat Immunol **12:**137-143.

196. **Varga ZT, Grant A, Manicassamy B, Palese P.** 2012. Influenza virus protein PB1-F2 inhibits the induction of type I interferon by binding to MAVS and decreasing mitochondrial membrane potential. J Virol **86:**8359-8366.

197. **Varga ZT, Ramos I, Hai R, Schmolke M, Garcia-Sastre A, Fernandez-Sesma A, Palese P.** 2011. The influenza virus protein PB1-F2 inhibits the induction of type I interferon at the level of the MAVS adaptor protein. PLoS Pathog **7:**e1002067.

198. **Kochs G, Garcia-Sastre A, Martinez-Sobrido L.** 2007. Multiple anti-interferon actions of the influenza A virus NS1 protein. J Virol **81:**7011-7021.

199. **Ayllon J, Garcia-Sastre A.** 2015. The NS1 protein: a multitasking virulence factor. Curr Top Microbiol Immunol **386:**73-107.

200. **Marc D.** 2014. Influenza virus non-structural protein NS1: interferon antagonism and beyond. J Gen Virol **95:**2594-2611.

201. **Hale BG, Randall RE, Ortin J, Jackson D.** 2008. The multifunctional NS1 protein of influenza A viruses. J Gen Virol **89:**2359-2376.

202. **Chen W, Calvo PA, Malide D, Gibbs J, Schubert U, Bacik I, Basta S, O'Neill R, Schickli J, Palese P, Henklein P, Bennink JR, Yewdell JW.** 2001. A novel influenza A virus mitochondrial protein that induces cell death. Nat Med **7:**1306-1312.

203. **Le Goffic R, Bouguyon E, Chevalier C, Vidic J, Da Costa B, Leymarie O, Bourdieu C, Decamps L, Dhorne-Pollet S, Delmas B.** 2010. Influenza A virus protein PB1-F2 exacerbates IFN-beta expression of human respiratory epithelial cells. J Immunol **185:**4812-4823.

204. **Jagger BW, Wise HM, Kash JC, Walters KA, Wills NM, Xiao YL, Dunfee RL, Schwartzman LM, Ozinsky A, Bell GL, Dalton RM, Lo A, Efstathiou S, Atkins JF, Firth AE, Taubenberger JK, Digard P.** 2012. An overlapping protein-coding region in influenza A virus segment 3 modulates the host response. Science **337:**199-204.

205. **Tauber S, Ligertwood Y, Quigg-Nicol M, Dutia BM, Elliott RM.** 2012. Behaviour of influenza A viruses differentially expressing segment 2 gene products in vitro and in vivo. J Gen Virol **93:**840-849.

206. **Wise HM, Foeglein A, Sun J, Dalton RM, Patel S, Howard W, Anderson EC, Barclay WS, Digard P.** 2009. A complicated message: Identification of a novel PB1-related protein translated from influenza A virus segment 2 mRNA. J Virol **83:**8021-8031.

207. **Wise HM, Barbezange C, Jagger BW, Dalton RM, Gog JR, Curran MD, Taubenberger JK, Anderson EC, Digard P.** 2011. Overlapping signals for translational regulation and packaging of influenza A virus segment 2. Nucleic Acids Res **39:**7775-7790.

208. **O'Neill RE, Talon J, Palese P.** 1998. The influenza virus NEP (NS2 protein) mediates the nuclear export of viral ribonucleoproteins. EMBO J **17:**288-296.

209. **Chen BJ, Leser GP, Jackson D, Lamb RA.** 2008. The influenza virus M2 protein cytoplasmic tail interacts with the M1 protein and influences virus assembly at the site of virus budding. J Virol **82:**10059-10070.

210. **Zhang J, Pekosz A, Lamb RA.** 2000. Influenza virus assembly and lipid raft microdomains: a role for the cytoplasmic tails of the spike glycoproteins. J Virol **74:**4634-4644.

211. **Ginting TE, Shinya K, Kyan Y, Makino A, Matsumoto N, Kaneda S, Kawaoka Y.** 2012. Amino acid changes in hemagglutinin contribute to the replication of oseltamivir-resistant H1N1 influenza viruses. J Virol **86:**121-127.

212. **Mitnaul LJ, Matrosovich MN, Castrucci MR, Tuzikov AB, Bovin NV, Kobasa D, Kawaoka Y.** 2000. Balanced hemagglutinin and neuraminidase activities are critical for efficient replication of influenza A virus. J Virol **74:**6015-6020.

213. **Wagner R, Matrosovich M, Klenk HD.** 2002. Functional balance between haemagglutinin and neuraminidase in influenza virus infections. Rev Med Virol **12:**159-166.

214. **Chambers BS, Li Y, Hodinka RL, Hensley SE.** 2014. Recent H3N2 influenza virus clinical isolates rapidly acquire hemagglutinin or neuraminidase mutations when propagated for antigenic analyses. J Virol **88:**10986-10989.

215. **Xu R, Zhu X, McBride R, Nycholat CM, Yu W, Paulson JC, Wilson IA.** 2012. Functional balance of the hemagglutinin and neuraminidase activities accompanies the emergence of the 2009 H1N1 influenza pandemic. J Virol **86:**9221-9232.

216. **Imai M, Kawaoka Y.** 2012. The role of receptor binding specificity in interspecies transmission of influenza viruses. Curr Opin Virol **2:**160-167.

217. **Hensley SE, Das SR, Bailey AL, Schmidt LM, Hickman HD, Jayaraman A, Viswanathan K, Raman R, Sasisekharan R, Bennink JR, Yewdell JW.** 2009. Hemagglutinin receptor binding avidity drives influenza A virus antigenic drift. Science **326:**734-736.

218. **Yewdell JW.** 2011. Viva la revolucion: rethinking influenza a virus antigenic drift. Curr Opin Virol **1:**177-183.

219. **Skehel JJ, Waterfield MD.** 1975. Studies on the primary structure of the influenza virus hemagglutinin. Proc Natl Acad Sci U S A **72:**93-97.

220. **Wiley DC, Skehel JJ.** 1987. The structure and function of the hemagglutinin membrane glycoprotein of influenza virus. Annu Rev Biochem **56:**365-394.

221. **Air GM, Laver WG, Webster RG.** 1987. Antigenic variation in influenza viruses. Contrib Microbiol Immunol **8:**20-59.

222. **Medina RA, Garcia-Sastre A.** 2011. Influenza A viruses: new research developments. Nat Rev Microbiol **9:**590-603.

223. **Nobusawa E, Aoyama T, Kato H, Suzuki Y, Tateno Y, Nakajima K.** 1991. Comparison of complete amino acid sequences and receptor-binding properties among 13 serotypes of hemagglutinins of influenza A viruses. Virology **182:**475-485.

224. **Tong S, Li Y, Rivailler P, Conrardy C, Castillo DA, Chen LM, Recuenco S, Ellison JA, Davis CT, York IA, Turmelle AS, Moran D, Rogers S, Shi M, Tao Y, Weil MR, Tang K, Rowe LA, Sammons S, Xu X, Frace M, Lindblade KA,**

Cox NJ, Anderson LJ, Rupprecht CE, Donis RO. 2012. A distinct lineage of influenza A virus from bats. Proc Natl Acad Sci U S A **109:**4269-4274.

225. **Tong S, Zhu X, Li Y, Shi M, Zhang J, Bourgeois M, Yang H, Chen X, Recuenco S, Gomez J, Chen LM, Johnson A, Tao Y, Dreyfus C, Yu W, McBride R, Carney PJ, Gilbert AT, Chang J, Guo Z, Davis CT, Paulson JC, Stevens J, Rupprecht CE, Holmes EC, Wilson IA, Donis RO.** 2013. New world bats harbor diverse influenza A viruses. PLoS Pathog **9:**e1003657.

226. **Zhou B, Ma J, Liu Q, Bawa B, Wang W, Shabman RS, Duff M, Lee J, Lang Y, Cao N, Nagy A, Lin X, Stockwell TB, Richt JA, Wentworth DE, Ma W.** 2014. Characterization of uncultivable bat influenza virus using a replicative synthetic virus. PLoS Pathog **10:**e1004420.

227. **Wu Y, Wu Y, Tefsen B, Shi Y, Gao GF.** 2014. Bat-derived influenza-like viruses H17N10 and H18N11. Trends Microbiol **22:**183-191.

228. **Nicholls JM, Bourne AJ, Chen H, Guan Y, Peiris JS.** 2007. Sialic acid receptor detection in the human respiratory tract: evidence for widespread distribution of potential binding sites for human and avian influenza viruses. Respir Res **8:**73.

229. **Shinya K, Ebina M, Yamada S, Ono M, Kasai N, Kawaoka Y.** 2006. Avian flu: influenza virus receptors in the human airway. Nature **440:**435-436.

230. **Ibricevic A, Pekosz A, Walter MJ, Newby C, Battaile JT, Brown EG, Holtzman MJ, Brody SL.** 2006. Influenza virus receptor specificity and cell tropism in mouse and human airway epithelial cells. J Virol **80:**7469-7480.

231. **Matrosovich M, Tuzikov A, Bovin N, Gambaryan A, Klimov A, Castrucci MR, Donatelli I, Kawaoka Y.** 2000. Early alterations of the receptor-binding properties of H1, H2, and H3 avian influenza virus hemagglutinins after their introduction into mammals. J Virol **74:**8502-8512.

232. **Collins PJ, Vachieri SG, Haire LF, Ogrodowicz RW, Martin SR, Walker PA, Xiong X, Gamblin SJ, Skehel JJ.** 2014. Recent evolution of equine influenza and the origin of canine influenza. Proc Natl Acad Sci U S A **111:**11175-11180.

233. **Webby RJ, Swenson SL, Krauss SL, Gerrish PJ, Goyal SM, Webster RG.** 2000. Evolution of swine H3N2 influenza viruses in the United States. J Virol **74:**8243-8251.

234. **Nelson MI, Vincent AL, Kitikoon P, Holmes EC, Gramer MR.** 2012. Evolution of novel reassortant A/H3N2 influenza viruses in North American swine and humans, 2009-2011. J Virol **86:**8872-8878.

235. **Kawaoka Y, Chambers TM, Sladen WL, Webster RG.** 1988. Is the gene pool of influenza viruses in shorebirds and gulls different from that in wild ducks? Virology **163:**247-250.

236. **Alexander DJ.** 2000. A review of avian influenza in different bird species. Vet Microbiol **74:**3-13.

237. **Lupiani B, Reddy SM.** 2009. The history of avian influenza. Comp Immunol Microbiol Infect Dis **32:**311-323.

238. **Wright PF, Neumann G, Kawaoka Y.** 2007. Orthomyxoviruses, p. 1691-1740. *In* Knipe DM, Howley PM (ed.), Fields Virology 5th edition, vol. 2. Lippincott Williams & Wilkins, Philadelphia.

239. **Richard M, Schrauwen EJ, de Graaf M, Bestebroer TM, Spronken MI, van Boheemen S, de Meulder D, Lexmond P, Linster M, Herfst S, Smith DJ, van den Brand JM, Burke DF, Kuiken T, Rimmelzwaan GF, Osterhaus AD, Fouchier RA.** 2013. Limited airborne transmission of H7N9 influenza A virus between ferrets. Nature **501:**560-563.

240. **Xiong X, Martin SR, Haire LF, Wharton SA, Daniels RS, Bennett MS, McCauley JW, Collins PJ, Walker PA, Skehel JJ, Gamblin SJ.** 2013. Receptor binding by an H7N9 influenza virus from humans. Nature **499:**496-499.

241. **Ito T, Couceiro JN, Kelm S, Baum LG, Krauss S, Castrucci MR, Donatelli I, Kida H, Paulson JC, Webster RG, Kawaoka Y.** 1998. Molecular basis for the generation in pigs of influenza A viruses with pandemic potential. J Virol **72:**7367-7373.

242. **Kida H, Ito T, Yasuda J, Shimizu Y, Itakura C, Shortridge KF, Kawaoka Y, Webster RG.** 1994. Potential for transmission of avian influenza viruses to pigs. J Gen Virol **75 (Pt 9):**2183-2188.

243. **Shu LL, Lin YP, Wright SM, Shortridge KF, Webster RG.** 1994. Evidence for interspecies transmission and reassortment of influenza A viruses in pigs in southern China. Virology **202:**825-833.

244. **Zhou NN, Senne DA, Landgraf JS, Swenson SL, Erickson G, Rossow K, Liu L, Yoon KJ, Krauss S, Webster RG.** 2000. Emergence of H3N2 reassortant influenza A viruses in North American pigs. Vet Microbiol **74:**47-58.

245. **Worobey M, Han GZ, Rambaut A.** 2014. Genesis and pathogenesis of the 1918 pandemic H1N1 influenza A virus. Proc Natl Acad Sci U S A **111:**8107-8112.

246. **Lowen AC, Steel J.** 2014. Roles of humidity and temperature in shaping influenza seasonality. J Virol **88:**7692-7695.

247. **Belser JA, Wadford DA, Pappas C, Gustin KM, Maines TR, Pearce MB, Zeng H, Swayne DE, Pantin-Jackwood M, Katz JM, Tumpey TM.** 2010. Pathogenesis of pandemic influenza A (H1N1) and triple-reassortant swine influenza A (H1) viruses in mice. J Virol **84:**4194-4203.

248. **Matsuoka Y, Lamirande EW, Subbarao K.** 2009. The mouse model for influenza. Curr Protoc Microbiol **Chapter 15:**Unit 15G 13.

249. **Bouvier NM, Lowen AC.** 2010. Animal Models for Influenza Virus Pathogenesis and Transmission. Viruses **2:**1530-1563.

250. **Pica N, Iyer A, Ramos I, Bouvier NM, Fernandez-Sesma A, Garcia-Sastre A, Lowen AC, Palese P, Steel J.** 2011. The DBA.2 mouse is susceptible to disease following infection with a broad, but limited, range of influenza A and B viruses. J Virol **85:**12825-12829.

251. **Kash JC, Basler CF, Garcia-Sastre A, Carter V, Billharz R, Swayne DE, Przygodzki RM, Taubenberger JK, Katze MG, Tumpey TM.** 2004. Global host immune response: pathogenesis and transcriptional profiling of type A influenza viruses expressing the hemagglutinin and neuraminidase genes from the 1918 pandemic virus. J Virol **78:**9499-9511.

252. **Kash JC, Tumpey TM, Proll SC, Carter V, Perwitasari O, Thomas MJ, Basler CF, Palese P, Taubenberger JK, Garcia-Sastre A, Swayne DE, Katze**

MG. 2006. Genomic analysis of increased host immune and cell death responses induced by 1918 influenza virus. Nature **443:**578-581.

253. **Perrone LA, Plowden JK, Garcia-Sastre A, Katz JM, Tumpey TM.** 2008. H5N1 and 1918 pandemic influenza virus infection results in early and excessive infiltration of macrophages and neutrophils in the lungs of mice. PLoS Pathog **4:**e1000115.

254. **Qi L, Kash JC, Dugan VG, Wang R, Jin G, Cunningham RE, Taubenberger JK.** 2009. Role of sialic acid binding specificity of the 1918 influenza virus hemagglutinin protein in virulence and pathogenesis for mice. J Virol **83:**3754-3761.

255. **Ilyushina NA, Khalenkov AM, Seiler JP, Forrest HL, Bovin NV, Marjuki H, Barman S, Webster RG, Webby RJ.** 2010. Adaptation of pandemic H1N1 influenza viruses in mice. J Virol **84:**8607-8616.

256. **O'Donnell CD, Subbarao K.** 2011. The contribution of animal models to the understanding of the host range and virulence of influenza A viruses. Microbes Infect **13:**502-515.

257. **Xu L, Bao L, Deng W, Zhu H, Chen T, Lv Q, Li F, Yuan J, Xiang Z, Gao K, Xu Y, Huang L, Li Y, Liu J, Yao Y, Yu P, Yong W, Wei Q, Zhang L, Qin C.** 2013. The mouse and ferret models for studying the novel avian-origin human influenza A (H7N9) virus. Virol J **10:**253.

258. **Boon AC, deBeauchamp J, Hollmann A, Luke J, Kotb M, Rowe S, Finkelstein D, Neale G, Lu L, Williams RW, Webby RJ.** 2009. Host genetic variation affects resistance to infection with a highly pathogenic H5N1 influenza A virus in mice. J Virol **83:**10417-10426.

259. **Staeheli P, Grob R, Meier E, Sutcliffe JG, Haller O.** 1988. Influenza virus-susceptible mice carry Mx genes with a large deletion or a nonsense mutation. Mol Cell Biol **8:**4518-4523.

260. **Staeheli P, Danielson P, Haller O, Sutcliffe JG.** 1986. Transcriptional activation of the mouse Mx gene by type I interferon. Mol Cell Biol **6:**4770-4774.

261. **Staeheli P, Pravtcheva D, Lundin LG, Acklin M, Ruddle F, Lindenmann J, Haller O.** 1986. Interferon-regulated influenza virus resistance gene Mx is localized on mouse chromosome 16. J Virol **58:**967-969.

262. **Haller O, Arnheiter H, Gresser I, Lindenmann J.** 1979. Genetically determined, interferon-dependent resistance to influenza virus in mice. J Exp Med **149:**601-612.

263. **Lednicky JA, Croutch CR, Lawrence SJ, Hamilton SB, Daniels DE, Astroff B.** 2010. A nonlethal young domesticated ferret (Mustela putorius furo) model for studying pandemic influenza virus A/California/04/2009 (H1N1). Comp Med **60:**364-368.

264. **Matsuoka Y, Lamirande EW, Subbarao K.** 2009. The ferret model for influenza. Curr Protoc Microbiol **Chapter 15:**Unit 15G 12.

265. **Reuman PD, Keely S, Schiff GM.** 1989. Assessment of signs of influenza illness in the ferret model. J Virol Methods **24:**27-34.

266. **Stark GV, Long JP, Ortiz DI, Gainey M, Carper BA, Feng J, Miller SM, Bigger JE, Vela EM.** 2013. Clinical profiles associated with influenza disease in the ferret model. PLoS One **8:**e58337.

267. **Jia N, Barclay WS, Roberts K, Yen HL, Chan RW, Lam AK, Air G, Peiris JS, Dell A, Nicholls JM, Haslam SM.** 2014. Glycomic characterization of respiratory tract tissues of ferrets: implications for its use in influenza virus infection studies. J Biol Chem **289:**28489-28504.

268. **Ng PS, Bohm R, Hartley-Tassell LE, Steen JA, Wang H, Lukowski SW, Hawthorne PL, Trezise AE, Coloe PJ, Grimmond SM, Haselhorst T, von Itzstein M, Paton AW, Paton JC, Jennings MP.** 2014. Ferrets exclusively synthesize Neu5Ac and express naturally humanized influenza A virus receptors. Nat Commun **5:**5750.

269. **McBrayer A, Camp JV, Tapp R, Yamshchikov V, Grimes S, Noah DL, Jonsson CB, Bruder CE.** 2010. Course of seasonal influenza A/Brisbane/59/07 H1N1 infection in the ferret. Virol J **7:**149.

270. **van den Brand JM, Stittelaar KJ, Leijten LM, van Amerongen G, Simon JH, Osterhaus AD, Kuiken T.** 2012. Modification of the ferret model for pneumonia from seasonal human influenza A virus infection. Vet Pathol **49:**562-568.

271. **Belser JA, Gustin KM, Maines TR, Blau DM, Zaki SR, Katz JM, Tumpey TM.** 2011. Pathogenesis and transmission of triple-reassortant swine H1N1 influenza viruses isolated before the 2009 H1N1 pandemic. J Virol **85:**1563-1572.

272. **Moore IN, Lamirande EW, Paskel M, Donahue D, Qin J, Subbarao K.** 2014. Severity of clinical disease and pathology in ferrets experimentally infected with influenza viruses is influenced by inoculum volume. J Virol **88:**13879-13891.

273. **Maines TR, Lu XH, Erb SM, Edwards L, Guarner J, Greer PW, Nguyen DC, Szretter KJ, Chen LM, Thawatsupha P, Chittaganpitch M, Waicharoen S, Nguyen DT, Nguyen T, Nguyen HH, Kim JH, Hoang LT, Kang C, Phuong LS, Lim W, Zaki S, Donis RO, Cox NJ, Katz JM, Tumpey TM.** 2005. Avian influenza (H5N1) viruses isolated from humans in Asia in 2004 exhibit increased virulence in mammals. J Virol **79:**11788-11800.

274. **Belser JA, Lu X, Maines TR, Smith C, Li Y, Donis RO, Katz JM, Tumpey TM.** 2007. Pathogenesis of avian influenza (H7) virus infection in mice and ferrets: enhanced virulence of Eurasian H7N7 viruses isolated from humans. J Virol **81:**11139-11147.

275. **Salomon R, Franks J, Govorkova EA, Ilyushina NA, Yen HL, Hulse-Post DJ, Humberd J, Trichet M, Rehg JE, Webby RJ, Webster RG, Hoffmann E.** 2006. The polymerase complex genes contribute to the high virulence of the human H5N1 influenza virus isolate A/Vietnam/1203/04. J Exp Med **203:**689-697.

276. **Tumpey TM, Maines TR, Van Hoeven N, Glaser L, Solorzano A, Pappas C, Cox NJ, Swayne DE, Palese P, Katz JM, Garcia-Sastre A.** 2007. A two-amino acid change in the hemagglutinin of the 1918 influenza virus abolishes transmission. Science **315:**655-659.

277. **Camp JV, Svensson TL, McBrayer A, Jonsson CB, Liljestrom P, Bruder CE.** 2012. De-novo transcriptome sequencing of a normalized cDNA pool from influenza infected ferrets. PLoS One **7:**e37104.

278. **Peng X, Alfoldi J, Gori K, Eisfeld AJ, Tyler SR, Tisoncik-Go J, Brawand D, Law GL, Skunca N, Hatta M, Gasper DJ, Kelly SM, Chang J, Thomas MJ, Johnson J, Berlin AM, Lara M, Russell P, Swofford R, Turner-Maier J, Young S, Hourlier T, Aken B, Searle S, Sun X, Yi Y, Suresh M, Tumpey TM, Siepel A, Wisely SM, Dessimoz C, Kawaoka Y, Birren BW, Lindblad-Toh K, Di Palma F, Engelhardt JF, Palermo RE, Katze MG.** 2014. The draft genome sequence of the ferret (Mustela putorius furo) facilitates study of human respiratory disease. Nat Biotechnol **32:**1250-1255.

279. **Rutigliano JA, Doherty PC, Franks J, Morris MY, Reynolds C, Thomas PG.** 2008. Screening monoclonal antibodies for cross-reactivity in the ferret model of influenza infection. J Immunol Methods **336:**71-77.

280. **Martel CJ, Aasted B.** 2009. Characterization of antibodies against ferret immunoglobulins, cytokines and CD markers. Vet Immunol Immunopathol **132:**109-115.

281. **Matrosovich MN, Matrosovich TY, Gray T, Roberts NA, Klenk HD.** 2004. Human and avian influenza viruses target different cell types in cultures of human airway epithelium. Proc Natl Acad Sci U S A **101:**4620-4624.

282. **Walther T, Karamanska R, Chan RW, Chan MC, Jia N, Air G, Hopton C, Wong MP, Dell A, Malik Peiris JS, Haslam SM, Nicholls JM.** 2013. Glycomic analysis of human respiratory tract tissues and correlation with influenza virus infection. PLoS Pathog **9:**e1003223.

283. **Gamblin SJ, Haire LF, Russell RJ, Stevens DJ, Xiao B, Ha Y, Vasisht N, Steinhauer DA, Daniels RS, Elliot A, Wiley DC, Skehel JJ.** 2004. The structure and receptor binding properties of the 1918 influenza hemagglutinin. Science **303:**1838-1842.

284. **Childs RA, Palma AS, Wharton S, Matrosovich T, Liu Y, Chai W, Campanero-Rhodes MA, Zhang Y, Eickmann M, Kiso M, Hay A, Matrosovich M, Feizi T.** 2009. Receptor-binding specificity of pandemic influenza A (H1N1) 2009 virus determined by carbohydrate microarray. Nat Biotechnol **27:**797-799.

285. **Gustin KM, Belser JA, Wadford DA, Pearce MB, Katz JM, Tumpey TM, Maines TR.** 2011. Influenza virus aerosol exposure and analytical system for ferrets. Proc Natl Acad Sci U S A **108:**8432-8437.

286. **Galloway SE, Reed ML, Russell CJ, Steinhauer DA.** 2013. Influenza HA subtypes demonstrate divergent phenotypes for cleavage activation and pH of fusion: implications for host range and adaptation. PLoS Pathog **9:**e1003151.

287. **Cotter CR, Jin H, Chen Z.** 2014. A single amino acid in the stalk region of the H1N1pdm influenza virus HA protein affects viral fusion, stability and infectivity. PLoS Pathog **10:**e1003831.

288. **Cross KJ, Wharton SA, Skehel JJ, Wiley DC, Steinhauer DA.** 2001. Studies on influenza haemagglutinin fusion peptide mutants generated by reverse genetics. EMBO J **20:**4432-4442.

289. **Daniels RS, Douglas AR, Skehel JJ, Wiley DC.** 1983. Analyses of the antigenicity of influenza haemagglutinin at the pH optimum for virus-mediated membrane fusion. J Gen Virol **64 (Pt 8):**1657-1662.

290. **Ruigrok RW, Aitken A, Calder LJ, Martin SR, Skehel JJ, Wharton SA, Weis W, Wiley DC.** 1988. Studies on the structure of the influenza virus haemagglutinin at the pH of membrane fusion. J Gen Virol **69 (Pt 11):**2785-2795.

291. **Marjuki H, Yen HL, Franks J, Webster RG, Pleschka S, Hoffmann E.** 2007. Higher polymerase activity of a human influenza virus enhances activation of the hemagglutinin-induced Raf/MEK/ERK signal cascade. Virol J **4:**134.

292. **Neumann G, Kawaoka Y.** 2002. Synthesis of influenza virus: new impetus from an old enzyme, RNA polymerase I. Virus Res **82:**153-158.

293. **Skehel JJ.** 1971. RNA-dependent RNA polymerase activity of the influenza virus. Virology **45:**793-796.

294. **Watanabe T, Tisoncik-Go J, Tchitchek N, Watanabe S, Benecke AG, Katze MG, Kawaoka Y.** 2013. 1918 Influenza virus hemagglutinin (HA) and the viral RNA polymerase complex enhance viral pathogenicity, but only HA induces aberrant host responses in mice. J Virol **87:**5239-5254.

295. **Mehle A, Doudna JA.** 2009. Adaptive strategies of the influenza virus polymerase for replication in humans. Proc Natl Acad Sci U S A **106:**21312-21316.

296. **Subbarao EK, London W, Murphy BR.** 1993. A single amino acid in the PB2 gene of influenza A virus is a determinant of host range. J Virol **67:**1761-1764.

297. **Shinya K, Hamm S, Hatta M, Ito H, Ito T, Kawaoka Y.** 2004. PB2 amino acid at position 627 affects replicative efficiency, but not cell tropism, of Hong Kong H5N1 influenza A viruses in mice. Virology **320:**258-266.

298. **Garcia-Sastre A.** 2011. Induction and evasion of type I interferon responses by influenza viruses. Virus Res **162:**12-18.

299. **Garcia-Sastre A, Egorov A, Matassov D, Brandt S, Levy DE, Durbin JE, Palese P, Muster T.** 1998. Influenza A virus lacking the NS1 gene replicates in interferon-deficient systems. Virology **252:**324-330.

300. **Mibayashi M, Martinez-Sobrido L, Loo YM, Cardenas WB, Gale M, Jr., Garcia-Sastre A.** 2007. Inhibition of retinoic acid-inducible gene I-mediated induction of beta interferon by the NS1 protein of influenza A virus. J Virol **81:**514-524.

301. **Wang X, Li M, Zheng H, Muster T, Palese P, Beg AA, Garcia-Sastre A.** 2000. Influenza A virus NS1 protein prevents activation of NF-kappaB and induction of alpha/beta interferon. J Virol **74:**11566-11573.

302. **Das K, Ma LC, Xiao R, Radvansky B, Aramini J, Zhao L, Marklund J, Kuo RL, Twu KY, Arnold E, Krug RM, Montelione GT.** 2008. Structural basis for

suppression of a host antiviral response by influenza A virus. Proc Natl Acad Sci U S A **105:**13093-13098.

303. **Pinto R, Herold S, Cakarova L, Hoegner K, Lohmeyer J, Planz O, Pleschka S.** 2011. Inhibition of influenza virus-induced NF-kappaB and Raf/MEK/ERK activation can reduce both virus titers and cytokine expression simultaneously in vitro and in vivo. Antiviral Res **92:**45-56.

304. **Pleschka S, Wolff T, Ehrhardt C, Hobom G, Planz O, Rapp UR, Ludwig S.** 2001. Influenza virus propagation is impaired by inhibition of the Raf/MEK/ERK signalling cascade. Nat Cell Biol **3:**301-305.

305. **Pang IK, Pillai PS, Iwasaki A.** 2013. Efficient influenza A virus replication in the respiratory tract requires signals from TLR7 and RIG-I. Proc Natl Acad Sci U S A **110:**13910-13915.

306. **Fernandez-Sesma A, Marukian S, Ebersole BJ, Kaminski D, Park MS, Yuen T, Sealfon SC, Garcia-Sastre A, Moran TM.** 2006. Influenza virus evades innate and adaptive immunity via the NS1 protein. J Virol **80:**6295-6304.

307. **Stasakova J, Ferko B, Kittel C, Sereinig S, Romanova J, Katinger H, Egorov A.** 2005. Influenza A mutant viruses with altered NS1 protein function provoke caspase-1 activation in primary human macrophages, resulting in fast apoptosis and release of high levels of interleukins 1beta and 18. J Gen Virol **86:**185-195.

308. **Hartshorn KL.** 2010. Role of surfactant protein A and D (SP-A and SP-D) in human antiviral host defense. Front Biosci (Schol Ed) **2:**527-546.

309. **Gordon S, Taylor PR.** 2005. Monocyte and macrophage heterogeneity. Nat Rev Immunol **5:**953-964.

310. **Hussell T, Bell TJ.** 2014. Alveolar macrophages: plasticity in a tissue-specific context. Nat Rev Immunol **14:**81-93.

311. **Thepen T, McMenamin C, Oliver J, Kraal G, Holt PG.** 1991. Regulation of immune response to inhaled antigen by alveolar macrophages: differential effects of in vivo alveolar macrophage elimination on the induction of tolerance vs. immunity. Eur J Immunol **21:**2845-2850.

312. **Spiteri MA, Knight RA, Jeremy JY, Barnes PJ, Chung KF.** 1994. Alveolar macrophage-induced suppression of peripheral blood mononuclear cell responsiveness is reversed by in vitro allergen exposure in bronchial asthma. Eur Respir J **7:**1431-1438.

313. **Ghoneim HE, Thomas PG, McCullers JA.** 2013. Depletion of alveolar macrophages during influenza infection facilitates bacterial superinfections. J Immunol **191:**1250-1259.

314. **Tarling JD, Lin HS, Hsu S.** 1987. Self-renewal of pulmonary alveolar macrophages: evidence from radiation chimera studies. J Leukoc Biol **42:**443-446.

315. **Hashimoto D, Chow A, Noizat C, Teo P, Beasley MB, Leboeuf M, Becker CD, See P, Price J, Lucas D, Greter M, Mortha A, Boyer SW, Forsberg EC, Tanaka M, van Rooijen N, Garcia-Sastre A, Stanley ER, Ginhoux F, Frenette PS, Merad M.** 2013. Tissue-resident macrophages self-maintain locally

throughout adult life with minimal contribution from circulating monocytes. Immunity **38:**792-804.

316. **Snelgrove RJ, Goulding J, Didierlaurent AM, Lyonga D, Vekaria S, Edwards L, Gwyer E, Sedgwick JD, Barclay AN, Hussell T.** 2008. A critical function for CD200 in lung immune homeostasis and the severity of influenza infection. Nat Immunol **9:**1074-1083.

317. **Rygiel TP, Rijkers ES, de Ruiter T, Stolte EH, van der Valk M, Rimmelzwaan GF, Boon L, van Loon AM, Coenjaerts FE, Hoek RM, Tesselaar K, Meyaard L.** 2009. Lack of CD200 enhances pathological T cell responses during influenza infection. J Immunol **183:**1990-1996.

318. **Wright GJ, Cherwinski H, Foster-Cuevas M, Brooke G, Puklavec MJ, Bigler M, Song Y, Jenmalm M, Gorman D, McClanahan T, Liu MR, Brown MH, Sedgwick JD, Phillips JH, Barclay AN.** 2003. Characterization of the CD200 receptor family in mice and humans and their interactions with CD200. J Immunol **171:**3034-3046.

319. **Fujisawa H, Tsuru S, Taniguchi M, Zinnaka Y, Nomoto K.** 1987. Protective mechanisms against pulmonary infection with influenza virus. I. Relative contribution of polymorphonuclear leukocytes and of alveolar macrophages to protection during the early phase of intranasal infection. J Gen Virol **68 (Pt 2):**425-432.

320. **Kim HM, Kang YM, Ku KB, Park EH, Yum J, Kim JC, Jin SY, Lee JS, Kim HS, Seo SH.** 2013. The severe pathogenicity of alveolar macrophage-depleted ferrets infected with 2009 pandemic H1N1 influenza virus. Virology **444:**394-403.

321. **Kim HM, Lee YW, Lee KJ, Kim HS, Cho SW, van Rooijen N, Guan Y, Seo SH.** 2008. Alveolar macrophages are indispensable for controlling influenza viruses in lungs of pigs. J Virol **82:**4265-4274.

322. **Schneider C, Nobs SP, Heer AK, Kurrer M, Klinke G, van Rooijen N, Vogel J, Kopf M.** 2014. Alveolar macrophages are essential for protection from respiratory failure and associated morbidity following influenza virus infection. PLoS Pathog **10:**e1004053.

323. **Tumpey TM, Garcia-Sastre A, Taubenberger JK, Palese P, Swayne DE, Pantin-Jackwood MJ, Schultz-Cherry S, Solorzano A, Van Rooijen N, Katz JM, Basler CF.** 2005. Pathogenicity of influenza viruses with genes from the 1918 pandemic virus: functional roles of alveolar macrophages and neutrophils in limiting virus replication and mortality in mice. J Virol **79:**14933-14944.

324. **Schindler C, Levy DE, Decker T.** 2007. JAK-STAT signaling: from interferons to cytokines. J Biol Chem **282:**20059-20063.

325. **Borden EC, Williams BR.** 2011. Interferon-stimulated genes and their protein products: what and how? J Interferon Cytokine Res **31:**1-4.

326. **Kato H, Sato S, Yoneyama M, Yamamoto M, Uematsu S, Matsui K, Tsujimura T, Takeda K, Fujita T, Takeuchi O, Akira S.** 2005. Cell type-specific involvement of RIG-I in antiviral response. Immunity **23:**19-28.

327. **Loo YM, Fornek J, Crochet N, Bajwa G, Perwitasari O, Martinez-Sobrido L, Akira S, Gill MA, Garcia-Sastre A, Katze MG, Gale M, Jr.** 2008. Distinct RIG-I and MDA5 signaling by RNA viruses in innate immunity. J Virol **82:**335-345.

328. **Dixit E, Kagan JC.** 2013. Intracellular pathogen detection by RIG-I-like receptors. Adv Immunol **117:**99-125.

329. **Koyama S, Ishii KJ, Kumar H, Tanimoto T, Coban C, Uematsu S, Kawai T, Akira S.** 2007. Differential role of TLR- and RLR-signaling in the immune responses to influenza A virus infection and vaccination. J Immunol **179:**4711-4720.

330. **Chan MC, Cheung CY, Chui WH, Tsao SW, Nicholls JM, Chan YO, Chan RW, Long HT, Poon LL, Guan Y, Peiris JS.** 2005. Proinflammatory cytokine responses induced by influenza A (H5N1) viruses in primary human alveolar and bronchial epithelial cells. Respir Res **6:**135.

331. **Gerlach RL, Camp JV, Chu YK, Jonsson CB.** 2013. Early host responses of seasonal and pandemic influenza A viruses in primary well-differentiated human lung epithelial cells. PLoS One **8:**e78912.

332. **Chan RW, Yuen KM, Yu WC, Ho CC, Nicholls JM, Peiris JS, Chan MC.** 2010. Influenza H5N1 and H1N1 virus replication and innate immune responses in bronchial epithelial cells are influenced by the state of differentiation. PLoS One **5:**e8713.

333. **Paquette SG, Banner D, Chi le TB, Leomicronn AJ, Xu L, Ran L, Huang SS, Farooqui A, Kelvin DJ, Kelvin AA.** 2014. Pandemic H1N1 influenza A directly induces a robust and acute inflammatory gene signature in primary human bronchial epithelial cells downstream of membrane fusion. Virology **448:**91-103.

334. **Zeng H, Pappas C, Katz JM, Tumpey TM.** 2011. The 2009 pandemic H1N1 and triple-reassortant swine H1N1 influenza viruses replicate efficiently but elicit an attenuated inflammatory response in polarized human bronchial epithelial cells. J Virol **85:**686-696.

335. **Patel JR, Vora KP, Tripathi S, Zeng H, Tumpey TM, Katz JM, Sambhara S, Gangappa S.** 2011. Infection of lung epithelial cells with pandemic 2009 A(H1N1) influenza viruses reveals isolate-specific differences in infectivity and host cellular responses. Viral Immunol **24:**89-99.

336. **Chan MC, Chan RW, Yu WC, Ho CC, Yuen KM, Fong JH, Tang LL, Lai WW, Lo AC, Chui WH, Sihoe AD, Kwong DL, Wong DS, Tsao GS, Poon LL, Guan Y, Nicholls JM, Peiris JS.** 2010. Tropism and innate host responses of the 2009 pandemic H1N1 influenza virus in ex vivo and in vitro cultures of human conjunctiva and respiratory tract. Am J Pathol **176:**1828-1840.

337. **Herold S, von Wulffen W, Steinmueller M, Pleschka S, Kuziel WA, Mack M, Srivastava M, Seeger W, Maus UA, Lohmeyer J.** 2006. Alveolar epithelial cells direct monocyte transepithelial migration upon influenza virus infection: impact of chemokines and adhesion molecules. J Immunol **177:**1817-1824.

338. **Arndt U, Wennemuth G, Barth P, Nain M, Al-Abed Y, Meinhardt A, Gemsa D, Bacher M.** 2002. Release of macrophage migration inhibitory factor and

CXCL8/interleukin-8 from lung epithelial cells rendered necrotic by influenza A virus infection. J Virol **76:**9298-9306.

339. **Tate MD, Pickett DL, van Rooijen N, Brooks AG, Reading PC.** 2010. Critical role of airway macrophages in modulating disease severity during influenza virus infection of mice. J Virol **84:**7569-7580.

340. **Tate MD, Schilter HC, Brooks AG, Reading PC.** 2011. Responses of mouse airway epithelial cells and alveolar macrophages to virulent and avirulent strains of influenza A virus. Viral Immunol **24:**77-88.

341. **van Riel D, Leijten LM, van der Eerden M, Hoogsteden HC, Boven LA, Lambrecht BN, Osterhaus AD, Kuiken T.** 2011. Highly pathogenic avian influenza virus H5N1 infects alveolar macrophages without virus production or excessive TNF-alpha induction. PLoS Pathog **7:**e1002099.

342. **Wang J, Nikrad MP, Travanty EA, Zhou B, Phang T, Gao B, Alford T, Ito Y, Nahreini P, Hartshorn K, Wentworth D, Dinarello CA, Mason RJ.** 2012. Innate immune response of human alveolar macrophages during influenza A infection. PLoS One **7:**e29879.

343. **Herold S, Steinmueller M, von Wulffen W, Cakarova L, Pinto R, Pleschka S, Mack M, Kuziel WA, Corazza N, Brunner T, Seeger W, Lohmeyer J.** 2008. Lung epithelial apoptosis in influenza virus pneumonia: the role of macrophage-expressed TNF-related apoptosis-inducing ligand. J Exp Med **205:**3065-3077.

344. **Hogner K, Wolff T, Pleschka S, Plog S, Gruber AD, Kalinke U, Walmrath HD, Bodner J, Gattenlohner S, Lewe-Schlosser P, Matrosovich M, Seeger W, Lohmeyer J, Herold S.** 2013. Macrophage-expressed IFN-beta contributes to apoptotic alveolar epithelial cell injury in severe influenza virus pneumonia. PLoS Pathog **9:**e1003188.

345. **Thepen T, Van Rooijen N, Kraal G.** 1989. Alveolar macrophage elimination in vivo is associated with an increase in pulmonary immune response in mice. J Exp Med **170:**499-509.

346. **Fukuyama S, Kawaoka Y.** 2011. The pathogenesis of influenza virus infections: the contributions of virus and host factors. Curr Opin Immunol **23:**481-486.

347. **Zhou J, Law HK, Cheung CY, Ng IH, Peiris JS, Lau YL.** 2006. Functional tumor necrosis factor-related apoptosis-inducing ligand production by avian influenza virus-infected macrophages. J Infect Dis **193:**945-953.

348. **Jeisy-Scott V, Kim JH, Davis WG, Cao W, Katz JM, Sambhara S.** 2012. TLR7 recognition is dispensable for influenza virus A infection but important for the induction of hemagglutinin-specific antibodies in response to the 2009 pandemic split vaccine in mice. J Virol **86:**10988-10998.

349. **Daidoji T, Koma T, Du A, Yang CS, Ueda M, Ikuta K, Nakaya T.** 2008. H5N1 avian influenza virus induces apoptotic cell death in mammalian airway epithelial cells. J Virol **82:**11294-11307.

350. **Fesq H, Bacher M, Nain M, Gemsa D.** 1994. Programmed cell death (apoptosis) in human monocytes infected by influenza A virus. Immunobiology **190:**175-182.

351. **Hofmann P, Sprenger H, Kaufmann A, Bender A, Hasse C, Nain M, Gemsa D.** 1997. Susceptibility of mononuclear phagocytes to influenza A virus infection and possible role in the antiviral response. J Leukoc Biol **61:**408-414.
352. **Mok CK, Lee DC, Cheung CY, Peiris M, Lau AS.** 2007. Differential onset of apoptosis in influenza A virus H5N1- and H1N1-infected human blood macrophages. J Gen Virol **88:**1275-1280.
353. **Seo SH, Webby R, Webster RG.** 2004. No apoptotic deaths and different levels of inductions of inflammatory cytokines in alveolar macrophages infected with influenza viruses. Virology **329:**270-279.
354. **Huang FF, Barnes PF, Feng Y, Donis R, Chroneos ZC, Idell S, Allen T, Perez DR, Whitsett JA, Dunussi-Joannopoulos K, Shams H.** 2011. GM-CSF in the lung protects against lethal influenza infection. Am J Respir Crit Care Med **184:**259-268.
355. **Helft J, Manicassamy B, Guermonprez P, Hashimoto D, Silvin A, Agudo J, Brown BD, Schmolke M, Miller JC, Leboeuf M, Murphy KM, Garcia-Sastre A, Merad M.** 2012. Cross-presenting CD103+ dendritic cells are protected from influenza virus infection. J Clin Invest **122:**4037-4047.
356. **Ho AW, Prabhu N, Betts RJ, Ge MQ, Dai X, Hutchinson PE, Lew FC, Wong KL, Hanson BJ, Macary PA, Kemeny DM.** 2011. Lung CD103+ dendritic cells efficiently transport influenza virus to the lymph node and load viral antigen onto MHC class I for presentation to CD8 T cells. J Immunol **187:**6011-6021.
357. **Diebold SS, Kaisho T, Hemmi H, Akira S, Reis e Sousa C.** 2004. Innate antiviral responses by means of TLR7-mediated recognition of single-stranded RNA. Science **303:**1529-1531.
358. **Lund JM, Alexopoulou L, Sato A, Karow M, Adams NC, Gale NW, Iwasaki A, Flavell RA.** 2004. Recognition of single-stranded RNA viruses by Toll-like receptor 7. Proc Natl Acad Sci U S A **101:**5598-5603.
359. **Geiler J, Michaelis M, Sithisarn P, Cinatl J, Jr.** 2011. Comparison of pro-inflammatory cytokine expression and cellular signal transduction in human macrophages infected with different influenza A viruses. Med Microbiol Immunol **200:**53-60.
360. **Teijaro JR, Walsh KB, Cahalan S, Fremgen DM, Roberts E, Scott F, Martinborough E, Peach R, Oldstone MB, Rosen H.** 2011. Endothelial cells are central orchestrators of cytokine amplification during influenza virus infection. Cell **146:**980-991.
361. **Griffith JW, Sokol CL, Luster AD.** 2014. Chemokines and chemokine receptors: positioning cells for host defense and immunity. Annu Rev Immunol **32:**659-702.
362. **Liu B, Mori I, Hossain MJ, Dong L, Takeda K, Kimura Y.** 2004. Interleukin-18 improves the early defence system against influenza virus infection by augmenting natural killer cell-mediated cytotoxicity. J Gen Virol **85:**423-428.
363. **Long JP, Kotur MS, Stark GV, Warren RL, Kasoji M, Craft JL, Albrecht RA, Garcia-Sastre A, Katze MG, Waters KM, Vasconcelos D, Sabourin PJ, Bresler HS, Sabourin CL.** 2013. Accumulation of CD11b(+)Gr-1(+) cells in the

lung, blood and bone marrow of mice infected with highly pathogenic H5N1 and H1N1 influenza viruses. Arch Virol **158:**1305-1322.

364. **Stein-Streilein J, Bennett M, Mann D, Kumar V.** 1983. Natural killer cells in mouse lung: surface phenotype, target preference, and response to local influenza virus infection. J Immunol **131:**2699-2704.

365. **Gazit R, Gruda R, Elboim M, Arnon TI, Katz G, Achdout H, Hanna J, Qimron U, Landau G, Greenbaum E, Zakay-Rones Z, Porgador A, Mandelboim O.** 2006. Lethal influenza infection in the absence of the natural killer cell receptor gene Ncr1. Nat Immunol **7:**517-523.

366. **Mandelboim O, Lieberman N, Lev M, Paul L, Arnon TI, Bushkin Y, Davis DM, Strominger JL, Yewdell JW, Porgador A.** 2001. Recognition of haemagglutinins on virus-infected cells by NKp46 activates lysis by human NK cells. Nature **409:**1055-1060.

367. **Draghi M, Pashine A, Sanjanwala B, Gendzekhadze K, Cantoni C, Cosman D, Moretta A, Valiante NM, Parham P.** 2007. NKp46 and NKG2D recognition of infected dendritic cells is necessary for NK cell activation in the human response to influenza infection. J Immunol **178:**2688-2698.

368. **Mao H, Tu W, Qin G, Law HK, Sia SF, Chan PL, Liu Y, Lam KT, Zheng J, Peiris M, Lau YL.** 2009. Influenza virus directly infects human natural killer cells and induces cell apoptosis. J Virol **83:**9215-9222.

369. **Orange JS, Fassett MS, Koopman LA, Boyson JE, Strominger JL.** 2002. Viral evasion of natural killer cells. Nat Immunol **3:**1006-1012.

370. **Spies T, Groh V.** 2006. Natural cytotoxicity receptors: influenza virus in the spotlight. Nat Immunol **7:**443-444.

371. **Kos FJ, Engleman EG.** 1996. Role of natural killer cells in the generation of influenza virus-specific cytotoxic T cells. Cell Immunol **173:**1-6.

372. **He XS, Draghi M, Mahmood K, Holmes TH, Kemble GW, Dekker CL, Arvin AM, Parham P, Greenberg HB.** 2004. T cell-dependent production of IFN-gamma by NK cells in response to influenza A virus. J Clin Invest **114:**1812-1819.

373. **Herold S, Tabar TS, Janssen H, Hoegner K, Cabanski M, Lewe-Schlosser P, Albrecht J, Driever F, Vadasz I, Seeger W, Steinmueller M, Lohmeyer J.** 2011. Exudate macrophages attenuate lung injury by the release of IL-1 receptor antagonist in gram-negative pneumonia. Am J Respir Crit Care Med **183:**1380-1390.

374. **Hoeve MA, Nash AA, Jackson D, Randall RE, Dransfield I.** 2012. Influenza virus A infection of human monocyte and macrophage subpopulations reveals increased susceptibility associated with cell differentiation. PLoS One **7:**e29443.

375. **Reading PC, Whitney PG, Pickett DL, Tate MD, Brooks AG.** 2010. Influenza viruses differ in ability to infect macrophages and to induce a local inflammatory response following intraperitoneal injection of mice. Immunol Cell Biol **88:**641-650.

376. **Friesenhagen J, Boergeling Y, Hrincius E, Ludwig S, Roth J, Viemann D.** 2012. Highly pathogenic avian influenza viruses inhibit effective immune responses of human blood-derived macrophages. J Leukoc Biol **92:**11-20.

377. **Osterlund P, Pirhonen J, Ikonen N, Ronkko E, Strengell M, Makela SM, Broman M, Hamming OJ, Hartmann R, Ziegler T, Julkunen I.** 2010. Pandemic H1N1 2009 influenza A virus induces weak cytokine responses in human macrophages and dendritic cells and is highly sensitive to the antiviral actions of interferons. J Virol **84:**1414-1422.

378. **Peschke T, Bender A, Nain M, Gemsa D.** 1993. Role of macrophage cytokines in influenza A virus infections. Immunobiology **189:**340-355.

379. **Wareing MD, Lyon A, Inglis C, Giannoni F, Charo I, Sarawar SR.** 2007. Chemokine regulation of the inflammatory response to a low-dose influenza infection in CCR2-/- mice. J Leukoc Biol **81:**793-801.

380. **Ichikawa A, Kuba K, Morita M, Chida S, Tezuka H, Hara H, Sasaki T, Ohteki T, Ranieri VM, dos Santos CC, Kawaoka Y, Akira S, Luster AD, Lu B, Penninger JM, Uhlig S, Slutsky AS, Imai Y.** 2013. CXCL10-CXCR3 enhances the development of neutrophil-mediated fulminant lung injury of viral and nonviral origin. Am J Respir Crit Care Med **187:**65-77.

381. **Narasaraju T, Yang E, Samy RP, Ng HH, Poh WP, Liew AA, Phoon MC, van Rooijen N, Chow VT.** 2011. Excessive neutrophils and neutrophil extracellular traps contribute to acute lung injury of influenza pneumonitis. Am J Pathol **179:**199-210.

382. **Zhu H, Wang D, Kelvin DJ, Li L, Zheng Z, Yoon SW, Wong SS, Farooqui A, Wang J, Banner D, Chen R, Zheng R, Zhou J, Zhang Y, Hong W, Dong W, Cai Q, Roehrl MH, Huang SS, Kelvin AA, Yao T, Zhou B, Chen X, Leung GM, Poon LL, Webster RG, Webby RJ, Peiris JS, Guan Y, Shu Y.** 2013. Infectivity, transmission, and pathology of human-isolated H7N9 influenza virus in ferrets and pigs. Science **341:**183-186.

383. **Bradley LM, Douglass MF, Chatterjee D, Akira S, Baaten BJ.** 2012. Matrix metalloprotease 9 mediates neutrophil migration into the airways in response to influenza virus-induced toll-like receptor signaling. PLoS Pathog **8:**e1002641.

384. **Seo SU, Kwon HJ, Song JH, Byun YH, Seong BL, Kawai T, Akira S, Kweon MN.** 2010. MyD88 signaling is indispensable for primary influenza A virus infection but dispensable for secondary infection. J Virol **84:**12713-12722.

385. **Le Goffic R, Balloy V, Lagranderie M, Alexopoulou L, Escriou N, Flavell R, Chignard M, Si-Tahar M.** 2006. Detrimental contribution of the Toll-like receptor (TLR)3 to influenza A virus-induced acute pneumonia. PLoS Pathog **2:**e53.

386. **Leung YH, Nicholls JM, Ho CK, Sia SF, Mok CK, Valkenburg SA, Cheung P, Hui KP, Chan RW, Guan Y, Akira S, Peiris JS.** 2014. Highly pathogenic avian influenza A H5N1 and pandemic H1N1 virus infections have different phenotypes in Toll-like receptor 3 knockout mice. J Gen Virol **95:**1870-1879.

387. **Ratcliffe D, Migliorisi G, Cramer E.** 1992. Translocation of influenza virus by migrating neutrophils. Cell Mol Biol **38:**63-70.

388. **Borregaard N, Sorensen OE, Theilgaard-Monch K.** 2007. Neutrophil granules: a library of innate immunity proteins. Trends Immunol **28:**340-345.
389. **Brinkmann V, Reichard U, Goosmann C, Fauler B, Uhlemann Y, Weiss DS, Weinrauch Y, Zychlinsky A.** 2004. Neutrophil extracellular traps kill bacteria. Science **303:**1532-1535.
390. **Prince LR, Whyte MK, Sabroe I, Parker LC.** 2011. The role of TLRs in neutrophil activation. Curr Opin Pharmacol **11:**397-403.
391. **Thomas CJ, Schroder K.** 2013. Pattern recognition receptor function in neutrophils. Trends Immunol **34:**317-328.
392. **Bjornson AB, Mellencamp MA, Schiff GM.** 1991. Complement is activated in the upper respiratory tract during influenza virus infection. Am Rev Respir Dis **143:**1062-1066.
393. **Fritz RS, Hayden FG, Calfee DP, Cass LM, Peng AW, Alvord WG, Strober W, Straus SE.** 1999. Nasal cytokine and chemokine responses in experimental influenza A virus infection: results of a placebo-controlled trial of intravenous zanamivir treatment. J Infect Dis **180:**586-593.
394. **Lee NL.** 2009. Role of cytokines and chemokines in severe and complicated influenza infections. Hong Kong Med J **15 Suppl 8:**38-41.
395. **Lee N, Chan PK, Wong CK, Wong KT, Choi KW, Joynt GM, Lam P, Chan MC, Wong BC, Lui GC, Sin WW, Wong RY, Lam WY, Yeung AC, Leung TF, So HY, Yu AW, Sung JJ, Hui DS.** 2011. Viral clearance and inflammatory response patterns in adults hospitalized for pandemic 2009 influenza A(H1N1) virus pneumonia. Antivir Ther **16:**237-247.
396. **Garcia CC, Weston-Davies W, Russo RC, Tavares LP, Rachid MA, Alves-Filho JC, Machado AV, Ryffel B, Nunn MA, Teixeira MM.** 2013. Complement C5 activation during influenza A infection in mice contributes to neutrophil recruitment and lung injury. PLoS One **8:**e64443.
397. **Schmitz N, Kurrer M, Bachmann MF, Kopf M.** 2005. Interleukin-1 is responsible for acute lung immunopathology but increases survival of respiratory influenza virus infection. J Virol **79:**6441-6448.
398. **Ichinohe T, Lee HK, Ogura Y, Flavell R, Iwasaki A.** 2009. Inflammasome recognition of influenza virus is essential for adaptive immune responses. J Exp Med **206:**79-87.
399. **Crowe CR, Chen K, Pociask DA, Alcorn JF, Krivich C, Enelow RI, Ross TM, Witztum JL, Kolls JK.** 2009. Critical role of IL-17RA in immunopathology of influenza infection. J Immunol **183:**5301-5310.
400. **Schliehe C, Flynn EK, Vilagos B, Richson U, Swaminathan S, Bosnjak B, Bauer L, Kandasamy RK, Griesshammer IM, Kosack L, Schmitz F, Litvak V, Sissons J, Lercher A, Bhattacharya A, Khamina K, Trivett AL, Tessarollo L, Mesteri I, Hladik A, Merkler D, Kubicek S, Knapp S, Epstein MM, Symer DE, Aderem A, Bergthaler A.** 2015. The methyltransferase Setdb2 mediates virus-induced susceptibility to bacterial superinfection. Nat Immunol **16:**67-74.

401. **Wheeler JL, Martin KC, Lawrence BP.** 2013. Novel cellular targets of AhR underlie alterations in neutrophilic inflammation and inducible nitric oxide synthase expression during influenza virus infection. J Immunol **190:**659-668.
402. **Teske S, Bohn AA, Hogaboam JP, Lawrence BP.** 2008. Aryl hydrocarbon receptor targets pathways extrinsic to bone marrow cells to enhance neutrophil recruitment during influenza virus infection. Toxicol Sci **102:**89-99.
403. **Neff-LaFord H, Teske S, Bushnell TP, Lawrence BP.** 2007. Aryl hydrocarbon receptor activation during influenza virus infection unveils a novel pathway of IFN-gamma production by phagocytic cells. J Immunol **179:**247-255.
404. **Teske S, Bohn AA, Regal JF, Neumiller JJ, Lawrence BP.** 2005. Activation of the aryl hydrocarbon receptor increases pulmonary neutrophilia and diminishes host resistance to influenza A virus. Am J Physiol Lung Cell Mol Physiol **289:**L111-124.
405. **Hayashi F, Means TK, Luster AD.** 2003. Toll-like receptors stimulate human neutrophil function. Blood **102:**2660-2669.
406. **Hattermann K, Picard S, Borgeat M, Leclerc P, Pouliot M, Borgeat P.** 2007. The Toll-like receptor 7/8-ligand resiquimod (R-848) primes human neutrophils for leukotriene B4, prostaglandin E2 and platelet-activating factor biosynthesis. FASEB J **21:**1575-1585.
407. **Andonegui G, Goyert SM, Kubes P.** 2002. Lipopolysaccharide-induced leukocyte-endothelial cell interactions: a role for CD14 versus toll-like receptor 4 within microvessels. J Immunol **169:**2111-2119.
408. **van Bruggen R, Drewniak A, Tool AT, Jansen M, van Houdt M, Geissler J, van den Berg TK, Chapel H, Kuijpers TW.** 2010. Toll-like receptor responses in IRAK-4-deficient neutrophils. J Innate Immun **2:**280-287.
409. **Hartshorn K, Chang D, Rust K, White M, Heuser J, Crouch E.** 1996. Interactions of recombinant human pulmonary surfactant protein D and SP-D multimers with influenza A. Am J Physiol **271:**L753-762.
410. **Hartshorn KL, Crouch EC, White MR, Eggleton P, Tauber AI, Chang D, Sastry K.** 1994. Evidence for a protective role of pulmonary surfactant protein D (SP-D) against influenza A viruses. J Clin Invest **94:**311-319.
411. **Hartshorn KL, White MR, Voelker DR, Coburn J, Zaner K, Crouch EC.** 2000. Mechanism of binding of surfactant protein D to influenza A viruses: importance of binding to haemagglutinin to antiviral activity. Biochem J **351 Pt 2:**449-458.
412. **LeVine AM, Whitsett JA, Hartshorn KL, Crouch EC, Korfhagen TR.** 2001. Surfactant protein D enhances clearance of influenza A virus from the lung in vivo. J Immunol **167:**5868-5873.
413. **Qi L, Kash JC, Dugan VG, Jagger BW, Lau YF, Sheng ZM, Crouch EC, Hartshorn KL, Taubenberger JK.** 2011. The ability of pandemic influenza virus hemagglutinins to induce lower respiratory pathology is associated with decreased surfactant protein D binding. Virology **412:**426-434.
414. **van Eijk M, Bruinsma L, Hartshorn KL, White MR, Rynkiewicz MJ, Seaton BA, Hemrika W, Romijn RA, van Balkom BW, Haagsman HP.** 2011.

Introduction of N-linked glycans in the lectin domain of surfactant protein D: impact on interactions with influenza A viruses. J Biol Chem **286:**20137-20151.

415. **Hartshorn KL, White MR, Tecle T, Holmskov U, Crouch EC.** 2006. Innate defense against influenza A virus: activity of human neutrophil defensins and interactions of defensins with surfactant protein D. J Immunol **176:**6962-6972.

416. **Tecle T, White MR, Gantz D, Crouch EC, Hartshorn KL.** 2007. Human neutrophil defensins increase neutrophil uptake of influenza A virus and bacteria and modify virus-induced respiratory burst responses. J Immunol **178:**8046-8052.

417. **Doss M, White MR, Tecle T, Gantz D, Crouch EC, Jung G, Ruchala P, Waring AJ, Lehrer RI, Hartshorn KL.** 2009. Interactions of alpha-, beta-, and theta-defensins with influenza A virus and surfactant protein D. J Immunol **182:**7878-7887.

418. **Salvatore M, Garcia-Sastre A, Ruchala P, Lehrer RI, Chang T, Klotman ME.** 2007. alpha-Defensin inhibits influenza virus replication by cell-mediated mechanism(s). J Infect Dis **196:**835-843.

419. **Daher KA, Selsted ME, Lehrer RI.** 1986. Direct inactivation of viruses by human granulocyte defensins. J Virol **60:**1068-1074.

420. **Ratcliffe DR, Michl J, Cramer EB.** 1993. Neutrophils do not bind to or phagocytize human immune complexes formed with influenza virus. Blood **82:**1639-1646.

421. **Hartshorn KL, Liou LS, White MR, Kazhdan MM, Tauber JL, Tauber AI.** 1995. Neutrophil deactivation by influenza A virus. Role of hemagglutinin binding to specific sialic acid-bearing cellular proteins. J Immunol **154:**3952-3960.

422. **Ivan FX, Tan KS, Phoon MC, Engelward BP, Welsch RE, Rajapakse JC, Chow VT.** 2013. Neutrophils infected with highly virulent influenza H3N2 virus exhibit augmented early cell death and rapid induction of type I interferon signaling pathways. Genomics **101:**101-112.

423. **Wang JP, Bowen GN, Padden C, Cerny A, Finberg RW, Newburger PE, Kurt-Jones EA.** 2008. Toll-like receptor-mediated activation of neutrophils by influenza A virus. Blood **112:**2028-2034.

424. **Allen IC, Moore CB, Schneider M, Lei Y, Davis BK, Scull MA, Gris D, Roney KE, Zimmermann AG, Bowzard JB, Ranjan P, Monroe KM, Pickles RJ, Sambhara S, Ting JP.** 2011. NLRX1 protein attenuates inflammatory responses to infection by interfering with the RIG-I-MAVS and TRAF6-NF-kappaB signaling pathways. Immunity **34:**854-865.

425. **Jaworska J, Coulombe F, Downey J, Tzelepis F, Shalaby K, Tattoli I, Berube J, Rousseau S, Martin JG, Girardin SE, McCullers JA, Divangahi M.** 2014. NLRX1 prevents mitochondrial induced apoptosis and enhances macrophage antiviral immunity by interacting with influenza virus PB1-F2 protein. Proc Natl Acad Sci U S A **111:**E2110-2119.

426. **Allen IC, Scull MA, Moore CB, Holl EK, McElvania-TeKippe E, Taxman DJ, Guthrie EH, Pickles RJ, Ting JP.** 2009. The NLRP3 inflammasome

mediates in vivo innate immunity to influenza A virus through recognition of viral RNA. Immunity **30:**556-565.

427. **Belisle SE, Tisoncik JR, Korth MJ, Carter VS, Proll SC, Swayne DE, Pantin-Jackwood M, Tumpey TM, Katze MG.** 2010. Genomic profiling of tumor necrosis factor alpha (TNF-alpha) receptor and interleukin-1 receptor knockout mice reveals a link between TNF-alpha signaling and increased severity of 1918 pandemic influenza virus infection. J Virol **84:**12576-12588.

428. **Huang CH, Chen CJ, Yen CT, Yu CP, Huang PN, Kuo RL, Lin SJ, Chang CK, Shih SR.** 2013. Caspase-1 deficient mice are more susceptible to influenza A virus infection with PA variation. J Infect Dis **208:**1898-1905.

429. **Perrone LA, Szretter KJ, Katz JM, Mizgerd JP, Tumpey TM.** 2010. Mice lacking both TNF and IL-1 receptors exhibit reduced lung inflammation and delay in onset of death following infection with a highly virulent H5N1 virus. J Infect Dis **202:**1161-1170.

430. **Szretter KJ, Gangappa S, Lu X, Smith C, Shieh WJ, Zaki SR, Sambhara S, Tumpey TM, Katz JM.** 2007. Role of host cytokine responses in the pathogenesis of avian H5N1 influenza viruses in mice. J Virol **81:**2736-2744.

431. **Abramson JS, Lewis JC, Lyles DS, Heller KA, Mills EL, Bass DA.** 1982. Inhibition of neutrophil lysosome-phagosome fusion associated with influenza virus infection in vitro. Role in depressed bactericidal activity. J Clin Invest **69:**1393-1397.

432. **Walzog B, Schuppan D, Heimpel C, Hafezi-Moghadam A, Gaehtgens P, Ley K.** 1995. The leukocyte integrin Mac-1 (CD11b/CD18) contributes to binding of human granulocytes to collagen. Exp Cell Res **218:**28-38.

433. **Yamamoto K, Miyoshi-Koshio T, Utsuki Y, Mizuno S, Suzuki K.** 1991. Virucidal activity and viral protein modification by myeloperoxidase: a candidate for defense factor of human polymorphonuclear leukocytes against influenza virus infection. J Infect Dis **164:**8-14.

434. **Foong RE, Sly PD, Larcombe AN, Zosky GR.** 2010. No role for neutrophil elastase in influenza-induced cellular recruitment, cytokine production or airway hyperresponsiveness in mice. Respir Physiol Neurobiol **173:**164-170.

435. **Abramson JS, Mills EL, Giebink GS, Quie PG.** 1982. Depression of monocyte and polymorphonuclear leukocyte oxidative metabolism and bactericidal capacity by influenza A virus. Infect Immun **35:**350-355.

436. **Schwarz KB.** 1996. Oxidative stress during viral infection: a review. Free Radic Biol Med **21:**641-649.

437. **Knobil K, Choi AM, Weigand GW, Jacoby DB.** 1998. Role of oxidants in influenza virus-induced gene expression. Am J Physiol **274:**L134-142.

438. **Lazrak A, Iles KE, Liu G, Noah DL, Noah JW, Matalon S.** 2009. Influenza virus M2 protein inhibits epithelial sodium channels by increasing reactive oxygen species. FASEB J **23:**3829-3842.

439. **Snelgrove RJ, Edwards L, Rae AJ, Hussell T.** 2006. An absence of reactive oxygen species improves the resolution of lung influenza infection. Eur J Immunol **36:**1364-1373.

440. **Cooper JA, Jr., Carcelen R, Culbreth R.** 1996. Effects of influenza A nucleoprotein on polymorphonuclear neutrophil function. J Infect Dis **173:**279-284.

441. **Buffinton GD, Christen S, Peterhans E, Stocker R.** 1992. Oxidative stress in lungs of mice infected with influenza A virus. Free Radic Res Commun **16:**99-110.

442. **Perrone LA, Belser JA, Wadford DA, Katz JM, Tumpey TM.** 2013. Inducible nitric oxide contributes to viral pathogenesis following highly pathogenic influenza virus infection in mice. J Infect Dis **207:**1576-1584.

443. **Suliman HB, Ryan LK, Bishop L, Folz RJ.** 2001. Prevention of influenza-induced lung injury in mice overexpressing extracellular superoxide dismutase. Am J Physiol Lung Cell Mol Physiol **280:**L69-78.

444. **Vlahos R, Stambas J, Bozinovski S, Broughton BR, Drummond GR, Selemidis S.** 2011. Inhibition of Nox2 oxidase activity ameliorates influenza A virus-induced lung inflammation. PLoS Pathog **7:**e1001271.

445. **Zhang WJ, Wei H, Tien YT, Frei B.** 2011. Genetic ablation of phagocytic NADPH oxidase in mice limits TNFalpha-induced inflammation in the lungs but not other tissues. Free Radic Biol Med **50:**1517-1525.

446. **Akaike T, Noguchi Y, Ijiri S, Setoguchi K, Suga M, Zheng YM, Dietzschold B, Maeda H.** 1996. Pathogenesis of influenza virus-induced pneumonia: involvement of both nitric oxide and oxygen radicals. Proc Natl Acad Sci U S A **93:**2448-2453.

447. **Imai Y, Kuba K, Neely GG, Yaghubian-Malhami R, Perkmann T, van Loo G, Ermolaeva M, Veldhuizen R, Leung YH, Wang H, Liu H, Sun Y, Pasparakis M, Kopf M, Mech C, Bavari S, Peiris JS, Slutsky AS, Akira S, Hultqvist M, Holmdahl R, Nicholls J, Jiang C, Binder CJ, Penninger JM.** 2008. Identification of oxidative stress and Toll-like receptor 4 signaling as a key pathway of acute lung injury. Cell **133:**235-249.

448. **Nhu QM, Shirey K, Teijaro JR, Farber DL, Netzel-Arnett S, Antalis TM, Fasano A, Vogel SN.** 2010. Novel signaling interactions between proteinase-activated receptor 2 and Toll-like receptors in vitro and in vivo. Mucosal Immunol **3:**29-39.

449. **Shirey KA, Lai W, Scott AJ, Lipsky M, Mistry P, Pletneva LM, Karp CL, McAlees J, Gioannini TL, Weiss J, Chen WH, Ernst RK, Rossignol DP, Gusovsky F, Blanco JC, Vogel SN.** 2013. The TLR4 antagonist Eritoran protects mice from lethal influenza infection. Nature **497:**498-502.

450. **Fuchs TA, Abed U, Goosmann C, Hurwitz R, Schulze I, Wahn V, Weinrauch Y, Brinkmann V, Zychlinsky A.** 2007. Novel cell death program leads to neutrophil extracellular traps. J Cell Biol **176:**231-241.

451. **Urban CF, Reichard U, Brinkmann V, Zychlinsky A.** 2006. Neutrophil extracellular traps capture and kill Candida albicans yeast and hyphal forms. Cell Microbiol **8:**668-676.

452. **Guimaraes-Costa AB, Nascimento MT, Froment GS, Soares RP, Morgado FN, Conceicao-Silva F, Saraiva EM.** 2009. Leishmania amazonensis

promastigotes induce and are killed by neutrophil extracellular traps. Proc Natl Acad Sci U S A **106:**6748-6753.

453. **Kessenbrock K, Krumbholz M, Schonermarck U, Back W, Gross WL, Werb Z, Grone HJ, Brinkmann V, Jenne DE.** 2009. Netting neutrophils in autoimmune small-vessel vasculitis. Nat Med **15:**623-625.

454. **Marcos V, Zhou Z, Yildirim AO, Bohla A, Hector A, Vitkov L, Wiedenbauer EM, Krautgartner WD, Stoiber W, Belohradsky BH, Rieber N, Kormann M, Koller B, Roscher A, Roos D, Griese M, Eickelberg O, Doring G, Mall MA, Hartl D.** 2010. CXCR2 mediates NADPH oxidase-independent neutrophil extracellular trap formation in cystic fibrosis airway inflammation. Nat Med **16:**1018-1023.

455. **Hakkim A, Furnrohr BG, Amann K, Laube B, Abed UA, Brinkmann V, Herrmann M, Voll RE, Zychlinsky A.** 2010. Impairment of neutrophil extracellular trap degradation is associated with lupus nephritis. Proc Natl Acad Sci U S A **107:**9813-9818.

456. **Raftery MJ, Lalwani P, Krautkrmer E, Peters T, Scharffetter-Kochanek K, Kruger R, Hofmann J, Seeger K, Kruger DH, Schonrich G.** 2014. beta2 integrin mediates hantavirus-induced release of neutrophil extracellular traps. J Exp Med **211:**1485-1497.

457. **Hemmers S, Teijaro JR, Arandjelovic S, Mowen KA.** 2011. PAD4-mediated neutrophil extracellular trap formation is not required for immunity against influenza infection. PLoS One **6:**e22043.

458. **Dean RA, Cox JH, Bellac CL, Doucet A, Starr AE, Overall CM.** 2008. Macrophage-specific metalloelastase (MMP-12) truncates and inactivates ELR+ CXC chemokines and generates CCL2, -7, -8, and -13 antagonists: potential role of the macrophage in terminating polymorphonuclear leukocyte influx. Blood **112:**3455-3464.

459. **Fadok VA, Bratton DL, Konowal A, Freed PW, Westcott JY, Henson PM.** 1998. Macrophages that have ingested apoptotic cells in vitro inhibit proinflammatory cytokine production through autocrine/paracrine mechanisms involving TGF-beta, PGE2, and PAF. J Clin Invest **101:**890-898.

460. **El Kebir D, Filep JG.** 2013. Targeting neutrophil apoptosis for enhancing the resolution of inflammation. Cells **2:**330-348.

461. **Godson C, Mitchell S, Harvey K, Petasis NA, Hogg N, Brady HR.** 2000. Cutting edge: lipoxins rapidly stimulate nonphlogistic phagocytosis of apoptotic neutrophils by monocyte-derived macrophages. J Immunol **164:**1663-1667.

462. **Poe SL, Arora M, Oriss TB, Yarlagadda M, Isse K, Khare A, Levy DE, Lee JS, Mallampalli RK, Chan YR, Ray A, Ray P.** 2013. STAT1-regulated lung MDSC-like cells produce IL-10 and efferocytose apoptotic neutrophils with relevance in resolution of bacterial pneumonia. Mucosal Immunol **6:**189-199.

463. **Dienz O, Rud JG, Eaton SM, Lanthier PA, Burg E, Drew A, Bunn J, Suratt BT, Haynes L, Rincon M.** 2012. Essential role of IL-6 in protection against H1N1 influenza virus by promoting neutrophil survival in the lung. Mucosal Immunol **5:**258-266.

464. **Simard JC, Girard D, Tessier PA.** 2010. Induction of neutrophil degranulation by S100A9 via a MAPK-dependent mechanism. J Leukoc Biol **87:**905-914.
465. **Tsai SY, Segovia JA, Chang TH, Morris IR, Berton MT, Tessier PA, Tardif MR, Cesaro A, Bose S.** 2014. DAMP molecule S100A9 acts as a molecular pattern to enhance inflammation during influenza A virus infection: role of DDX21-TRIF-TLR4-MyD88 pathway. PLoS Pathog **10:**e1003848.
466. **Eruslanov EB, Lyadova IV, Kondratieva TK, Majorov KB, Scheglov IV, Orlova MO, Apt AS.** 2005. Neutrophil responses to Mycobacterium tuberculosis infection in genetically susceptible and resistant mice. Infect Immun **73:**1744-1753.
467. **Seiler P, Aichele P, Bandermann S, Hauser AE, Lu B, Gerard NP, Gerard C, Ehlers S, Mollenkopf HJ, Kaufmann SH.** 2003. Early granuloma formation after aerosol Mycobacterium tuberculosis infection is regulated by neutrophils via CXCR3-signaling chemokines. Eur J Immunol **33:**2676-2686.
468. **Moolenaar RL, Dalton C, Lipman HB, Umland ET, Gallaher M, Duchin JS, Chapman L, Zaki SR, Ksiazek TG, Rollin PE, et al.** 1995. Clinical features that differentiate hantavirus pulmonary syndrome from three other acute respiratory illnesses. Clin Infect Dis **21:**643-649.
469. **Smits SL, van den Brand JM, de Lang A, Leijten LM, van Ijcken WF, van Amerongen G, Osterhaus AD, Andeweg AC, Haagmans BL.** 2011. Distinct severe acute respiratory syndrome coronavirus-induced acute lung injury pathways in two different nonhuman primate species. J Virol **85:**4234-4245.
470. **Schomacker H, Schaap-Nutt A, Collins PL, Schmidt AC.** 2012. Pathogenesis of acute respiratory illness caused by human parainfluenza viruses. Curr Opin Virol **2:**294-299.
471. **Bataki EL, Evans GS, Everard ML.** 2005. Respiratory syncytial virus and neutrophil activation. Clin Exp Immunol **140:**470-477.
472. **Kolaczkowska E, Kubes P.** 2013. Neutrophil recruitment and function in health and inflammation. Nat Rev Immunol **13:**159-175.
473. **Kennedy JL, Turner RB, Braciale T, Heymann PW, Borish L.** 2012. Pathogenesis of rhinovirus infection. Curr Opin Virol **2:**287-293.
474. **Levandowski RA, Weaver CW, Jackson GG.** 1988. Nasal-secretion leukocyte populations determined by flow cytometry during acute rhinovirus infection. J Med Virol **25:**423-432.
475. **van Kempen M, Bachert C, Van Cauwenberge P.** 1999. An update on the pathophysiology of rhinovirus upper respiratory tract infections. Rhinology **37:**97-103.
476. **Racaniello V.** 2007. Picornaviridae: the viruses and their replication, p. 795-838. *In* Knipe DM, Howley PM (ed.), Fields virology 5th edition, vol. 1. Lippincott Williams & Wilkins, Philadelphia.
477. **Winther B.** 1994. Effects on the nasal mucosa of upper respiratory viruses (common cold). Dan Med Bull **41:**193-204.
478. **Winther B, Gwaltney JM, Jr., Mygind N, Hendley JO.** 1998. Viral-induced rhinitis. Am J Rhinol **12:**17-20.

479. **Gern JE, Busse WW.** 1999. Association of rhinovirus infections with asthma. Clin Microbiol Rev **12:**9-18.
480. **Gern JE, Martin MS, Anklam KA, Shen K, Roberg KA, Carlson-Dakes KT, Adler K, Gilbertson-White S, Hamilton R, Shult PA, Kirk CJ, Da Silva DF, Sund SA, Kosorok MR, Lemanske RF, Jr.** 2002. Relationships among specific viral pathogens, virus-induced interleukin-8, and respiratory symptoms in infancy. Pediatr Allergy Immunol **13:**386-393.
481. **Wang Q, Nagarkar DR, Bowman ER, Schneider D, Gosangi B, Lei J, Zhao Y, McHenry CL, Burgens RV, Miller DJ, Sajjan U, Hershenson MB.** 2009. Role of double-stranded RNA pattern recognition receptors in rhinovirus-induced airway epithelial cell responses. J Immunol **183:**6989-6997.
482. **Murawski MR, Bowen GN, Cerny AM, Anderson LJ, Haynes LM, Tripp RA, Kurt-Jones EA, Finberg RW.** 2009. Respiratory syncytial virus activates innate immunity through Toll-like receptor 2. J Virol **83:**1492-1500.
483. **Kelly JT, Busse WW.** 2008. Host immune responses to rhinovirus: mechanisms in asthma. J Allergy Clin Immunol **122:**671-682; quiz 683-674.
484. **Lamb RA, Parks GD.** 2007. Paramyxoviridae: the viruses and their replication, p. 1449-1496. *In* Knipe DM, Howley PM (ed.), Fields virology 5th edition, vol. 2. Lippincott Williams & Wilkins, Philadelphia.
485. **Pickles RJ, DeVincenzo JP.** 2015. Respiratory syncytial virus (RSV) and its propensity for causing bronchiolitis. J Pathol **235:**266-276.
486. **Domachowske JB, Rosenberg HF.** 1999. Respiratory syncytial virus infection: immune response, immunopathogenesis, and treatment. Clin Microbiol Rev **12:**298-309.
487. **McNamara PS, Ritson P, Selby A, Hart CA, Smyth RL.** 2003. Bronchoalveolar lavage cellularity in infants with severe respiratory syncytial virus bronchiolitis. Arch Dis Child **88:**922-926.
488. **McNamara PS, Flanagan BF, Selby AM, Hart CA, Smyth RL.** 2004. Pro- and anti-inflammatory responses in respiratory syncytial virus bronchiolitis. Eur Respir J **23:**106-112.
489. **McNamara PS, Smyth RL.** 2002. The pathogenesis of respiratory syncytial virus disease in childhood. Br Med Bull **61:**13-28.
490. **Konig B, Krusat T, Streckert HJ, Konig W.** 1996. IL-8 release from human neutrophils by the respiratory syncytial virus is independent of viral replication. J Leukoc Biol **60:**253-260.
491. **Hooper P, Zaki S, Daniels P, Middleton D.** 2001. Comparative pathology of the diseases caused by Hendra and Nipah viruses. Microbes Infect **3:**315-322.
492. **Koh YY, Jung da E, Koh JY, Kim JY, Yoo Y, Kim CK.** 2007. Bronchoalveolar cellularity and interleukin-8 levels in measles bronchiolitis obliterans. Chest **131:**1454-1460.
493. **Vargas SO, Kozakewich HP, Perez-Atayde AR, McAdam AJ.** 2004. Pathology of human metapneumovirus infection: insights into the pathogenesis of a newly identified respiratory virus. Pediatr Dev Pathol **7:**478-486; discussion 421.

494. **Schildgen V, van den Hoogen B, Fouchier R, Tripp RA, Alvarez R, Manoha C, Williams J, Schildgen O.** 2011. Human Metapneumovirus: lessons learned over the first decade. Clin Microbiol Rev **24:**734-754.

495. **Downham MA, Gardner PS, McQuillin J, Ferris JA.** 1975. Role of respiratory viruses in childhood mortality. Br Med J **1:**235-239.

496. **Schomacker H, Hebner RM, Boonyaratanakornkit J, Surman S, Amaro-Carambot E, Collins PL, Schmidt AC.** 2012. The C proteins of human parainfluenza virus type 1 block IFN signaling by binding and retaining Stat1 in perinuclear aggregates at the late endosome. PLoS One **7:**e28382.

497. **El Feghaly RE, McGann L, Bonville CA, Branigan PJ, Suryadevera M, Rosenberg HF, Domachowske JB.** 2010. Local production of inflammatory mediators during childhood parainfluenza virus infection. Pediatr Infect Dis J **29:**e26-31.

498. **Lai MMC, Perlman S, Anderson LJ.** 2007. Coronaviridae: the viruses and their replication, p. 1305-1335. *In* Knipe DM, Howley PM (ed.), Fields virology 5th edition, vol. 2. Lippincott Williams & Wilkins, Philadelphia.

499. **van der Hoek L.** 2007. Human coronaviruses: what do they cause? Antivir Ther **12:**651-658.

500. **Pyrc K, Berkhout B, van der Hoek L.** 2007. The novel human coronaviruses NL63 and HKU1. J Virol **81:**3051-3057.

501. **Jiang Y, Xu J, Zhou C, Wu Z, Zhong S, Liu J, Luo W, Chen T, Qin Q, Deng P.** 2005. Characterization of cytokine/chemokine profiles of severe acute respiratory syndrome. Am J Respir Crit Care Med **171:**850-857.

502. **Wu W, Booth JL, Duggan ES, Patel KB, Coggeshall KM, Metcalf JP.** 2010. Human lung innate immune cytokine response to adenovirus type 7. J Gen Virol **91:**1155-1163.

503. **Kim EA, Lee KS, Primack SL, Yoon HK, Byun HS, Kim TS, Suh GY, Kwon OJ, Han J.** 2002. Viral pneumonias in adults: radiologic and pathologic findings. Radiographics **22 Spec No:**S137-149.

504. **Zaki SR, Greer PW, Coffield LM, Goldsmith CS, Nolte KB, Foucar K, Feddersen RM, Zumwalt RE, Miller GL, Khan AS, et al.** 1995. Hantavirus pulmonary syndrome. Pathogenesis of an emerging infectious disease. Am J Pathol **146:**552-579.

505. **Zinman G, Brower-Sinning R, Emeche CH, Ernst J, Huang GT, Mahony S, Myers AJ, O'Dee DM, Flynn JL, Nau GJ, Ross TM, Salter RD, Benos PV, Bar Joseph Z, Morel PA.** 2011. Large scale comparison of innate responses to viral and bacterial pathogens in mouse and macaque. PLoS One **6:**e22401.

506. **Don M, Valent F, Korppi M, Canciani M.** 2009. Differentiation of bacterial and viral community-acquired pneumonia in children. Pediatr Int **51:**91-96.

507. **Virkki R, Juven T, Rikalainen H, Svedstrom E, Mertsola J, Ruuskanen O.** 2002. Differentiation of bacterial and viral pneumonia in children. Thorax **57:**438-441.

508. **Byeon JH, Lee JC, Choi IS, Yoo Y, Park SH, Choung JT.** 2009. Comparison of cytokine responses in nasopharyngeal aspirates from children with viral lower respiratory tract infections. Acta Paediatr **98:**725-730.

509. **Holub M, Lawrence DA, Andersen N, Davidova A, Beran O, Maresova V, Chalupa P.** 2013. Cytokines and chemokines as biomarkers of community-acquired bacterial infection. Mediators Inflamm **2013:**190145.

510. **Kragsbjerg P, Jones I, Vikerfors T, Holmberg H.** 1995. Diagnostic value of blood cytokine concentrations in acute pneumonia. Thorax **50:**1253-1257.

511. **Korppi M.** 2004. Non-specific host response markers in the differentiation between pneumococcal and viral pneumonia: what is the most accurate combination? Pediatr Int **46:**545-550.

512. **Ruuskanen O, Putto A, Sarkkinen H, Meurman O, Irjala K.** 1985. C-reactive protein in respiratory virus infections. J Pediatr **107:**97-100.

513. **Fares M, Mourad S, Rajab M, Rifai N.** 2011. The use of C-reactive protein in predicting bacterial co-Infection in children with bronchiolitis. N Am J Med Sci **3:**152-156.

514. **Kolb JP, Casella CR, SenGupta S, Chilton PM, Mitchell TC.** 2014. Type I interferon signaling contributes to the bias that Toll-like receptor 4 exhibits for signaling mediated by the adaptor protein TRIF. Sci Signal **7:**ra108.

515. **Honda K, Taniguchi T.** 2006. IRFs: master regulators of signalling by Toll-like receptors and cytosolic pattern-recognition receptors. Nat Rev Immunol **6:**644-658.

516. **Ljungberg K, McBrayer A, Camp JV, Chu YK, Tapp R, Noah DL, Grimes S, Proctor ML, Liljestrom P, Jonsson CB, Bruder CE.** 2012. Host gene expression signatures discriminate between ferrets infected with genetically similar H1N1 strains. PLoS One **7:**e40743.

517. **Gentile DA, Skoner DP.** 2001. Viral rhinitis. Curr Allergy Asthma Rep **1:**227-234.

518. **Sung RY, Hui SH, Wong CK, Lam CW, Yin J.** 2001. A comparison of cytokine responses in respiratory syncytial virus and influenza A infections in infants. Eur J Pediatr **160:**117-122.

519. **Shirey KA, Pletneva LM, Puche AC, Keegan AD, Prince GA, Blanco JC, Vogel SN.** 2010. Control of RSV-induced lung injury by alternatively activated macrophages is IL-4R alpha-, TLR4-, and IFN-beta-dependent. Mucosal Immunol **3:**291-300.

520. **Paul WE, Seder RA.** 1994. Lymphocyte responses and cytokines. Cell **76:**241-251.

521. **Chan MC, Chan RW, Yu WC, Ho CC, Chui WH, Lo CK, Yuen KM, Guan YI, Nicholls JM, Peiris JS.** 2009. Influenza H5N1 virus infection of polarized human alveolar epithelial cells and lung microvascular endothelial cells. Respir Res **10:**102.

522. **Sumino KC, Walter MJ, Mikols CL, Thompson SA, Gaudreault-Keener M, Arens MQ, Agapov E, Hormozdi D, Gaynor AM, Holtzman MJ, Storch GA.**

2010. Detection of respiratory viruses and the associated chemokine responses in serious acute respiratory illness. Thorax **65:**639-644.

523. **Luster AD, Unkeless JC, Ravetch JV.** 1985. Gamma-interferon transcriptionally regulates an early-response gene containing homology to platelet proteins. Nature **315:**672-676.

524. **Neville LF, Mathiak G, Bagasra O.** 1997. The immunobiology of interferon-gamma inducible protein 10 kD (IP-10): a novel, pleiotropic member of the C-X-C chemokine superfamily. Cytokine Growth Factor Rev **8:**207-219.

525. **Moser B, Wolf M, Walz A, Loetscher P.** 2004. Chemokines: multiple levels of leukocyte migration control. Trends Immunol **25:**75-84.

526. **Cella M, Jarrossay D, Facchetti F, Alebardi O, Nakajima H, Lanzavecchia A, Colonna M.** 1999. Plasmacytoid monocytes migrate to inflamed lymph nodes and produce large amounts of type I interferon. Nat Med **5:**919-923.

527. **Groom JR, Luster AD.** 2011. CXCR3 in T cell function. Exp Cell Res **317:**620-631.

528. **Bonizzi G, Karin M.** 2004. The two NF-kappaB activation pathways and their role in innate and adaptive immunity. Trends Immunol **25:**280-288.

529. **Furuya Y, Steiner D, Metzger DW.** 2014. Does Type I Interferon Limit Protective Neutrophil Responses during Pulmonary Francisella Tularensis Infection? Front Immunol **5:**355.

530. **Martinelli S, Urosevic M, Daryadel A, Oberholzer PA, Baumann C, Fey MF, Dummer R, Simon HU, Yousefi S.** 2004. Induction of genes mediating interferon-dependent extracellular trap formation during neutrophil differentiation. J Biol Chem **279:**44123-44132.

531. **Garcia-Romo GS, Caielli S, Vega B, Connolly J, Allantaz F, Xu Z, Punaro M, Baisch J, Guiducci C, Coffman RL, Barrat FJ, Banchereau J, Pascual V.** 2011. Netting neutrophils are major inducers of type I IFN production in pediatric systemic lupus erythematosus. Sci Transl Med **3:**73ra20.

532. **Decker P.** 2011. Neutrophils and interferon-alpha-producing cells: who produces interferon in lupus? Arthritis Res Ther **13:**118.

533. **Stock AT, Smith JM, Carbone FR.** 2014. Type I IFN suppresses Cxcr2 driven neutrophil recruitment into the sensory ganglia during viral infection. J Exp Med **211:**751-759.

534. **Xin L, Vargas-Inchaustegui DA, Raimer SS, Kelly BC, Hu J, Zhu L, Sun J, Soong L.** 2010. Type I IFN receptor regulates neutrophil functions and innate immunity to Leishmania parasites. J Immunol **184:**7047-7056.

535. **Thomas PG, Dash P, Aldridge JR, Jr., Ellebedy AH, Reynolds C, Funk AJ, Martin WJ, Lamkanfi M, Webby RJ, Boyd KL, Doherty PC, Kanneganti TD.** 2009. The intracellular sensor NLRP3 mediates key innate and healing responses to influenza A virus via the regulation of caspase-1. Immunity **30:**566-575.

536. **Salomon R, Hoffmann E, Webster RG.** 2007. Inhibition of the cytokine response does not protect against lethal H5N1 influenza infection. Proc Natl Acad Sci U S A **104:**12479-12481.

537. **Dawson TC, Beck MA, Kuziel WA, Henderson F, Maeda N.** 2000. Contrasting effects of CCR5 and CCR2 deficiency in the pulmonary inflammatory response to influenza A virus. Am J Pathol **156:**1951-1959.

538. **Wareing MD, Shea AL, Inglis CA, Dias PB, Sarawar SR.** 2007. CXCR2 is required for neutrophil recruitment to the lung during influenza virus infection, but is not essential for viral clearance. Viral Immunol **20:**369-378.

539. **Wareing MD, Lyon AB, Lu B, Gerard C, Sarawar SR.** 2004. Chemokine expression during the development and resolution of a pulmonary leukocyte response to influenza A virus infection in mice. J Leukoc Biol **76:**886-895.

540. **Yang Z, Delgado R, Xu L, Todd RF, Nabel EG, Sanchez A, Nabel GJ.** 1998. Distinct cellular interactions of secreted and transmembrane Ebola virus glycoproteins. Science **279:**1034-1037.

541. **Sullivan N, Yang ZY, Nabel GJ.** 2003. Ebola virus pathogenesis: implications for vaccines and therapies. J Virol **77:**9733-9737.

542. **Itoh Y, Shinya K, Kiso M, Watanabe T, Sakoda Y, Hatta M, Muramoto Y, Tamura D, Sakai-Tagawa Y, Noda T, Sakabe S, Imai M, Hatta Y, Watanabe S, Li C, Yamada S, Fujii K, Murakami S, Imai H, Kakugawa S, Ito M, Takano R, Iwatsuki-Horimoto K, Shimojima M, Horimoto T, Goto H, Takahashi K, Makino A, Ishigaki H, Nakayama M, Okamatsu M, Warshauer D, Shult PA, Saito R, Suzuki H, Furuta Y, Yamashita M, Mitamura K, Nakano K, Nakamura M, Brockman-Schneider R, Mitamura H, Yamazaki M, Sugaya N, Suresh M, Ozawa M, Neumann G, Gern J, Kida H, Ogasawara K, Kawaoka Y.** 2009. In vitro and in vivo characterization of new swine-origin H1N1 influenza viruses. Nature **460:**1021-1025.

543. **Van Kerkhove MD, Vandemaele KA, Shinde V, Jaramillo-Gutierrez G, Koukounari A, Donnelly CA, Carlino LO, Owen R, Paterson B, Pelletier L, Vachon J, Gonzalez C, Hongjie Y, Zijian F, Chuang SK, Au A, Buda S, Krause G, Haas W, Bonmarin I, Taniguichi K, Nakajima K, Shobayashi T, Takayama Y, Sunagawa T, Heraud JM, Orelle A, Palacios E, van der Sande MA, Wielders CC, Hunt D, Cutter J, Lee VJ, Thomas J, Santa-Olalla P, Sierra-Moros MJ, Hanshaoworakul W, Ungchusak K, Pebody R, Jain S, Mounts AW.** 2011. Risk Factors for Severe Outcomes following 2009 Influenza A (H1N1) Infection: A Global Pooled Analysis. PLoS Med **8:**e1001053.

544. **Louie JK, Jean C, Acosta M, Samuel MC, Matyas BT, Schechter R.** 2011. A review of adult mortality due to 2009 pandemic (H1N1) influenza A in California. PLoS One **6:**e18221.

545. **Lucker LM, Kherad O, Iten A, Wagner N, Descombes M, Camus V, Kaiser L, Louis-Simonet M.** 2011. Clinical features and outcome of hospitalised adults and children with the 2009 influenza A H1N1 infection at Geneva's University Hospital. Swiss Med Wkly **141:**w13177.

546. **Kuster SP, Drews S, Green K, Blair J, Davis I, Downey J, Fowler R, Katz K, Lapinsky S, McRitchie D, Pataki J, Powis J, Rose D, Sarabia A, Simone C, Simor A, Stewart T, McGeer A.** 2010. Epidemiology of influenza-associated

hospitalization in adults, Toronto, 2007/8. Eur J Clin Microbiol Infect Dis **29:**835-843.

547. **Wang B, Dwyer DE, Soedjono M, Shi H, Matlho K, Ratnamohan M, Blyth C, McPhie K, Cunningham AL, Saksena NK.** 2011. Evidence of the circulation of pandemic influenza (H1N1) 2009 with D222D/G/N/S hemagglutinin polymorphisms during the first wave of the 2009 influenza pandemic. J Clin Virol **52:**304-306.

548. **Fezeu L, Julia C, Henegar A, Bitu J, Hu FB, Grobbee DE, Kengne AP, Hercberg S, Czernichow S.** 2011. Obesity is associated with higher risk of intensive care unit admission and death in influenza A (H1N1) patients: a systematic review and meta-analysis. Obes Rev **12:**653-659.

549. **Ghedin E, Laplante J, DePasse J, Wentworth DE, Santos RP, Lepow ML, Porter J, Stellrecht K, Lin X, Operario D, Griesemer S, Fitch A, Halpin RA, Stockwell TB, Spiro DJ, Holmes EC, St George K.** 2011. Deep sequencing reveals mixed infection with 2009 pandemic influenza A (H1N1) virus strains and the emergence of oseltamivir resistance. J Infect Dis **203:**168-174.

550. **Ozawa M, Basnet S, Burley LM, Neumann G, Hatta M, Kawaoka Y.** 2011. Impact of amino acid mutations in PB2, PB1-F2, and NS1 on the replication and pathogenicity of pandemic (H1N1) 2009 influenza viruses. J Virol **85:**4596-4601.

551. **Kao CL, Chan TC, Tsai CH, Chu KY, Chuang SF, Lee CC, Li ZR, Wu KW, Chang LY, Shen YH, Huang LM, Lee PI, Yang C, Compans R, Rouse BT, King CC.** 2012. Emerged HA and NA mutants of the pandemic influenza H1N1 viruses with increasing epidemiological significance in Taipei and Kaohsiung, Taiwan, 2009-10. PLoS One **7:**e31162.

552. **Reid AH, Janczewski TA, Lourens RM, Elliot AJ, Daniels RS, Berry CL, Oxford JS, Taubenberger JK.** 2003. 1918 influenza pandemic caused by highly conserved viruses with two receptor-binding variants. Emerg Infect Dis **9:**1249-1253.

553. **Ilyushina NA, Khalenkov AM, Seiler JP, Forrest HL, Bovin NV, Marjuki H, Barman S, Webster RG, Webby RJ.** 2010. Adaptation of pandemic H1N1 influenza viruses in mice. Journal of virology **84:**8607-8616.

554. **Ye J, Sorrell EM, Cai Y, Shao H, Xu K, Pena L, Hickman D, Song H, Angel M, Medina RA, Manicassamy B, Garcia-Sastre A, Perez DR.** 2010. Variations in the hemagglutinin of the 2009 H1N1 pandemic virus: potential for strains with altered virulence phenotype? PLoS pathogens **6:**e1001145.

555. **Suphaphiphat P, Franti M, Hekele A, Lilja A, Spencer T, Settembre E, Palmer G, Crotta S, Tuccino AB, Keiner B, Trusheim H, Balabanis K, Sackal M, Rothfeder M, Mandl CW, Dormitzer PR, Mason PW.** 2010. Mutations at positions 186 and 194 in the HA gene of the 2009 H1N1 pandemic influenza virus improve replication in cell culture and eggs. Virol J **7:**157.

556. **Blair PJ, Wierzba TF, Touch S, Vonthanak S, Xu X, Garten RJ, Okomo-Adhiambo MA, Klimov AI, Kasper MR, Putnam SD.** 2010. Influenza epidemiology and characterization of influenza viruses in patients seeking treatment for acute fever in Cambodia. Epidemiology and infection **138:**199-209.

557. **Van Kerkhove MD, Vandemaele KA, Shinde V, Jaramillo-Gutierrez G, Koukounari A, Donnelly CA, Carlino LO, Owen R, Paterson B, Pelletier L, Vachon J, Gonzalez C, Hongjie Y, Zijian F, Chuang SK, Au A, Buda S, Krause G, Haas W, Bonmarin I, Taniguichi K, Nakajima K, Shobayashi T, Takayama Y, Sunagawa T, Heraud JM, Orelle A, Palacios E, van der Sande MA, Wielders CC, Hunt D, Cutter J, Lee VJ, Thomas J, Santa-Olalla P, Sierra-Moros MJ, Hanshaoworakul W, Ungchusak K, Pebody R, Jain S, Mounts AW.** 2011. Risk factors for severe outcomes following 2009 influenza A (H1N1) infection: a global pooled analysis. PLoS medicine **8:**e1001053.

558. **Kilander A, Rykkvin R, Dudman SG, Hungnes O.** 2010. Observed association between the HA1 mutation D222G in the 2009 pandemic influenza A(H1N1) virus and severe clinical outcome, Norway 2009-2010. Euro Surveill **15**.

559. **Mak GC, Au KW, Tai LS, Chuang KC, Cheng KC, Shiu TC, Lim W.** 2010. Association of D222G substitution in haemagglutinin of 2009 pandemic influenza A (H1N1) with severe disease. Euro Surveill **15**.

560. **Berdal JE, Mollnes TE, Waehre T, Olstad OK, Halvorsen B, Ueland T, Laake JH, Furuseth MT, Maagaard A, Kjekshus H, Aukrust P, Jonassen CM.** 2011. Excessive innate immune response and mutant D222G/N in severe A (H1N1) pandemic influenza. The Journal of infection **63:**308-316.

561. **Chan PK, Lee N, Joynt GM, Choi KW, Cheung JL, Yeung AC, Lam P, Wong R, Leung BW, So HY, Lam WY, Hui DC.** 2011. Clinical and virological course of infection with haemagglutinin D222G mutant strain of 2009 pandemic influenza A (H1N1) virus. J Clin Virol **50:**320-324.

562. **Anton A, Marcos MA, Martinez MJ, Ramon S, Martinez A, Cardenosa N, Godoy P, Torner N, De Molina P, Isanta R, Jimenez de Anta MT, Pumarola T.** 2010. D225G mutation in the hemagglutinin protein found in 3 severe cases of 2009 pandemic influenza A (H1N1) in Spain. Diagn Microbiol Infect Dis **67:**207-208.

563. **Liu Y, Childs RA, Matrosovich T, Wharton S, Palma AS, Chai W, Daniels R, Gregory V, Uhlendorff J, Kiso M, Klenk HD, Hay A, Feizi T, Matrosovich M.** 2010. Altered receptor specificity and cell tropism of D222G hemagglutinin mutants isolated from fatal cases of pandemic A(H1N1) 2009 influenza virus. J Virol **84:**12069-12074.

564. **Takemae N, Ruttanapumma R, Parchariyanon S, Yoneyama S, Hayashi T, Hiramatsu H, Sriwilaijaroen N, Uchida Y, Kondo S, Yagi H, Kato K, Suzuki Y, Saito T.** 2010. Alterations in receptor-binding properties of swine influenza viruses of the H1 subtype after isolation in embryonated chicken eggs. J Gen Virol **91:**938-948.

565. **Watanabe T, Shinya K, Watanabe S, Imai M, Hatta M, Li C, Wolter BF, Neumann G, Hanson A, Ozawa M, Yamada S, Imai H, Sakabe S, Takano R, Iwatsuki-Horimoto K, Kiso M, Ito M, Fukuyama S, Kawakami E, Gorai T, Simmons HA, Schenkman D, Brunner K, Capuano SV, 3rd, Weinfurter JT, Nishio W, Maniwa Y, Igarashi T, Makino A, Travanty EA, Wang J, Kilander A, Dudman SG, Suresh M, Mason RJ, Hungnes O, Friedrich TC,**

Kawaoka Y. 2011. Avian-type receptor-binding ability can increase influenza virus pathogenicity in macaques. Journal of virology **85:**13195-13203.

566. **Xu L, Bao L, Zhou J, Wang D, Deng W, Lv Q, Ma Y, Li F, Sun H, Zhan L, Zhu H, Ma C, Shu Y, Qin C.** 2011. Genomic polymorphism of the pandemic A (H1N1) influenza viruses correlates with viral replication, virulence, and pathogenicity in vitro and in vivo. PLoS One **6:**e20698.

567. **Patel JR, Vora KP, Tripathi S, Zeng H, Tumpey TM, Katz JM, Sambhara S, Gangappa S.** 2011. Infection of lung epithelial cells with pandemic 2009 A(H1N1) influenza viruses reveals isolate-specific differences in infectivity and host cellular responses. Viral immunology **24:**89-99.

568. **Pappas C, Aguilar PV, Basler CF, Solorzano A, Zeng H, Perrone LA, Palese P, Garcia-Sastre A, Katz JM, Tumpey TM.** 2008. Single gene reassortants identify a critical role for PB1, HA, and NA in the high virulence of the 1918 pandemic influenza virus. Proc Natl Acad Sci U S A **105:**3064-3069.

569. **Pica N, Iyer A, Ramos I, Bouvier NM, Fernandez-Sesma A, Garcia-Sastre A, Lowen AC, Palese P, Steel J.** 2011. The DBA.2 mouse is susceptible to disease following infection with a broad, but limited, range of influenza A and B viruses. Journal of virology **85:**12825-12829.

570. **Srivastava B, Blazejewska P, Hessmann M, Bruder D, Geffers R, Mauel S, Gruber AD, Schughart K.** 2009. Host genetic background strongly influences the response to influenza a virus infections. PLoS One **4:**e4857.

571. **Trammell RA, Liberati TA, Toth LA.** 2012. Host genetic background and the innate inflammatory response of lung to influenza virus. Microbes Infect **14:**50-58.

572. **Everitt AR, Clare S, Pertel T, John SP, Wash RS, Smith SE, Chin CR, Feeley EM, Sims JS, Adams DJ, Wise HM, Kane L, Goulding D, Digard P, Anttila V, Baillie JK, Walsh TS, Hume DA, Palotie A, Xue Y, Colonna V, Tyler-Smith C, Dunning J, Gordon SB, Smyth RL, Openshaw PJ, Dougan G, Brass AL, Kellam P.** 2012. IFITM3 restricts the morbidity and mortality associated with influenza. Nature **484:**519-523.

573. **Hayden FG, Treanor JJ, Fritz RS, Lobo M, Betts RF, Miller M, Kinnersley N, Mills RG, Ward P, Straus SE.** 1999. Use of the oral neuraminidase inhibitor oseltamivir in experimental human influenza: randomized controlled trials for prevention and treatment. JAMA **282:**1240-1246.

574. **Kobasa D, Takada A, Shinya K, Hatta M, Halfmann P, Theriault S, Suzuki H, Nishimura H, Mitamura K, Sugaya N, Usui T, Murata T, Maeda Y, Watanabe S, Suresh M, Suzuki T, Suzuki Y, Feldmann H, Kawaoka Y.** 2004. Enhanced virulence of influenza A viruses with the haemagglutinin of the 1918 pandemic virus. Nature **431:**703-707.

575. **Baskin CR, Bielefeldt-Ohmann H, Tumpey TM, Sabourin PJ, Long JP, Garcia-Sastre A, Tolnay AE, Albrecht R, Pyles JA, Olson PH, Aicher LD, Rosenzweig ER, Murali-Krishna K, Clark EA, Kotur MS, Fornek JL, Proll S, Palermo RE, Sabourin CL, Katze MG.** 2009. Early and sustained innate

immune response defines pathology and death in nonhuman primates infected by highly pathogenic influenza virus. Proc Natl Acad Sci U S A **106:**3455-3460.

576. **To KK, Hung IF, Li IW, Lee KL, Koo CK, Yan WW, Liu R, Ho KY, Chu KH, Watt CL, Luk WK, Lai KY, Chow FL, Mok T, Buckley T, Chan JF, Wong SS, Zheng B, Chen H, Lau CC, Tse H, Cheng VC, Chan KH, Yuen KY.** 2010. Delayed clearance of viral load and marked cytokine activation in severe cases of pandemic H1N1 2009 influenza virus infection. Clinical infectious diseases : an official publication of the Infectious Diseases Society of America **50:**850-859.

577. **Tumpey TM, Garcia-Sastre A, Taubenberger JK, Palese P, Swayne DE, Pantin-Jackwood MJ, Schultz-Cherry S, Solorzano A, Van Rooijen N, Katz JM, Basler CF.** 2005. Pathogenicity of influenza viruses with genes from the 1918 pandemic virus: functional roles of alveolar macrophages and neutrophils in limiting virus replication and mortality in mice. Journal of virology **79:**14933-14944.

578. **Perrone LA, Plowden JK, Garcia-Sastre A, Katz JM, Tumpey TM.** 2008. H5N1 and 1918 pandemic influenza virus infection results in early and excessive infiltration of macrophages and neutrophils in the lungs of mice. PLoS pathogens **4:**e1000115.

579. **Tate MD, Brooks AG, Reading PC, Mintern JD.** 2012. Neutrophils sustain effective CD8(+) T-cell responses in the respiratory tract following influenza infection. Immunology and cell biology **90:**197-205.

580. **Hashimoto Y, Moki T, Takizawa T, Shiratsuchi A, Nakanishi Y.** 2007. Evidence for phagocytosis of influenza virus-infected, apoptotic cells by neutrophils and macrophages in mice. Journal of immunology **178:**2448-2457.

581. **Stein-Streilein J, Bennett M, Mann D, Kumar V.** 1983. Natural killer cells in mouse lung: surface phenotype, target preference, and response to local influenza virus infection. Journal of immunology **131:**2699-2704.

582. **Stein-Streilein J, Guffee J, Fan W.** 1988. Locally and systemically derived natural killer cells participate in defense against intranasally inoculated influenza virus. Regional immunology **1:**100-105.

583. **Stein-Streilein J, Guffee J.** 1986. In vivo treatment of mice and hamsters with antibodies to asialo GM1 increases morbidity and mortality to pulmonary influenza infection. J Immunol **136:**1435-1441.

584. **Mao H, Tu W, Liu Y, Qin G, Zheng J, Chan PL, Lam KT, Peiris JS, Lau YL.** 2010. Inhibition of human natural killer cell activity by influenza virions and hemagglutinin. J Virol **84:**4148-4157.

585. **Vance RE, Jamieson AM, Cado D, Raulet DH.** 2002. Implications of CD94 deficiency and monoallelic NKG2A expression for natural killer cell development and repertoire formation. Proc Natl Acad Sci U S A **99:**868-873.

586. **Abdul-Careem MF, Mian MF, Yue G, Gillgrass A, Chenoweth MJ, Barra NG, Chew MV, Chan T, Al-Garawi AA, Jordana M, Ashkar AA.** 2012. Critical role of natural killer cells in lung immunopathology during influenza infection in mice. J Infect Dis **206:**167-177.

587. **Reading PC, Whitney PG, Pickett DL, Tate MD, Brooks AG.** 2010. Influenza viruses differ in ability to infect macrophages and to induce a local inflammatory response following intraperitoneal injection of mice. Immunology and cell biology **88:**641-650.

588. **Reading PC, Miller JL, Anders EM.** 2000. Involvement of the mannose receptor in infection of macrophages by influenza virus. Journal of virology **74:**5190-5197.

589. **Hofmann P, Sprenger H, Kaufmann A, Bender A, Hasse C, Nain M, Gemsa D.** 1997. Susceptibility of mononuclear phagocytes to influenza A virus infection and possible role in the antiviral response. Journal of leukocyte biology **61:**408-414.

590. **Weinheimer VK, Becher A, Tonnies M, Holland G, Knepper J, Bauer TT, Schneider P, Neudecker J, Ruckert JC, Szymanski K, Temmesfeld-Wollbrueck B, Gruber AD, Bannert N, Suttorp N, Hippenstiel S, Wolff T, Hocke AC.** 2012. Influenza A Viruses Target Type II Pneumocytes in the Human Lung. J Infect Dis.

591. **Osterlund P, Pirhonen J, Ikonen N, Ronkko E, Strengell M, Makela SM, Broman M, Hamming OJ, Hartmann R, Ziegler T, Julkunen I.** 2010. Pandemic H1N1 2009 influenza A virus induces weak cytokine responses in human macrophages and dendritic cells and is highly sensitive to the antiviral actions of interferons. Journal of virology **84:**1414-1422.

592. **Josset L, Belser JA, Pantin-Jackwood MJ, Chang JH, Chang ST, Belisle SE, Tumpey TM, Katze MG.** 2012. Implication of inflammatory macrophages, nuclear receptors, and interferon regulatory factors in increased virulence of pandemic 2009 H1N1 influenza A virus after host adaptation. J Virol **86:**7192-7206.

593. **Tate MD, Pickett DL, van Rooijen N, Brooks AG, Reading PC.** 2010. Critical role of airway macrophages in modulating disease severity during influenza virus infection of mice. Journal of virology **84:**7569-7580.

594. **Wijburg OL, DiNatale S, Vadolas J, van Rooijen N, Strugnell RA.** 1997. Alveolar macrophages regulate the induction of primary cytotoxic T-lymphocyte responses during influenza virus infection. J Virol **71:**9450-9457.

595. **Hui KP, Lee SM, Cheung CY, Ng IH, Poon LL, Guan Y, Ip NY, Lau AS, Peiris JS.** 2009. Induction of proinflammatory cytokines in primary human macrophages by influenza A virus (H5N1) is selectively regulated by IFN regulatory factor 3 and p38 MAPK. J Immunol **182:**1088-1098.

596. **Sakabe S, Iwatsuki-Horimoto K, Takano R, Nidom CA, Le MQ, Nagamura-Inoue T, Horimoto T, Yamashita N, Kawaoka Y.** 2011. Cytokine production by primary human macrophages infected with highly pathogenic H5N1 or pandemic H1N1 2009 influenza viruses. J Gen Virol **92:**1428-1434.

597. **Reed LJ, Muench H.** 1938. A simple method of estimating fifty percent endpoints. American Journal of Hygiene **27:**493-497.

598. **Inoue E, Wang X, Osawa Y, Okazaki K.** 2010. Full genomic amplification and subtyping of influenza A virus using a single set of universal primers. Microbiol Immunol **54:**129-134.

599. **Patel M, Dennis A, Flutter C, Khan Z.** 2010. Pandemic (H1N1) 2009 influenza. British journal of anaesthesia **104:**128-142.

600. **Rowe T, Leon AJ, Crevar CJ, Carter DM, Xu L, Ran L, Fang Y, Cameron CM, Cameron MJ, Banner D, Ng DC, Ran R, Weirback HK, Wiley CA, Kelvin DJ, Ross TM.** 2010. Modeling host responses in ferrets during A/California/07/2009 influenza infection. Virology **401:**257-265.

601. **Safronetz D, Rockx B, Feldmann F, Belisle SE, Palermo RE, Brining D, Gardner D, Proll SC, Marzi A, Tsuda Y, Lacasse RA, Kercher L, York A, Korth MJ, Long D, Rosenke R, Shupert WL, Aranda CA, Mattoon JS, Kobasa D, Kobinger G, Li Y, Taubenberger JK, Richt JA, Parnell M, Ebihara H, Kawaoka Y, Katze MG, Feldmann H.** 2011. Pandemic swine-origin H1N1 influenza A virus isolates show heterogeneous virulence in macaques. J Virol **85:**1214-1223.

602. **Mollura DJ, Morens DM, Taubenberger JK, Bray M.** 2010. The role of radiology in influenza: novel H1N1 and lessons learned from the 1918 pandemic. J Am Coll Radiol **7:**690-697.

603. **Bray M, Lawler J, Paragas J, Jahrling PB, Mollura DJ.** 2011. Molecular imaging of influenza and other emerging respiratory viral infections. J Infect Dis **203:**1348-1359.

604. **Qureshi NR, Hien TT, Farrar J, Gleeson FV.** 2006. The radiologic manifestations of H5N1 avian influenza. J Thorac Imaging **21:**259-264.

605. **Hansell DM, Bankier AA, MacMahon H, McLoud TC, Muller NL, Remy J.** 2008. Fleischner Society: glossary of terms for thoracic imaging. Radiology **246:**697-722.

606. **Davis SL, Be NA, Lamichhane G, Nimmagadda S, Pomper MG, Bishai WR, Jain SK.** 2009. Bacterial thymidine kinase as a non-invasive imaging reporter for Mycobacterium tuberculosis in live animals. PLoS One **4:**e6297.

607. **Davis SL, Nuermberger EL, Um PK, Vidal C, Jedynak B, Pomper MG, Bishai WR, Jain SK.** 2009. Noninvasive pulmonary [18F]-2-fluoro-deoxy-D-glucose positron emission tomography correlates with bactericidal activity of tuberculosis drug treatment. Antimicrob Agents Chemother **53:**4879-4884.

608. **Salem N, Balkman JD, Wang J, Wilson DL, Lee Z, King CL, Basilion JP.** 2010. In vivo imaging of schistosomes to assess disease burden using positron emission tomography (PET). PLoS Negl Trop Dis **4**.

609. **Bellani G, Guerra L, Pesenti A, Messa C.** 2010. Imaging of lung inflammation during severe influenza A: H1N1. Intensive Care Med **36:**717-718.

610. **Chen DL, Rosenbluth DB, Mintun MA, Schuster DP.** 2006. FDG-PET imaging of pulmonary inflammation in healthy volunteers after airway instillation of endotoxin. J Appl Physiol **100:**1602-1609.

611. **Jones HA, Sriskandan S, Peters AM, Pride NB, Krausz T, Boobis AR, Haslett C.** 1997. Dissociation of neutrophil emigration and metabolic activity in lobar pneumonia and bronchiectasis. Eur Respir J **10:**795-803.

612. **Chen DL, Schuster DP.** 2004. Positron emission tomography with [18F]fluorodeoxyglucose to evaluate neutrophil kinetics during acute lung injury. Am J Physiol Lung Cell Mol Physiol **286:**L834-840.

613. **Jones HA, Schofield JB, Krausz T, Boobis AR, Haslett C.** 1998. Pulmonary fibrosis correlates with duration of tissue neutrophil activation. Am J Respir Crit Care Med **158:**620-628.

614. **Chutinimitkul S, Herfst S, Steel J, Lowen AC, Ye J, van Riel D, Schrauwen EJ, Bestebroer TM, Koel B, Burke DF, Sutherland-Cash KH, Whittleston CS, Russell CA, Wales DJ, Smith DJ, Jonges M, Meijer A, Koopmans M, Rimmelzwaan GF, Kuiken T, Osterhaus AD, Garcia-Sastre A, Perez DR, Fouchier RA.** 2010. Virulence-associated substitution D222G in the hemagglutinin of 2009 pandemic influenza A(H1N1) virus affects receptor binding. J Virol **84:**11802-11813.

615. **Veldhuis Kroeze EJ, van Amerongen G, Dijkshoorn ML, Simon JH, de Waal L, Hartmann IJ, Krestin GP, Kuiken T, Osterhaus AD, Stittelaar KJ.** 2011. Pulmonary pathology of pandemic influenza A/H1N1 virus (2009)-infected ferrets upon longitudinal evaluation by computed tomography. J Gen Virol **92:**1854-1858.

616. **Shim SS, Kim Y, Ryu YJ.** 2011. Novel influenza A (H1N1) infection: chest CT findings from 21 cases in Seoul, Korea. Clin Radiol **66:**118-124.

617. **Lee EJ, Moore WE, Fryer HC, Minocha HC.** 1982. Haematological and serum chemistry profiles of ferrets (Mustela putorius furo). Lab Anim **16:**133-137.

618. **Reed LJ, Muench H.** 1938. A simple method of estimating fifty percent endpoints. American Journal of Hygiene **27:**493-497.

619. **Preaud E, Durand L, Macabeo B, Farkas N, Sloesen B, Palache A, Shupo F, Samson SI, Vaccines Europe influenza working g.** 2014. Annual public health and economic benefits of seasonal influenza vaccination: a European estimate. BMC Public Health **14:**813.

620. **Lu PJ, Santibanez TA, Williams WW, Zhang J, Ding H, Bryan L, O'Halloran A, Greby SM, Bridges CB, Graitcer SB, Kennedy ED, Lindley MC, Ahluwalia IB, LaVail K, Pabst LJ, Harris L, Vogt T, Town M, Singleton JA, Centers for Disease C, Prevention.** 2013. Surveillance of influenza vaccination coverage--United States, 2007-08 through 2011-12 influenza seasons. MMWR Surveill Summ **62:**1-28.

621. **Nichol KL, Treanor JJ.** 2006. Vaccines for seasonal and pandemic influenza. J Infect Dis **194 Suppl 2:**S111-118.

622. **Pearce MB, Belser JA, Houser KV, Katz JM, Tumpey TM.** 2011. Efficacy of seasonal live attenuated influenza vaccine against virus replication and transmission of a pandemic 2009 H1N1 virus in ferrets. Vaccine **29:**2887-2894.

623. **Hancock K, Veguilla V, Lu X, Zhong W, Butler EN, Sun H, Liu F, Dong L, DeVos JR, Gargiullo PM, Brammer TL, Cox NJ, Tumpey TM, Katz JM.**

2009. Cross-reactive antibody responses to the 2009 pandemic H1N1 influenza virus. N Engl J Med **361:**1945-1952.

624. **Ellebedy AH, Ducatez MF, Duan S, Stigger-Rosser E, Rubrum AM, Govorkova EA, Webster RG, Webby RJ.** 2011. Impact of prior seasonal influenza vaccination and infection on pandemic A (H1N1) influenza virus replication in ferrets. Vaccine **29:**3335-3339.

625. **Shinya K, Makino A, Kawaoka Y.** 2010. Emerging and reemerging influenza virus infections. Vet Pathol **47:**53-57.

626. **Kilbourne ED.** 2006. Influenza pandemics of the 20th century. Emerg Infect Dis **12:**9-14.

627. **Neumann G, Kawaoka Y.** 2006. Host range restriction and pathogenicity in the context of influenza pandemic. Emerg Infect Dis **12:**881-886.

628. **Tscherne DM, Garcia-Sastre A.** 2011. Virulence determinants of pandemic influenza viruses. J Clin Invest **121:**6-13.

629. **van Riel D, Munster VJ, de Wit E, Rimmelzwaan GF, Fouchier RA, Osterhaus AD, Kuiken T.** 2006. H5N1 Virus Attachment to Lower Respiratory Tract. Science **312:**399.

630. **Munster VJ, de Wit E, van den Brand JM, Herfst S, Schrauwen EJ, Bestebroer TM, van de Vijver D, Boucher CA, Koopmans M, Rimmelzwaan GF, Kuiken T, Osterhaus AD, Fouchier RA.** 2009. Pathogenesis and transmission of swine-origin 2009 A(H1N1) influenza virus in ferrets. Science **325:**481-483.

631. **Jonsson CB, Camp JV, Wu A, Zheng H, Kraenzle JL, Biller AE, Vanover CD, Chu YK, Ng CK, Proctor M, Sherwood L, Steffen MC, Mollura DJ.** 2012. Molecular imaging reveals a progressive pulmonary inflammation in lower airways in ferrets infected with 2009 H1N1 pandemic influenza virus. PLoS One **7:**e40094.

632. **Belser JA, Katz JM, Tumpey TM.** 2011. The ferret as a model organism to study influenza A virus infection. Dis Model Mech **4:**575-579.

633. **Tran V, Moser LA, Poole DS, Mehle A.** 2013. Highly sensitive real-time in vivo imaging of an influenza reporter virus reveals dynamics of replication and spread. J Virol **87:**13321-13329.

634. **Chen DL, Mintun MA, Schuster DP.** 2004. Comparison of methods to quantitate 18F-FDG uptake with PET during experimental acute lung injury. J Nucl Med **45:**1583-1590.

635. **Goldsmith SJ, Vallabhajosula S.** 2009. Clinically proven radiopharmaceuticals for infection imaging: mechanisms and applications. Semin Nucl Med **39:**2-10.

636. **Jones HA, Clark RJ, Rhodes CG, Schofield JB, Krausz T, Haslett C.** 1994. In vivo measurement of neutrophil activity in experimental lung inflammation. Am J Respir Crit Care Med **149:**1635-1639.

637. **Fujisawa H.** 2001. Inhibitory role of neutrophils on influenza virus multiplication in the lungs of mice. Microbiol Immunol **45:**679-688.

638. **Fujisawa H.** 2008. Neutrophils play an essential role in cooperation with antibody in both protection against and recovery from pulmonary infection with influenza virus in mice. J Virol **82:**2772-2783.

639. **Narasaraju T, Yang E, Samy RP, Ng HH, Poh WP, Liew AA, Phoon MC, van Rooijen N, Chow VT.** 2011. Excessive neutrophils and neutrophil extracellular traps contribute to acute lung injury of influenza pneumonitis. Am J Pathol **179:**199-210.

640. **Nicholls JM, Wong LP, Chan RW, Poon LL, So LK, Yen HL, Fung K, van Poucke S, Peiris JS.** 2012. Detection of highly pathogenic influenza and pandemic influenza virus in formalin fixed tissues by immunohistochemical methods. J Virol Methods **179:**409-413.

641. **Schindelin J, Arganda-Carreras I, Frise E, Kaynig V, Longair M, Pietzsch T, Preibisch S, Rueden C, Saalfeld S, Schmid B, Tinevez JY, White DJ, Hartenstein V, Eliceiri K, Tomancak P, Cardona A.** 2012. Fiji: an open-source platform for biological-image analysis. Nat Methods **9:**676-682.

642. **Ogino J, Asanuma H, Hatanaka Y, Matsuno Y, Gotoda H, Muraoka S, Tsuji T, Fukazawa Y, Yamashiro K, Kondo N, Iwaki H, Miyokawa N, Hasegawa T.** 2013. Validity and reproducibility of Ki-67 assessment in gastrointestinal stromal tumors and leiomyosarcomas. Pathol Int **63:**102-107.

643. **Hasegawa T, Yamamoto S, Nojima T, Hirose T, Nikaido T, Yamashiro K, Matsuno Y.** 2002. Validity and reproducibility of histologic diagnosis and grading for adult soft-tissue sarcomas. Hum Pathol **33:**111-115.

644. **Wu A, Zheng H, Kraenzle J, Biller A, Vanover CD, Proctor M, Sherwood L, Steffen M, Ng C, Mollura DJ, Jonsson CB.** 2012. Ferret thoracic anatomy by 2-deoxy-2-(18F)fluoro-D-glucose (18F-FDG) positron emission tomography/computed tomography (18F-FDG PET/CT) imaging. ILAR J **53:**E9-21.

645. **Bagci U, Foster B, Miller-Jaster K, Luna B, Dey B, Bishai WR, Jonsson CB, Jain S, Mollura DJ.** 2013. A computational pipeline for quantification of pulmonary infections in small animal models using serial PET-CT imaging. EJNMMI research **3:**55.

646. **Foster B, Bagci U, Ziyue X, Dey B, Luna B, Bishai W, Jain S, Mollura DJ.** 2014. Segmentation of PET images for computer-aided functional quantification of tuberculosis in small animal models. IEEE transactions on bio-medical engineering **61:**711-724.

647. **Xu Z, Bagci U, Foster B, Mansoor A, Mollura DJ.** 2013. Spatially constrained random walk approach for accurate estimation of airway wall surfaces. Medical image computing and computer-assisted intervention : MICCAI ... International Conference on Medical Image Computing and Computer-Assisted Intervention **16:**559-566.

648. **Czernin J, Benz MR, Allen-Auerbach MS.** 2010. PET/CT imaging: The incremental value of assessing the glucose metabolic phenotype and the structure of cancers in a single examination. Eur J Radiol **73:**470-480.

649. **Ramos CD, Canetti C, Souto JT, Silva JS, Hogaboam CM, Ferreira SH, Cunha FQ.** 2005. MIP-1alpha[CCL3] acting on the CCR1 receptor mediates neutrophil migration in immune inflammation via sequential release of TNF-alpha and LTB4. J Leukoc Biol **78:**167-177.
650. **Reichel CA, Puhr-Westerheide D, Zuchtriegel G, Uhl B, Berberich N, Zahler S, Wymann MP, Luckow B, Krombach F.** 2012. C-C motif chemokine CCL3 and canonical neutrophil attractants promote neutrophil extravasation through common and distinct mechanisms. Blood **120:**880-890.
651. **Mukaida N.** 2003. Pathophysiological roles of interleukin-8/CXCL8 in pulmonary diseases. Am J Physiol Lung Cell Mol Physiol **284:**L566-577.
652. **De Filippo K, Henderson RB, Laschinger M, Hogg N.** 2008. Neutrophil chemokines KC and macrophage-inflammatory protein-2 are newly synthesized by tissue macrophages using distinct TLR signaling pathways. J Immunol **180:**4308-4315.
653. **Wolpe SD, Davatelis G, Sherry B, Beutler B, Hesse DG, Nguyen HT, Moldawer LL, Nathan CF, Lowry SF, Cerami A.** 1988. Macrophages secrete a novel heparin-binding protein with inflammatory and neutrophil chemokinetic properties. J Exp Med **167:**570-581.
654. **Wagner JG, Roth RA.** 2000. Neutrophil migration mechanisms, with an emphasis on the pulmonary vasculature. Pharmacol Rev **52:**349-374.
655. **Zhang X, Kluger Y, Nakayama Y, Poddar R, Whitney C, DeTora A, Weissman SM, Newburger PE.** 2004. Gene expression in mature neutrophils: early responses to inflammatory stimuli. J Leukoc Biol **75:**358-372.
656. **Newburger PE, Subrahmanyam YV, Weissman SM.** 2000. Global analysis of neutrophil gene expression. Curr Opin Hematol **7:**16-20.
657. **Manz MG, Boettcher S.** 2014. Emergency granulopoiesis. Nat Rev Immunol **14:**302-314.
658. **Kreisel D, Nava RG, Li W, Zinselmeyer BH, Wang B, Lai J, Pless R, Gelman AE, Krupnick AS, Miller MJ.** 2010. In vivo two-photon imaging reveals monocyte-dependent neutrophil extravasation during pulmonary inflammation. Proc Natl Acad Sci U S A **107:**18073-18078.
659. **McBrayer A, Camp JV, Tapp R, Yamshchikov V, Grimes S, Noah DL, Jonsson CB, Bruder CE.** 2010. Course of seasonal influenza A/Brisbane/59/07 H1N1 infection in the ferret. Virology journal **7:**149.
660. **Ratcliffe DR, Nolin SL, Cramer EB.** 1988. Neutrophil interaction with influenza-infected epithelial cells. Blood **72:**142-149.
661. **Daigneault DE, Hartshorn KL, Liou LS, Abbruzzi GM, White MR, Oh SK, Tauber AI.** 1992. Influenza A virus binding to human neutrophils and cross-linking requirements for activation. Blood **80:**3227-3234.
662. **Hartshorn KL, Daigneault DE, White MR, Tauber AI.** 1992. Anomalous features of human neutrophil activation by influenza A virus are shared by related viruses and sialic acid-binding lectins. J Leukoc Biol **51:**230-236.

663. **Hartshorn KL, Daigneault DE, White MR, Tuvin M, Tauber JL, Tauber AI.** 1992. Comparison of influenza A virus and formyl-methionyl-leucyl-phenylalanine activation of the human neutrophil. Blood **79:**1049-1057.

664. **Cassidy LF, Lyles DS, Abramson JS.** 1989. Depression of polymorphonuclear leukocyte functions by purified influenza virus hemagglutinin and sialic acid-binding lectins. J Immunol **142:**4401-4406.

665. **Koma T, Yoshimatsu K, Nagata N, Sato Y, Shimizu K, Yasuda SP, Amada T, Nishio S, Hasegawa H, Arikawa J.** 2014. Neutrophil depletion suppresses pulmonary vascular hyperpermeability and occurrence of pulmonary edema caused by hantavirus infection in C.B-17 SCID mice. J Virol **88:**7178-7188.

666. **Kohio HP, Adamson AL.** 2013. Glycolytic control of vacuolar-type ATPase activity: a mechanism to regulate influenza viral infection. Virology **444:**301-309.

667. **Marjuki H, Gornitzky A, Marathe BM, Ilyushina NA, Aldridge JR, Desai G, Webby RJ, Webster RG.** 2011. Influenza A virus-induced early activation of ERK and PI3K mediates V-ATPase-dependent intracellular pH change required for fusion. Cell Microbiol **13:**587-601.

668. **Kurata T, Oguri T, Isobe T, Ishioka S, Yamakido M.** 1999. Differential expression of facilitative glucose transporter (GLUT) genes in primary lung cancers and their liver metastases. Jpn J Cancer Res **90:**1238-1243.

669. **de Geus-Oei LF, van Krieken JH, Aliredjo RP, Krabbe PF, Frielink C, Verhagen AF, Boerman OC, Oyen WJ.** 2007. Biological correlates of FDG uptake in non-small cell lung cancer. Lung Cancer **55:**79-87.

670. **Gerdes J, Lemke H, Baisch H, Wacker HH, Schwab U, Stein H.** 1984. Cell cycle analysis of a cell proliferation-associated human nuclear antigen defined by the monoclonal antibody Ki-67. J Immunol **133:**1710-1715.

671. **Brown DC, Gatter KC.** 1990. Monoclonal antibody Ki-67: its use in histopathology. Histopathology **17:**489-503.

672. **Yamamoto Y, Nishiyama Y, Ishikawa S, Nakano J, Chang SS, Bandoh S, Kanaji N, Haba R, Kushida Y, Ohkawa M.** 2007. Correlation of 18F-FLT and 18F-FDG uptake on PET with Ki-67 immunohistochemistry in non-small cell lung cancer. Eur J Nucl Med Mol Imaging **34:**1610-1616.

673. **Buck AK, Halter G, Schirrmeister H, Kotzerke J, Wurziger I, Glatting G, Mattfeldt T, Neumaier B, Reske SN, Hetzel M.** 2003. Imaging proliferation in lung tumors with PET: 18F-FLT versus 18F-FDG. J Nucl Med **44:**1426-1431.

674. **Kotton DN, Morrisey EE.** 2014. Lung regeneration: mechanisms, applications and emerging stem cell populations. Nat Med **20:**822-832.

675. **Cameron CM, Cameron MJ, Bermejo-Martin JF, Ran L, Xu L, Turner PV, Ran R, Danesh A, Fang Y, Chan PK, Mytle N, Sullivan TJ, Collins TL, Johnson MG, Medina JC, Rowe T, Kelvin DJ.** 2008. Gene expression analysis of host innate immune responses during Lethal H5N1 infection in ferrets. J Virol **82:**11308-11317.

676. **Kumar PA, Hu Y, Yamamoto Y, Hoe NB, Wei TS, Mu D, Sun Y, Joo LS, Dagher R, Zielonka EM, Wang de Y, Lim B, Chow VT, Crum CP, Xian W,**

McKeon F. 2011. Distal airway stem cells yield alveoli in vitro and during lung regeneration following H1N1 influenza infection. Cell **147:**525-538.

677. **Lee SM, Gardy JL, Cheung CY, Cheung TK, Hui KP, Ip NY, Guan Y, Hancock RE, Peiris JS.** 2009. Systems-level comparison of host-responses elicited by avian H5N1 and seasonal H1N1 influenza viruses in primary human macrophages. PLoS One **4:**e8072.

678. **Murphy EA, Davis JM, McClellan JL, Carmichael MD, Rooijen NV, Gangemi JD.** 2011. Susceptibility to infection and inflammatory response following influenza virus (H1N1, A/PR/8/34) challenge: role of macrophages. J Interferon Cytokine Res **31:**501-508.

679. **Filardy AA, Pires DR, Nunes MP, Takiya CM, Freire-de-Lima CG, Ribeiro-Gomes FL, DosReis GA.** 2010. Proinflammatory clearance of apoptotic neutrophils induces an IL-12(low)IL-10(high) regulatory phenotype in macrophages. J Immunol **185:**2044-2050.

680. **Ramirez JA, Anzueto AR.** 2011. Changing needs of community-acquired pneumonia. J Antimicrob Chemother **66 Suppl 3:**iii3-9.

681. **Shrestha SS, Swerdlow DL, Borse RH, Prabhu VS, Finelli L, Atkins CY, Owusu-Edusei K, Bell B, Mead PS, Biggerstaff M, Brammer L, Davidson H, Jernigan D, Jhung MA, Kamimoto LA, Merlin TL, Nowell M, Redd SC, Reed C, Schuchat A, Meltzer MI.** 2011. Estimating the burden of 2009 pandemic influenza A (H1N1) in the United States (April 2009-April 2010). Clin Infect Dis **52 Suppl 1:**S75-82.

682. **Regan J, Fowlkes A, Biggerstaff M, Jhung MA, Gindler J, Kennedy E, Fields V, Finelli L, Pandemic Influenza AFCSIT.** 2012. Epidemiology of influenza A (H1N1)pdm09-associated deaths in the United States, September-October 2009. Influenza Other Respir Viruses **6:**e169-177.

683. **Le VL, Courtney CL, Steel J, Compans RW.** 2013. Closely related influenza viruses induce contrasting respiratory tract immunopathology. PLoS One **8:**e76708.

684. **Otte A, Sauter M, Alleva L, Baumgarte S, Klingel K, Gabriel G.** 2011. Differential host determinants contribute to the pathogenesis of 2009 pandemic H1N1 and human H5N1 influenza A viruses in experimental mouse models. Am J Pathol **179:**230-239.

685. **Sakabe S, Ozawa M, Takano R, Iwastuki-Horimoto K, Kawaoka Y.** 2011. Mutations in PA, NP, and HA of a pandemic (H1N1) 2009 influenza virus contribute to its adaptation to mice. Virus Res **158:**124-129.

686. **Watanabe T, Imai M, Watanabe S, Shinya K, Hatta M, Li C, Neumann G, Ozawa M, Hanson A, Zhong G, Fukuyama S, Kawakami E, Simmons HA, Schenkman D, Brunner K, Capuano SV, 3rd, Weinfurter JT, Kilander A, Dudman SG, Suresh M, Hungnes O, Friedrich TC, Kawaoka Y.** 2012. Characterization in vitro and in vivo of pandemic (H1N1) 2009 influenza viruses isolated from patients. J Virol **86:**9361-9368.

687. **Sun Y, Xu Q, Shen Y, Liu L, Wei K, Sun H, Pu J, Chang KC, Liu J.** 2014. Naturally occurring mutations in the PA gene are key contributors to increased virulence of pandemic H1N1/09 influenza virus in mice. J Virol **88:**4600-4604.

688. **Lakdawala SS, Shih AR, Jayaraman A, Lamirande EW, Moore I, Paskel M, Sasisekharan R, Subbarao K.** 2013. Receptor specificity does not affect replication or virulence of the 2009 pandemic H1N1 influenza virus in mice and ferrets. Virology **446:**349-356.

689. **Watanabe T, Shinya K, Watanabe S, Imai M, Hatta M, Li C, Wolter BF, Neumann G, Hanson A, Ozawa M, Yamada S, Imai H, Sakabe S, Takano R, Iwatsuki-Horimoto K, Kiso M, Ito M, Fukuyama S, Kawakami E, Gorai T, Simmons HA, Schenkman D, Brunner K, Capuano SV, 3rd, Weinfurter JT, Nishio W, Maniwa Y, Igarashi T, Makino A, Travanty EA, Wang J, Kilander A, Dudman SG, Suresh M, Mason RJ, Hungnes O, Friedrich TC, Kawaoka Y.** 2011. Avian-type receptor-binding ability can increase influenza virus pathogenicity in macaques. J Virol **85:**13195-13203.

690. **Berdal JE, Mollnes TE, Waehre T, Olstad OK, Halvorsen B, Ueland T, Laake JH, Furuseth MT, Maagaard A, Kjekshus H, Aukrust P, Jonassen CM.** 2011. Excessive innate immune response and mutant D222G/N in severe A (H1N1) pandemic influenza. J Infect **63:**308-316.

691. **Wedde M, Wahlisch S, Wolff T, Schweiger B.** 2013. Predominance of HA-222D/G polymorphism in influenza A(H1N1)pdm09 viruses associated with fatal and severe outcomes recently circulating in Germany. PLoS One **8:**e57059.

692. **Elderfield RA, Watson SJ, Godlee A, Adamson WE, Thompson CI, Dunning J, Fernandez-Alonso M, Blumenkrantz D, Hussell T, Investigators M, Zambon M, Openshaw P, Kellam P, Barclay WS.** 2014. Accumulation of human-adapting mutations during circulation of A(H1N1)pdm09 influenza virus in humans in the United Kingdom. J Virol **88:**13269-13283.

693. **Lin YP, Wharton SA, Martin J, Skehel JJ, Wiley DC, Steinhauer DA.** 1997. Adaptation of egg-grown and transfectant influenza viruses for growth in mammalian cells: selection of hemagglutinin mutants with elevated pH of membrane fusion. Virology **233:**402-410.

694. **Zaraket H, Bridges OA, Russell CJ.** 2013. The pH of activation of the hemagglutinin protein regulates H5N1 influenza virus replication and pathogenesis in mice. J Virol **87:**4826-4834.

695. **Grimm D, Staeheli P, Hufbauer M, Koerner I, Martinez-Sobrido L, Solorzano A, Garcia-Sastre A, Haller O, Kochs G.** 2007. Replication fitness determines high virulence of influenza A virus in mice carrying functional Mx1 resistance gene. Proc Natl Acad Sci U S A **104:**6806-6811.

696. **Memoli MJ, Bristol T, Proudfoot KE, Davis AS, Dunham EJ, Taubenberger JK.** 2012. In vivo evaluation of pathogenicity and transmissibility of influenza A(H1N1)pdm09 hemagglutinin receptor binding domain 222 intrahost variants isolated from a single immunocompromised patient. Virology **428:**21-29.

697. **Neumann G, Kawaoka Y.** 2001. Reverse genetics of influenza virus. Virology **287:**243-250.

698.   **Neumann G, Watanabe T, Ito H, Watanabe S, Goto H, Gao P, Hughes M, Perez DR, Donis R, Hoffmann E, Hobom G, Kawaoka Y.** 1999. Generation of influenza A viruses entirely from cloned cDNAs. Proc Natl Acad Sci U S A **96:**9345-9350.

APPENDIX

PUBLISHED WORK

Listed below are co-authorship statements and acknowledgments for each of the previously-published chapters (chapters II and III). This information includes funding sources, author affiliations, author contributions, and complete citation information. Also included below is the co-authorship statement and acknowledgments for Chapter IV, which was undergoing peer review for publication at the time this dissertation was submitted. As stated below, previously-published chapters (*i.e.*, chapters II and III) are open-access articles distributed under the terms of the Creative Commons Attribution License, which permits unrestricted use, distribution, and reproduction in any medium, provided the original author and source are credited. More information about Creative Commons licenses can be found at the following website: creativecommons.org/licenses. Reproduction of Chapter IV may be subject to publisher permission after the fact when it and if it is accepted for publication.

Chapter II – Co-authorship statements

Chapter II is composed of the following publications:

Camp JV, Chu Y-K, Chung D-H, McAllister RC, Adcock RS, Gerlach RL, Wiemken TL, Peyrani P, Ramirez JA, Summersgill JT, Jonsson CB (2013). Phenotypic Differences in

Virulence and Immune Response in Closely Related Clinical Isolates of Influenza A 2009 H1N1 Pandemic Viruses in Mice. PLoS ONE 8(2):e56602. doi: 10.1371/journal.pone.0056602

The following analyses were performed by authors other than me:

(1) Collection of clinical specimens was performed by TLW, PP, JAR, and JTS

(2) Virus isolation from clinical specimens and collection of mouse samples from the screen of all isolates in DBA2 mice was performed by YKC.

(3) Sequencing of virus isolates was performed by DHC, YKC, RCM and RSA

(4) The final manuscript was written and edited by JVC and CBJ.

Coauthor affiliations:

Jeremy V. Camp[1], Yong-Kyu Chu[2], Dong-Hoon Chung[1,2], Ryan C. McAllister[1], Robert S. Adcock[1], Rachael L. Gerlach[1], Timothy L. Wiemken[3], Paula Peyrani[3], Julio A. Ramirez[3], James T. Summersgill[3], and Colleen B. Jonsson[1,2]

1Department of Microbiology and Immunology, University of Louisville, KY USA; **2** Center for Predictive Medicine for Biodefense and Emerging Infectious Diseases, University of Louisville, KY USA; **3** Division of Infectious Diseases, University of Louisville, Louisville, KY USA

Chapter III – Co-authorship statements

Chapter III is composed of the following publication:

Jonsson CB, Camp JV, Wu A, Zheng H, Kraenzle JL, Biller AE, Vanover CD, Chu Y-K, Ng CK, Proctor M, Sherwood L, Steffern MC, Mollura DJ (2012) Molecular Imaging Reveals a Progressive Pulmonary Inflammation in Lower Airways in Ferrets Infected

with 2009 H1N1 Pandemic Influenza Virus. PLoS ONE 7(7): e40094.

doi:10.1371/journal.pone.0040094.

The following analysis was performed by authors other than me:

(1) CT and PET imaging was performed by HZ and CN,

(2) Image processing and analysis was performed by AW, DJM

(3) Histopathology interpretation and scoring was performed by MP and LS

(4) The final manuscript was written by CBJ and DJMCo-author affiliations:

Colleen B. Jonsson[1,2], Jeremy V. Camp[1], Albert Wu[3], Huaiyu Zheng[4], Jennifer L. Kraenzle[1], Ashley E. Biller[1], Carol D. Vanover[1], Yong-Kyu Chu[1], Chin K. Ng[4], Mary Proctor[5], Leslie Sherwood[5], Marlene C. Steffen[1], Daniel J. Mollura[3]

1 Center for Predictive Medicine for Biodefense and Emerging Infectious Diseases, and **2** Department of Microbiology and Immunology, University of Louisville, Louisville, KY 40202, USA; **3** Center for Infectious Disease Imaging, Department of Radiology and Imaging Sciences, National Institutes of Health, Bethesda, MD 20892, USA; **4** Department of Radiology and **5** Department of Research Resources Facilities, University of Louisville, Louisville, KY 40202, USA

Chapter IV – Co-authorship statements

Chapter IV has been submitted to the Journal of Virology and is under peer review as of 4/24/2015.

The following analyses were performed by co-authors other than me:

(1) Ferret PET-CT image acquisition was performed by HG,

(2) PET-CT image analysis was performed by UB and DJM

286

Co-author affiliations:

Jeremy V. Camp[1,2], Ulas Bagci[3], Yong-Kyu Chu[2], Brendan Squier[4], Mostafa Fraig[5,6], Silvia M. Uriarte[1,5], Haixun Guo[2,7], Daniel J. Mollura[3], Colleen B. Jonsson[1,2]

1 Department of Microbiology and Immunology, **2** Center for Predictive Medicine for Infectious Diseases and Biodefense, **4** School of Dentistry, **5** Department of Medicine, **6** Department of Pathology, **7** Department of Radiology, University of Louisville, Louisville, KY 40202 USA, **3** Center for Infectious Disease Imaging, Department of Radiology and Imaging Sciences, National Institutes of Health, Bethesda, MD, 20892 USA

CURRICULUM VITAE

Jeremy V. Camp

Work: Dept of Microbiology and Immunology
        University of Louisville
        505 S Hancock Street Rm 626
        Louisville, KY 40202 USA
Home: 1280 Cherokee Rd. Apt 6
        Louisville, KY 40204 USA
Born: 03 June 1980 (age 34); Opelika, AL USA
Tel.:   +1 (334) 787-2376
Email: jeremy.camp.1@louisville.edu

Education
Ph.D. Microbiology and Immunology, May 2015
        University of Louisville, Louisville, KY
        Mentor: Colleen B. Jonsson, Ph.D.
        Dissertation topic: "Critical insights into the pathogenesis of clinical isolates of
                pandemic influenza A(H1N1)2009 virus in mouse and ferret models."
M.S. Biology (Medical Entomology), December 2006
        Georgia Southern University, Statesboro, GA
        Mentor: William S. Irby, Ph.D.
        Thesis: "Biology of Corethrellidae (Diptera): host feeding and host attraction."
B.S. Zoology, December 2003
        Music minor in piano performance
        Auburn University, Auburn, AL

Peer-reviewed Scientific Papers
1. Alpert, M.D., A.R. Rahmberg, W. Neidermyer, S.K. Ng, A. Carville, J.V. Camp, R. L. Wilson, M. Piatak Jr., K.G. Mansfield, W. Li, C.J. Miller, J.D. Lifson, P.A. Kozlowski, D.T. Evans. 2010. "Envelope-modified single-cycle SIV selectively enhances antibody responses, and partially protects against repeated, low-dose vaginal challenge." Journal of Virology. 84(20): pp. 10748-64.
2. Song, K., D.L. Bolton, R.L. Wilson, J.V. Camp, S. Bao, J.J. Mattapallil, L.A. Herzenberg, L.A. Herzenberg, C.A. Andrews, J.C. Sadoff, J. Goudsmit, M.G. Pau, R.A. Seder, P.A. Kozlowski, G.J. Nabel, M. Roederer, S.S. Rao. 2010. "Genetic immunization in the lung induces potent local and systemic immune responses." Proceedings of the National Academy of Sciences. 107(51): 22213-8.

3. McBrayer, A., J.V. Camp, R. Tapp, V. Yamshchikov, S. Grimes, D. Noah, C. B. Jonsson, C. E. Bruder. 2010. "Course of Seasonal Influenza A/Brisbane/59/07 H1N1 Infection in the Ferret Model." Virology Journal. 7:149.
4. Bruder, C. E., S. Yao, F. Larson, J.V. Camp, R. Tapp, A. McBrayer, N. Powers, W. V. Granda, C. B. Jonsson. 2010. "Transcriptome sequencing and development of an expression microarray platform for the domestic ferret" BMC Genomics. 11:251.
5. Camp, J.V., T.L. Svensson, A. McBrayer, C.B. Jonsson, P. Liljestrom, C.E. Bruder. 2012. "De-novo transcriptome sequencing of a normalized cDNA pool from influenza-infected ferrets." PLoS One. 7(5):e37104.
6. Ljungberg, K., A. McBrayer, J.V. Camp, Y.K Chu, R. Tapp, D.L. Noah, S. Grimes, M.L. Proctor, P. Liljestrom, C.B. Jonsson, C.E. Bruder. 2012. "Host gene expression signatures discriminate between ferrets infected with genetically similar H1N1 strains." PLoS One. 7(7):e40743.
7. Jonsson, C.B., J.V. Camp, A. Wu, H. Zheng, J.L. Kraenzle, A.E. Biller, C.D. Vanover, Y.K Chu, C.K. Ng, M. Proctor, L. Sherwood, M.C. Steffen, D.J. Mollura. 2012. "Molecular imaging reveals a progressive pulmonary inflammation in lower airways in ferrets infected with 2009 H1N1 pandemic Influenza virus." PLoS One. 7(7):e40094.
8. Camp, J.V., Y.K. Chu, D.H. Chung, R.C. McAllister, R.S. Adcock, R.L. Gerlach, T.L. Wiemken, P. Peyrani, J.A. Ramirez, J.T. Summersgill, C.B. Jonsson. 2013. "Phenotypic differences in virulence and immune response in closely related clinical isolates of influenza A 2009 H1N1 pandemic viruses in mice." PLoS One. 2013;8(2):e56602.
9. Chung*, D.H., A. Västermark*, J.V. Camp*, R. McAllister*, S.K. Remold, Y.K. Chu, C. Bruder, C.B. Jonsson. 2013. "The murine model for Hantaan virus-induced lethal disease shows two distinct paths in viral evolutionary trajectory with or without ribavirin treatment." Journal of Virology. 87(20): 10997-11007. * = equal contributions
10. Gerlach, R.L., J.V. Camp, Y.K. Chu, C.B. Jonsson. 2013. "Early host responses of seasonal and pandemic influenza A viruses in primary well-differentiated human lung epithelial cells." PLoS One. 8(11): e78912.
11. Ogg, M., C.B. Jonsson, J.V. Camp, J. Hooper. 2013. "Ribavirin protects Syrian hamsters against lethal Hantavirus Pulmonary Syndrome after exposure to Andes virus." Viruses. 5(11): 2704-20.
12. Xu, Z, U. Bagci, A. Mansoor, G. Kramer-Marek, B. Luna, A. Kubler, B. Dey, B. Foster, G.Z. Papadakis, J.V. Camp, C.B. Jonsson, W.R. Bishai, S. Jain, J.K. Udupa, and D. Mollura. 2015. "Computer-Aided Pulmonary Image Analysis in Small Animal Models." Medical Physics. *In press.
13. *Camp, J.V., U. Bağcı, B. Squier, Y-K. Chu, M. Fraig, S. Uriarte, H. Guo, D.J. Mollura, C B. Jonsson. 2015. "Lower respiratory tract infection of the ferret by 2009 H1N1 pandemic influenza A virus triggers biphasic, systemic and local neutrophil recruitment." Journal of Virology. *In review.

Presentations and other scientific contributions

"Biology of the Corethrellidae.'
Poster at Entomological Society of America Conference 2005,
Ft. Lauderdale, FL
Presentation at Georgia Entomological Society Conference 2005,
Athens, GA
Presentation at Georgia Entomological Society Conference 2006,
Jekyll Island, GA.

"Differential virulence of 2009 H1N1 influenza A strains isolated from patients with severe influenza pneumonia in Kentucky as tested in mice." Poster at 2011 American Society for Virology Conference, Minneapolis, MN.

"Phenotypic differences in virulence and immune response in closely related clinical isolates of influenza A 2009 H1N1 pandemic viruses in mice." Poster at 2013 American Society for Virology Conference, State College, PA.

"Multi-focal Neutrophil Infiltration and Inflammation in Lungs of Ferrets Infected with 2009 H1N1 Influenza A Virus Clinical Isolate." Orthomyxovirus Pathogenesis Workshop Presentation at 2014 American Society for Virology Conference, Ft. Collins, CO

Invited Lectures and Teaching

"Biology of Organisms" and "Environmental Biology" undergraduate laboratory courses. Georgia Southern University, Statesboro, GA; Fall 2004 – Fall 2006

"Pathogenesis and virulence of H1N1 influenza A viruses." Division of Infectious Diseases Grand Rounds, University of Louisville Hospital, Louisville, KY; 26 March 2014

"Ebola: What is it? How do we treat it? And should we be worried." Beer with a Scientist public seminar series, 12 Nov 2014, Louisville, KY

"Viral Pathogenesis" Lecturer for the following courses:
- MBIO618 Cell Biology of Viruses, Spring 2014
- MBIO687 Microbial Pathogenesis, Spring 2015
Department of Microbiology and Immunology, University of Louisville

Academic Service

President - Biology Organization of Graduate Students, Georgia Southern University, 2006
Student Tutor in Statistics – University of Louisville, 2013
Curriculum Committee Representative – Microbiology and Immunology Student Organization, University of Louisville, 2013-2014

Admissions Committee Representative – Microbiology and Immunology Student
Organization, University of Louisville, 2014-2015

Awards and Memberships
- Eagle Scout Award - June 1998
- Interface, Inc. Scholarship - August 1998-May 2000
- Graduate Student Professional Development Fund, Georgia Southern University,
2005
- Dr. Sturgis McKeever Zoology Scholarship, Georgia Southern University, 2005
- T. L. Bissell Award, Georgia Entomological Society, 2006
- Georgia Entomological Society Scholarship, 2005
- Member, Georgia Entomological Society, 2004 - 2006
- Member, Entomological Society of America, 2005 – 2007
- Member, American Society for Virology, 2010 – present
- American Society for Virology Student Travel Grant, 2011, 2013
- Integrated Program in Biomedical Sciences Fellowship, University of Louisville,
2011-2013

Employment History

Immunology Core Manager, August 2010 – August 2011
Center for Predictive Medicine for Biodefense and Emerging Infectious Diseases
Regional Biocontainment Laboratory
University of Louisville, Louisville, KY

Biologist, January 2009 – August 2010
Project: NIH C26 contract, Development of the ferret model of influenza
Laboratory of Colleen B. Jonsson, Ph.D.; Supervisor, Carl E. Bruder, Ph.D.
Department of Viral Biochemistry
Southern Research Institute, Birmingham, AL

Research Associate, February 2007- December 2008
Project: Mucosal immunology and HIV vaccination strategies
Laboratory of Pamela Kozlowski, Ph.D.
Gene Therapy Group
LSU Health Sciences Center, New Orleans, LA

Research Assistant, June 2005- December 2006
Exhibit curation and population genetics of the tick, Ixodes scapularis
Laboratory of Lorenza Beati, M.D., Ph.D.
U.S. National Tick Collection
Institute for Arthropodology and Parasitology, Statesboro, GA

Graduate Teaching Assistant, August 2004- December 2006
Department of Biology

Georgia Southern University, Statesboro, GA

Field Biologist, September 2001 – August 2004
  Project: Ecology of Eastern Equine Encephalitis virus mosquito vectors
  Laboratory of Eddie W. Cupp, Ph.D.
  Vector Biology Laboratory
  Auburn University, Auburn, AL